Doctoral theses at NTNU, 2022:273

Juan Hou

Investigation of Model Predictive Control Application in District Heating Systems with Distributed Sources

Doctoral thesis

NTNU
Norwegian University of Science and Technology
Thesis for the Degree of
Philosophiae Doctor
Faculty of Engineering
Department of Energy and Process Engineering

NTNU
Norwegian University of
Science and Technology

Juan Hou

Investigation of Model Predictive Control Application in District Heating Systems with Distributed Sources

Thesis for the Degree of Philosophiae Doctor

Trondheim, September 2022

Norwegian University of Science and Technology
Faculty of Engineering
Department of Energy and Process Engineering

NTNU
Norwegian University of
Science and Technology

NTNU
Norwegian University of Science and Technology

Thesis for the Degree of Philosophiae Doctor

Faculty of Engineering
Department of Energy and Process Engineering

© Juan Hou

ISBN 978-82-326-6697-3 (printed ver.)
ISBN 978-82-326-5523-6 (electronic ver.)
ISSN 1503-8181 (printed ver.)
ISSN 2703-8084 (online ver.)

Doctoral theses at NTNU, 2022:273

Printed by NTNU Grafisk senter

PREFACE

This thesis is submitted to the Norwegian University of Science and Technology in partial fulfilment of the requirements for the degree of Doctor of Philosophy (PhD).

This work was carried out at the Department of Energy and Process Engineering, Norwegian University of Science and Technology, Trondheim, Norway. The work was under the supervision of Professor Natasa Nord from the Norwegian University of Science and Technology and the co-supervision of Associate Professor Gongsheng Huang from the City University of Hong Kong, Hong Kong, China.

This PhD project was under financial support by the Research Council of Norway through the FRIPRO/FRINATEK program, project number 262707.

ACKNOWLEDGMENTS

The four years journey as a PhD candidate must be an amazing chapter in my whole life, and it has been an adventure full of inspiring, stressful yet joyful experiences. Throughout this journey, I have always been surrounded by wonderful people who are supporting me in some way. I would like to express my heartfelt gratitude to all of them.

First of all, my special thanks to Natasa Nord, my main supervisor, for all the scientific and personal suggestions throughout my PhD studies. I highly appreciate her trust, patience and understanding, especially for the two years that I am being a new mother. Her advice and experiences both from work and life keep me always on the right track to finishing my PhD, especially in times of doubt and frustration.

I would like to acknowledge my co-supervisor, Gongsheng Huang, for his professional advice as an expert in HVAC system control and optimization. I appreciate all his valuable suggestions to boost my research.

I am grateful to the staff at the Department of Engineering Cybernetics, who gave me access to obtain the valuable resources in their courses, which help me from zero to have knowledge of numerical optimal control.

Furthermore, I would like to thank my colleagues and friends at NTNU. Thank you all for making this journey fun and memorable. I appreciate all the brain centre talks and the countless cakes and coffees.

I am forever grateful to my family for their unconditional love and support. To my parents for bringing me up in a positive family atmosphere and always providing me with their help in my tough times. To my husband, Haoran, for being my team partner both in work and life and always insisting on our dreams when I was about to give up. The last but not least, to my lovely son, Jixi, for joining the family and bringing us all unprecedented moments of happiness. Your healthy growth is the biggest motivation to keep me going.

Trondheim, Norway

May 1, 2022

Juan Hou

ACKNOWLEDGMENTS

ABSTRACT

District heating (DH) systems, which can integrate various available heat sources, have proven to be an energy-efficient and environment-friendly way to satisfy buildings' heating demands. However, with the transition from current energy systems to future sustainable energy solutions, the DH system, as an essential part of the energy systems, must undergo a generational transition to maintain its competitiveness compared with alternative heating technologies. As a result, the current DH systems are transitioning to the 4th and 5th generation DH systems. Developing intelligent control strategies to optimally operate the DH system is one of the crucial measures to realize the transition. Numerous studies have reported that intelligent control strategies can notably reduce energy use, mitigate greenhouse gas emissions and improve economic performance for heating systems. However, most of the existing DH systems still use rule-based control (RBC) strategies with limited energy-saving and cost-saving potential.

This thesis, therefore, aimed to explore the intelligent control strategies for the existing DH by utilizing model predictive control (MPC) strategies. With a focus on the DH systems dedicated to Nordic climate conditions, this thesis investigated the implementation of MPC on both the demand and supply side of the DH system to improve the energy and economic performance of the system. To achieve this goal, a step-by-step simulation-based study, was conducted, driven by four research questions.

Question 1: What is the economic boundary when using MPC to improve the economic performance of a DH system? Literature reviews and energy contract investigations revealed that generalized heating and electricity price models can be used as the basis for the economic boundary for the MPC schemes. The generalized heating price model included the load demand component (LDC) and the energy demand component (EDC), and the generalized electricity price model was made up of the power price and the grid rent. This economic boundary was incorporated into the objective functions of the MPC schemes based on their specific needs.

Question 2: What is the system energy and economic performance when using MPC on the demand side of the DH systems? The research on the MPC application in a building space heating (SH) system was conducted to answer this question. The modelling method for a

building SH system was proposed, and then an MPC scheme was formulated by defining an economic-related objective function and system constraints, as well as incorporating the developed SH system model and an optimization framework. Finally, this MPC scheme was evaluated by comparing its performance to that of a conventional RBC strategy. A case study on the SH system in a university building showed that the MPC scheme with perfect future weather information could cut the weekly heating cost by 4.1% and decrease the violation numbers of indoor temperature by 65% compared to an RBC strategy. However, these benefits may be impaired when the MPC scheme directly used weather forecast information. Since any prediction has some uncertainties and hence the MPC controller may receive inaccurate weather information, leading to incorrect control actions that may deteriorate the system performance. Therefore, the third research question was proposed as follows.

Question 3: What is the impact of weather forecast uncertainty on MPC performance, and how to handle it? To answer the impact of weather forecast uncertainty on MPC performance, another MPC scenario that directly used weather forecast information was proposed. The simulation results showed that the MPC scheme directly using weather forecast information cut the heating cost by only 0.7% and even increased the violation numbers of indoor temperature by 20% compared to the RBC strategy. To tackle the weather forecast uncertainty, an error model was proposed to improve the quality of weather forecast information. Meanwhile, one more MPC scenario that incorporated weather forecast information and the error model was proposed. Results showed that introducing the error model for the MPC scheme was able to address the weather forecast uncertainty and hence achieve almost the full theoretical potential of the MPC in terms of heating cost-saving and indoor temperature control. The MPC scheme with weather forecast information and the error model cut the weekly heating cost by 3.4% and decreased the violation numbers of indoor temperature by 73% compared to the RBC strategy.

Question 4: What is the system energy and economic performance when using MPC on the supply side of the DH systems with distributed sources? The research on the MPC application for a heat prosumer with data centre (DC) waste heat recovery and thermal energy storage (TES) was conducted to answer this question. The modelling method for a typical heat prosumer with DC waste heat and TES was proposed firstly, and then an MPC scheme was formulated by defining an economic-related objective function and system constraints, as well as incorporating the developed DH system model and an optimization framework. A case study on a campus DH system showed that the MPC scheme optimized the heat supply allocation

between the multiple heat sources and the TES so that the economic performance of the DH system was improved. The MPC scheme was more stable and robust expressed as the smaller fluctuating ranges of the outlet temperature at the heat pump (HP) evaporator, which is crucial for the DC cooling system's safe operation. In addition, the MPC scheme made an optimized trade-off between the heat and electricity use to achieve the best economic performance of the heat prosumer, and the resulting monthly energy cost saving was up to 3.2%.

In conclusion, this thesis provided a systematic research method on the implementation of MPC in DH systems with distributed sources from both the demand and supply sides. Meanwhile, the investigation of weather forecast uncertainty may facilitate the real application of the MPC in building energy systems. Lastly, this study may enrich the research on the intelligent control strategies for the DH system.

ABSTRACT

LIST OF PUBLICATIONS

Paper 1:

Hou J, Li H, Nord N. Nonlinear model predictive control for the space heating system of a university building in Norway. Energy. 2022; 253: 124157.

Paper 2:

Hou J, Li H, Nord N, Huang G. Model predictive control under weather forecast uncertainty for HVAC systems in university buildings. Energy and Buildings. 2022; 257: 111793.

Paper 3:

Hou J, Li H, Nord N, Huang G. Model predictive control for a university heat prosumer with data centre waste heat and thermal energy storage. Submitted to Journal of Energy (Status: Under review).

Paper 4:

Li H, Hou J, Tian Z, Hong T, Nord N, Rohde D. Optimize heat prosumers' economic performance under current heating price models by using water tank thermal energy storage. Energy. 2022; 239: 122103.

Paper 5:

Hou J, Li H, Nord N. Model predictive control for a data centre waste heat-based heat prosumer in Norway. Submitted to the 10th BuildSim Nordic conference and the 2nd International Nordic conference for IBPSA. (Status: Accepted for full paper, and oral presentation).

Paper 6:

Hou J, Li H, Nord N. Optimal control of secondary side supply water temperature for substation in district heating systems. E3S Web Conf. 2019; 111: 06015. The 13th REHVA World Congress CLIMA 2019.

Paper 7:

Li H, Hou J, Hong T, Ding Y, Nord N. Energy, economic, and environmental analysis of integration of thermal energy storage into district heating systems using waste heat from data centres. Energy. 2021; 219: 119582.

Paper 8:

Li H, Hou J, Hong T, Nord N. Distinguish between the economic optimal and lowest distribution temperatures for heat-prosumer-based district heating systems with short-term thermal energy storage. Energy. 2022; 248: 123601.

Paper 9:

Li H, Hou J, Nord N. Using thermal storages to solve the mismatch between waste heat feedin and heat demand: a case study of a district heating system of a university campus. Energy Proceedings. 2019;04. The 11th International Conference on Applied Energy.

Paper 10:

Li H, Hou J, Ding Y, Nord N. Techno-economic analysis of implementing thermal storage for peak load shaving in a campus district heating system with waste heat from the data centre. E3S Web Conf; 2021;246: 09003. The 10th International SCANVAC Cold Climate Conference.

Paper 11:

Li H, Hou J, Nord N. Optimal design and operation for heat prosumer-based district heating systems. The 14th REHVA HVAC World Congress CLIMA 2022.

ABBREVIATIONS

AHU	Air-handling unit
CHP	Combined heat and power
COP	Coefficient of performance
CP	Circulator pump
DC	Data centre
DH	District heating
DHS	Distributed heat source
EDC	Energy demand component
HE	Heat exchanger
HP	Heat pump
IPOPT	Interior Point OPTimizer
KKT	Karush-Kuhn-Tucker
LDC	Load demand component
MEPS	MetCoOp Ensemble Prediction System
MPC	Model predictive control
MS	Main substation
NLP	Nonlinear programming
NWPM	Numerical weather prediction model
P controller	Proportional controller
PI controller	Proportional-integral controller
RBC	Rule-based control
RC	Resistance-capacitance
RMSE	Root mean square error
R2R	Return to return
R2S	Return to supply
SH	Space heating
TES	Thermal energy storage
WCC	Weather compensation controller
WTTES	Water tank thermal energy storage

LIST OF CONTENTS

LIST OF TABLES

LIST OF FIGURES

1 INTRODUCTION

This chapter introduces the motivation, research questions and tasks of the doctoral work. The thesis structure and list of publications that support this thesis are presented as well.

1.1 Motivation

The energy use of buildings accounts for a large share of total energy use and significantly contributes to global warming. In the European Union countries, buildings are responsible for nearly 40% of the total energy use and about 36% of the total greenhouse gas emissions [1]. Moreover, in the EU's residential sector, around 80% of the buildings' energy use is for heating purposes including space heating (SH) and domestic hot water, especially during the winter season [2]. District heating (DH) systems, which can integrate various available heat sources, have proven to be an energy-efficient and environment-friendly way to satisfy buildings' heating demands. Nowadays, the total number of DH systems has been estimated to be around 80 000 all overall the world, and thereof about 6 000 systems in Europe [3, 4]. However, with the transition from current energy systems to future sustainable energy solutions, the DH system, as an essential part of the energy systems, must undergo a generational transition to maintain its competitiveness compared with alternative heating technologies [5]. As a result, the current DH systems are transitioning to the 4^{th} and 5^{th} generation DH systems. Developing intelligent control strategies to optimally operate the DH system is one of the crucial measures to realize the transition [6]. Numerous studies have reported that intelligent control strategies can notably reduce energy use, mitigate greenhouse gas emissions and improve economic performance for heating systems [7-11]. However, most of the existing DH systems still use rule-based control (RBC) strategies with limited energy-saving and cost-saving potential. With decreasing computational and sensing costs, a digital age that is paving the way for the adoption of intelligent control strategies is coming. In the last decade, model predictive control (MPC) has dominated the research on intelligent control strategies in building energy systems [12].

MPC is a potential control solution that can be focused on the reduction of energy use, energy cost, and associated greenhouse gas emissions while maintaining and potentially improving occupant comfort [13]. MPC uses a dynamic system model to predict the future behaviour of the system and generates an optimal control vector that minimizes an objective function over the prediction horizon in the presence of disturbances and technical operational constraints. The

objective function can combine several conflicting performance targets, such as maximization of thermal comfort and minimization of energy use, and an optimal trade-off among them can be obtained by running the MPC algorithm [14, 15]. However, despite intensive research efforts, the transfer of this technique to real application in building energy systems is still in the early stages [12]. One difficulty stems from the fact that every energy system is unique, which requires a tailored modelling method and control design for its MPC scheme. Building an MPC scheme to control a district-level energy system even increases the complexity, and this is the reason that most previous MPC research has been dedicated to the heating, ventilation and air-conditioning systems of single buildings [16]. The implementation of MPC at the district level, i.e. the control of the energy supplied to a cluster of buildings has not yet been fully explored [17]. Moreover, weather forecast uncertainty is one challenge as well hindering the implementation of the MPC. A building MPC is based on the prediction of future weather and many studies consider a perfect weather forecast for MPC. However, any prediction has some uncertainties that may influence system performance such as energy use and thermal comfort. Therefore, the MPC controller may receive inaccurate information and lead to incorrect control actions that may cause thermal discomfort or energy waste [18]. Finally, the MPC performance may vary depending on the test cases and climate conditions [19]. Further research should be conducted to test the concept in different types of climates and buildings. This thesis, therefore, aimed to contribute to the implementation of MPC in DH systems dedicated to Nordic climate conditions to improve their economic performance, and weather forecast uncertainty was investigated as well. This study was conducted in two steps: 1) design an MPC scheme on the demand side of a DH system and then investigate the impact of weather forecast uncertainty on the MPC performance; 2) design an MPC scheme on the supply side of a DH system and then realize the optimal control of the heat supplied to a cluster of buildings.

Nowadays, in most DH systems, SH demand is managed by a weather compensation controller (WCC) at the building substation level. Meanwhile, proportional control valves are often installed inside buildings to regulate the water flow rate to maintain the indoor air temperature close to its set point. However, this control technique does not contain any information about the building dynamics and lacks flexibility. It does not consider making smart decisions like strategically lowering the heating output to exploit the intrinsic building thermal inertia and hence reduce the heating cost [11]. In contrast, MPC can realize the intelligent management of SH systems, as the building dynamic model, future disturbances, energy price, energy demand,

and intelligent algorithms are incorporated into the controller. Particularly, the passive thermal mass storage of the buildings can be considered in the MPC control strategy to further improve the system's economic performance. However, the weather forecast uncertainty may impair the benefits brought by using the MPC control strategy, as explained before. Therefore, the implementation of MPC in the SH system to improve the system energy and economic performance, as well as the impact of weather forecast uncertainty on MPC performance were investigated as the first step of this thesis.

Moreover, integrating renewables and waste heat into the DH system is one significant characteristic of the future DH system [5, 20]. Specifically, the renewables and waste heat may be integrated into the heat user side as distributed heat sources (DHSs), and these heat users with DHSs are known as heat prosumers because of their dual roles of producer and consumer. Heat prosumers will become critical participants in future DH systems due to the increasing integration of renewables and waste heat [21]. Among these DHSs, waste heat recovery from data centres (DCs) is a promising option. DCs are energy-intensive facilities that continuously convert most of their energy use into waste heat, resulting in a considerable amount of stable and available waste heat. In addition, many DCs are built close to an existing DH network, which makes the DC waste heat easy to access for the DH network. As a result, there is an increasing effort to capture DC waste heat for DH systems, and many studies have explored the possibilities and proposed technical solutions for recovering DC waste heat for DH systems [22-27]. However, the solutions for optimal control of the DH system after recovering DC waste heat to further improve the economic performance of the system are rarely investigated, particularly for a heat prosumer with DC waste heat and thermal energy storage (TES). The optimal control of a heat prosumer with DC waste heat and TES is challenging, and the difficulties come from the following aspects: 1) a complex economic boundary involving not only dynamic heating prices but also electricity prices due to the electricity use of DC waste heat recovery units, 2) multi-level technical operation constraints from both the DH system and the DC cooling system and 3) numerous manipulated variables need to be optimized originating from the multi-components, such as heat substation, heat users, DC and TES. An MPC scheme, which can employ an economic-related objective function for real-time control, may be one way to realize the maximized possible economic performance of the system while satisfying different technical operational constraints [12, 15]. Therefore, the implementation of MPC in a heat prosumer with DC waste heat and TES was investigated in this thesis as the second step,

particularly focusing on the heat supply allocation between the multiple heat sources to realize the optimal control of the heat supplied to a cluster of buildings.

1.2 Research questions and research tasks

The following research questions and tasks were proposed as a step-by-step approach to achieve the thesis's aim.

Question 1: **What is the economic boundary when using MPC to improve the economic performance of a district heating system?**

Task 1.1: Identify key factors that affect heating and electricity costs based on literature reviews and widely used energy contracts in Nordic countries.

Task 1.2: Define the economic boundary by developing a generalized heating price model as well as a generalized electricity price model that incorporates the identified key factors.

Question 2: What is the system energy and economic performance when using MPC on the demand side of the DH systems?

Task 2.1: Propose the modelling method for a building SH system.

Task 2.2: Formulate an MPC scheme by defining an economic-related objective function and system constraints, as well as incorporating the developed SH system model and an optimization framework.

Task 2.3: Evaluate the MPC scheme by comparing its performance to that of a conventional RBC strategy.

Question 3: What is the impact of weather forecast uncertainty on MPC performance, and how to handle it?

Task 3.1: Develop an error model to estimate the error existing in the weather forecast.

Task 3.2: Propose an improved MPC scheme that integrates with the error model to tackle weather forecast uncertainty.

Task 3.3: Evaluate the improved MPC scheme by comparing its performance to that of the standard one without the error model.

Question 4: What is the system energy and economic performance when using MPC on the supply side of the DH systems with distributed sources?

Task 4.1: Propose the modelling method for a typical heat prosumer with DC waste heat and TES.

Task 4.2: Formulate an MPC scheme by defining an economic-related objective function and system constraints, as well as incorporating the developed DH system model and an optimization framework.

Task 4.3: Evaluate the MPC scheme by comparing its performance to that of a conventional RBC strategy.

The above research questions are logically connected and organized in Figure 1-1.

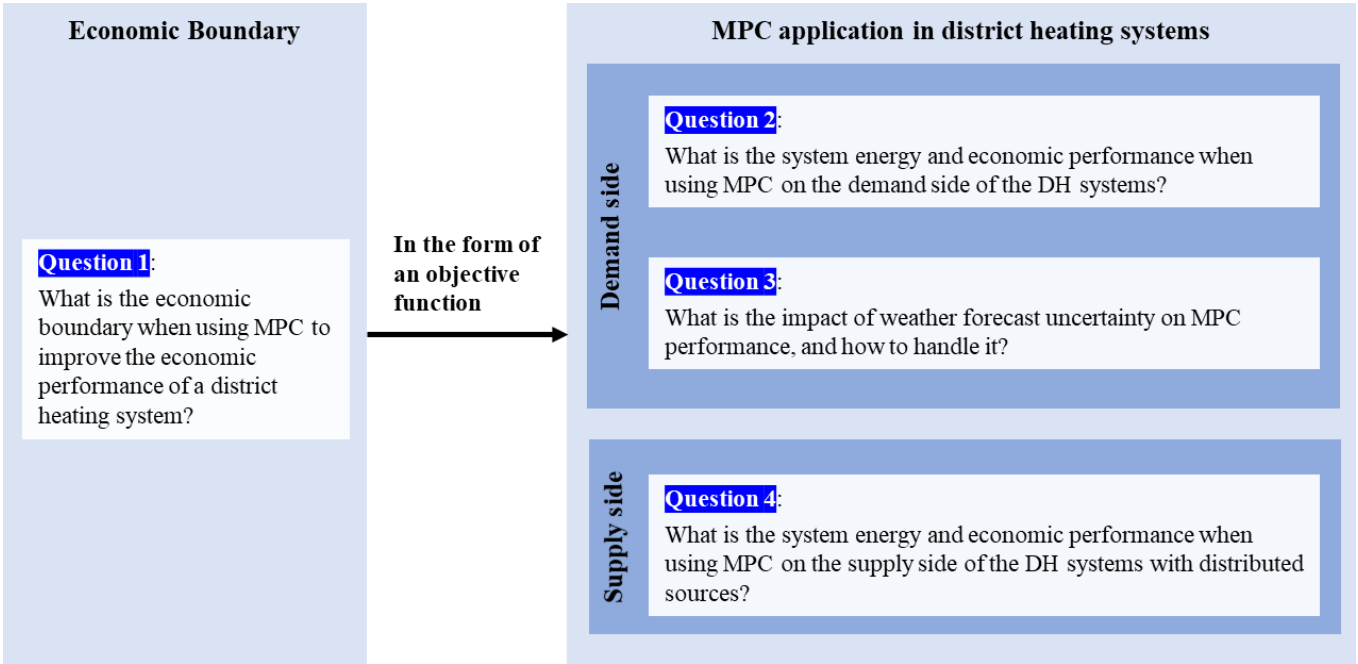

Figure 1-1. Connection and organization of the research questions

1.3 Structure of the thesis

The main body of the thesis is illustrated in Figure 1-2. Chapter 2 introduces the background of the study. Chapter 3 presents the research methodology, including the modelling language, optimization framework, economic boundary, formulation of MPCs on the demand and supply sides of a DH system and the error model to handle weather forecast uncertainties. Chapter 3.5 describes the case studies: a university building SH system and the university campus DH system connected to the introduced SH system. Chapter 5 presents and discusses the key results. Chapter 6 outlines the main conclusions, acknowledges the major limitations and gives recommendations for future research. As shown in Figure 1-2, the first research question, **Question 1**, which establishes the economic boundary of the study, is addressed in Chapter 3. The other research questions, from **Question 2** to **Question 4**, are addressed and answered in Chapter 3 to Chapter 5 of the thesis.

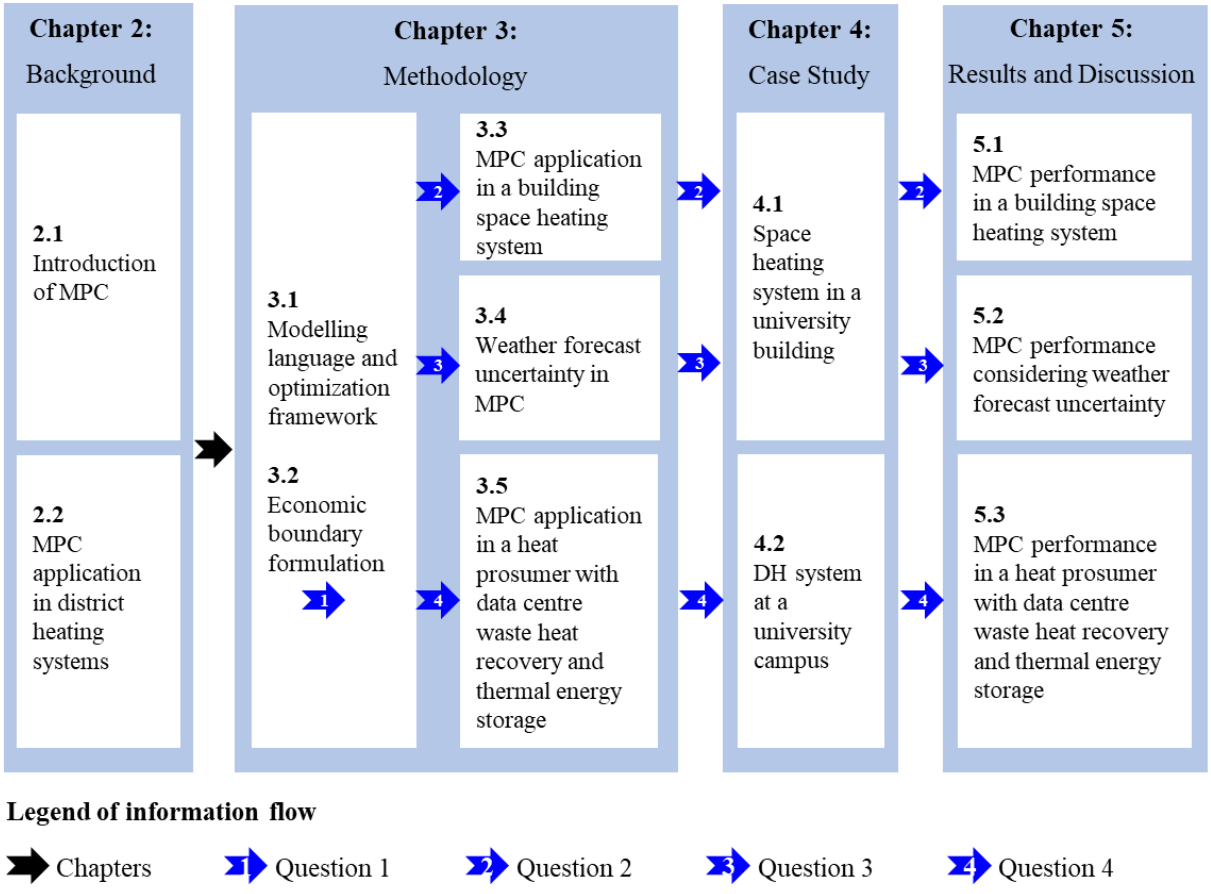

Figure 1-2. Structure and information flow from Chapter 2 to Chapter 5 of the thesis

1.4 List of publications

This thesis is built on four journal papers and one conference paper. Figure 1-3 presents an overview of these papers and distinguishes them into primary and supporting papers. The primary papers address the key research questions and the supporting papers present the preparatory work for the primary papers. The following are the papers that make up this thesis, as well as the author's contributions.

Primary papers:

Paper 1:

Hou J, Li H, Nord N. Nonlinear model predictive control for the space heating system of a university building in Norway. Energy. 2022; 253: 124157.

Contribution: The paper is invited to the 'Special Issue of Energy Dedicated to SDEWES 2021'. The type of this paper is Full Length Article. The conceptualization was done together with Haoran Li and Natasa Nord. The methodology and the original draft preparation were done in collaboration with Haoran Li. Natasa Nord reviewed and commented on the work.

Paper 2:

Hou J, Li H, Nord N, Huang G. Model predictive control under weather forecast uncertainty for HVAC systems in university buildings. Energy and Buildings. 2022; 257: 111793.

Contribution: The type of this paper is Full Length Article. The conceptualization was done together with Haoran Li. The methodology and the original draft preparation were done in collaboration with Haoran Li. Natasa Nord and Gongsheng Huang reviewed and commented on the work.

Paper 3:

Hou J, Li H, Nord N, Huang G. Model predictive control for a university heat prosumer with data centre waste heat and thermal energy storage. Submitted to Journal of Energy (Status: Under review).

Contribution: The type of this paper is Full Length Article. The conceptualization was done together with Haoran Li. The methodology and the original draft preparation were done in

collaboration with Haoran Li. Natasa Nord and Gongsheng Huang reviewed and commented on the work.

Supporting papers

Paper 4:

Li H, Hou J, Tian Z, Hong T, Nord N, Rohde D. Optimize heat prosumers' economic performance under current heating price models by using water tank thermal energy storage. Energy. 2022; 239: 122103.

Contribution: The type of this paper is Full Length Article. The author assisted in the methodology and original draft preparation.

Paper 5:

Hou J, Li H, Nord N. Model predictive control for a data centre waste heat-based heat prosumer in Norway. Submitted to BuildSim Nordic 2022 conference. (Status: Accepted for full paper, and oral presentation).

Contribution: The type of this paper is Full Length Article. The author did the conceptualization, methodology and original draft preparation. Haoran Li and Natasa Nord reviewed and commented on the work.

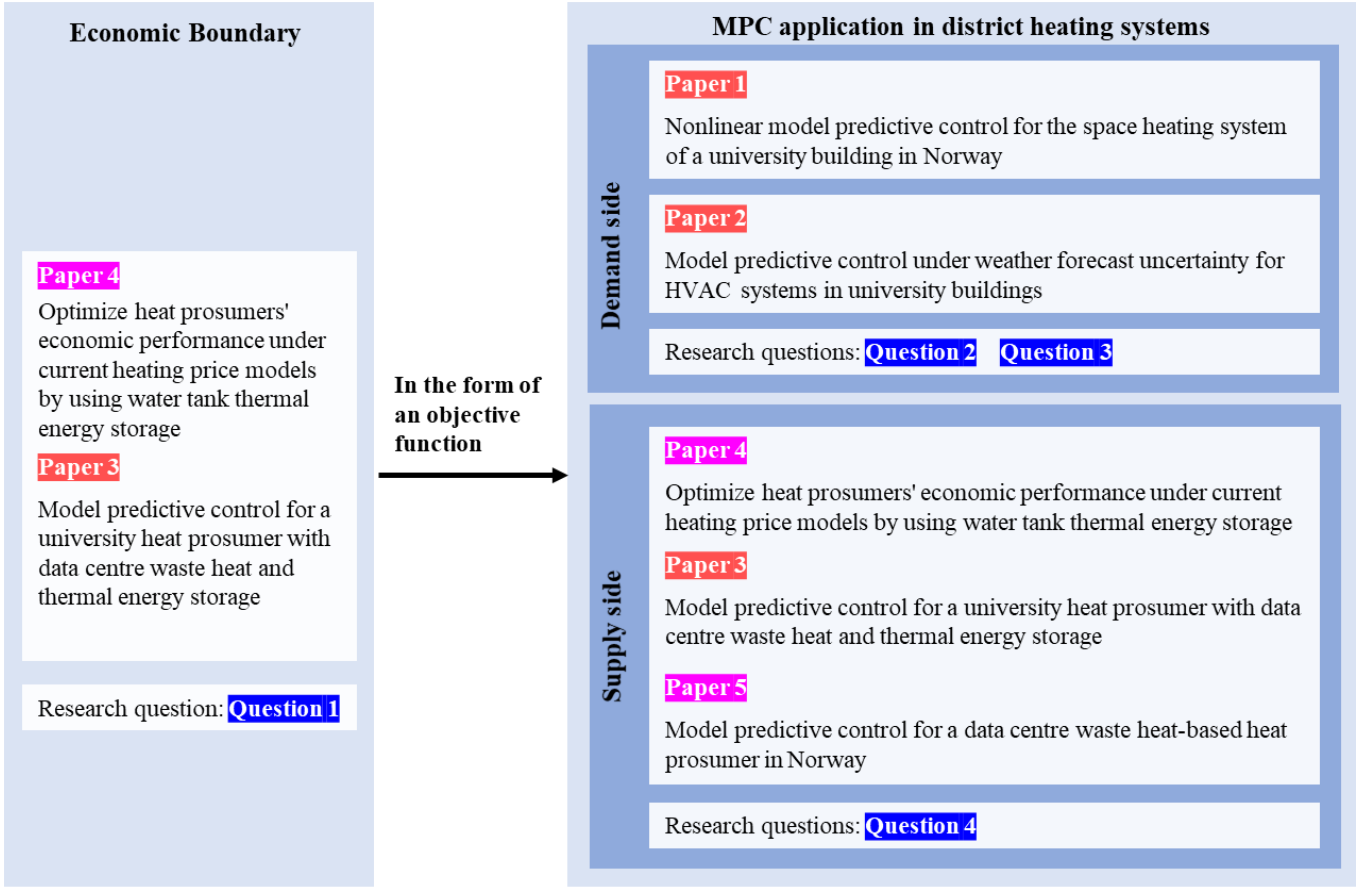

Figure 1-3. Overview of the publications considered in this thesis and their connections with the research questions

Additional papers:

Collaboration within the research project *'Understanding Behaviour of District Heating Systems Integrating Distributed Sources'* has led to further publications:

Paper 6:

Hou J, Li H, Nord N. Optimal control of secondary side supply water temperature for substation in district heating systems. E3S Web Conf. 2019; 111: 06015. The 13th REHVA World Congress CLIMA 2019.

Contribution: The type of this paper is Full Length Article. The author did the conceptualization, methodology and the original draft preparation. Haoran Li and Natasa Nord reviewed and commented on the work.

Paper 7:

Li H, Hou J, Hong T, Ding Y, Nord N. Energy, economic, and environmental analysis of integration of thermal energy storage into district heating systems using waste heat from data centres. Energy. 2021; 219: 119582.

Contribution: The type of this paper is Full Length Article. The author assisted in the conceptualization and the original draft preparation.

Paper 8:

Li H, Hou J, Hong T, Nord N. Distinguish between the economic optimal and lowest distribution temperatures for heat-prosumer-based district heating systems with short-term thermal energy storage. Energy. 2022; 248: 123601.

Contribution: The type of this paper is Full Length Article. The author assisted in the conceptualization and the original draft preparation.

Paper 9:

Li H, Hou J, Nord N. Using thermal storages to solve the mismatch between waste heat feedin and heat demand: a case study of a district heating system of a university campus. Energy Proceedings. 2019;04. The 11th International Conference on Applied Energy.

Contribution: The type of this paper is Full Length Article. The author assisted in the original draft preparation.

Paper 10:

Li H, Hou J, Ding Y, Nord N. Techno-economic analysis of implementing thermal storage for peak load shaving in a campus district heating system with waste heat from the data centre. E3S Web Conf; 2021;246: 09003. The 10th International SCANVAC Cold Climate Conference.

Contribution: The type of this paper is Full Length Article. The author assisted in the original draft preparation.

Paper 11:

Li H, Hou J, Nord N. Optimal design and operation for heat prosumer-based district heating systems. The 14th REHVA HVAC World Congress CLIMA 2022.

Contribution: The type of this paper is Full Length Article. The author assisted in the original draft preparation.

2 BACKGROUND

This chapter introduces how the MPC scheme was applied in building energy systems and reviews the literature on the MPC application in DH systems.

2.1 Introduction of MPC

MPC originated in the late 1970s and early 1980s in the process industries, and it recently has been receiving extensive attention from researchers in the field of building energy system control. MPC is a constrained optimal control approach that minimizes a given objective function over a finite prediction horizon to calculate an optimal trajectory of control inputs. Figure 2-1 illustrates a typical abstract closed-loop MPC scheme that can describe most of the control applications in building energy systems [12].

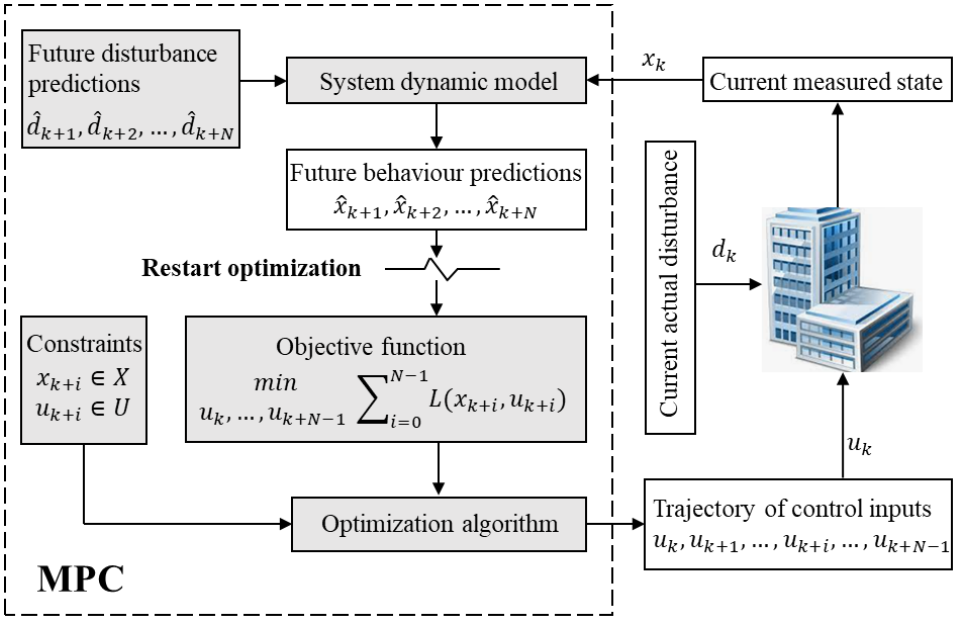

Figure 2-1. MPC scheme for building energy system control [12]

As shown in Figure 2-1, the fundamental components of an MPC are 1) a system dynamic model, 2) future disturbance predictions, 3) an objective function and system constraints, and 4) an optimization algorithm. At each time step, the future disturbance predictions ($\hat{d}_k, \hat{d}_{k+1}, \ldots, \hat{d}_{k+N-1}$) together with the candidate MPC control input trajectory are used as

simulation inputs to the system dynamic model. This simulation is carried out over the prediction horizon (N) that typically ranges between 8 and 72 hours in building energy system applications [14]. The optimizer evaluates the objective function for each simulation run and adapts the candidate MPC control input trajectory until an optimal solution ($u_k, u_{k+1}, \ldots, u_{k+i}, \ldots, u_{k+N-1}$) is obtained. Only the first control inputs in the optimal trajectory (u_k) are supplied to the system that is affected by the current actual disturbance (d_k). At the next time step, the MPC changes the initial states of the system dynamic model according to the current measurement system state (x_k), receives a new sequence of future disturbance predictions ($\hat{d}_{k+1}, \hat{d}_{k+2}, \ldots, \hat{d}_{k+N}$), and restart the optimization [15].

2.2 MPC application in district heating systems

The application of MPC in heating systems has attracted lots of attention in recent years, but most of these studies are exclusively devoted to buildings with individual heating systems [7, 8, 28-31]. The building heating systems connected to a DH system imply higher system complexity and a larger computational burden, and this leads the MPC application in DH systems to be challenging. However, despite the inherent difficulties, some researchers still proved the feasibility of the MPC application in DH systems from both the demand side and the supply side.

Currently, studies focused on the MPC application on the demand side of the DH system to minimize operating costs of the SH system and maximize occupant comfort are relatively rare. One example is from Aoun et al [11]. They proposed a mixed-integer linear programming-based MPC strategy to optimize the operation of the SH system connected to a DH system based on minimizing operating costs. The proposed methods were tested on a DH system located in France by numerical simulation method, and the results showed that the adopted MPC proved to be more cost-effective than a conventional WCC while maintaining satisfying indoor temperature [11].

More researchers focused on the MPC application on the supply side of the DH system to optimize the operation of the heat production plants. Verrilli et al. designed an MPC controller to optimize the operation of a DH system that integrates TES and uses a combined heat and power (CHP) plant as a heat source. The designed MPC focused on reducing the operating and maintenance cost of the CHP plant by scheduling boilers, TES units, and flexible loads. The

proposed approach was tested using the data obtained from a DH system in Finland by both simulation and experiment methods, and the results showed the cost benefits of the approach [32]. Moreover, Saletti et al. developed an MPC controller to optimize the management and heat distribution of the CHP in a DH system by utilizing the thermal capacity of the connected buildings as TES. The approach was tested on a DH system located in central Sweden, and one week's simulation results demonstrated the effectiveness of the MPC with a peak load shaving of 16% and a mass flow rate reduction of 23% [33]. Similarly, Zwan et al. presented an MPC approach to minimize fossil peak loads and maximize the use of renewable sources for DH systems with multi-heat sources by using the thermal mass of buildings as daily storage without violating temperature constraints. The approach was tested on a virtual DH system. Simulation results showed that the peak fossil heat supply was reduced by 50%, and the cheap renewable heat source could deliver most of the heat demand in continuous operation since the supply temperature was minimised [34]. Furthermore, Hermansen et al. proposed an MPC strategy for a heat booster substation in an ultra-low temperature DH system to minimize the operation costs of the heat pump, which was used to charge the TES, by optimizing the charging schedule of the TES. The proposed MPC strategy was successfully implemented in a real DH system in Copenhagen to verify the control strategy. A comparison of the proposed MPC scheduling to a standard RBC showed average daily savings of 23% on the electricity costs [35].

In summary, these previous studies have demonstrated the enormous energy and economic benefits of applying MPC schemes in DH systems. However, these limited literature resources reveal the fact that the research on the application of MPC in DH systems is still a relatively new field both from the demand side and the supply side due to some inherent challenges. Regarding the demand side, although many researchers have investigated the MPC application in electricity-based SH systems, like electrical radiators and electric underfloor heating, the research on the MPC application in a hydronic SH system connected to a DH system is still limited as illustrated in the literature review. One challenge is that typical building heating systems connected to DH networks are comprised of hydronic heat emitters, such as radiators, that are characterized by nonlinearities in their heat rate output driven by the temperature difference between the radiator and room [4]. In a real DH system, the supply water temperature and the water flow rate for a radiator system are often used as the manipulated variables to achieve the desired heating rate. As a result, a nonlinear radiator model involving the supply water temperature and the water flow rate as the manipulated variables is needed to support the

simulation of the real control strategy, which results in a nonlinear MPC. Nonlinear MPCs are much more challenging in terms of stability and robustness issues. Regarding the supply side, the literature review shows that MPC is commonly used to optimize the operation of a single heat production plant, like a CHP plant, in a DH system. The research on the DH system with multiple heat sources, especially on the DH system integrated with renewables and TES, is hard to find. The challenge is that the DH systems with multiple heat sources are much more complex than the DH systems with a single heat source, which makes the already complex modelling and control design method of the MPC schemes even more complicated. Moreover, most of the research on the MPC application in DH systems considers a perfect future disturbance prediction. However, any prediction has some uncertainties that may impair the MPC performance. Since the MPC controller may receive inaccurate information and lead to incorrect control actions that may cause thermal discomfort or energy waste [18]. Finally, the MPC performance may vary depending on the test cases and climate conditions [19].

Therefore, this thesis aimed to contribute to the implementation of MPC in DH systems as well, from both the demand side and the supply side. The investigated DH system was a heat prosumer with DC waste heat and TES, which is affected by the Nordic climate conditions. Regarding the demand side, a nonlinear MPC scheme involving a hydronic heat emitter model was designed for a typical SH system connected to the investigated heat prosumer. Weather forecast uncertainty was investigated as well on the demand side. Regarding the supply side, an MPC scheme was designed to optimize the operation and management of the multiple heat sources and TES in the investigated heat prosumer.

3 METHODOLOGY

This chapter presents the methodology used in the thesis. Section 3.1 introduces the modelling language and the simulation and optimization platform. Afterwards, the MPC optimization framework used in this doctoral work is elaborated. Section 3.2 formulates the economic boundary used in the MPC scheme. Section 3.3 presents the MPC application on the demand side of a DH system. Based on the methods and results of Section 3.3, Section 3.4 introduces an error model to address the weather forecast uncertainty in the MPC scheme. Finally, Section 3.5 presents the MPC application on the supply side of a DH system that is a DC waste heat-based heat prosumer.

3.1 Modelling language and optimization framework

This doctoral work was a simulation-based study. Modelica language was chosen as the modelling language and JModelica.org was used as the simulation and optimization platform. Modelica language is an object-oriented, declarative, multi-domain modelling language for component-oriented modelling of complex systems, such as systems containing hydraulic, thermal, control, or process-oriented subcomponents. It supports the acausal connection of components governed by mathematical equations to facilitate modelling from first principles and provides object-oriented constructs that facilitate the reuse of subcomponent models [36]. JModelica.org is a platform for modelling, simulation and optimization of complex dynamic systems that are based on the Modelica modelling language. JModelica.org can formulate and solve dynamic optimization problems, including optimal control, trajectory optimization, parameter optimization and model calibration. The platform promotes open interfaces for integration with numerical packages, such as the nonlinear programming (NLP) solver, Interior Point OPTimizer (IPOPT), and the symbolic framework for automatic differentiation, CasADi. Moreover, JModelica.org supports user interaction by integrating a Python package. Python provides access to all parts of the platform, including model compilation and loading, simulation and optimization [37]. Based on the optimization platform JModelica.org, Figure 3-1 presents the main steps of the MPC optimization framework in this doctoral work.

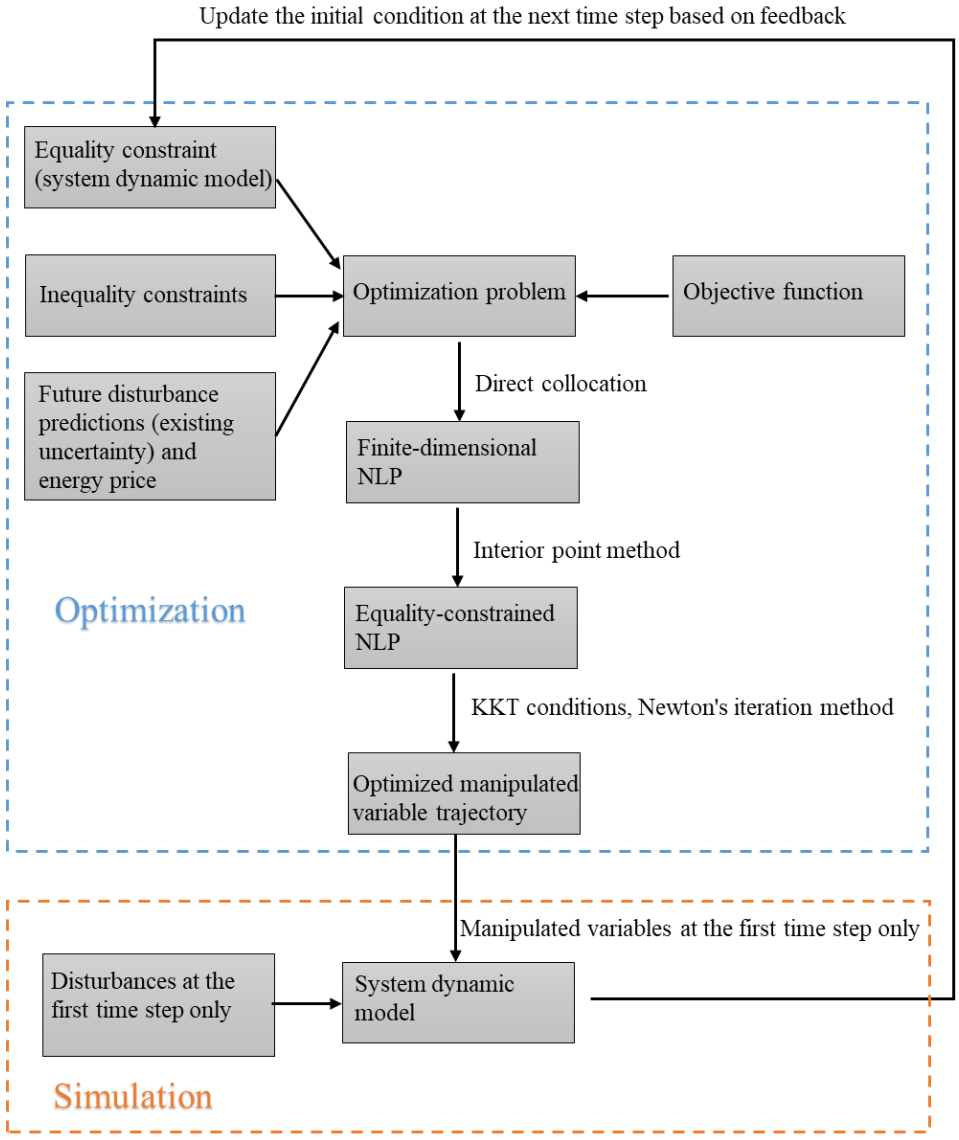

Figure 3-1. Main steps of the MPC optimization framework based on the optimization platform JModelica

The optimization algorithm applied in the optimization process is illustrated in the upper part of Figure 3-1. The optimization problem in the optimization process was an infinite-dimensional problem, which is challenging for computers to handle. In this doctoral work, a direct collocation method was used to transcribe the original infinite-dimensional problem into

a finite-dimensional NLP problem, which can be solved using NLP solvers. However, the discretised finite-dimensional NLP problem had inequality constraints, which led the Karush-Kuhn-Tucker (KKT) conditions of the NLP cannot be solved using Newton's iteration method. To tackle this problem, an interior-point method was used to approximate the discretised NLP problem by an equality-constrained NLP problem. Finally, a local optimized manipulated variable trajectory was found by solving the KKT conditions of the equality-constrained NLP based on Newton's iteration method. A more comprehensive description of the optimization algorithm is presented in **Paper 2**.

3.2 Economic boundary formulation

The economic boundary was formulated based on the system energy bill, and the formulated economic boundary was incorporated into the objective functions of the MPC schemes to improve system economic performance. The system energy bill comes from two parts: 1) heating bill paid for the DH use and 2) electricity bill paid for the electricity use. Therefore, this section illustrates the economic boundary by considering the pricing mechanism in Nordic countries for the heating price model and electricity price model simultaneously.

3.2.1 Heating price model

A generalized heating price model was proposed and used in this doctoral work. This generalized heating price model only considered the energy demand component (EDC) and the load demand component (LDC), because the EDC and the LDC are the most commonly used components in the existing heating price models in Nordic countries. For example, one survey on heating pricing models in Sweden shows that the EDC and LDC together account for around 96% of the total heating cost [38]. The EDC is used to cover the DH companies' fuel costs, and it is charged based on the total heat use of heat users. The LDC is typically used to compensate DH companies' costs of maintaining a particular level of capacity for peak load, as well as new facility investment costs, depreciation, and other expenses, and it is charged based on the peak load of the heat users. This generalized heating price model is discussed in detail and presented in **Paper 4**, and it is described by Equations (1), (2), and (3).

$$C_{hea} = C_{edc} + C_{ldc} \tag{1}$$

$$C_{edc} = \int_{t_0}^{t_f} EP(t) \cdot \dot{Q}(t) \cdot dt \quad (2)$$

$$C_{ldc} = LP \cdot \dot{Q}_p \quad (3)$$

where C_{hea} is the total heating cost. C_{edc} is the EDC and calculated by Equations (2). C_{ldc} is the LDC and calculated by Equation (3). $EP(t)$ and $\dot{Q}(t)$ are the EDC heating price and the heat rate supplied to the heat user at time *t*, respectively. LP and $\dot{Q}_p$ are the LDC heating price and the peak heat rate. The units of $EP(t)$ and LP are NOK[1]/kWh and NOK/kW, respectively.

3.2.2 Electricity price model

A generalized electricity price model was proposed and used in this doctoral work. This generalized electricity price model was based on the investigation of electricity contracts in Norway. In Norway, the end-users have to pay for two parts when using electricity: 1) power price to a power supplier for purchasing electricity and 2) grid rent to the local grid distribution company for transporting the power [39, 40]. Regarding the power price paid to a power supplier, it is determined by the different contracts provided by the power supplier. According to Statistics Norway, the spot-price contract is the most common and widely used contract type in Norway [41]. Therefore, the spot-price contract was used regarding the power price paid to a power supplier. In a spot-price contract, the power price follows the market price determined by Nord Pool [42]. A mark-up must also be paid by the customer [43]. The power price for the spot-price contract is calculated by Equations (4), (5) and (6).

$$C_{ele\_pow} = C_{spo} + C_{sur} + C_{mfi} \quad (4)$$

$$C_{spo} = \int_{t_0}^{t_f} PP_{spo}(t) \cdot \dot{E}(t) \cdot dt \quad (5)$$

$$C_{sur} = \int_{t_0}^{t_f} PP_{sur} \cdot \dot{E}(t) \cdot dt \quad (6)$$

where C_{ele_pow} is the power price paid to a power supplier. C_{spo} is the spot price-related fee and calculated by Equation (5). C_{sur} is the surcharge-related fee and calculated by Equation (6).

1 The currency rate between NOK and EUR can be found from https://www.xe.com/, in this study 1 EUR=10.0 NOK.

C_{mfi} is the monthly fixed fee. $PP_{spo}(t)$ is the spot price at time t and obtained from Nord Pool [42]. PP_{sur} is the surcharge including electricity certificate, and $\dot{E}(t)$ is the electricity use at time t. Both the units of $PP_{spo}(t)$ and PP_{sur} are NOK/kWh.

Regarding the grid rent paid to the grid distribution company, it is decided by the local grid distribution company. For a big business end-user, the grid rent consists of an energy link fee, a power link fee and an annual fixed link fee [44]. The grid rent price is calculated by Equations (7), (8) and (9).

$$C_{ele\_gri} = C_{ene} + C_{pow} + C_{afi} \tag{7}$$

$$C_{ene} = \int_{t_0}^{t_f} GP_{ene} \cdot \dot{E}(t) \cdot dt \tag{8}$$

$$C_{pow} = GP_{pow} \cdot \dot{E}_p \tag{9}$$

where C_{ele_gri} is the grid rent paid to the local grid distribution company. C_{ene} is the energy link fee and calculated by Equation (8). C_{pow} is the power link fee and calculated by Equation (9). C_{afi} is the annual fixed fee. GP_{ene} is the energy link fee per energy unit, and $\dot{E}(t)$ is the electricity use at time t. GP_{pow} is the power extraction price per power unit, and $\dot{E}_p$ is the highest hourly power output. The units of GP_{ene} and GP_{pow} are NOK/kWh and NOK/kW, respectively.

Finally, a generalized electricity price model was proposed based on the above explanation. A more comprehensive description of this generalized electricity price model is presented in **Paper 3**, and it is calculated as Equation (10).

$$C_{ele} = C_{ele\_pow} + C_{ele\_gri} \tag{10}$$

where C_{ele} is the total electricity cost, C_{ele_pow} is the power price paid to a power supplier as shown in Equation (4), and C_{ele_gri} is the grid rent paid to the local grid distribution company as shown in Equation (7).

Based on the above explanation, the first research question of this thesis is answered:

Question 1: **What is the economic boundary when using MPC to improve the economic performance of a district heating system?**

Answer: The generalized heating price model and the generalized electricity price model formulate the basis of the economic boundary for the MPC schemes. The generalized heating price model consists of the LDC and the EDC, and the generalized electricity price model consists of the power price and the grid rent.

3.3 MPC application in a building space heating system

This section briefly introduces the method of MPC application on the demand side of DH systems. It addresses the second research question - **Question 2**: What is the system energy and economic performance when using MPC on the demand side of the DH systems? A more comprehensive description of the methods can be found in **Paper 1**.

Firstly, an SH system dynamic model was developed by Modelica language. Afterwards, the developed model together with the economic boundary, future disturbances and system constraints formulated the MPC optimization problem. Finally, the formulated MPC optimization problem was solved on the JModelica.org optimization platform as described in Figure 3-1. The following content presents the above steps and the research scenarios.

3.3.1 System dynamic model

Among commonly used models, the resistance-capacitance (RC) model has been demonstrated to be reliable and precise in predicting the thermal behaviour of buildings [45]. Therefore, an RC model was developed in this work to capture the key characteristics of the building, and it was built by using the Modelica language. Figure 3-2 illustrates the components of the developed RC model and the heat fluxes exchanged among them. The model mainly consists of four components including the internal thermal mass, indoor air, building envelopes, and outdoor environment. Due to the low solar radiation in the analysed location during the study period, solar radiation was not taken into account in this work [46]. In addition, this work aimed to incorporate the building thermal mass as TES into the MPC controller to further improve the energy and economic performance of the system. Therefore, as presented in Figure 3-2, a third-order RC model was developed with special attention to the thermal mass of building envelopes and the interior thermal mass, besides considering the thermal mass of indoor air, because their corresponding thermal inertia is necessary for the short-term TES in the intended MPC [11].

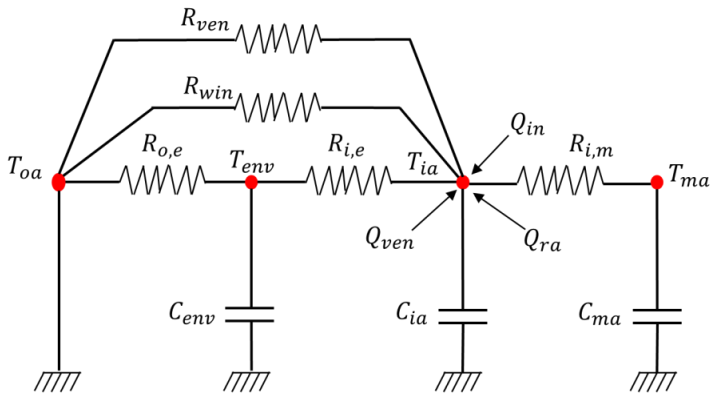

Figure 3-2. Schematic of building resistance-capacitance model structure

In this work, the parameters, including heat resistance and heat capacitance, were determined by an estimation method according to the available information of the investigated building and the recommended values in the European standard ISO 52016-1 [47]. Detailed calculations for the energy balances among each component given in Figure 3-2 are shown in Equations (11), (12) and (13), as the following:

$$C_{env} \cdot \frac{dT_{env}}{dt} = \frac{T_{ia} - T_{env}}{R_{i,e}} + \frac{T_{oa} - T_{env}}{R_{o,e}} \tag{11}$$

$$C_{ia} \cdot \frac{dT_{ia}}{dt} = \frac{T_{ma} - T_{ia}}{R_{i,m}} + \frac{T_{env} - T_{ia}}{R_{i,e}} + \frac{T_{oa} - T_{ia}}{R_{win}} + \frac{T_{oa} - T_{ia}}{R_{ven}} + \dot{Q}_{ra} + \dot{Q}_{ven} + \dot{Q}_{in} \tag{12}$$

$$C_{ma} \cdot \frac{dT_{ma}}{dt} = \frac{T_{ia} - T_{ma}}{R_{i,m}} \tag{13}$$

where R and C represent the heat resistance and capacitance, respectively, whose values were obtained by the estimation method. T denotes the temperature. Subscripts ia, oa, env, ma, win, and ven represent indoor air, outdoor air, building envelopes, internal thermal mass, windows, and ventilation, respectively. In addition, $R_{i,e}$ represents the heat resistance between the indoor air and the building envelopes. $R_{o,e}$ represents the heat resistance between the outdoor air and the building envelopes. $R_{i,m}$ represents the heat resistance between the indoor air and the interior thermal mass. $\dot{Q}_{in}$ is the internal heat gains, $\dot{Q}_{ven}$ is the heat flow rate from

the mechanical ventilation system, and $\dot{Q}_{ra}$ is the heat flow rate from the radiator system. Specifically, $\dot{Q}_{in}$ was obtained by historical measurement data and the Norwegian standard SN-NSPEK 3031 [48]. $\dot{Q}_{ven}$ is described as Equation (14) according to Norwegian standard SN-NSPEK 3031 [48]. $\dot{Q}_{ra}$ is determined by Equations (15), (16), (17) and (18). In this work, to get a more accurate dynamical description of the radiator, a discrete-element radiator model with N lumps was utilized and coupled to the RC model. This discrete-element radiator model was based on the European Standard EN 442-2 [49], which refers to it as the characteristic equation of the radiator. Meanwhile, previous studies have confirmed this model [50-52]. $\dot{Q}_{sh}$ is the total heat flow rate of the SH system as shown in Equation (19).

$$\dot{Q}_{ven} = 0.33 \cdot \dot{V}_{air} \cdot (1 - \eta_T) \cdot (T_{ia}^{ref} - T_{oa}) \tag{14}$$

$$\dot{Q}_{ra} = \sum_{n=1}^{N} \dot{Q}_n \tag{15}$$

$$\dot{Q}_n = K_n \cdot F_n \cdot (T_n - T_{ia}) \tag{16}$$

$$K_n = (T_n - T_{ia})^a \tag{17}$$

$$c_{p\_ra} \cdot \frac{dT_n}{dt} = c_{p\_w} \cdot \dot{m}_{ra} \cdot (T_{n-1} - T_n) - \dot{Q}_n \tag{18}$$

$$\dot{Q}_{sh} = \dot{Q}_{ven} + \dot{Q}_{ra} \tag{19}$$

where $\dot{V}_{air}$ describes the mechanical ventilation volume flow rate, which was determined by the measured data and the Norwegian standard SN-NSPEK 3031 [48]. T_{ia}^{ref} is the indoor temperature's reference value. η_T denotes the temperature efficiency of heat recovery in the mechanical ventilation system. For each radiator section n, $\dot{Q}_n$ represents the heat flow rate, T_n describes the average water temperature, F_n is the surface area and K_n is the equivalent heat transfer coefficient. a is a characteristic coefficient of the radiator, which can be obtained from the radiator manufacturer. In addition, c_{p_ra} is the radiator material's heat capacity for each section n. c_{p_w} and $\dot{m}_{ra}$ are the specific water heat capacity and the water mass flow rate, respectively. The radiator model was nonlinear in this work due to the definition of K_n, and hence made the dynamic system model in this work nonlinear.

3.3.2 Optimization formulation

The proposed MPC control strategy was used to improve the energy and economic performance of the SH system with satisfying indoor temperatures. Therefore, the generalized heating price model was utilized in the objective function. In addition, the achieved indoor temperature was used as an indicator to estimate the thermal environment. Finally, a multi-objective optimization problem was formulated with two conflicting optimization goals as presented in Equations (20), (21), (22), (23) and (24).

Minimize:

$$\int_0^H EP(t) \cdot \dot{Q}_{sh}(t) \cdot dt + LP \cdot \dot{Q}_p + W \cdot \int_0^H (T_{ia}(t) - T_{ia}^{ref}(t))^2 \cdot dt \qquad (20)$$

subject to:

$$x(0) = A \qquad (21)$$

$$\dot{x}(t) - F\big(x(t), u(t)\big) = 0 \qquad (22)$$

$$\dot{Q}(t) \leq \dot{Q}_p \qquad (23)$$

$$u_{min} \leq u(t) \leq u_{max} \qquad (24)$$

where H denotes the prediction horizon and was 12 hours in this work. $EP(t)$ and LP are the dynamic EDC price at time t, and the LDC price, respectively. $\dot{Q}_{sh}(t)$ is the heat rate at time t and $\dot{Q}_p$ denotes the peak heat rate which is a free parameter that needed to be optimized. The first two terms in Equation (20) are the heating cost, including the EDC and the LDC. In addition, the third term in Equation (20) is the achieved indoor temperature target, which is expressed as a quadratic form to avoid high violations of the desired indoor temperature. A weighting factor W was used in the achieved indoor temperature term to represent the "price" that the occupants are willing to pay for certain indoor temperatures, just like the energy prices in the heating cost term of the objective function [12]. In this work, the value of W was decided by the following criterion: when the deviation between the indoor temperature and the reference value was 0.5 K, the heating cost term and the achieved indoor temperature term contributed equally to the objective function. $T_{ia}(t)$ and $T_{ia}^{ref}(t)$ are the achieved indoor temperature and

the reference value at time t. The initial states of the dynamic system are described as Equation (21), and the values of these initial states are represented by the vector A. Equation (22) is the equality constraint of the formulated optimization problem, which is the developed dynamic system model. Equations (23) and (24) are the inequality constraints of the formulated optimization problem, of which Equation (24) describes the bounds of manipulated variables. u_{min} and u_{max} are the lower and upper bounds of manipulated variables. In this work, the manipulated variables $u(t)$ was defined as $u(t) = [T_{sh}(t)\ \dot{m}_{sh}(t)]^T$, of which $T_{sh}(t)$ and $\dot{m}_{sh}(t)$ are the supply water temperature and the water mass flow rate of SH system.

3.3.3 Simulation scenarios

In this section, the occupancy schedule was based on historical measurement data in the case building and the Norwegian standard SN-NSPEK 3031 [32], and it was assumed to be perfectly predicted. In addition, the measured outdoor temperature from the case building was used instead of the weather forecast information to explore the theoretical potential of the MPC.

Two research scenarios were proposed to evaluate the proposed MPC method for the SH system in a building, as shown in Figure 3-3. The reference scenario was based on an RBC strategy, which was the common control strategy of the SH system in a building. As presented in Figure 3-3 a), the supply water temperature was controlled by a WCC according to the current outdoor temperature. In addition, a proportional (P) controller was used to adjust the SH system's water flow rate according to the deviation between the indoor temperature and its reference value. In this scenario, the optimal control of the SH system was difficult to realize, as the future disturbances (weather and occupancy), energy price, and the system dynamics were not able to be incorporated into the controllers. The MPC scenario proposed in this work, however, was able to realize the optimal control of the SH system. As shown in Figure 3-3 b), during the optimization process, the perfect future disturbance predictions (weather and occupancy) together with a candidate manipulated variable trajectory (the water flow rate and the supply water temperature) were used as simulation inputs for the dynamic system model. An iterative simulation was conducted over a certain prediction horizon. The optimizer assessed the objective function for each simulation run and updated the candidate manipulated variable trajectory until an optimized trajectory was found. Afterwards, only the optimized manipulated variables at the first time step were used to control the SH system of the building. In the next

time step, the MPC updated the initial states of the dynamic system model based on the feedback from the building and restart the optimization [15].

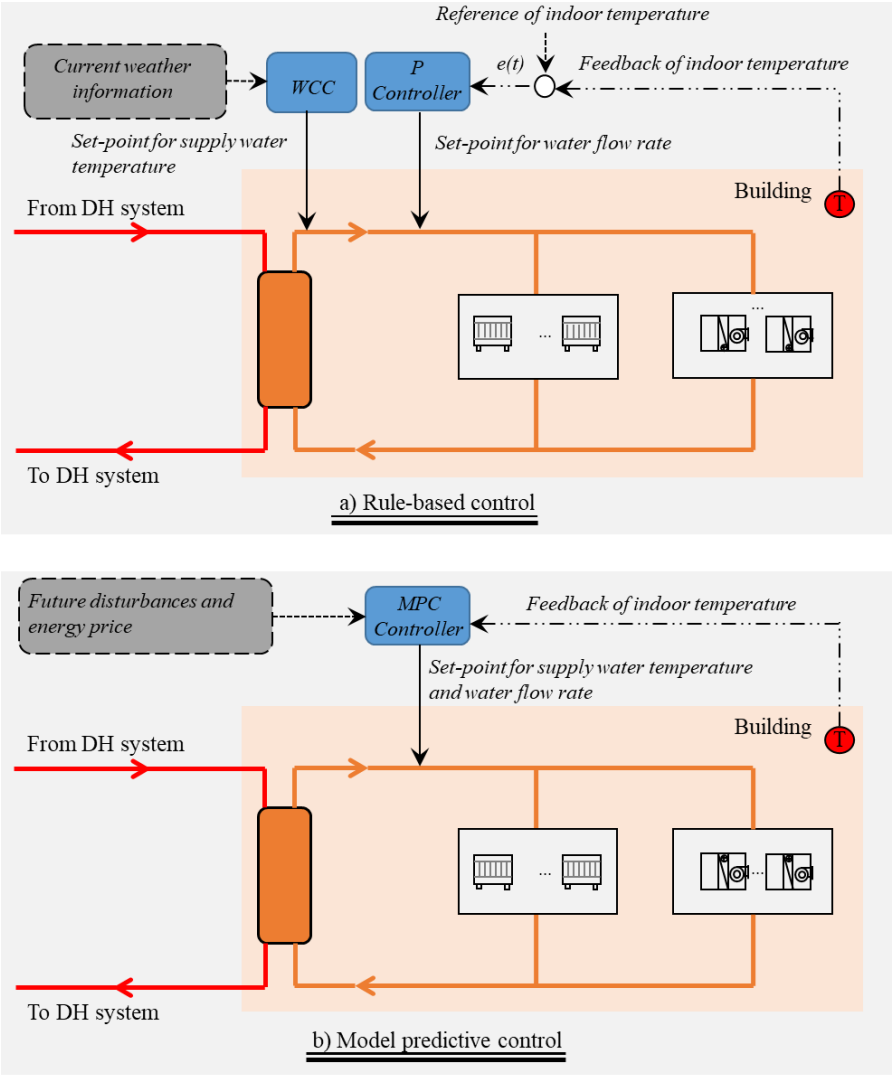

Figure 3-3. Research scenarios utilizing rule-based control and model predictive control for the space heating system in a building

3.4 Weather forecast uncertainty in MPC

This section followed the research methods of Section 3.3, by introducing an error model. This error model was used to handle the weather forecast uncertainty in the MPC scheme, and address the third research question- **Question 3**: What is the impact of weather forecast uncertainty on MPC performance, and how to handle it? A comprehensive description of the work is presented in **Paper 2**.

3.4.1 An error model for weather forecast

One challenge with the direct use of the weather forecast data in the MPC is the uncertainty of forecasted data resulting from the uncertainty of the numerical weather prediction model (NWPM). Inherent uncertainty lies in the NWPM due to the stochastic nature of atmospheric processes, the imperfect knowledge of the weather model's initial conditions, as well as modelling errors [53]. Therefore, the exact actual weather data may not be reflected by the forecasted data well. The forecast weather data in this work considered only the outdoor temperature due to the low solar radiation in the studied area during the studied period [46]. The actual outdoor temperature acting on the building can be decomposed as in Equation (25):

$$T_k = \bar{T}_k + e_k \tag{25}$$

where T_k and $\bar{T}_k$ denote the actual and the NWPM forecasted outdoor temperature at the time step *k*, and e_k is the prediction error of NWPM at the time step *k*.

To improve the prediction of future disturbance acting on the building, the prediction error of the NWPM, e_k, may be estimated by an error model. The prediction error of the NWPM means the deviation between the actual outdoor temperature and the corresponding NWPM forecasted data. In practice, the current prediction error is known, because of the availability of the measured data. According to [54, 55], this work assumed that the unknown future prediction error of the NWPM was correlated to the known current prediction error, however, the correlation decreased along with the increasing time distance. For example, the NWPM prediction error in the near future was approximated by the current prediction error, while the NWPM prediction error in the distant future had a limited relationship with the current prediction error and hence the forecasted data from the NWPM was the best estimation for the outdoor temperature. The error model is illustrated as Equation (26).

$$\tilde{e}_{k+t} = r(t) \cdot e_k, \quad t = 1,2,3,\dots,12 \tag{26}$$

where $\tilde{e}_{k+t}$ is the estimated prediction error of the NWPM in the future, e_k is the known prediction error of the NWPM at the current time step k. Parameter $0 \leq r(t) \leq 1$ which is a weighting function, describes the decreasing predictive effect of the current prediction error on the future NWPM prediction error along with the increasing time distance. In this work, the value of parameter $r(t)$ was given by Equation (27) based on [54]. Therefore, the future outdoor temperature was estimated as Equation (28).

$$r(t) = 1 - \frac{e^{t-6}}{1 + e^{t-6}}, \quad t = 1,2,3,\dots,12 \tag{27}$$

$$\tilde{T}_{k+t} = \bar{T}_{k+t} + \tilde{e}_{k+t}, \quad t = 1,2,3,\dots,12 \tag{28}$$

where $\tilde{T}_{k+t}$ is the estimated outdoor temperature in the future, $\bar{T}_{k+t}$ is the forecasted outdoor temperature from NWPM, and $\tilde{e}_{k+t}$ is the estimated prediction error of NWPM given by the error model as illustrated by Equation (26).

3.4.2 Simulation scenarios

Two more MPC research scenarios were proposed in this section except the scenarios introduced in Section 3.3.3. Therefore, four research scenarios were used in this section, including a reference scenario, two benchmark MPC scenarios, and one improved MPC scenario integrated with the error model. The reference scenario represented the RBC strategy for the SH system without using any MPC controller, as introduced in Section 3.3.3. The other scenarios represented the MPC strategies with different weather information provided for their MPC controllers. The ideal benchmark MPC scenario assumed perfect weather forecasts, i.e. providing the actual weather data for its MPC controller, as presented in Section 3.3.3. The standard benchmark MPC scenario did not address the weather forecast error, i.e. directly providing the forecasted weather data for its MPC controller. Finally, the improved MPC scenario handles the weather forecast error by integrating with the error model, i.e. providing the estimated weather data from the error model for its MPC controller.

The four research scenarios were presented in Figure 3-4. The reference scenario, RBC in Figure 3-4 a), presented the RBC strategy for the SH system and has been described in Section 3.3.3.

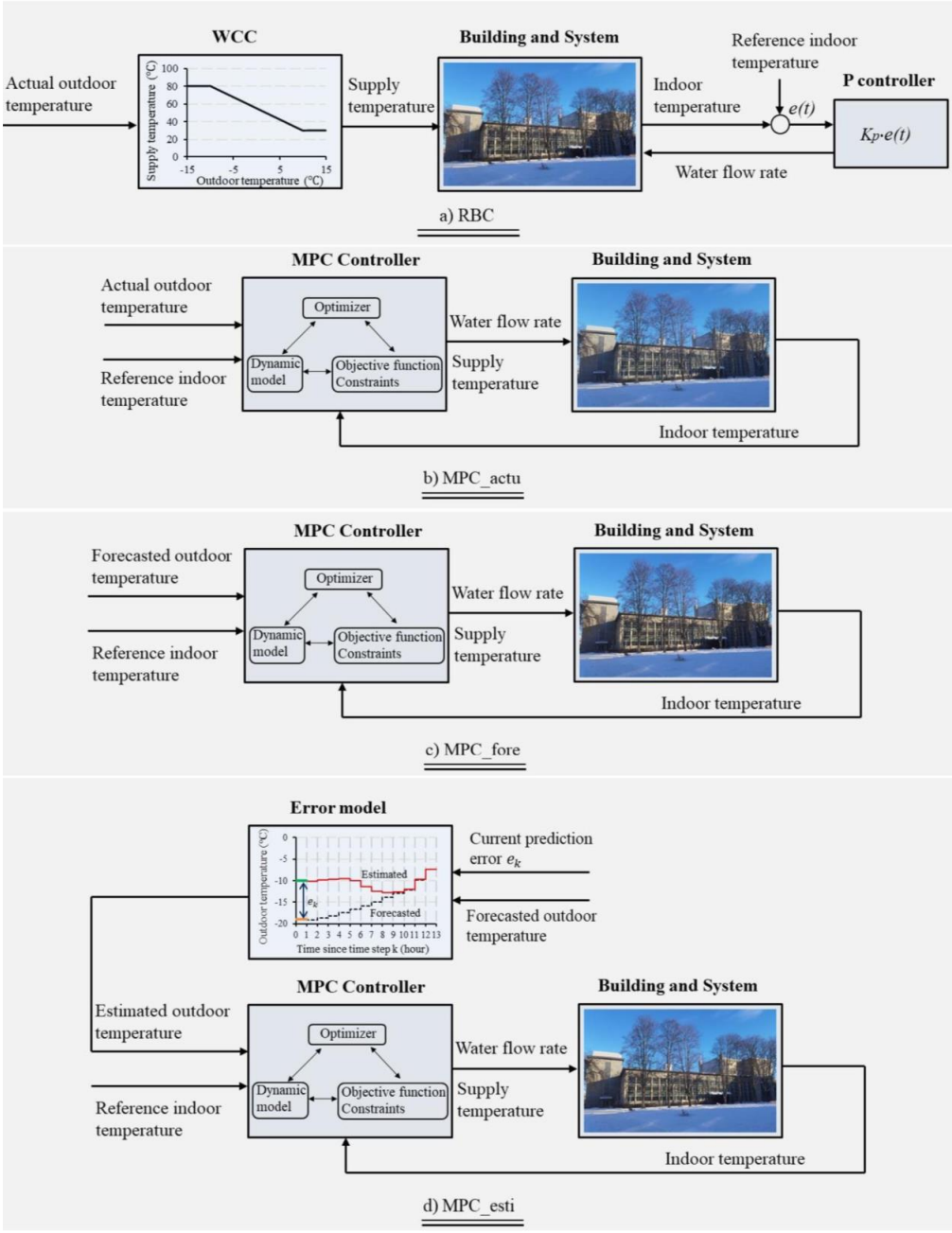

Figure 3-4. Schematics of the four scenarios

The ideal MPC scenario, MPC_actu in Figure 3-4 b), was an ideal MPC control strategy, which was defined as optimal control with the perfect weather prediction as described in Section 3.3.3,

i.e. assuming no deviation between the forecasted weather and the actual weather. As shown in Figure 3-4 b), the actual outdoor temperature was used by the MPC controller to present the perfect weather prediction. This is not an implementable controller but a concept, which was used to investigate the theoretical potential of MPC.

The standard MPC scenario, MPC_fore in Figure 3-4 c), was a standard MPC control strategy in practice. It used the imperfect weather forecast of the NWPM but determined its control actions under the assumption that the predictions were correct. As presented in Figure 3-4 c), the forecasted outdoor temperature from the NWPM was used by the MPC controller. This scenario demonstrated the practical potential of MPC.

The improved MPC scenario, MPC_esti in Figure 3-4 d), was proposed considering the uncertainty of weather predictions in the MPC control strategy. As shown in Figure 3-4 d), the error model described in Section 3.4.1 was integrated to improve the quality of forecasted outdoor temperature from the NWPM, and then the high-quality estimated outdoor temperature was used by the MPC controller. This scenario made the handling of the weather forecast uncertainty straightforward, meanwhile maintaining the computationally tractable MPC.

3.5 MPC application in a heat prosumer with data centre waste heat recovery and thermal energy storage

This section briefly introduces the method of MPC application on the supply side of DH systems with distributed sources. It addressed the fourth research question - **Question 4**: What is the system energy and economic performance when using MPC on the supply side of the DH systems with distributed sources? A more comprehensive description of the methods can be found in **Paper 3**.

Firstly, a typical DC waste heat-based heat prosumer with short-term TES was proposed and its dynamic model was developed by Modelica language. Afterwards, the developed model together with the economic boundary, future heating demand and system constraints formulated the MPC optimization problem. Finally, the formulated MPC optimization problem was solved on the JModelica.org optimization platform as described in Figure 3-1. The following content presents the above steps and the research scenarios.

3.5.1 System dynamic model

Figure 3-5 illustrates a typical DC waste heat-based heat prosumer with short-term TES. A water tank thermal energy storage (WTTES) was chosen as the short-term TES in this work because it is easily implemented and economically reasonable for DH systems [21].

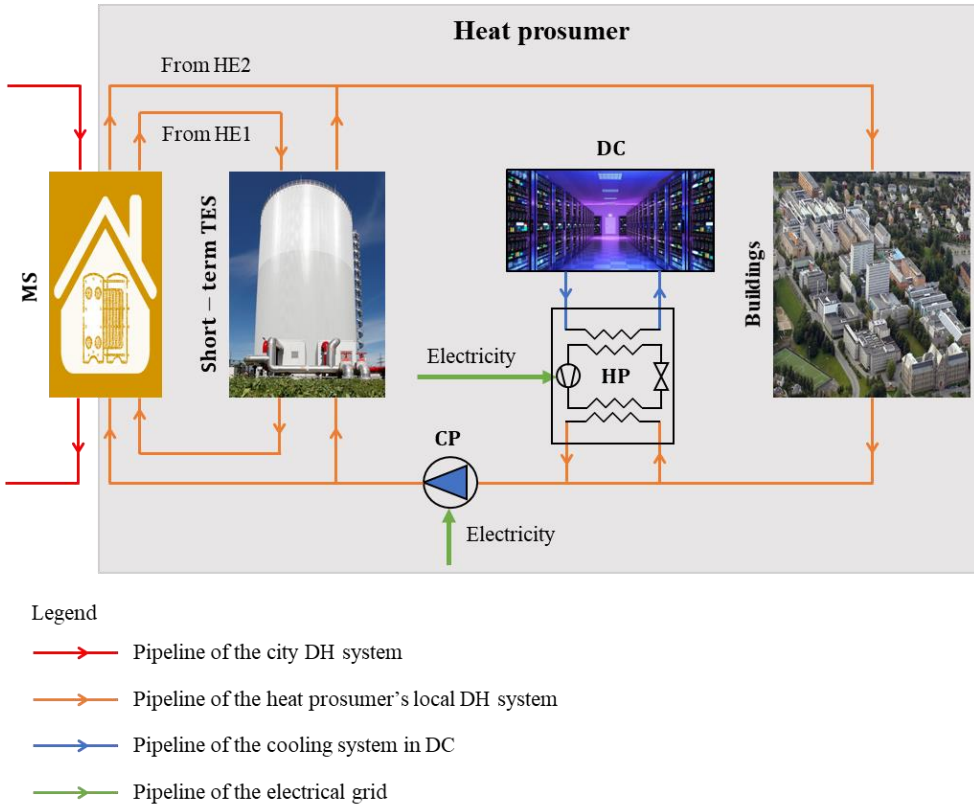

Figure 3-5. Typical data centre waste heat-based heat prosumer with short-term thermal energy storage

A main substation (MS) is usually used to connect the city DH network with the distribution network of the heat prosumer and to physically separate the flows so that the local DH system of the heat prosumer can be managed independently from its city DH network. There are two heat exchangers (HEs) in the MS, HE1 is used to charge the WTTES and HE2 is used to supply heat from the city DH network to the heat prosumer's local DH network. A heat pump (HP) was used to cool down the DC and harvest the DC waste heat for the heat prosumer's local DH network, as shown in Figure 3-5. There are usually two common connection ways between the

DC and the DH systems: the return to supply (R2S) and the return to return (R2R) connection. The R2S connection implies that water is extracted from the return pipe, heated to a proper temperature, and then fed into the supply pipe of the DH system. The R2R connection implies that water is extracted from the return pipe and heated to any temperature, because it already has a higher temperature than the return water of the DH system, and fed into the return pipe [56, 57]. In this work, the R2R connection was chosen, because it is preferable for low-temperature heat sources and no extra heat sources are required to raise the temperature of water delivered into the DH system [20, 56]. Finally, a cluster of buildings is the heat user, and a circulator pump (CP) is used to circulate the hot water for the heat prosumer's local DH network.

The system dynamic model was based on the energy and mass flow exchanging connection between the individual component models. The individual components consisted of the MS, DC, buildings, WTTES, CP and pipeline, as shown in Figure 3-5. The energy and mass flow exchanges between various components, as well as the modelling method for each component of the MS, buildings, WTTES and pipelines, are elaborated in **Paper 4**. The modelling methods of the DC's HP and CP are discussed in this section.

Based on research [58], the operational conditions are the key factors that determine an HP's electricity use, aside from the HP's inherent performance characteristics. The operational conditions include the inlet and outlet water temperature as well as the water mass flow rate both at the evaporator and condenser sides of an HP. Moreover, extensive measured data on these operational conditions were available in this study. Therefore, an HP model including these operational conditions was developed, as shown in Equation (29).

$$\hat{E}_{HP} = a \cdot T_{in\_eva} + b \cdot T_{out\_eva} + c \cdot T_{in\_con} + d \cdot T_{out\_con} + e \cdot \dot{m}_{eva} + f \cdot \dot{m}_{con} \quad (29)$$

where $\hat{E}_{HP}$ is the simulated HP compressor power. T_{in_eva} and T_{out_eva} are the inlet and outlet water temperatures at the evaporator side. T_{in_con} and T_{out_con} are the inlet and outlet temperatures at the condenser side. $\dot{m}_{eva}$ and $\dot{m}_{con}$ are the water mass flow rate at the evaporator and condenser sides, respectively. a, b, c, d, e, and f are the parameters needed to be identified. In this work, the Evolutionary Engine provided by the Excel Solver was used to identify these parameter values.

To overcome pipeline hydraulic resistance and local pipeline accessory resistance, a CP was employed to circulate warm water for the campus DH network. This work used a variable-speed CP because it can dramatically minimize pumping electricity use [59]. The total pumping power needed to circulate the water in a distribution system can be calculated by Equations (30) and (31).

$$E_{CP} = \frac{\Delta P \cdot \dot{V}}{\eta_{CP}} \tag{30}$$

$$\Delta P = S \cdot \dot{m}^2 \tag{31}$$

where E_{CP} is the CP electricity use. $\dot{V}$ is the water volume flow rate. η_{CP} is the total conversion efficiency of the CP and was 0.7 in this study [60]. ΔP is the total pressure drop of the DH distribution network. $\dot{m}$ is the mass flow rate of water. S is the resistance friction coefficient of the DH distribution network that is related to the characteristics of the pipeline. One assumption was adopted in this study: the water mass flow rate was regulated by the variable-speed CP, and the pipeline valves had no actions. As a result, the resistance friction coefficient S was a constant value that could be inferred from the DH system's design condition.

3.5.2 Optimization formulation

In this work, the MPC scheme employed an economic-related objective function to maximize the heat prosumer's economic performance. The heating and electricity price models described in Section 3.2 were involved in this objective function as shown in Equation (32). However, the monthly fixed fee involved in the power price and the annual fixed fee involved in grid rent were not included, because they are not related to real-time electricity use. In addition, the power link fee involved in the grid rent of electricity price model was not considered as well. This is because only the electricity use for the HP and CP was involved in the optimization problem, the electricity use for other equipment, lighting, etc. was not involved, but the power link fee is charged based on the highest hourly total electricity use of the whole energy system. Therefore, at each time step, the MPC controller solves the following optimization problem:
Minimize:

$$\begin{aligned}\int_0^H EP(t) \cdot \dot{Q}_{MS}(t) \cdot dt + LP \cdot \dot{Q}_{MS\_p} \\ + \int_0^H (PP_{spo}(t) + PP_{sur} + GP_{ene}) \cdot (\dot{E}_{HP}(t) \\ + \dot{E}_{CP}(t)) \cdot dt\end{aligned} \tag{32}$$

subject to:

$$\dot{Q}_{MS}(t) \leq \dot{Q}_{MS\_p} \tag{33}$$

$$F(t, \boldsymbol{z}(t)) = 0 \tag{34}$$

$$F_0(t_0, \boldsymbol{z}(t_0)) = 0 \tag{35}$$

$$z_L \leq \boldsymbol{z}(t) \leq z_U \tag{36}$$

where H is the predictive horizon, which was 12 hours in this work. $\dot{Q}_{MS}(t)$ is the heat flow rate of MS at time t. $\dot{Q}_{MS\_p}$ is the peak heat rate of MS, and it was a parameter to be optimized. $EP(t)$, LP, $PP_{spo}(t)$, PP_{sur} and GP_{ene} have been explained in Section 3.2. Moreover, $\dot{E}_{HP}(t)$ and $\dot{E}_{CP}(t)$ are the electricity use of the HP and CP at time t, respectively. The equality constraints of Equation (34) and Equation (35) are the system dynamics as explained in Section 3.5.1 and the initial condition of the system, respectively. Finally, Equation (36) defines the inequality constraint including the technical operational constraints. $\boldsymbol{z} \in \mathbb{R}^{n_z}$ is the set of time-dependent variables, which includes the manipulated variables $\boldsymbol{u} \in \mathbb{R}^{n_u}$ to be optimized, the differential variables $\boldsymbol{x} \in \mathbb{R}^{n_x}$, and the algebraic variables $\boldsymbol{y} \in \mathbb{R}^{n_y}$. $z_L \in [-\infty, \infty]^{n_z}$ and $z_U \in [-\infty, \infty]^{n_z}$ are the lower and upper limits, respectively.

3.5.3 Simulation scenarios

Two research scenarios were proposed to evaluate the MPC scheme. The reference scenario was based on an RBC strategy, as shown in Figure 3-6. A WCC was used to control the supply water temperature of HE2 based on the outdoor air temperature. The water flow rate of HE2 was adjusted by a proportional-integral (PI) controller based on the feedback of return water temperature. The reference values of return water temperature were obtained by the linear regression based on the measured data of the case system, as explained in **Paper 4**. Another PI controller was used to determine the HP compressor power based on the feedback of the outlet water temperature of the evaporator. The reference value of the outlet water temperature of the evaporator was set as 6.5℃ because most of the measured outlet temperatures of the evaporator fluctuated between 6.0 and 7.0℃ and the average value was 6.5℃ based on the case system. Finally, the charging and discharging processes of the WTTES were decided by a pre-defined schedule elaborated in **Paper 3**.

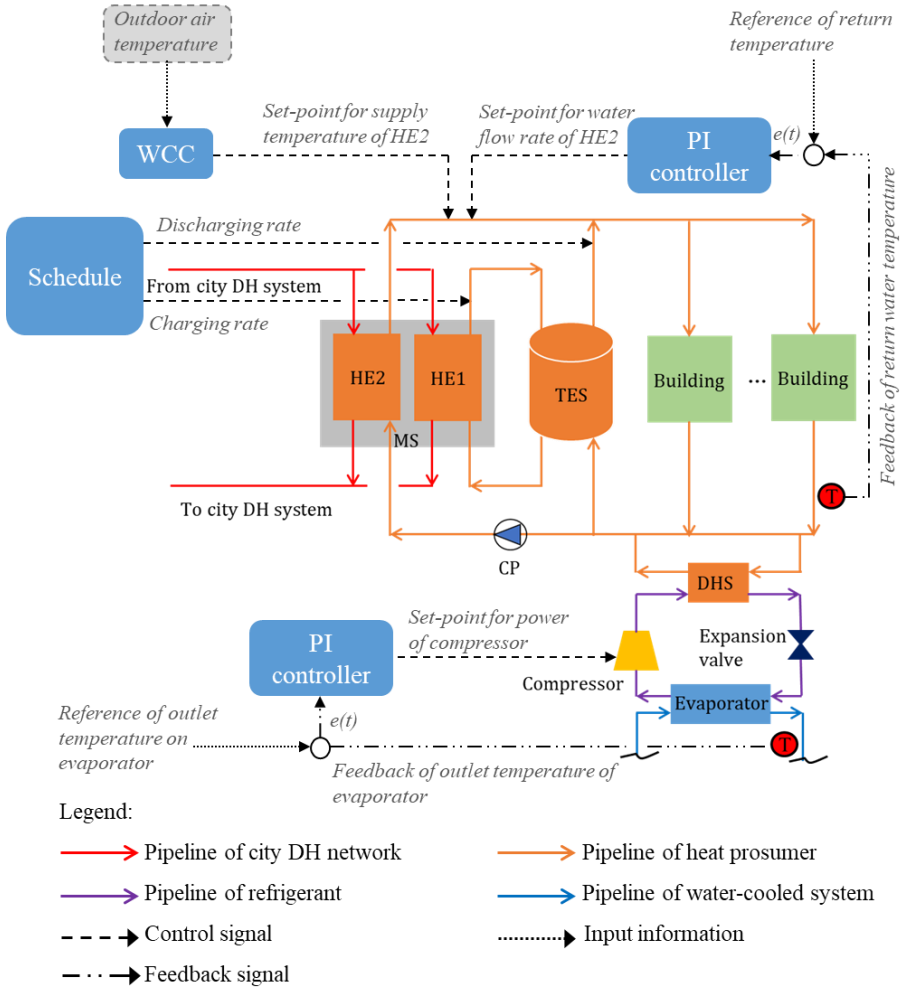

Figure 3-6. The scenario of rule-based control

The MPC scenario is illustrated in Figure 3-7. In this scenario, the building's heating demand and the energy price over the predictive horizon were incorporated into the MPC controller. The controller evaluated the objective function with various manipulated variable trajectories until an optimal trajectory was found. As presented in Figure 3-7, the manipulated variables were the supply water temperature and water mass flow rate of the HEs, the water mass flow rate of the WTTES and the power of the HP compressor. These manipulated variables were constrained to their feasible regions in the real system, which formulates the technique operational constraints of the MPC. The constraint settings for the supply water temperature and water mass flow rate of the HEs, and the water mass flow rate of the WTTES were

elaborated in **Paper 4**. Moreover, the upper bound and lower bound of the HP compressor power were defined by the measured data. Another critical operational constraint was that the DC cooling requirement had to be satisfied. In this work, the DC cooling requirement was guaranteed by maintaining the outlet water temperature of the evaporator in the range of 6.0-7.0℃, because the measured inlet water temperature and mass flow of the evaporator for the case system were almost constant values while most of the measured outlet water temperature of the evaporator fluctuated in the range of 6.0- 7.0℃.

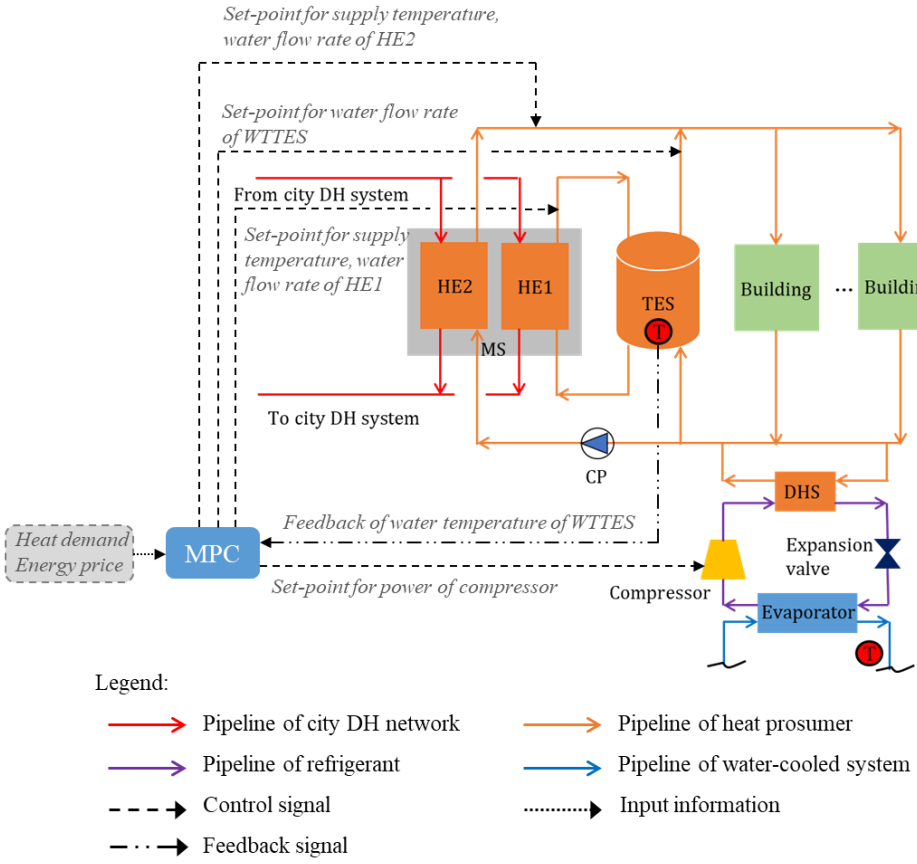

Figure 3-7. The scenario of model predictive control

4 CASE STUDY

This chapter briefly introduces the case studies of the thesis. Firstly, the case study of an SH system in a university building is described. This typical SH system was used for the study on the demand side of the DH system. Afterwards, the campus DH system connected to the described SH system is presented, which is a heat prosumer with DC waste heat. This campus DH system was used for the study on the supply side of the DH systems.

4.1 Space heating system in a university building

A university building that is located in Trondheim, Norway was used as the case study for the SH system, as shown in Figure 4-1 a). The building was built in 1962, and it has six floors with a total floor area of 15 000 m^2. This building is mainly used for education, offices, and laboratory [61].

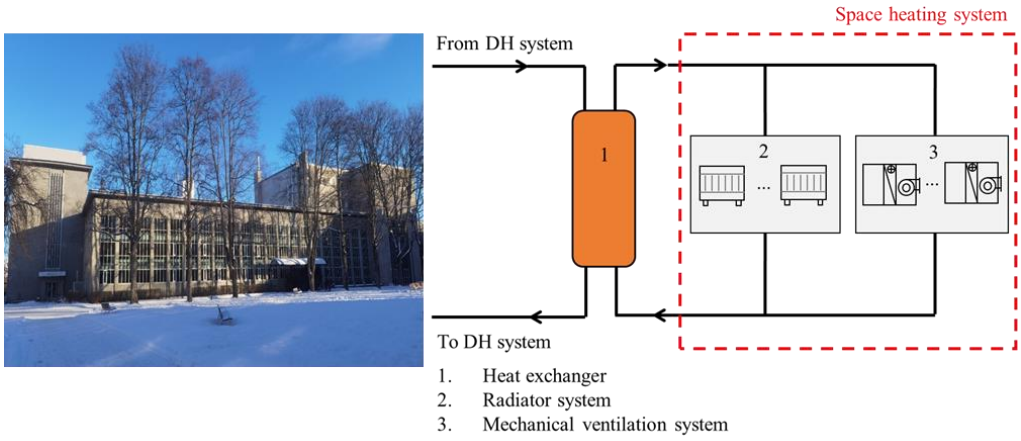

a) The university building b) Space heating system in the building

Figure 4-1. The university building and its space heating system investigated in the case study

The SH system in this building is presented in Figure 4-1 b). A HE in the building heat substation is used to connect the SH system and the campus DH system. The SH system includes a radiator system and a mechanical ventilation system. The radiator system is used to compensate for the heat loss to the environment through building envelopes, as well as heat the entering cold air due to air infiltration. The mechanical ventilation system consists of several

air-handling units (AHUs) and is used to heat the entering cold air due to mechanical ventilation and provide the occupants with heated fresh air.

To improve the energy and economic performance of the SH system, the MPC scheme proposed in Section 3.3 was tested on this university building by simulation. Meanwhile, the MPC scheme integrated with the error model was simulated on this building as well. Table 4-1 summarizes the key information of the case building. Detailed information on the estimation method of heat resistance and capacitance and the local heating prices can be found in **Paper 1** and **Paper 2**.

Table 4-1. The key information of the case building

Category	**Parameter**	**Value**
Areas of building elements (m^2)	Exterior wall	5 504
	Roof	4 315
	Windows, doors, and glass	2 293
	Interior wall	8 256
U-values of building elements (W/(m^2·K))	Exterior wall	0.35
	Roof	0.35
	Windows, doors, and glass	2.04
Specific heat capacities of elements (J/ m^2·K) [1]	Exterior opaque	175 000
	Interior wall	75 000
	Air and furniture	10 000
Ventilation	Air infiltration (h^{-1})	2.70[2]
	Mechanical ventilation (h^{-1})	0-1.50[3]
	Temperature efficiency of heat recovery (%)	62
	Heated air volume (m^3)	73 600
Internal heat gains	Equipment, lighting, person (W/ m^2)	5.5-19.0[3]

[1] Based on the thermal properties of the building, the European standard ISO 52016-1 [47], and the Norwegian standard SN-NSPEK 3031 [48].

[2] Air change rate at 50 Pa, n_{50}.

[3] Based on the measurement data and the Norwegian standard SN-NSPEK 3031 [48].

4.2 DH system at a university campus

The campus DH system connected to the introduced SH system was used as the case study for the heat prosumer, as presented in Figure 4-2. There is an MS to connect the campus DH system with the city DH network via HEs, and hence the campus DH system can be managed

independently. A DC acts as a DHS because the return water of the campus DH network is used to harvest the DC's waste heat by cooling down the high-temperature refrigerant vapour at the HP condenser. The heat users in this campus DH system are buildings whose total building area is about 300 000 m², and more detailed information about the buildings can be found in research [61].

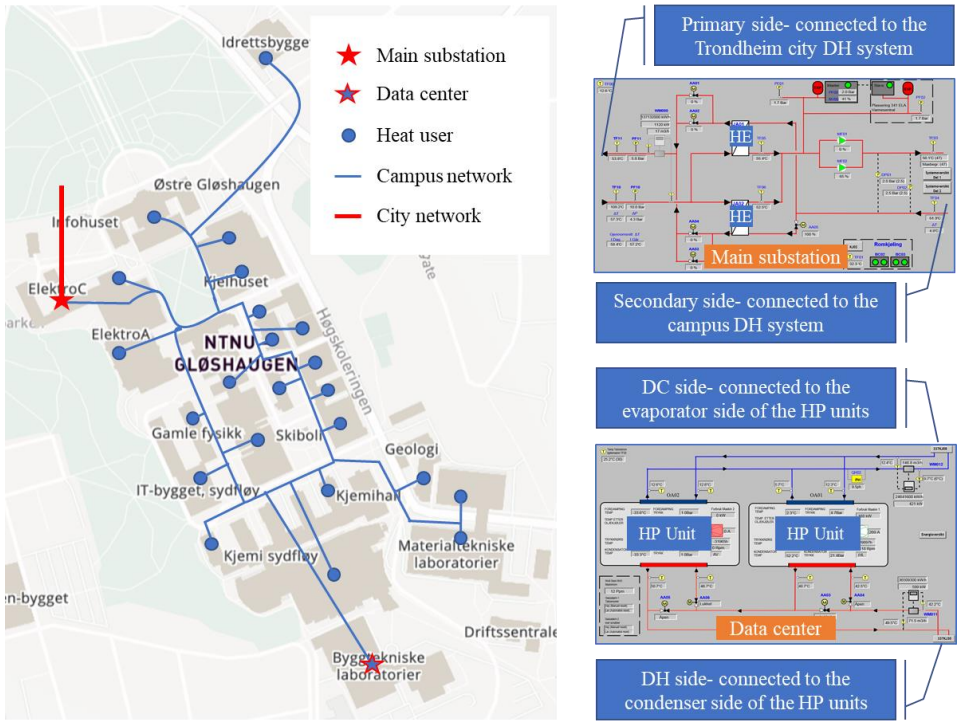

Figure 4-2. Campus district heating system

According to the measurement data from June 2017 to May 2018, as shown in Figure 4-3, the total heating demand of the buildings was 32.8 GWh. The DC provided around 20% of the heat for buildings, while the rest 80% of the heat was supplied from the city DH network via the MS. Therefore, this campus DH system is a DC waste heat-based heat prosumer. Another phenomenon observed in Figure 4-3 is that the buildings' heating demand was not evenly distributed and there were high peak loads from the MS, especially during the heating season. The heating price model adopted by the local DH company takes peak loads into account, and the peak load-related heating cost, LDC, accounted for about 26% of the total heating cost each year. **Paper 7** has proven that introducing a short-term TES, WTTES, for the case system was

able to address the high peak load problem and improve the system's economic performance [21]. Moreover, an in-depth investigation of the optimal storage size of WTTES has been conducted in **Paper 4**. Therefore, considering the trade-off between investment and heating cost-saving, a WTTES with a storage volume of 900 m^3, which was able to supply heat to the campus DH system for up to 12 hours, was introduced in this study.

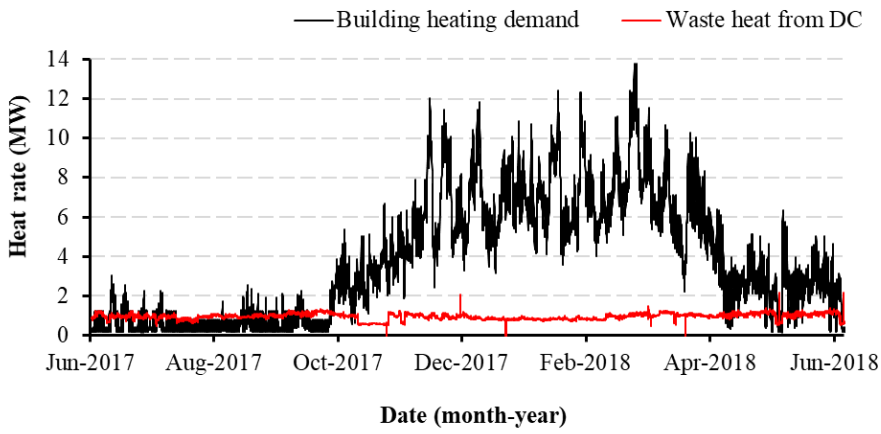

Figure 4-3. Heating demand and waste heat recovery of the campus district heating system

To further improve the economic performance of this DH system integrated with the DC waste heat, the MPC scheme proposed in Section 3.5 was tested on this campus DH system by simulation. Detailed simulation settings including the local heating and electricity prices, can be found in **Paper 3**.

5 RESULTS AND DISCUSSION

This chapter presents the key results of this doctoral work and answers research questions from **Question 2** to **Question 4**. The results evaluate the MPC schemes applied on both the demand and supply side of a DH system and identify the effectiveness of the error model.

5.1 MPC performance in a building space heating system

This section summarizes the key results of the research in Section 3.3 on the MPC scheme applied on the demand side of a DH system under perfect future disturbances. By presenting the achieved indoor temperature, peak load shaving effect and heating cost saving in the proposed research scenarios, it answers the second research question - **Question 2:** What is the system energy and economic performance when using MPC on the demand side of the DH systems? A more comprehensive elaboration on the results and the model validation can be found in **Paper 2**.

5.1.1 Indoor air temperature

The proposed MPC scheme in Section 3.3 was tested on the case building by simulation for one week (from 17th to 24th of January 2018), and measured outdoor air temperature was used in this MPC scheme to explore its theoretical potential. Figure 5-1 shows the indoor air temperature and the violation numbers of indoor temperature for the MPC scenario and its corresponding RBC scenario. The indoor temperature was collected every ten minutes, and the violation number was counted when the difference between the indoor temperature and the reference value was higher than 0.5 K.

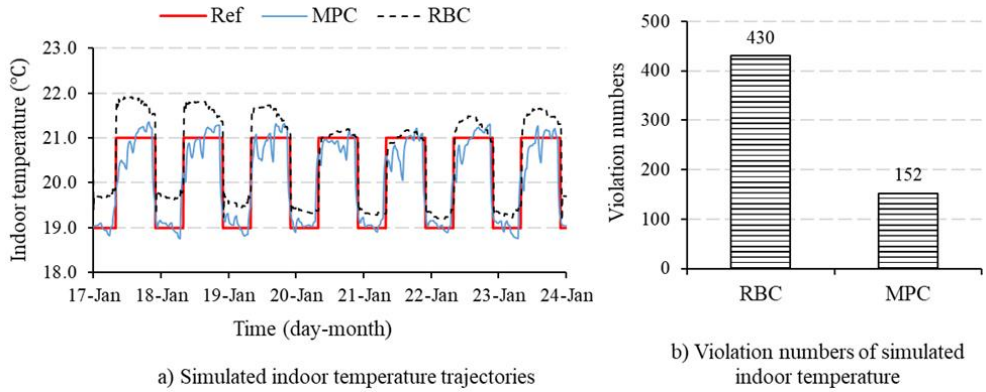

Figure 5-1. Simulated indoor air temperatures for RBC and MPC scenarios

According to the measured data and the Norwegian standard SN-NSPEK 3031 [48], the reference indoor temperature values for the two research scenarios were both defined as 21°C from 8:00 am to 10:00 pm and 19°C from 10:00 pm to 8:00 am, as shown by the red solid line in Figure 5-1 a). The P controller in the RBC scenario was tuned to achieve the required indoor temperature under all the conditions according to the principle of the actual building controller, as shown by the black dash line in Figure 5-1 a). The proposed MPC scenario achieved better indoor temperature control performance than the conventional RBC. As shown by the blue solid line in Figure 5-1 a), the over-heating phenomenon that occurred in the RBC scenario was effectively decreased in the MPC scenario, and the deviations between the indoor temperature and its reference values were decreased as well. Furthermore, as presented in Figure 5-1 b), the violation numbers of the indoor temperature were also decreased by the MPC control strategy from 430 to 152, with a reduction of nearly 65%.

5.1.2 Peak load shaving

The proposed MPC scheme for the SH system incorporated the building thermal mass as TES to shift the heat loads away from peak hours and realize peak load shaving. Figure 5-2 illustrates the heat rate for the MPC and RBC scenarios.

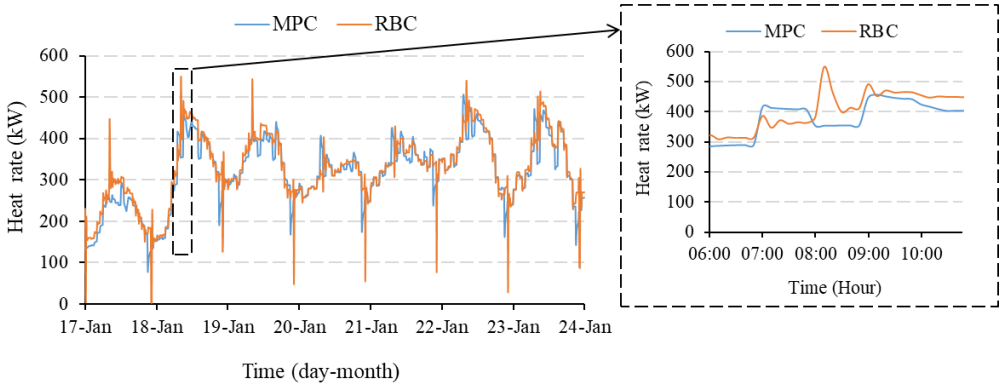

Figure 5-2. Simulated heat rates of space heating systems for RBC and MPC scenarios

As presented in Figure 5-2, significant peak loads were observed around 8:00 am in the RBC scenario, when the reference values of the indoor temperature raised from 19°C to 21°C. Meanwhile, these peak hours coincided with the occupancy as well. The MPC scenario, however, handled this sudden rise of the reference indoor temperature by preheating the

building one hour ahead (from 7:00 am to 8:00 am). Afterwards, the MPC control strategy slightly lowered its heat supply for the building to avoid the peak loads that appeared in the RBC scenario. Meanwhile, the indoor temperature of the MPC scenario was controlled at its acceptable range, as shown in Figure 5-1. Therefore, the MPC scenario shifted part of its heat load from the peak hours to the non-peak hours, and this heat load shifting contributed to its peak load shaving effect.

5.1.3 Heating cost

The heating price model used in this work only considered the LDC and the EDC. Therefore, the peak load and the heat use for the two scenarios are presented firstly. Figure 5-3 presents the peak load and heat use for two scenarios. Coinciding with Section 5.1.2, the MPC scenario presented a significant peak load shaving effect, and the peak load was decreased from 549 kW to 506 kW, a reduction of almost 8.0% compared to the benchmark scenario RBC, as shown in Figure 5-3 a). In addition, due to the elimination of the over-heating phenomenon, heating use was saved as well in the MPC scenario. As presented in Figure 5-3 b), the MPC scenario saved the heat use from 54.9 MWh to 53.1 MWh, with a heat use saving of around 3.2%.

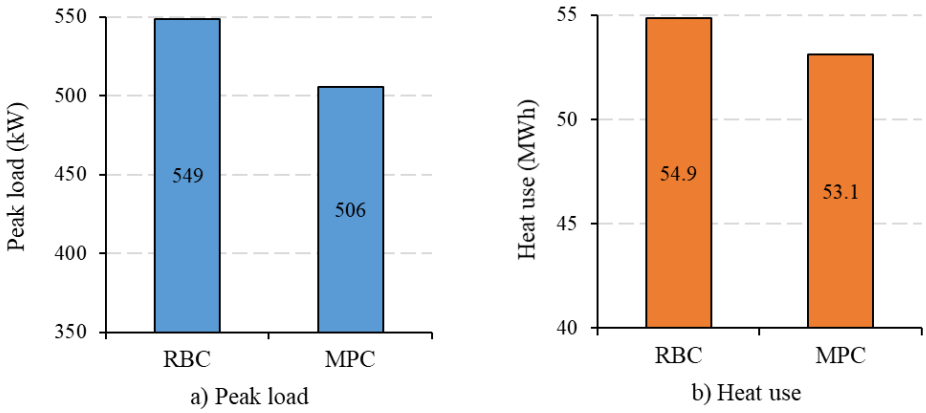

Figure 5-3. Simulated peak loads and heat use of space heating system for RBC and MPC scenarios

Figure 5-4 presents the heating cost including the LDC and the EDC for different scenarios. In the MPC scenario, both the LDC and the EDC were reduced because of the peak load shaving and heat use saving effects brought by the MPC controller, as illustrated in Figure 5-4. As a

result, the MPC scenario saved the heating cost from 38 600 NOK to 37 000 NOK, a weekly heating cost saving of 4.1%.

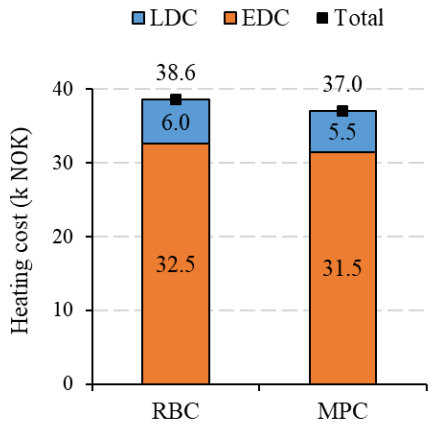

Figure 5-4. Simulated heating costs of space heating systems for RBC and MPC scenarios

5.2 MPC performance considering weather forecast uncertainty

This section summarizes the key results of the research in Section 3.4 on the weather forecast uncertainty in the MPC scheme. By firstly evaluating the error model and then presenting the achieved indoor temperature and heating cost saving in the proposed research scenarios, it answers the third research question - **Question 3:** What is the impact of weather forecast uncertainty on MPC performance, and how to handle it? A more comprehensive elaboration on the results and the error model can be found in **Paper 2**.

5.2.1 Evaluation of error model for weather forecast

Two more MPC scenarios, one directly using the weather forecast data and one using the estimated weather data generated by the error model, were tested during the same week (from 17th to 23rd of January 2018). Figure 5-5 presents the comparison between the forecasted and the actual outdoor temperature during the simulation period. The weather forecast data were given by the archived forecasts of the NWPM, MetCoOp Ensemble Prediction System (MEPS), which is cooperated by the meteorological services of Norway, Sweden, and Finland. The location of the case building was used as the input for the NWPM to download the corresponding historical weather forecast data. As shown in Figure 5-5, the deviations between the forecasted and the actual outdoor temperature were large and most of the forecasted values

were lower than the actual values. The mean value of these deviations was -2.7 K, and the maximum deviation was -9.2 K. To improve the quality of MEPS forecasted outdoor temperature as shown in Figure 5-5, the error model proposed in Section 3.4.1 was used to estimate the prediction error of MEPS, and then the estimated MEPS prediction error together with the MEPS forecasted outdoor temperature were combined to generate a sequence of estimated outdoor temperature. According to [62, 63], the accuracy of these estimated outdoor temperatures was quantified using a standard metric, root mean square error (RMSE). RMSE represents the sample standard deviation of the differences between predicted values and actual values.

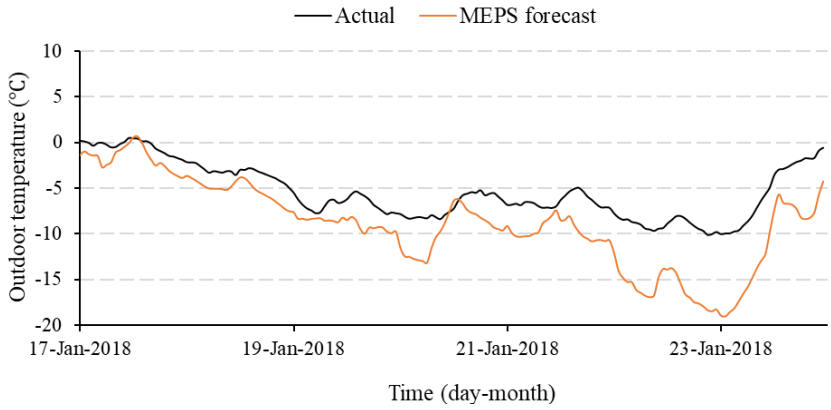

Figure 5-5. Forecasted and actual outdoor air temperature

Figure 5-6 presents the RMSEs of each hour in the predictive horizon, in which the black line represents the RMSE of the MEPS forecasted outdoor temperature, and the orange line represents the RMSE of the estimated outdoor temperature. The predictive horizon was 12 hours in this work, and hence the X-axis of Figure 5-6 ranged from 1 to 12. In addition, the studied typical week had 168 hours, and therefore the RMSEs of each hour in the predictive horizon were calculated based on 168 pairs of data including actual and predicted values. As presented in Figure 5-6, the RMSEs of the forecasted outdoor temperature direct from MEPS were larger and fluctuated around 4.2 K for each hour in the predictive horizon. In contrast, after introducing the error model for MEPS forecasted outdoor temperature, the accuracy of the outdoor temperature was increased. As shown in Figure 5-6, the estimated outdoor temperatures had higher accuracy with the lower RMSEs from 0.5 to 4.2 K, especially for the near future as presented on the left side of Figure 5-6.

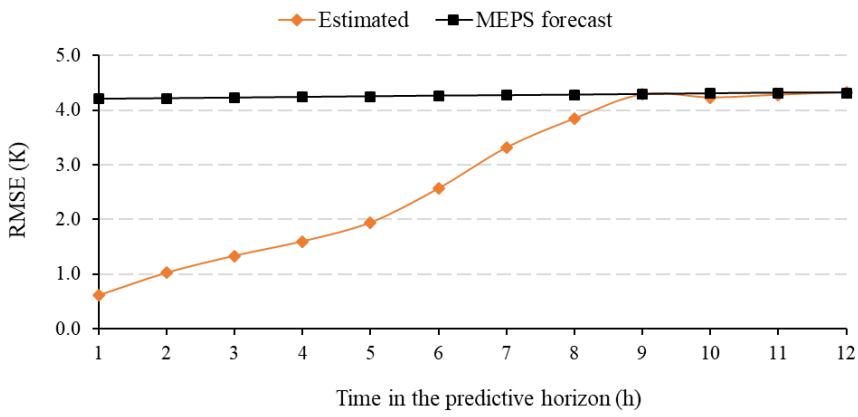

Figure 5-6. RMSEs of the MEPS forecasted and the estimated outdoor temperature

5.2.2 Indoor air temperature

Figure 5-7 presents the indoor air temperature and its reference values for different scenarios. Moreover, the violation numbers of the indoor temperature are presented in Figure 5-8. The indoor temperature reference values and violation numbers were set as described in Section 5.1.1. The ideal MPC scenario that used the measured outdoor air temperature, MPC_actu, demonstrated the theoretical control performance of the MPC and it coincides with the MPC scenario in Section 5.1.1. This ideal MPC scenario eliminated the over-heating phenomenon occurring in the reference scenario RBC, and reduced the deviations between indoor temperature and its reference values. The violation numbers were decreased from 430 to 152, with a reduction of almost 65%.

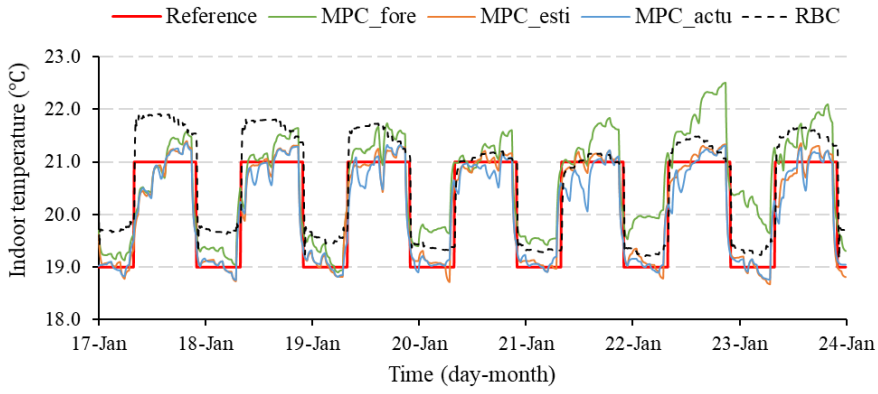

Figure 5-7. Simulated indoor temperature for RBC and MPC scenarios

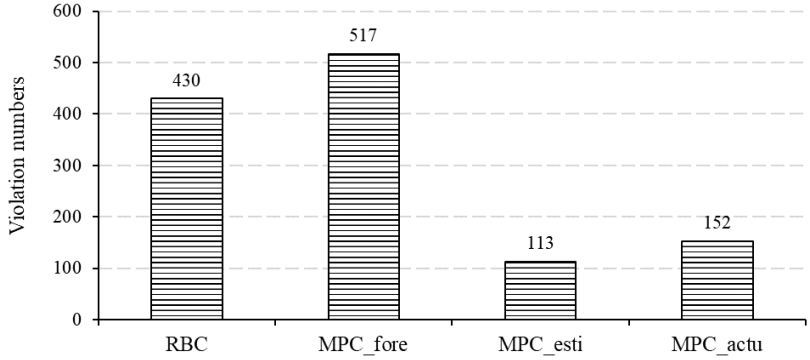

Figure 5-8. Simulated violation numbers of indoor temperature for RBC and MPC scenarios

The standard MPC scenario that directly used weather forecast outdoor air temperature, MPC_fore, presented the practical indoor temperature control performance of MPC, as depicted in Figure 5-7 by the green solid line. The MEPS forecasted outdoor temperature was directly used by the MPC controller in this scenario. Due to receiving inaccurate outdoor temperature, this scenario did not perform well, especially when the MEPS forecasted weather largely varied from the actual one. The over-heating phenomenon in this scenario was even worse than that in the reference scenario RBC, as shown in Figure 5-7. In addition, compared to the reference scenario, RBC, the deviations between the indoor temperature and its reference values were increased and the violation numbers of the indoor temperature were even higher, an increase of 20%, as shown in Figure 5-8. Due to receiving the low-quality predictions for the future weather, this standard MPC scenario presented even worse control performance than the conventional RBC in terms of the indoor temperature.

In contrast, the improved MPC scenario that used the estimated outdoor air temperature from the error model, MPC_esti, was able to guarantee satisfying indoor temperature by introducing the error model. As presented in Figure 5-6, the error model together with the MEPS forecasted outdoor temperature generated the high-quality estimated future outdoor temperature, and then the estimated outdoor temperature was used by the MPC controller in this scenario. Due to receiving the high-quality weather data, this scenario achieved almost the same indoor temperature control performance as the ideal MPC scenario, as depicted in Figure 5-7 by the orange solid line. The over-heating phenomenon was removed and the deviations between the indoor temperature and its reference values were small in this scenario. Moreover, as presented in Figure 5-8, the violation numbers of the indoor temperature dropped by almost 80%

compared to the standard MPC scenario (MPC_fore) and by 73% compared to the reference scenario RBC.

5.2.3 Heating cost

The heating cost was charged based on the peak heat rate and the heat use of end-users. Figure 5-9 presents the peak heat rate for different scenarios. The ideal MPC scenario, MPC_actu, presented a remarkable peak load shaving effect with a reduction of 8.0% compared to the reference scenario RBC. However, due to receiving inaccurate weather data, the peak load shaving performance of the MPC deteriorated. As shown in Figure 5-9, the standard MPC scenario, MPC_fore, shaved the peak load by only 3.6% compared to the reference scenario RBC. In contrast, introducing the error model was able to improve the peak load shaving performance of MPC a bit. As the improved MPC scenario (MPC_esti) showed, the peak load was decreased by 4.6%, which was higher than the standard MPC scenario (MPC_fore).

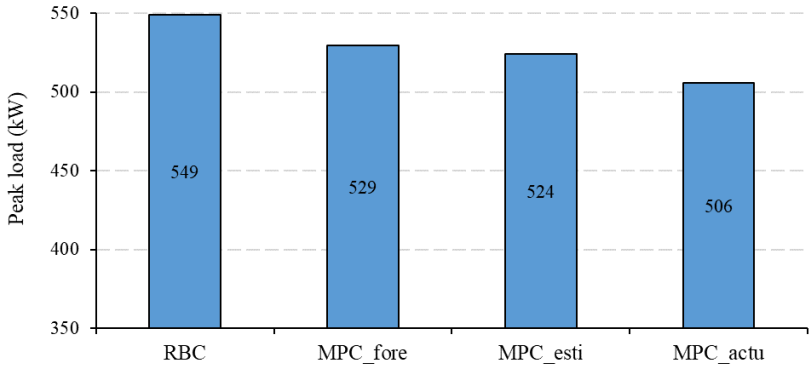

Figure 5-9. Simulated peak load for RBC and MPC scenarios

Figure 5-10 presents the heat use for different scenarios. The ideal MPC scenario, MPC_actu, demonstrated the theoretical heat use saving potential of the MPC, with a heat use saving of 3.3%. However, the low-quality predictions of weather degraded the heat use saving performance of the MPC. As the standard MPC scenario (MPC_fore) showed, its heat use was almost the same as the reference scenario RBC. In this scenario, its MPC controller received lower forecasted outdoor temperatures, which led to incorrect control actions of MPC. The MPC controller provided more heat than the building demand and hence resulted in the over-heating phenomenon and heat waste. Introducing the error model was able to improve the quality of weather information and significantly improve the MPC performance in terms of heat

use saving. As shown in Figure 5-10, the improved MPC scenario (MPC_esti) reduced the heat use by 3.0%, which was very close to the theoretical heat use saving potential of the MPC.

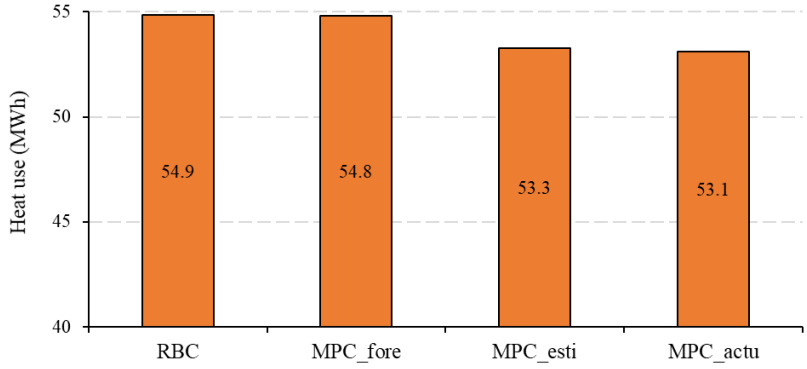

Figure 5-10. Simulated heat use for RBC and MPC scenarios

Figure 5-11 presents the heating cost for different scenarios. The theoretical heating cost saving was 4.1%, as the ideal MPC scenario MPC_actu showed. The standard MPC scenario, MPC_fore, saved only 0.7% of heating cost compared to the reference scenario RBC. The heating cost saving performance of the MPC was degraded a lot due to the low-quality weather forecast information. However, introducing the error model for the weather forecast brought remarkable improvement in terms of heat use saving for the MPC controller, as described above. Therefore, about 3.4% of the heating cost was saved by the improved MPC scenario MPC_esti.

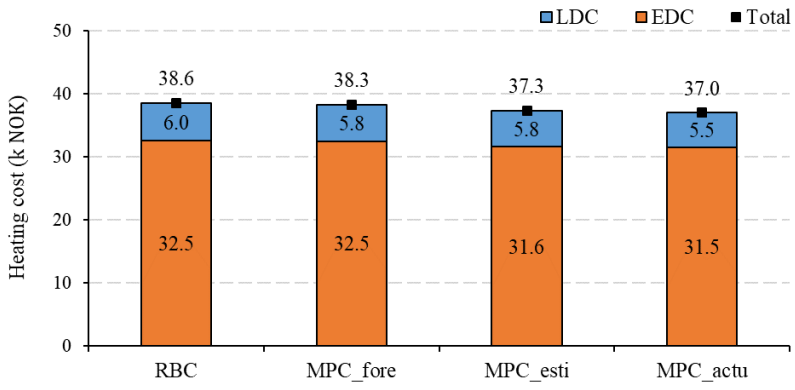

Figure 5-11. Simulated heating costs for RBC and MPC scenarios

5.3 MPC performance in a heat prosumer with data centre waste heat recovery and thermal energy storage

This section summarizes the key results of the research in Section 3.5 on the MPC scheme applied on the supply side of a DH system with distributed sources. The DH system used in the case study is a heat prosumer with DC waste heat. By presenting the DC performance, the local DH system performance and the overall performance of heat prosumer in the proposed research scenarios, it answers the fourth research question - **Question 4**: What is the system energy and economic performance when using MPC on the supply side of the DH systems with distributed sources? A more comprehensive elaboration on the results and the model validation can be found in **Paper 3**.

5.3.1 Data centre performance

This simulation-based study was conducted during the heating season (from October to April) of the year 2017- 2018. January and April of 2018 were chosen as the typical month for the midwinter and the transitional period, respectively, to conduct the study. The outlet temperature of the evaporator, the coefficient of performance (COP) of the HP, and the electricity use of the HP were used as indicators to evaluate the DC performance. Figure 5-12 presents the outlet temperature of the evaporator in January and April, respectively. Two obvious phenomena can be observed: 1) Both the MPC scenarios had smaller outlet temperature fluctuating ranges compared to the RBC scenarios, especially in April; 2) Both the MPC scenarios preferred lower outlet temperatures with average values of 6.0 and 6.1℃, respectively. The average values of the outlet temperatures were 6.5℃ in the RBC scenarios. Moreover, one conclusion was obtained as well: the cooling requirement of DC was satisfied in both MPC and RBC scenarios because most of the outlet water temperatures of the evaporator were within its feasible region from 6.0 to 7.0℃.

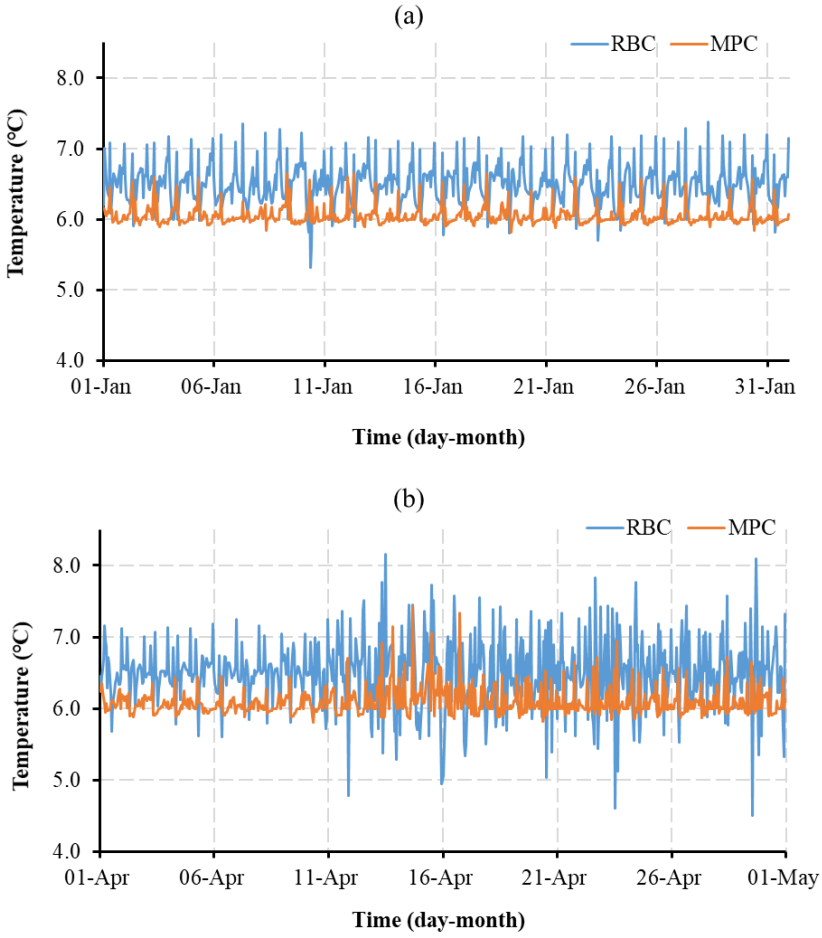

Figure 5-12. Simulated outlet temperatures of the evaporator for RBC and MPC scenarios (a) January 2018 (b) April 2018

Figure 5-13 presents the COPs of HP in January and April. Similar to the outlet temperature of the evaporator, the COPs of the HP in the MPC scenarios varied within a smaller range compared to the RBC scenarios, especially in April. In terms of the average value of COP, the MPC scenario was higher than that of the RBC scenario in January, with values of 3.1 and 2.9 respectively. However, the average value of COP in the RBC scenario was a bit higher than that of the MPC scenario in April, with values of 3.1 and 3.0 respectively. These results indicated that the MPC scheme was more robust than the RBC scheme expressed by the smaller

fluctuating ranges of both the outlet temperature of the evaporator and the COP of the HP, which are crucial for the DC cooling system's safe operation.

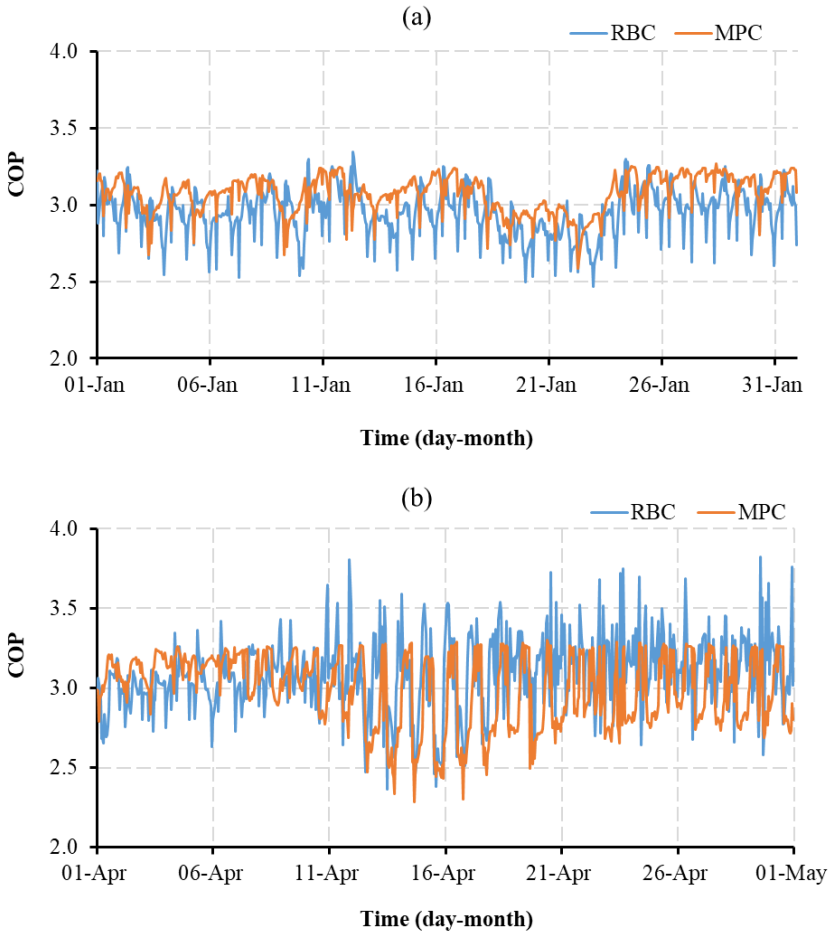

Figure 5-13. Simulated COPs of the heat pump for RBC and MPC scenarios (a) January 2018 (b) April 2018

Figure 5-14 presents the monthly electricity use of the HP for two scenarios, respectively. Two main phenomena can be noticed in Figure 5-14: 1) The MPC scenarios used more electricity for HPs than the RBC scenarios in both January and April; 2) The electricity use of the HP in the MPC scenarios had no big difference in January and April, while the RBC scenario used much more electricity in January than in April. These phenomena indicated that the electricity use of the HP in the MPC scenarios was much more stable, and the MPC scenarios preferred to

generate more waste heat from the HP by using more electricity because the COPs of the HP were always higher than 1.0 and maintained at around 3.0-3.1.

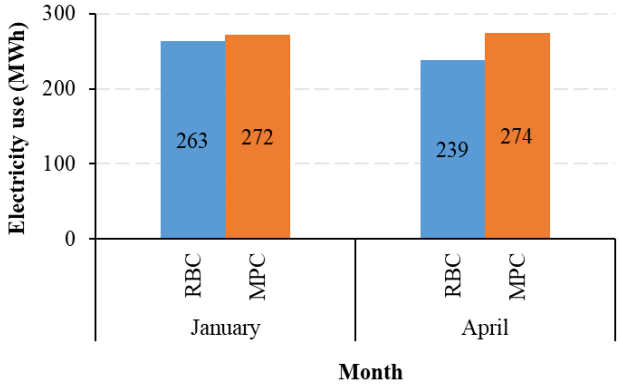

Figure 5-14. Simulated electricity use of heat pump for RBC and MPC scenarios

5.3.2 Local district heating performance

Peak heat rate and heat use were chosen as the indicators to evaluate the performance of the local DH system. Figure 5-15 presents the peak load of the MS for the two scenarios in January and April, respectively. As shown in Figure 5-15, both MPC scenarios, in January and April, took better advantage of the WTTES flexibilities, which was demonstrated by the lower peak loads compared to their corresponding RBC scenarios. In January, the peak load of the MPC scenario dropped to around 10.9 MW, a reduction of about 5.6% compared to the RBC scenario. In April, the peak load reduction of the MPC scenario was even more, with a reduction of almost 12.0% compared to the RBC scenario. Figure 5-16 presents the heat use of the local DH system for two scenarios in January and April, respectively. As shown in Figure 5-16, each MPC scenario saved the heat use compared to its corresponding RBC scenario, with savings of 2.0% and 3.7%, respectively.

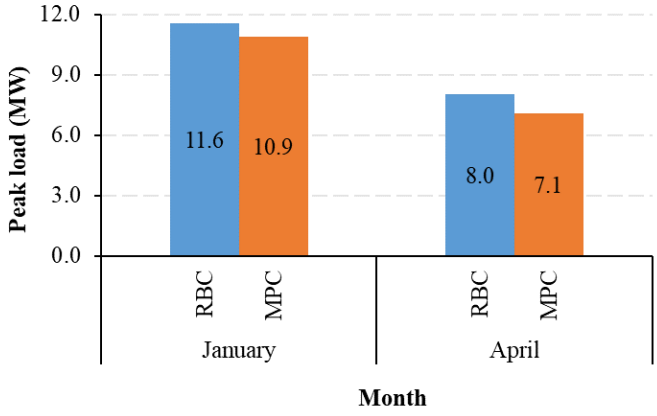

Figure 5-15. Simulated peak load for RBC and MPC scenarios

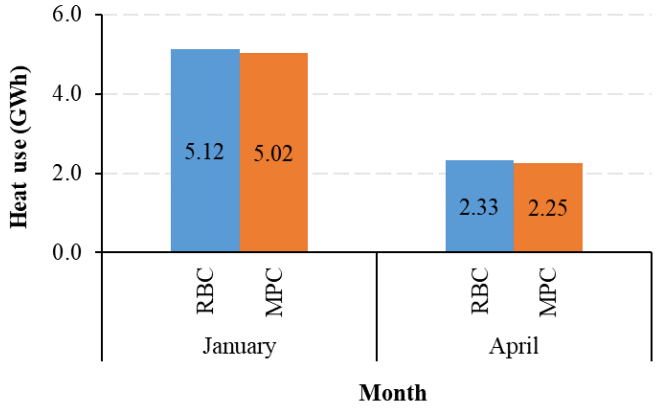

Figure 5-16. Simulated heat use for RBC and MPC scenarios

5.3.3 Overall performance of heat prosumer

The total energy use and energy bill were used to evaluate the heat prosumer's overall performance. Figure 5-17 presents the monthly total energy use for the two scenarios. The energy use included the heat supplied from the MS and the electricity supplied to power the DC's HP and the CP. One obvious result that can be noticed in Figure 5-17 was that both the MPC scenarios preferred to use more electricity but less heat. In January, the heat supplied from the MS for the MPC scenario was decreased by 2.0% compared to the RBC scenario. In contrast, more electricity was used in the MPC scenario, with an increase of 8.1%. A similar phenomenon

could be found in April as well: the heat use decrease was 3.7% and the electricity use increase was almost 19.0% in the MPC scenario. This result can be explained by the following reason: the MPC scenarios tended to gain heat as much as possible from the HP of DC to achieve the maximum economic performance because the COPs of HP were always higher than 1.0 and maintained at around 3.0-3.1. For example, to supply 3.0 kWh of heat for the heat user, the electricity use of HP would be only around 1.0 kWh while the MS would need to supply exactly 3.0 kWh heat. Meanwhile, the prices of electricity were only a bit higher than the heat during the studied period. Therefore, gaining heat as much as possible from the HP was the way that the MPC scheme used to achieve the maximum possible economic performance, and this will be further illustrated in the following text.

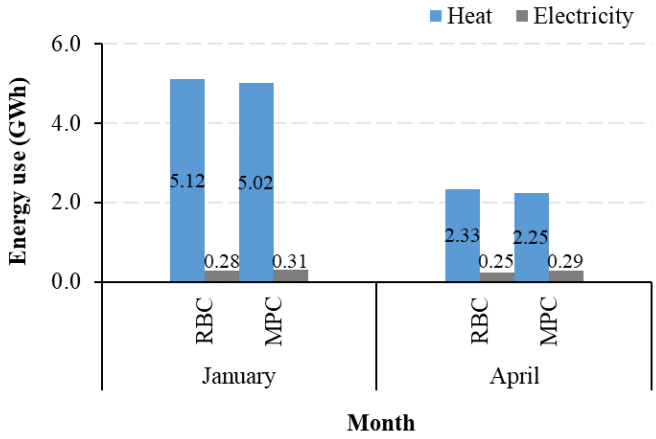

Figure 5-17. Simulated energy use for RBC and MPC scenarios

Figure 5-18 presents the monthly total energy bill for the two scenarios. The energy bill consisted of heating cost and electricity cost. Thereof, the heating cost included the LDC based on the heat user's peak load and the EDC based on the total heat use of the heat user. There were several similar results presented both in January and April as follows: 1) Both the MPC scenarios saved the total energy bill compared to their corresponding RBC scenarios, with savings of 1.8% and 3.2% in January and April, respectively; 2) Both the MPC scenarios reduced the heating costs, which were brought by both the reductions of the LDC and the EDC, with the reduction of 2.3% and 5.1% in January and April; 3) Both the MPC scenarios increased the electricity cost due to the increased electricity use as explained by Figure 5-17. The increases were 8.2% and 19.1% in January and April, respectively. However, the electricity

cost accounted for less than 10% of the total energy bill and hence the increased electricity cost was not able to impair the total economic performance of MPC scenarios. Based on the above analysis, one important result was found as follows: the MPC scheme made an optimized trade-off between the heat use and the electricity use to achieve the possible maximum economic performance of the heat prosumer.

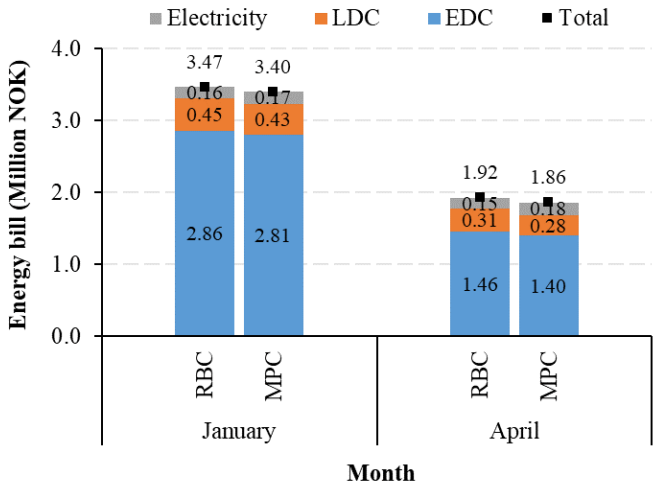

Figure 5-18. Simulated energy bill for RBC and MPC scenarios

6 CONCLUSIONS

This chapter highlights the key results of this thesis. Section 6.1 presents the key conclusions, while Section 6.2 acknowledges the limitations of this doctoral work. In Section 6.3, recommendations for future research are given.

6.1 Concluding remarks

This thesis aimed to contribute to the implementation of MPC in DH systems that are dedicated to Nordic climate conditions to improve the energy and economic performance of the system. The most important conclusions are listed as follows.

Firstly, the MPC application on the demand side of the investigated DH system can realize the intelligent management of SH systems, as the building dynamic model, future disturbances, energy price, energy demand, and intelligent algorithms are incorporated into the controller. Particularly, the passive thermal mass storage of the buildings can be considered as TES in the MPC strategy to further improve the system's economic performance. The case study indicated that the MPC scheme with perfect future weather information could cut the weekly heating cost by 4.1% and decrease the violation numbers of indoor temperature by 65% compared to the current RBC strategy. However, the weather forecast uncertainty impaired these benefits brought by using the MPC, which was illustrated by the deteriorated economic performance of the SH system when the MPC scheme directly used weather forecast information. The MPC scheme with direct weather forecast information cut the heating cost by only 0.7% and even increased the violation numbers of indoor temperature by 20% compared to the RBC strategy. Introducing the error model for the MPC scheme was proven an efficient way to tackle the weather forecast uncertainty existing in the practical MPC. Therefore, the second important conclusion is obtained: introducing the error model for the MPC scheme was able to address the weather forecast uncertainty and hence achieve almost the full theoretical potential of the MPC in terms of heating cost-saving and indoor temperature control. The MPC scheme with weather forecast information and the error model cut the weekly heating cost by 3.4% and decreased the violation numbers of indoor temperature by 73% compared to the RBC strategy.

Lastly, the MPC application on the supply side of the investigated DH system can obtain the optimal heat supply allocation between the multiple heat sources and hence further improve the

economic performance of the DH system after introducing DC waste heat. The case study indicated that the MPC scheme was more stable and robust expressed as the smaller fluctuating ranges of both the outlet temperature of the evaporator and the COP of the HP in DC, which are crucial for the DC cooling system's safe operation. In addition, the MPC scheme took better advantage of the WTTES flexibilities, which was demonstrated by the lower peak loads. The peak load reduction of the MPC scheme was up to 12.0% compared to the RBC strategy. Finally, the MPC scheme tended to gain waste heat as much as possible from the DC by using more electricity for the HP but extracting less heat from the MS to achieve the maximum possible economic performance, and the resulting monthly energy cost saving was up to 3.2%. In total, the MPC scheme made an optimized trade-off between heat use and electricity use to achieve the best economic performance of the heat prosumer.

6.2 Limitation

The first limitation comes from the RC model used in the research on the MPC application on the demand side of the DH system. As for the parameter settings of the RC model, it is commonly conducted either by estimation methods if the detailed information of the building geometry and thermal properties is well-known, or by system identification methods that use historical measured data to tune the values of the parameters, or a mix of both [64]. In this work, the parameter values of the RC model were determined by an estimation method according to the known detailed information of the case building, the on-site measured data, and the recommended values in the European standard ISO 52016-1 [47], which results in a white-box RC model. However, for many buildings, detailed building information and complete on-site measured data are often unavailable. In this case, it is challenging to develop a white-box model based on the limited information about the building.

The second limitation is the objective function used in the research on the MPC application on the supply side of the DH system. The objective function was set to minimize the energy bill of the system by incorporating the heating and electricity costs. Spot price-related components account for a large share of both the heating and electricity costs according to the local DH company [65] and the power supplier company [66]. Therefore, the MPC controller tended to control both the MS and the HP providing more heat and storing the heat in the TES during the low spot price period and then reusing the heat during the high spot price period to minimize the energy bill. However, the objective function based solely on the energy bill may cause an

increase in CO_2 emissions. Time-varying CO_2 intensity was commonly used to evaluate the CO_2 emissions of electricity generation, and the low CO_2 intensity period does not coincide with the low spot price period in some countries [28, 67]. In Norway, electricity is mostly generated from hydropower, which features lower CO_2 intensities. However, the interaction between the continental European and the Norwegian power grids significantly increases the CO_2 intensity, i.e. the CO_2 intensity is increased a lot when importing electricity from other European countries. The Norwegian hydropower reservoirs are generally operated in a cost-optimal way, with electricity imported at night when electricity is cheap and exported to continental Europe during the day when electricity is expensive, which results in the negative correlation between the spot price and the CO_2 intensity [67]. Figure 6-1 shows one example that is from the research [67] to explain it. For the illustrated biding zone in Norway, electricity is generated from hydropower during the high demand period (high spot prices), which results in low CO_2 intensities. In contrast, electricity is imported from continental Europe during the low demand period (low spot price), which results in high CO_2 intensities. This negative correlation between the spot price and the CO_2 intensity results that the proposed MPC scheme may increase CO_2 emissions despite the reduction of the energy bill.

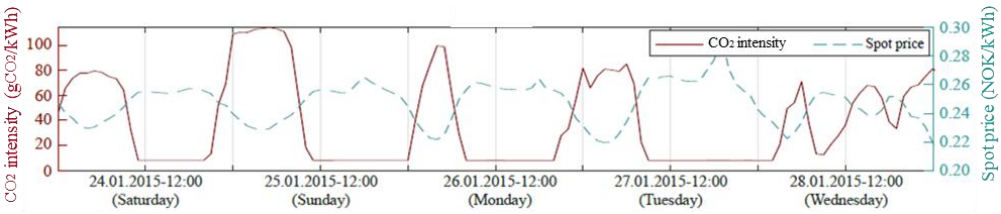

Figure 6-1. Hourly CO_2 intensities and spot prices for a biding zone in Norway [67].

6.3 Future research

Possible future studies are suggested based on the presented research results and the acknowledged limitations.

Firstly, a more generalized research method to set the parameter values of the RC model is needed. Using system identification techniques to develop a grey-box RC model may be one way when the building information is limited. A grey-box RC model builds the model structure using the system's dominating physical attributes and estimates the model parameters using measurement data. Grey-box models have better generalization properties and usually require

less building information compared to white-box models. Therefore, to have a more generalized research method, a grey-box RC model may be developed in future work to test the MPC schemes proposed in this work.

Secondly, with the concerns of energy and climate crisis, it is better to involve CO_2 emissions as one performance target in the objective function of the MPC that is applied on the supply side of the DH system. The objective function of the MPC can be set by adding a weighting factor for the energy costs and a weighting factor for the CO_2 emissions. These two weighting factors can be adjusted either to balance the performance of the MPC with respect to both targets or to minimize it with respect to one target of particular interest. To achieve this goal, the method to determine the time-varying CO_2 intensity for the biding zone where the case system is located may be investigated firstly in future work.

BIBLIOGRAPHY

[1] European Commission. Energy Performance of Buildings Directive, https://ec.europa.eu/energy/topics/energy-efficiency/energy-efficient-buildings/energy-performance-buildings-directive_en; 2021 [Accessed 06 April 2021].

[2] European Commission. Heating and cooling, https://ec.europa.eu/energy/topics/energy-efficiency/heating-and-cooling_en?redir=1; 2021 [Accessed 06 April 2021].

[3] Werner S. International review of district heating and cooling. Energy. 2017;137:617-31.

[4] Frederiksen S, Werner S. District heating and cooling, Vol. 579, Studentlitteratur Lund, 2013.

[5] Lund H, Østergaard PA, Chang M, Werner S, Svendsen S, Sorknæs P, et al. The status of 4th generation district heating: Research and results. Energy. 2018;164:147-59.

[6] Werner S. District heating and cooling in Sweden. Energy. 2017;126:419-29.

[7] Seal S, Boulet B, Dehkordi VR. Centralized model predictive control strategy for thermal comfort and residential energy management. Energy. 2020;212:118456.

[8] Ławryńczuk M, Ocłoń P. Model Predictive Control and energy optimisation in residential building with electric underfloor heating system. Energy. 2019;182:1028-44.

[9] Privara S, Široký J, Ferkl L, Cigler J. Model predictive control of a building heating system: The first experience. Energy and Buildings. 2011;43(2-3):564-72.

[10] Široký J, Oldewurtel F, Cigler J, Prívara S. Experimental analysis of model predictive control for an energy efficient building heating system. Applied Energy. 2011;88(9):3079-87.

[11] Aoun N, Bavière R, Vallee M, Aurousseau A, Sandou G. Modelling and flexible predictive control of buildings space-heating demand in district heating systems. Energy. 2019;188:116042.

[12] Drgoňa J, Arroyo J, Cupeiro Figueroa I, Blum D, Arendt K, Kim D, et al. All you need to know about model predictive control for buildings. Annual Reviews in Control. 2020;50:190-232.

[13] Hilliard T, Kavgic M, Swan L. Model predictive control for commercial buildings: trends and opportunities. Advances in Building Energy Research. 2016;10(2):172-90.

[14] Afram A, Janabi-Sharifi F. Theory and applications of HVAC control systems–A review of model predictive control (MPC). Building and Environment. 2014;72:343-55.

[15] Killian M, Kozek M. Ten questions concerning model predictive control for energy efficient buildings. Building and Environment. 2016;105:403-12.
[16] Afram A, Janabi-Sharifi F. Theory and applications of HVAC control systems - A review of model predictive control (MPC). Building and Environment. 2014;72:343-55.
[17] Saletti C, Gambarotta A, Morini M. Development, analysis and application of a predictive controller to a small-scale district heating system. Applied Thermal Engineering. 2020;165:114558.
[18] Thieblemont H, Haghighat F, Ooka R, Moreau A. Predictive control strategies based on weather forecast in buildings with energy storage system: A review of the state-of-the art. Energy and Buildings. 2017;153:485-500.
[19] Petersen S, Bundgaard KW. The effect of weather forecast uncertainty on a predictive control concept for building systems operation. Applied Energy. 2014;116:311-21.
[20] Li H, Nord N. Transition to the 4th generation district heating-possibilities, bottlenecks, and challenges. Energy Procedia. 2018;149:483-98.
[21] Li H, Hou J, Hong T, Ding Y, Nord N. Energy, economic, and environmental analysis of integration of thermal energy storage into district heating systems using waste heat from data centres. Energy. 2021;219:119582.
[22] Li J, Yang Z, Li H, Hu S, Duan Y, Yan J. Optimal schemes and benefits of recovering waste heat from data center for district heating by CO2 transcritical heat pumps. Energy Conversion and Management. 2021;245:114591.
[23] Wahlroos M, Pärssinen M, Manner J, Syri S. Utilizing data center waste heat in district heating–Impacts on energy efficiency and prospects for low-temperature district heating networks. Energy. 2017;140:1228-38.
[24] Hiltunen P, Syri S. Low-temperature waste heat enabling abandoning coal in Espoo district heating system. Energy. 2021;231:120916.
[25] Davies G, Maidment G, Tozer R. Using data centres for combined heating and cooling: An investigation for London. Applied Thermal Engineering. 2016;94:296-304.
[26] He Z, Ding T, Liu Y, Li Z. Analysis of a district heating system using waste heat in a distributed cooling data center. Applied Thermal Engineering. 2018;141:1131-40.
[27] Wahlroos M, Pärssinen M, Rinne S, Syri S, Manner J. Future views on waste heat utilization–Case of data centers in Northern Europe. Renewable and Sustainable Energy Reviews. 2018;82:1749-64.

[28] Knudsen MD, Petersen S. Demand response potential of model predictive control of space heating based on price and carbon dioxide intensity signals. Energy and Buildings. 2016;125:196-204.

[29] Pedersen TH, Hedegaard RE, Petersen S. Space heating demand response potential of retrofitted residential apartment blocks. Energy and Buildings. 2017;141:158-66.

[30] Gholamibozanjani G, Tarragona J, De Gracia A, Fernández C, Cabeza LF, Farid MM. Model predictive control strategy applied to different types of building for space heating. Applied energy. 2018;231:959-71.

[31] Hedegaard RE, Pedersen TH, Petersen S. Multi-market demand response using economic model predictive control of space heating in residential buildings. Energy and Buildings. 2017;150:253-61.

[32] Verrilli F, Srinivasan S, Gambino G, Canelli M, Himanka M, Del Vecchio C, et al. Model predictive control-based optimal operations of district heating system with thermal energy storage and flexible loads. IEEE Transactions on Automation Science and Engineering. 2016;14(2):547-57.

[33] Saletti C, Zimmerman N, Morini M, Kyprianidis K, Gambarotta A. Enabling smart control by optimally managing the State of Charge of district heating networks. Applied Energy. 2021;283:116286.

[34] van der Zwan S, Pothof I. Operational optimization of district heating systems with temperature limited sources. Energy and Buildings. 2020;226:110347.

[35] Hermansen R, Smith K, Thorsen JE, Wang J, Zong Y. Model predictive control for a heat booster substation in ultra low temperature district heating systems. Energy. 2022;238:121631.

[36] The Modelica Association. https://www.modelica.org/; 2020 [accessed 20 December 2020].

[37] Åkesson J, Årzén K-E, Gäfvert M, Bergdahl T, Tummescheit H. Modeling and optimization with Optimica and JModelica. org—Languages and tools for solving large-scale dynamic optimization problems. Computers & Chemical Engineering. 2010;34(11):1737-49.

[38] Song J, Wallin F, Li H. District heating cost fluctuation caused by price model shift. Applied Energy. 2017;194:715-24.

[39] Norwegian Water Resources and Energy Directorate. Energy Regulatory Authority, https://www.nve.no/reguleringsmyndigheten/kunde/nett/nettleie/?ref=mainmenu; 2021 [Accessed 3 November 2021].

[40] Karlsen SS. Investigation of Grid Rent Business Models as Incentive for Demand-Side Management in Buildings-A case study on fully electric operated houses in Norway. Master thesis: Norwegian University of Science and Technology. 2018.

[41] Statistics Norway. Energy and Manufacturing, https://www.ssb.no/en/energi-og-industri/artikler-og-publikasjoner/twofold-increase-in-electricity-price-for-households; 2021 [Accessed 3 November 2021].

[42] Nord Pool. https://www.nordpoolgroup.com/; 2021 [Accessed 3 November 2021].

[43] Energy Facts Norway. Norway's Energy Supply System, https://energifaktanorge.no/en/utskrift/#toc-2; 2021 [Accessed 3 November 2021].

[44] Tensio. Grid Rental, https://ts.tensio.no/kunde/nettleie-priser-og-avtaler; 2021 [Accessed 3 November 2021].

[45] Bacher P, Madsen H. Identifying suitable models for the heat dynamics of buildings. Energy and Buildings. 2011;43(7):1511-22.

[46] Hagos DA, Gebremedhin A, Zethraeus B. Solar water heating as a potential source for inland Norway energy mix. Journal of Renewable Energy. 2014;2014.

[47] European standard. Energy performance of buildings- Energy needs for heating and cooling, internal temperatures and sensible and latent heat loads- Part 1: Calculation procedures; ISO 52016-1:2017.

[48] Standard norge. Energy performance of buildings- Calculation of energy needs and energy supply (in Norwegian); SN-NSPEK 3031:2020.

[49] EN 442-2 Radiators and convectors - Part 2: Test methods and rating. 2014.

[50] Xu B, Fu L, Di H. Dynamic simulation of space heating systems with radiators controlled by TRVs in buildings. Energy and Buildings. 2008;40(9):1755-64.

[51] Li H, Nord N. Operation strategies to achieve low supply and return temperature in district heating system. E3S Web Conf. 2019;111:05022.

[52] IBPSA Project 1. 2019.

[53] Oldewurtel F, Parisio A, Jones CN, Gyalistras D, Gwerder M, Stauch V, et al. Use of model predictive control and weather forecasts for energy efficient building climate control. Energy and Buildings. 2012;45:15-27.

[54] Groß A, Wittwer C, Diehl M. Stochastic Model Predictive Control of Photovoltaic Battery Systems using a Probabilistic Forecast Model. European Journal of Control. 2020.

[55] Hedegaard RE, Pedersen TH, Knudsen MD, Petersen S. Towards practical model predictive control of residential space heating: Eliminating the need for weather measurements. Energy and Buildings. 2018;170:206-16.

[56] Huang P, Copertaro B, Zhang X, Shen J, Löfgren I, Rönnelid M, et al. A review of data centers as prosumers in district energy systems: Renewable energy integration and waste heat reuse for district heating. Applied Energy. 2020;258:114109.

[57] Nord N, Shakerin M, Tereshchenko T, Verda V, Borchiellini R. Data informed physical models for district heating grids with distributed heat sources to understand thermal and hydraulic aspects. Energy. 2021;222:119965.

[58] Shu H-W, Duanmu L, Zhu Y-X, Li X-L. Critical COP value of heat pump unit for energy-saving in the seawater-source heat pump district heating system and the analysis of its impact factors. Harbin Gongye Daxue Xuebao(Journal of Harbin Institute of Technology). 2010;42(12):1995-8.

[59] Liu X, Zheng ON, Niu F. A simulation-based study on different control strategies for variable speed pump in distributed ground source heat pump systems. ASHRAE Transactions. 2016;122.

[60] Grundfos. Circulator pump, https://product-selection.grundfos.com/no/products/nbg-nbge/nbg/nbg-100-80-160177-97839346?pumpsystemid=1406357823&tab=variant-sizing-results; 2021 [accessed 15 December 2021].

[61] Guan J, Nord N, Chen S. Energy planning of university campus building complex: Energy usage and coincidental analysis of individual buildings with a case study. Energy and Buildings. 2016;124:99-111.

[62] Chakraborty D, Elzarka H, Bhatnagar R. Generation of accurate weather files using a hybrid machine learning methodology for design and analysis of sustainable and resilient buildings. Sustainable Cities and Society. 2016;24:33-41.

[63] Henze GP, Kalz DE, Felsmann C, Knabe G. Impact of forecasting accuracy on predictive optimal control of active and passive building thermal storage inventory. HVAC&R Research. 2004;10(2):153-78.

[64] Ogunsola OT, Song L. Review and evaluation of using RC thermal modeling of cooling load prediction for HVAC system control purpose. ASME International Mechanical Engineering Congress and Exposition. 2012;45233:735-43.

[65] Statkraft varme at Tronheim. Products and services, https://www.statkraftvarme.no/globalassets/0/statkraft-varme/produkter-og-

tjenester/prisark/jan-2021/trondheim-bedrift-uten-volumledd-bt1.pdf; 2021 [accessed 16 December 2021].

[66] NordlysEnergi. Company, https://www.nordlysenergi.com/bedrift; 2021 [accessed 16 December 2021].

[67] Clauß J, Stinner S, Solli C, Lindberg KB, Madsen H, Georges L. Evaluation method for the hourly average CO2eq. Intensity of the electricity mix and its application to the demand response of residential heating. Energies. 2019;12(7):1345.

APPENDIX- PUBLICATIONS

This section contains the publications that make up the thesis.

APPENDIX- PUBLICATIONS

PAPER 1

Hou J, Li H, Nord N. Nonlinear model predictive control for the space heating system of a university building in Norway. Energy. 2022; 253: 124157.

APPENDIX- PUBLICATIONS

Energy 253 (2022) 124157

Contents lists available at ScienceDirect

Energy

journal homepage: www.elsevier.com/locate/energy

Nonlinear model predictive control for the space heating system of a university building in Norway

Juan Hou*, Haoran Li, Natasa Nord

Department of Energy and Process Technology, Norwegian University of Science and Technology, Kolbjørn Hejes vei 1 B, Trondheim, 7491, Norway

ARTICLE INFO

Article history:
Received 10 December 2021
Received in revised form
4 April 2022
Accepted 28 April 2022
Available online 30 April 2022

Keywords:
Thermal energy storage
Peak load
Heating cost
Indoor temperature
Optimal control

ABSTRACT

Space heating accounts for a significant share of a building's energy use; moreover, occupants' desires for better thermal comfort may further increase the energy use and peak load of the space heating system, as well as its total energy cost. The goal of this study was to use an optimal control technique: model-based predictive controller, to improve the energy and economic performance of space heating systems with satisfying indoor temperature. The proposed optimal controller incorporated the dynamic energy prices, the disturbances from weather and occupancy, as well as a nonlinear system dynamic model that considered the building thermal mass as thermal energy storage. The model-based predictive controller was tested by simulation on a university building in central Norway, and its control performance was compared to a conventional rule-based control approach, which is currently employed by the case system. The model-based predictive controller's effectiveness was demonstrated by a 2.8% reduction in heat use, 8.8% shaving in peak load, 3.8% saving in heating cost, and a 59% drop in indoor temperature violation. Furthermore, a sensitivity study revealed that the model-based predictive controller still maintained high energy and economic performance even under lightweight building constructions with decreased building thermal mass.

© 2022 Elsevier Ltd. All rights reserved.

1. Introduction

The energy use of buildings accounts for a large share of total energy use and significantly contributes to global warming. In the European Union (EU) countries, buildings are responsible for nearly 40% of the total energy use and about 36% of the total greenhouse gas emissions [1]. Among buildings' energy use, heating and cooling accounts for a significant portion and plays a crucial role in the EU's ambition to transition into a clean and carbon-neutral economy by 2050. According to 2019 figures from Eurostat, approximately 75% of heating and cooling is still generated from fossil fuels while only 22% is generated from renewable energy [2]. As a result, reducing the energy use of the heating and cooling sector is imperative, and many researchers contribute to it by exploring different techniques. Regarding the cooling system, some researchers focus on the techniques of energy monitoring and diagnosis to facilitate energy use saving. Sorrentino et al. proposed a method, which joints deployment of two estimators, for online monitoring of cooling load supplied by Telecommunication (TLC) cooling systems. The results confirmed the suitability of the proposed procedure as a reliable and effective energy monitoring and diagnostic tool for TLC applications [3]. Afterwards, D'Aniello et al. deepened the theme of monitoring and energetic diagnosis of TLC central offices, via the development and application of innovative performance parameters [4]. Meanwhile, Sorrentino et al. developed a model-based tool for advanced monitoring and diagnosis of TLC sites, and pointed out that the proposed diagnostic tools could be embedded in advanced energy intelligence platforms [5]. Despite building cooling being an important element of the decarbonisation policy, the building heating system plays an even more important role in the EU's residential sector. In the EU residential sector, around 80% of the buildings' energy use is for heating purposes including space heating (SH) and domestic hot water, especially during the winter season [6]. This figure indicates that minor energy savings in building heating systems might have a significant impact on the energy use of the building sector, and hence on the energy use of the entire energy system. Therefore, this study focus on exploring techniques for reducing the energy use of building heating systems. Nevertheless, there is a growing trend for building occupants to demand higher thermal comfort, which may

* Corresponding author.
E-mail address: juan.hou@ntnu.no (J. Hou).

https://doi.org/10.1016/j.energy.2022.124157
0360-5442/© 2022 Elsevier Ltd. All rights reserved.

result in increased building energy use. As a result, building heating system control must make a trade-off between the two conflicting goals: 1) improve thermal comfort, and 2) reduce energy use as well as energy costs. The application of intelligent control techniques for the SH system may be one way to achieve the above conflicting goals simultaneously [7]. Model predictive control (MPC), originated in the process industries (oil refineries, chemical plants, etc.), is an ideal intelligent control strategy to deal with an optimal control problem of buildings [8]. In the presence of disturbances and constraints, an MPC controller in a building employs a dynamic building model to predict the building's thermal behaviour and outputs a control vector minimizing an objective function over the prediction horizon. MPC is a potential control solution that may be focused on the reduction of energy use, energy cost, and associated greenhouse gas emissions while maintaining and potentially improving occupant comfort [9].

The suitability of MPC to tackle the optimal control of the SH system has been proven both by theory and real-life experiments. Aoun et al. proposed a mixed-integer linear programming-based MPC strategy to improve the operation of the SH systems in buildings. The proposed methods were tested by numerical simulation method, and the simulation results showed that the adopted MPC proved to be more cost-effective than the conventional weather compensation controller (WCC), while maintaining satisfied indoor temperature [10]. Seal et al. implemented a centralized MPC for a zone with a hybrid electric heating system, considering indoor temperature and energy management. Results showed that a 13.5% reduction of the energy cost was achieved by the proposed MPC during a 7-day simulation period [11]. Ławryńczuk et al. investigated the optimization of an underfloor electric heating system in a residential building by using an MPC controller. Simulation results demonstrated the effectiveness of the MPC regarding energy use saving, and around 1430 kWh electricity was reduced during the investigated heating season [12]. Privara et al. explored applying an MPC controller for the building heating system. The MPC controller was tested on a real university building. During the studied heating season, the achieved energy savings by the MPC controller were 17–24% compared to the conventional controller [13]. Similarly, Široký et al. analysed the implementation of MPC for the SH system in buildings and tested the proposed methods on a real building. Two months' experiments showed that the energy savings potential of the investigated building were 15%–28% by using an MPC controller [14].

Another benefit from the implementation of MPC in building energy systems is that thermal energy storage (TES) can be easily incorporated into the MPC design. TESs together with control techniques are becoming increasingly significant in shifting the peak energy demand and consequently reducing the system energy cost. For example, the peak energy demand contributes significantly to the energy cost for both heat suppliers and heat users in a district heating (DH) system. Regarding the heat supplier side, the peak loads decide the installed capacity of the heat production plants, which directly affects the investment and operation costs of the plants [15]. In some cases, peaks loads are provided by fossil-

Nomenclature

Abbreviations

AHU	Air-handling unit
CV(RMSE)	Coefficient of variation of the root mean square error
DH	District heating
FXC	Fix component
HDC	Heat demand component
LDC	Load demand component
MPC	Model predictive control
NLP	Nonlinear programming
NMBE	Normalized mean bias error
NMPC	Nonlinear model predictive control
RBC	Rule-based control
RC	Resistance-capacitance
SH	Space heating
SSE	Sum of squared errors
TES	Thermal energy storage
TLC	Telecommunication
VFC	Volume flow rate component
WCC	Weather compensation controller

Symbols

a	Characteristic coefficient of the radiator [−]
C	Heat capacitance [J/K]
c_p	Specific heat capacity [J/(kg•K)]
EP	Heat demand component price [NOK[1]/kWh]
F	Surface area [m^2]
H	Predictive horizon [h]
K	Equivalent heat transfer coefficient [W/(m^2•K)]
LP	Load demand component price [NOK/kW/month]
$\dot{m}$	Water mass flow rate [kg/s]
N	Number of radiator sections [−]
$\dot{Q}$	Heat flow rate [W]
R	Heat resistance [(m^2•K)/W]
T	Temperature [°C]
W	Weighting factor [−]
$\dot{Q}_p$	Peak heat rate of space heating system [W]
$\dot{V}_{air}$	Mechanical ventilation volume flow rate [m^3/h]
η_T	Temperature efficiency of heat recovery in the mechanical ventilation system [%]

Subscripts

env	Building envelopes
ia	Indoor air
in	Internal heat gains
ma	Internal thermal mass
n	Radiator section
oa	Outdoor air
ra	Radiator
sh	Space heating
ven	Ventilation
win	Windows
i,e	Indoor air and the building envelopes
o,e	Outdoor air and the building envelopes
i,m	Indoor air and the interior thermal mass

Superscripts

ref	Reference

[1] The currency rate between NOK and EUR can be found from https://www.xe.com/, in this study 1 EUR = 10.0 NOK.

based boilers, which makes peak load shaving even more imperative [16]. This is why many heating suppliers include the peak loads of heat users as an important component in their heating price models. For instance, a survey on Swedish heating price models finds that around 87% of the investigated heating price models take heat users' peak load into account, with the peak load charging fee accounting for 10–50% of the total heating cost for the heat users [17]. Therefore, the investigation of control techniques integrated with TESs has attracted lots of attention in recent years. Some researchers have investigated the possibility of reducing energy costs by introducing a borehole TES or a water tank as TESs into building heating systems and incorporating these TESs with control techniques. Rohde et al. introduced an ice TES and a borehole TES into an integrated heating and cooling system for a building complex. Afterwards, a dynamic optimization control technique was applied to optimize the system operation. The simulation results showed that the electricity use of the system was reduced by about 5% for the analysed year [18]. Similarly, Li et al. introduced a water tank and a borehole TES to a campus DH system, and incorporated these TESs with control techniques to improve system performance in terms of energy, economy and environment. The simulation results showed the effectiveness of the proposed method with an annual energy cost saving of 5–6% and CO_2 emission reduction of up to 8% [19]. However, integrating these TESs into buildings necessitates additional initial investment as well as maintenance costs. Buildings with large thermal mass, in fact, can be used as short-term TESs and have been proven to have large energy flexibility potential that allows peak load shaving and energy cost-saving [20]. Therefore, many researchers have started to explore the potential of integrating building thermal mass with control techniques, especially with MPC control strategy, to reduce the energy cost of the building heating system.

Dominković et al. investigated the potential of using building thermal mass as TESs for DH systems to optimize the energy systems' operation from the energy supply side, whose cost function was set to minimize the energy plants' investment, operating and maintenance costs, as well as their fuel costs and CO_2 emission costs. Simulation results showed that the building thermal mass could be used as intra-day storage to perform peak load shaving, and the operational cost saving of the investigated DH system was up to 4.6%, which was originated from the less utilized peak boilers and more effectively utilized solar thermal sources [21]. Pedersen et al. studied incorporating the building thermal mass as TES into an MPC scheme to perform peak load shaving and reduce heating costs for an individual electrical heating system. The cost function was set to minimize the electricity cost used by the SH system. Simulation results showed that around 6% of the electricity cost can be saved for the heat user [22]. Hu et al. designed an economic MPC controller for floor heating systems considering building thermal mass as TES. Simulation results showed that the designed MPC controller was able to utilize the thermal mass of the building to optimally shift energy use to low-price periods [23].

In summary, MPC assists in realizing the energy-efficient operation of the building heating system and ensuring satisfying indoor temperature. Moreover, the incorporation of the building thermal mass into an MPC controller as TES can lead to further improvements. However, as pointed in Ref. [24], the MPC's performance may vary depending on the building type and climate conditions. Therefore, further research on the application of MPC in various types of buildings under various climate conditions is required. Additionally, most previous research focused on the implementation of linear MPC in building heating systems. The dynamics of a building heating system, however, are usually nonlinear, especially in the case of a hydronic heating system connected to a DH system. Typical building heating systems connected to DH networks are comprised of hydronic heat emitters, such as radiators, that are characterized by nonlinearities in their heat rate output driven by the temperature difference between the radiator and room [25]. In a real DH system, the supply water temperature and the water flow rate for a radiator system are often used as the manipulated variables to achieve the desired heating rate. As a result, a nonlinear radiator model involving the supply water temperature and the water flow rate as the manipulated variables may support the simulation of the real control strategy. Therefore, the purpose of this study was to explore the utilization of nonlinear MPC (NMPC) for SH systems of university buildings in Nordic climates. A university building located in Trondheim, Norway, was selected as the case study, which has detailed measurements from the building energy management system to support the research. The proposed NMPC controller optimized the operation of the building SH system, making a trade-off between the heating costs and the indoor temperature, while taking into account future disturbances (weather and occupancy), energy price, and energy demand. The main contributions of this study are summarized as the following. Firstly, this study investigated a university building located in central Norway, whose building type and climate zone are rarely addressed by previous studies. Secondly, this research proposed and validated a nonlinear dynamic model that can be used in NMPC controllers, enabling a reasonable compromise between the model accuracy and computational tractability. Finally, a sensitivity study was carried out to assess the impact of building thermal mass on MPC performance, providing a full picture of MPC's effectiveness over a wide variety of building constructions, from lightweight to heavyweight.

The remainder of this article is organised as follows. Section 2 presents the modelling approach for the nonlinear system model, the formulation method of the objective function and constraints for the MPC, and the optimization framework to solve the MPC. Section 3 introduces the case study and research scenarios. Section 4 shows the model validation and the simulation results. Section 5 conducts a sensitivity analysis to investigate the impacts of building thermal mass on the MPC performance, and discusses the limitation of this study. Finally, in Section 6, conclusions are summarized.

2. Method

This section firstly presents the modelling methods for the building and SH system, and then detailed information on the formulation of MPC and the optimization framework is introduced.

2.1. System model

As highlighted in Ref. [8], the performance of MPC strongly depends on its embedded model, and developing an appropriate model is typically the most challenging part when designing an MPC controller. The main factor driving how to develop an appropriate model is the compromise between the model accuracy and computational tractability. The model must be accurate enough to predict the thermal behaviour of buildings, meanwhile, it should be as simple as possible to be computationally tractable and numerical stable [26]. Among commonly used models, the resistance-capacitance (RC) model has been demonstrated to be reliable and precise in predicting the thermal behaviour of buildings [27]. Therefore, an RC model was developed to capture the key characteristics of the building. The model was built by using the Modelica language, which is an object-oriented language to conveniently model physical systems [28]. Fig. 1 illustrates the components of the developed RC model and the heat fluxes exchanging among them.

The model mainly consists of four components including the

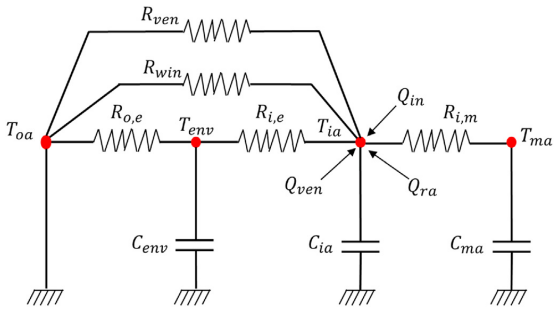

Fig. 1. Schematic of building resistance-capacitance model structure.

internal thermal mass, indoor air, building envelopes, and outdoor environment. Due to the low solar radiation in the analysed location during the study period, solar radiation was not taken into account in this study [29]. In addition, this study aimed to incorporate the building thermal mass as TES into the MPC controller to further improve the energy and economic performance of the system. Therefore, as presented in Fig. 1, a third-order RC model was developed with special attention to the thermal mass of building envelopes and the interior thermal mass, besides considering the thermal mass of indoor air, because their corresponding thermal inertia is necessary for the short-term TES in the intended MPC [10]. As for parameters' setting, it is commonly conducted either by estimation methods if the detailed information of the building geometry and thermal properties is well-known, or by system identification methods that use historical measured data to tune the values of the parameters, or a mix of both [30]. In this study, the parameters, including heat resistance and heat capacitance, were determined by an estimation method according to the available information of the investigated building and the recommended values in the European standard ISO 52016−1 [31]. Detailed calculations for the energy balances among each component given in Fig. 1 are shown in Equations (1)–(3) as the following:

$$C_{env} \times \frac{dT_{env}}{dt} = \frac{T_{ia} - T_{env}}{R_{i,e}} + \frac{T_{oa} - T_{env}}{R_{o,e}} \tag{1}$$

$$C_{ia} \times \frac{dT_{ia}}{dt} = \frac{T_{ma} - T_{ia}}{R_{i,m}} + \frac{T_{env} - T_{ia}}{R_{i,e}} + \frac{T_{oa} - T_{ia}}{R_{win}} + \frac{T_{oa} - T_{ia}}{R_{ven}} + \dot{Q}_{ra} + \dot{Q}_{ven} + \dot{Q}_{in} \tag{2}$$

$$C_{ma} \times \frac{dT_{ma}}{dt} = \frac{T_{ia} - T_{ma}}{R_{i,m}} \tag{3}$$

where R and C represent the heat resistance and capacitance, respectively, whose values were obtained by the estimation method. T denotes the temperature. Subscripts *ia*, *oa*, *env*, *ma*, *win*, and *ven* represent indoor air, outdoor air, building envelopes, internal thermal mass, windows, and ventilation, respectively. In addition, $R_{i,e}$ represents the heat resistance between the indoor air and the building envelopes. $R_{o,e}$ represents the heat resistance between the outdoor air and the building envelopes. $R_{i,m}$ represents the heat resistance between the indoor air and the interior thermal mass. $\dot{Q}_{in}$ is the internal heat gains, $\dot{Q}_{ven}$ is the heat flow rate from the mechanical ventilation system, and $\dot{Q}_{ra}$ is the heat flow rate from the radiator system. All the above heat capacitances, heat resistances, temperatures, and heat flow rates in Equations (1)–(3) are depicted in Fig. 1. Specifically, $\dot{Q}_{in}$ was obtained by historical measurement data and the Norwegian standard SN-NSPEK 3031 [32]. $\dot{Q}_{ven}$ is described as Equation (4) according to Norwegian standard SN-NSPEK 3031 [32]. $\dot{Q}_{ra}$ is determined by Equations (5)–(8). In this study, to get a more accurate dynamical description of the radiator, a discrete-element radiator model with N lumps was utilized and coupled to the RC model. This discrete-element radiator model was based on the European Standard EN 442−2 [33], which refers to it as the characteristic equation of the radiator. Meanwhile, previous studies have confirmed this model. In research [34], this discrete-element radiator model was developed and validated. Comparisons between simulation and experimental data indicated the effectiveness of the model. Similarly, in research [35], this discrete radiator model was validated using measured data, and the results suggested that the model is capable of accurately describing the dynamics of radiators. Furthermore, the Modelica IBPSA library, which was co-developed by research teams from RWTH Aachen University and the Lawrence Berkeley National Laboratory, etc., uses this discrete radiator model as well [36]. Finally, $\dot{Q}_{sh}$ is the total heat flow rate of the SH system as shown in Equation (9).

$$\dot{Q}_{ven} = 0.33 \times \dot{V}_{air} \times (1 - \eta_T) \times \left(T_{ia}^{ref} - T_{oa}\right) \tag{4}$$

$$\dot{Q}_{ra} = \sum_{n=1}^{N} \dot{Q}_n \tag{5}$$

$$\dot{Q}_n = K_n \times F_n \times (T_n - T_{ia}) \tag{6}$$

$$K_n = (T_n - T_{ia})^a \tag{7}$$

$$c_{p\_ra} \times \frac{dT_n}{dt} = c_{p\_w} \times \dot{m}_{ra} \times (T_{n-1} - T_n) - \dot{Q}_n \tag{8}$$

$$\dot{Q}_{sh} = \dot{Q}_{ven} + \dot{Q}_{ra} \tag{9}$$

where $\dot{V}_{air}$ describes the mechanical ventilation volume flow rate, which was determined by the measured data and the Norwegian standard SN-NSPEK 3031 [32]. T_{ia}^{ref} is the indoor temperature's reference value. η_T denotes the temperature efficiency of heat recovery in the mechanical ventilation system. For each radiator section n, $\dot{Q}_n$ represents the heat flow rate, T_n describes the average water temperature, F_n is the surface area and K_n is the equivalent heat transfer coefficient. a is a characteristic coefficient of the radiator, which can be obtained from the radiator manufacturer and was 0.28 in this study [37]. In addition, c_{p_ra} is the radiator material's heat capacity for each section n. c_{p_w} and $\dot{m}_{ra}$ are the specific water heat capacity and the water mass flow rate, respectively. The radiator model was nonlinear in this study due to the definition of K_n, and hence made the dynamic system model in this study nonlinear.

2.2. Formulation of model predictive control

In this study, the proposed MPC control strategy was used to improve the energy and economic performance of the SH system with satisfying indoor temperature. According to the research [17], heating price models generally include four components, fixed component (FXC), volume flow rate component (VFC), heat demand component (HDC), and load demand component (LDC). The FXC is the fee that a user must pay to stay connected to the DH

network. The VFC is a fee based on the volume of hot water required to provide heat to users and is intended to encourage a low return temperature. The HDC covers the cost of fuel and is charged based on the users' heat use. The LDC covers the costs of DH companies maintaining a certain level of capacity for peak loads, as well as the initial investment in new facilities, depreciation, and other expenses. It is charged based on the users' peak loads. However, the FXC and the VFC usually only account for around 1–2% of the total heating cost. The HDC and the LDC contribute to about 96% of the total heating cost. Therefore, the generalized heating price model in Ref. [38], which only considered the HDC and LDC, was utilized as well in this study. In addition, the achieved indoor temperature was used as an indicator to estimate the thermal environment. Finally, a multi-objective optimization problem was formulated with two conflicting optimization goals as presented in Equations (10)–(14).

Minimize:

$$\int_0^H EP(t) \times \dot{Q}_{sh}(t) \times dt + LP \times \dot{Q}_p + W \times \int_0^H \left(T_{ia}(t) - T_{ia}^{ref}(t)\right)^2 \times dt \tag{10}$$

subject to:

$$x(0) = A \tag{11}$$

$$\dot{x}(t) - F(x(t), u(t)) = 0 \tag{12}$$

$$\dot{Q}(t) \leq \dot{Q}_p \tag{13}$$

$$u_{min} \leq u(t) \leq u_{max} \tag{14}$$

where H denotes the prediction horizon and was 12 h in this study. $EP(t)$ and LP are the dynamic HDC price at time t, and the LDC price, respectively. These energy prices were gained from the website of the local DH company [39]. The HDC price varied between 0.5 and 0.8 NOK/kWh, and the LDC price was 47 NOK/kW/month in this study. $\dot{Q}_{sh}(t)$ is the heat rate at time t and $\dot{Q}_p$ denotes the peak heat rate which is a free parameter that needed to be optimized. The peak heat rate was defined as the maximum hourly heat use in the simulation period in this study according to the research [40]. The first two terms in Equation (10) are the heating cost, including the HDC and the LDC. In addition, the third term in Equation (10) is the achieved indoor temperature target, which is expressed as a quadratic form to avoid high violations of the desired indoor temperature. In MPC, the sum of squared errors (SSE) is usually used in the trajectory-tracking target of an objective function [41]. Meanwhile, previous research has shown that minimizing SSE in the reference signal tracking problem is effective regarding the control of building energy systems [42]. Afterwards, a weighting factor W was used in the achieved indoor temperature term to represent the "price" that the occupants are willing to pay for certain indoor temperatures, just like the energy prices in the heating cost term of the objective function [42]. In this study, the value of W was decided by the following criterion: when the deviation between the indoor temperature and the reference value was 0.5 K, the heating cost term and the achieved indoor temperature term contributed equally to the objective function. However, the value of W can be modified to other values based on the preferences of the system operators. $T_{ia}(t)$ and $T_{ia}^{ref}(t)$ are the achieved indoor temperature and the reference value at time t. The initial states of the dynamic system are described as Equation (11), and the values of these initial states are represented by the vector A. Equation (12) is the equality constraint of the formulated optimization problem, which is the dynamic system model developed in Section 2.1. Equation (13) and (14) are the inequality constraints of the formulated optimization problem, of which Equation (14) describes the bounds of manipulated variables. u_{min} and u_{max} are the lower and upper bounds of manipulated variables. In this study, the manipulated variables $u(t)$ was defined as $u(t) = [T_{sh}(t)\ \dot{m}_{sh}(t)]^T$, of which $T_{sh}(t)$ and $\dot{m}_{sh}(t)$ are the supply water temperature and the water flow rate of SH system.

2.3. Optimization framework

In this study, the optimization problem formulated in Section 2.2 was solved on the optimization platform JModelica. JModelica is a software platform for modelling, simulation, and optimization of complex dynamic systems that are based on the Modelica modelling language [43]. This section describes the main steps of the optimization framework, as shown in Fig. 2, which includes two main processes, the optimization process and the simulation process. At each time step, the future disturbances (weather and occupancy) and energy price, the objective function, and the equality and inequality constraints were incorporated into an optimization problem. This optimization problem was solved over the prediction horizon, and an optimized manipulated variable trajectory was generated for the next several hours to several days. However, only the optimized manipulated variables at the first time step were sent to the system dynamic model for the simulation process. In the simulation process, the system dynamic model was simulated under the first time step's disturbances by using the received optimized manipulated variables from the optimization process, and then yielded the state variables. These state variables were sent back to the system dynamic model used in the optimization process. The initial conditions of the system dynamic model were updated based on the feedback, and a new optimization problem was formulated and solved over the next prediction horizon.

The optimization algorithm applied in the optimization process is illustrated in the upper part of Fig. 2. The optimization problem in the optimization process was an infinite-dimensional problem, which is challenging for computers to handle. One common method to solve the infinite-dimensional problem is to discretize it firstly and optimize it afterwards by direct approaches [44]. The main idea of the direct approach is to discretize the original infinite-dimensional problem into a finite-dimensional nonlinear programming (NLP) problem, which can be solved using NLP solvers. The direct approaches can be classified into two categories: simultaneous and sequential methods. The simultaneous method discretizes the state and manipulated variables simultaneously, while the sequential method only discretizes the manipulated variables [44]. In this study, a direct collocation method belonging to the simultaneous category was used to transcribe the original infinite-dimensional problem into a finite-dimensional NLP problem, as shown in Fig. 2. The more detailed information about the direct collocation method was presented in previous research [45]. However, the discretised finite-dimensional NLP problem had the inequality constraints defined by the constraints of manipulated variables as described in Section 2.2, which led the Karush-Kuhn-Tucker (KKT) conditions of the NLP cannot be solved using the Newton's iteration method. To tackle this problem, an interior-point method was used to approximate the discretised NLP problem by an equality-constrained NLP problem. Finally, a local optimized manipulated variable trajectory was found by solving the KKT conditions of the equality-constrained NLP based on Newton's iteration method.

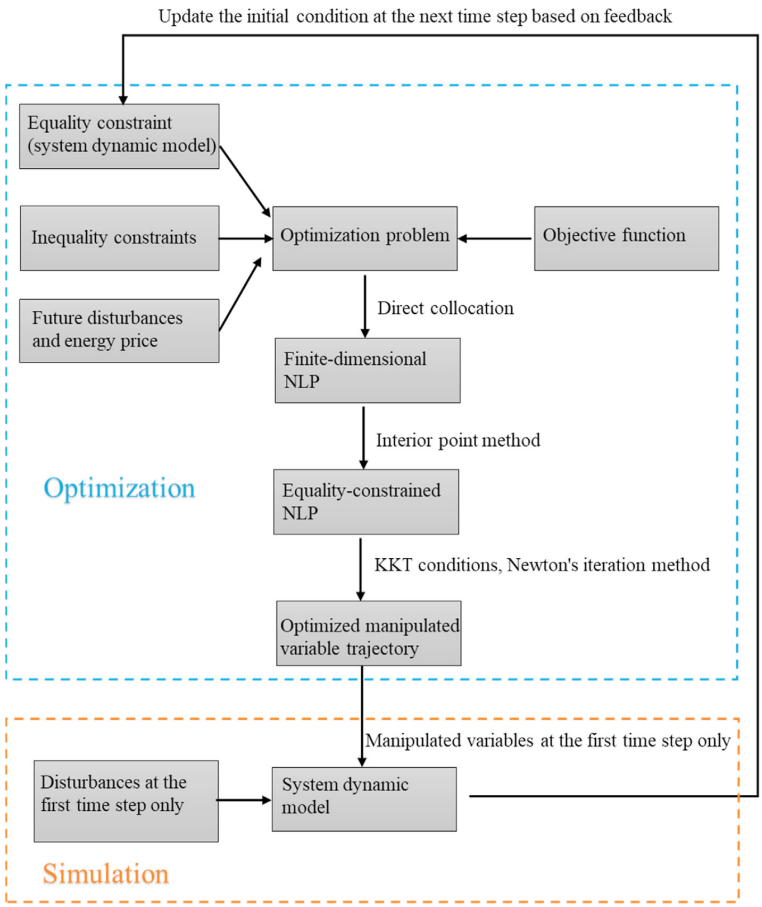

Fig. 2. Main steps of the optimization framework based on the optimization platform JModelica.

3. Case study and research scenarios

The method introduced in Section 2 was tested on a university building by simulation. The background of the case building and the research scenarios are illustrated in this section.

3.1. Background of the case building

A university building that is located in Trondheim, Norway was used to test the method proposed in Section 2, as shown in Fig. 3 a). The building was built in 1962, and it has six floors with a total floor area of 15 000 m^2. This building is mainly used for education, offices, and laboratory [46]. The SH system in this building is presented in Fig. 3 b). A heat exchanger in the building heat substation is used to connect the SH system and the DH system of the campus. The SH system includes a radiator system and a mechanical ventilation system. The radiator system is used to compensate for the heat loss to the environment through building envelopes, as well as heat the entering cold air due to air infiltration. The mechanical ventilation system consists of several air-handling units (AHUs) and is used to heat the entering cold air due to mechanical ventilation and provide the occupants with heated fresh air.

Table 1 summarizes the key information of the case building. The estimation method was used to acquire the heat resistance and heat capacitance values for the RC model proposed in Section 2.1. Firstly, the heat resistance and heat capacitance of each exterior thermal mass component exposed to the outdoor environment, such as the exterior walls or roof et al., were estimated by using the calculation method described in the European standard ISO 6946 [47]. Secondly, all of the building's exterior thermal mass components' heat resistances and capacitances were lumped into a single equivalent heat resistance and capacitance according to the suggested method in Ref. [48]. The equivalent heat resistance and capacitance reflected the overall thermal characteristics of all the exterior thermal mass components. When calculating the window's heat capacitance, one specific assumption was made: the window's thermal mass was assumed as zero because it could be neglected in comparison to the other exterior thermal mass components. The heat resistance and capacitance of interior thermal mass were estimated by using the same method described above. Finally, the estimated values for the heat resistance and capacitance marked in Fig. 1 are listed in Table 2.

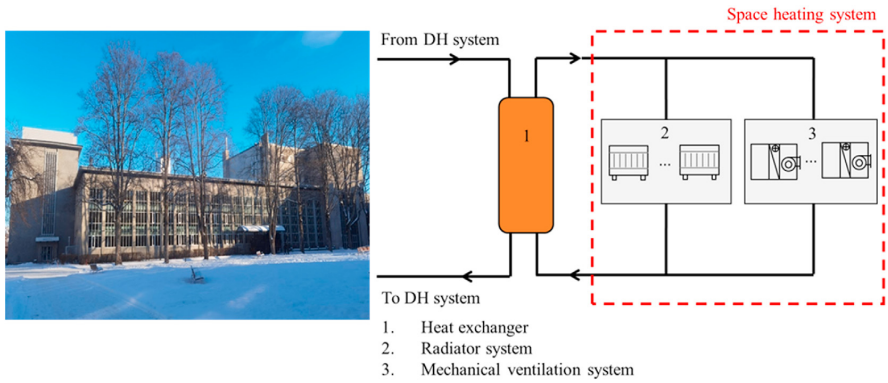

Fig. 3. The university building and its space heating system investigated as the case study in this research.

Table 1
The key parameters of the case building used to develop the building resistance-capacitance model, except the parameters of heat resistance and heat capacitance.

Category	Parameter	Value
Areas of building elements (m^2)	Exterior wall	5504
	Roof	4315
	Windows, doors, and glass	2293
	Interior wall	8256
U-values of building elements ($W/(m^2 \cdot K)$)	Exterior wall	0.35
	Roof	0.35
	Windows, doors, and glass	2.04
Specific heat capacities of elements ($J/m^2 \cdot K$)[a]	Exterior opaque	175 000
	Interior wall	75 000
	Air and furniture	10 000
Ventilation	Air infiltration (h^{-1})	2.70[b]
	Mechanical ventilation (h^{-1})	0–1.50[c]
	Temperature efficiency of heat recovery (%)	62
	Heated air volume (m^3)	73 600
Internal heat gains	Equipment, lighting, person (W/m^2)	5.5–19.0[c]

[a] Based on the thermal properties of the building, the European standard ISO 52016–1 [31], and the Norwegian standard SN-NSPEK 3031 [32].
[b] Air change rate at 50 Pa, n_{50}.
[c] Based on the measurement data and the Norwegian standard SN-NSPEK 3031 [32].

Table 2
The estimated values of heat resistance and heat capacitance of the case building used to develop the building resistance-capacitance model.

Parameter	Value
$R_{o,e}$	1.39×10^{-4} K/W
$R_{i,e}$	1.52×10^{-4} K/W
$R_{i,m}$	7.37×10^{-6} K/W
R_{win}	2.13×10^{-4} K/W
C_{env}	1.72×10^{9} J/K
C_{ia}	8.74×10^{7} J/K
C_{ma}	6.88×10^{8} J/K

3.2. Research scenarios

In this study, the occupancy schedule was based on historical measurement data and the Norwegian standard SN-NSPEK 3031 [32], and it was assumed to be perfectly predicted. In addition, the measured outdoor temperature from the campus energy management platform was used instead of the weather forecast information to explore the theoretical potential of the MPC. Two research scenarios were proposed in this study to evaluate the proposed MPC method, as shown in Fig. 4. The reference scenario was based on a rule-based control (RBC) strategy, which was the control strategy of the current SH system in the case study building. As presented in Fig. 4 a), the supply water temperature was controlled by a WCC according to the current outdoor temperature. In addition, to achieve better control performance than a simple on-off controller, a proportional (P) controller was used to adjust the SH system's water flow rate according to the deviation between the indoor temperature and its reference value. In this scenario, the optimal control of the SH system was difficult to realize, as the future disturbances (weather and occupancy), energy price, and the system dynamics were not able to be incorporated into the controllers.

The MPC scenario proposed in this study, however, was able to realize the optimal control of the SH system. As shown in Fig. 4 b), during the optimization process, the perfect future disturbance predictions (weather and occupancy) together with a candidate manipulated variable trajectory (the water flow rate and the supply

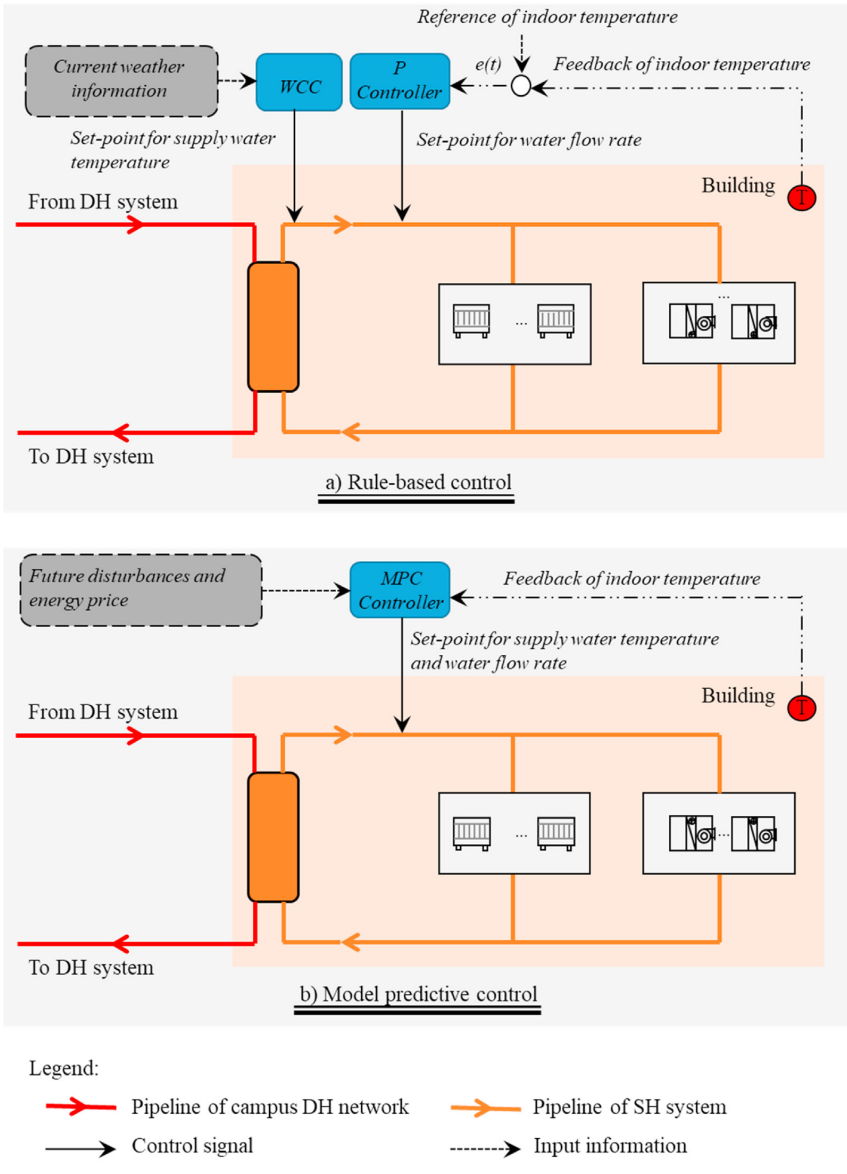

Fig. 4. Research scenarios utilizing different control strategies for the space heating system of case building.

water temperature) were used as simulation inputs for the dynamic system model. An iterative simulation was conducted over a certain prediction horizon. The optimizer assessed the objective function for each simulation run and updated the candidate manipulated variable trajectory until an optimized trajectory was found. Afterwards, only the optimized manipulated variables at the first time step were used to control the SH system of the building. At the next time step, the MPC updated the initial states of the dynamic system model based on the feedback from the building and repeated the optimization [8].

4. Results

The model validation is presented firstly in this section, and then one-week simulation results of the two research scenarios were evaluated in terms of achieved indoor temperature, peak load shaving, and heating cost.

4.1. Model validation

As explained in Section 2.1, the system model must be

sufficiently precise to predict the thermal behaviour of the building. To ensure the accuracy of the embedded model of the MPC controller, the dynamic system model proposed in Section 2.1 was validated by one month's measured data from the university energy management platform. A Building Energy Management System and a web-based Energy Monitoring System were utilized for the data collection on the campus building energy use. Besides the total energy use of the entire campus, the real-time energy use data of each building were intensively monitored, such as the heat use and the electricity use [46]. Therefore, these measured data of the case building with an hourly resolution were available to validate the developed model. For the validation process, a reasonable initial guess was given for the state variables of the dynamic system model, and the mechanical ventilation and internal heat gains specified in Table 1 were used as inputs for the system model. Afterwards, the dynamic system model was simulated under the given weather conditions and tracked the reference values of indoor temperature by using the RBC control strategy. The indoor temperature reference values were defined as 21 °C from 8:00 a.m. to 10:00 p.m., and 19 °C from 10:00 p.m. to 8:00 a.m., according to the measured data and modified by the recommended values of the Norwegian standard SN-NSPEK 3031 [32]. The simulation was conducted in the Dymola environment. Finally, the simulated hourly heat rate was compared to the measured hourly heat rate.

The validation results are presented in Fig. 5. The measured and simulated hourly heat rate of the SH system showed the same trend. During working hours, the hourly heat rate was higher because of the higher airflow rate of the AHUs. During non-working hours or weekends, the hourly heat rate was lower due to the lower airflow rate of the AHUs caused by fewer occupants. To quantify the deviation between the simulated and the measured data, coefficient of variation of the root mean square error (CV(RMSE)) and normalized mean bias error (NMBE) were used according to the ASHRAE Guideline 14−2014 [49]. ASHRAE Guideline 14−2014 requires the validation criteria within ±30% for CV(RMSE) and within ±10% for NMBE when using hourly data. In this study, the CV(RMSE) and the NMBE were 16.9% and 0.4%, respectively, which satisfied the requirements.

4.2. Indoor air temperature

The proposed MPC scenario was tested on the case building by simulation for one week (from 17th to 24th of January of 2018), and the simulation results for the achieved indoor air temperature are presented in this section. The simulation inputs including outdoor air temperature, internal heat gains and mechanical ventilation during this period are shown in Section Appendix A. The time period studied was a typical week during the heating season, with an average outdoor temperature of −5.4 °C and no holidays other than weekends. In addition, for the investigation of the MPC application in SH systems, a one-week simulation is a common time period. For example, both the research [50,51] adopted one week as the simulation period to investigate the MPC application in SH systems. Fig. 6 shows the indoor air temperature and the violation numbers of indoor temperature for different scenarios. The indoor temperature was collected every 10 min, and the violation number was counted when the difference between the indoor temperature and the reference value was higher than 0.5 K.

According to the measured data and modified by the Norwegian standard SN-NSPEK 3031 [32], the indoor temperature reference values for the two research scenarios were both defined as 21 °C from 8:00 a.m. to 10:00 p.m. and 19 °C from 10:00 p.m. to 8:00 a.m., as shown by the red solid line in Fig. 6 a). The P controller in the RBC scenario was tuned to achieve the required indoor temperature under all the conditions according to the principle of the actual building controller, as shown by the black dash line in Fig. 6 a). The proposed MPC scenario achieved better indoor temperature control performance than the conventional RBC. As shown by the blue solid line in Fig. 6 a), the over-heating phenomenon that occurred in the RBC scenario was effectively decreased in the MPC scenario, and the deviations between the indoor temperature and its reference values were decreased as well. Furthermore, as presented in Fig. 6 b), the violation numbers of the indoor temperature were also decreased from 374 to 153, with a reduction of nearly 59%, by the MPC control strategy.

4.3. Peak load shaving

As explained in Section 2.2, the LDC based on a heat use's peak load is one of the most important components in the heating price model, and hence peak load shaving is a critical measure to reduce heating cost. The proposed MPC in this study incorporated the building thermal mass as TES to shift the heat loads away from peak hours and realize peak load shaving.

Fig. 7 illustrates the heat rate for the RBC and the MPC scenario. In the RBC scenario, significant peak loads were observed around 8:00 a.m., when the reference values of the indoor temperature raised from 19 °C to 21 °C. Meanwhile, these peak hours coincided with the occupancy as well. The MPC scenario, however, handled this sudden rise of the reference indoor temperature by preheating the building 1 h ahead (from 7:00 a.m. to 8:00 a.m.). Afterwards, the MPC control strategy slightly lowered its heat supply for the

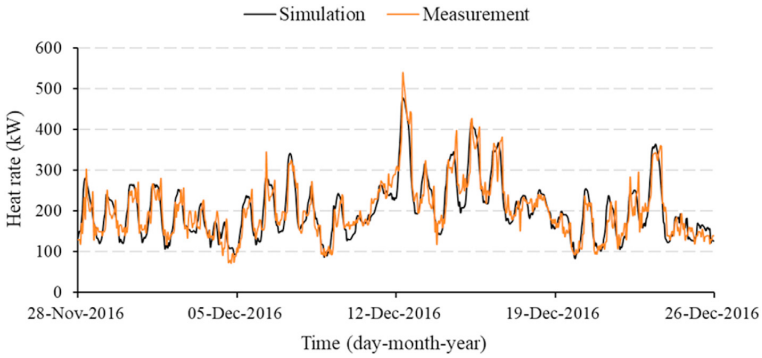

Fig. 5. Comparison between simulated and measured hourly heat use of the space heating system in the case building.

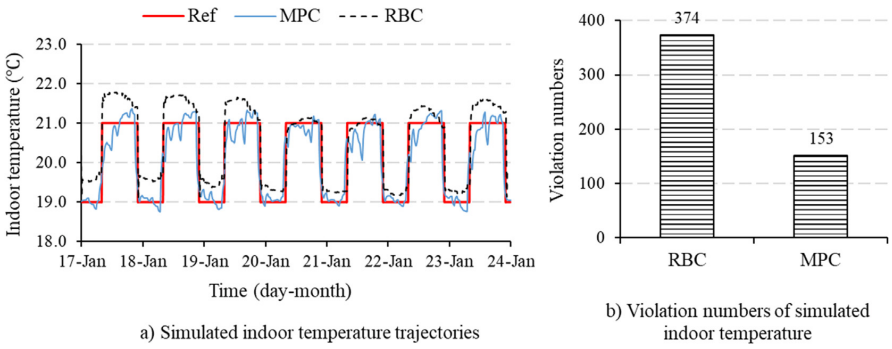

Fig. 6. Comparison between simulated indoor air temperatures in different research scenarios.

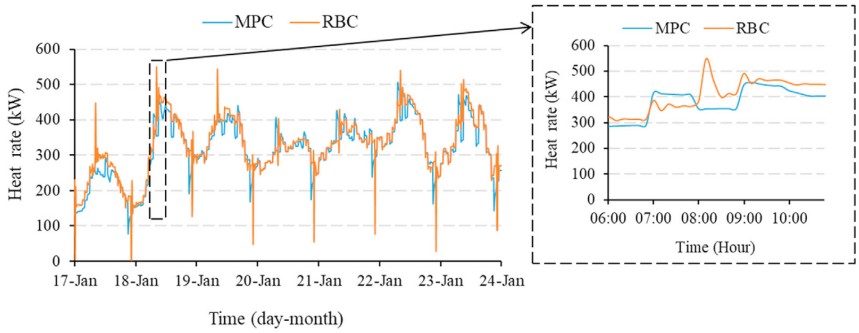

Fig. 7. Comparison between simulated heat rates of space heating system in different research scenarios.

building to avoid the peak loads that appeared in the RBC scenario. Meanwhile, the indoor temperature of the MPC scenario was controlled at its acceptable range, as shown in Section 4.2. Therefore, the MPC scenario shifted part of its heat load from the peak hours to the non-peak hours, and this heat load shifting contributed to its peak load shaving effect.

4.4. Heating cost

As described in Section 2.2, the heating price model used in this study only considered the LDC and the HDC. Therefore, the peak load and the heat use for the two scenarios are presented firstly in this section.

Fig. 8 presents the peak load and heat use for two scenarios. As mentioned in Section 4.3, the passive thermal mass storage of the building was integrated into the MPC control strategy to shave the peak load of the SH system. Therefore, the MPC scenario presented a significant peak load shaving effect, and the peak load was decreased from 555 kW to 506 kW, a reduction of almost 8.8% compared to the benchmark scenario RBC, as shown in Fig. 8 a). In addition, due to the elimination of the over-heating phenomenon, heating use was saved as well in the MPC scenario. As presented in Fig. 8 b), the MPC scenario saved the heat use from 55.4 MWh to 53.9 MWh, with a heat use saving of around 2.8%.

Finally, Fig. 9 presents the heating cost including the LDC and the HDC for different scenarios. In the MPC scenario, both the LDC and the HDC were reduced because of the peak load shaving and heat use saving effects brought by the MPC controller, as illustrated in Fig. 9. As a result, the MPC scenario saved the heating cost from 39 000 NOK to 37 500 NOK, a weekly heating cost saving of 3.8%.

5. Discussion

The impact of building thermal mass on the MPC performance is discussed firstly in this section to get more generalized conclusions, followed by the limitation of this study.

5.1. Impact of building thermal mass

The results from Section 4 assumed that the specific heat capacity of the building exterior opaque element was 175 000 J/m^2·K, which was based on the recommended value for the 'Heavy Class' construction in the European standard ISO 52016−1 [31]. However, the construction materials of building exterior envelopes vary from case to case, and hence the building exterior envelopes may range from 'Very light Class' to 'Very heavy Class' construction. Different construction classes of building exterior envelopes may lead to different TES capacities when the building thermal mass is used as short-term TES, and thus the MPC performance may be influenced. To get more generalized conclusions, a sensitivity analysis was conducted to investigate the impact of building thermal mass on the performance of MPC by involving further scenarios, as listed in Table 3. In Table 3, the specific heat capacities in different scenarios are set according to the reference values in the European standard ISO 52016−1 [31]. The only difference among each MPC scenario is the specific heat capacity settings of the building exterior opaque elements. Their corresponding benchmark scenarios RBC are introduced as well.

Fig. 10 presents the indoor temperature violation numbers for different scenarios. All the MPC scenarios demonstrated better indoor temperature control performance, which was observed by the

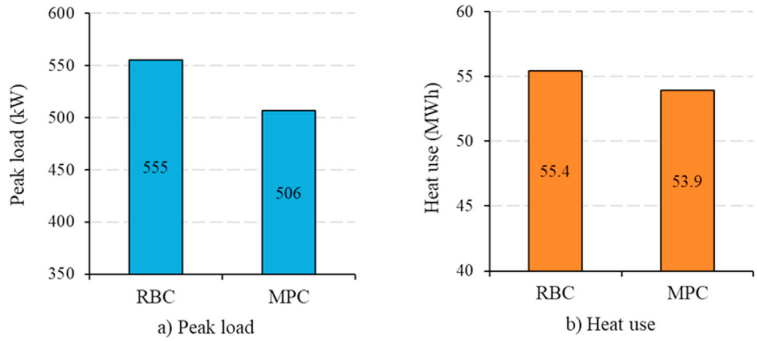

Fig. 8. Comparison between simulated peak loads and simulated heat use of space heating system in different research scenarios.

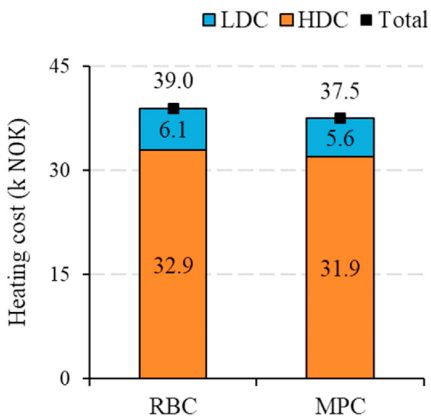

Fig. 9. Comparison between simulated heating costs of space heating system in different research scenarios.

Table 3
Research scenarios used for the sensitivity analysis, grouped according to different construction classes of building exterior envelopes.

Abbreviation	Specific heat capacity (J/m^2·K)	Class
Benchmark scenarios		
RBC_1	50 000	Very light
RBC_2	75 000	Light
RBC_3	110 000	Medium
RBC_4	175 000	Heavy
RBC_5	250 000	Very heavy
MPC scenarios		
MPC_1	50 000	Very light
MPC_2	75 000	Light
MPC_3	110 000	Medium
MPC_4	175 000	Heavy
MPC_5	250 000	Very heavy

much lower violation numbers compared to the corresponding RBC scenarios. In addition, there was no obvious difference between each MPC scenario regarding the violation numbers of indoor temperature.

Fig. 11 presents the peak load and heat use for different scenarios. As observed in Fig. 11 a), all the MPC scenarios, even the scenario MPC_1 with 'Very light' building exterior envelopes, took full advantage of the building thermal mass as TES to shift the heat load away from peak hours, which resulted in the peak load reduction ranging from 8.0% to 9.1% compared to their corresponding benchmark RBC scenarios. The MPC scenarios with larger building thermal mass tended to have a larger peak load shaving effect. However, in terms of heat use saving, all the MPC scenarios had almost the same ability, with savings of 2.7–2.8%, as presented in Fig. 11 b). Finally, Fig. 12 presents the heating cost for different scenarios. Similarly, all the MPC scenarios saved heating costs, which was brought by the reduction of the LDC and the HDC in the heating price model. However, due to the small difference of heat use saving in the MPC scenarios and the small share of the LDC in the heating price model compared to the HDC, the heating cost saving in different MPC scenarios demonstrated similar reductions, with the reductions changing from 3.6% to 3.9%. However, these reductions may present a larger difference if the share of the LDC in the heating price model is increased. Therefore, future work may consider how the heating price model influences the performance of the MPC controller. In addition, the objective function formulated in this study considered maintaining the indoor temperatures close to their setpoints as an important performance target, which may impair the potential of building thermal mass as TES, especially for the heavier building construction. Because the setpoint of indoor temperature was set as low as 19 °C during non-working hours (coincide with lower HDC price period). In contrast, the setpoint of indoor temperature was set as high as 21 °C during working hours (coincide with higher HDC price period). These indoor temperature setpoints were based on the recommended values in the Norwegian standard SN-NSPEK 3031 [32]. Due to this strict indoor temperature setting limitation, the MPC controller could not control the SH system to provide a bit more heat and store this heat in building thermal mass during the lower HDC price period, and then reuse this stored heat to reduce the heat output of SH system during the higher HDC price period. Therefore, future work may consider slacking the indoor temperature to a bit more flexible yet reasonable range, like setting as a range of 18 °C and 23 °C both in working and non-working hours, to fully unlock the flexibility of building thermal mass as TES.

5.2. Limitation

This study considered a perfect future disturbance prediction, and hence the actual weather data and occupancy schedule were provided for all the MPC controllers to explore the theoretical potential of MPC. However, any prediction contains some uncertainties that may lead to deviations between the predicted and

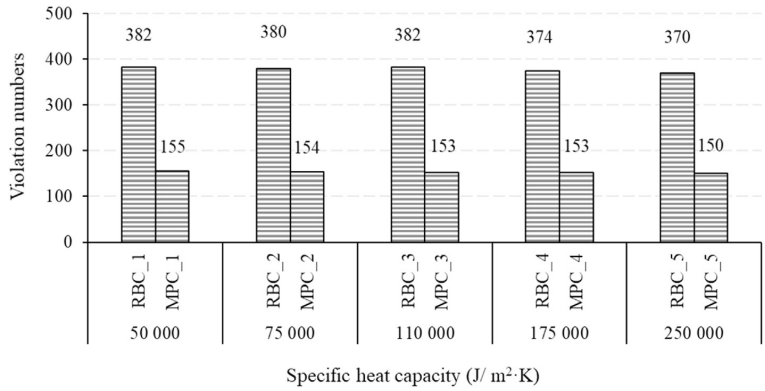

Fig. 10. Comparison between simulated indoor temperature violation numbers in different research scenarios dedicated to the sensitivity analysis.

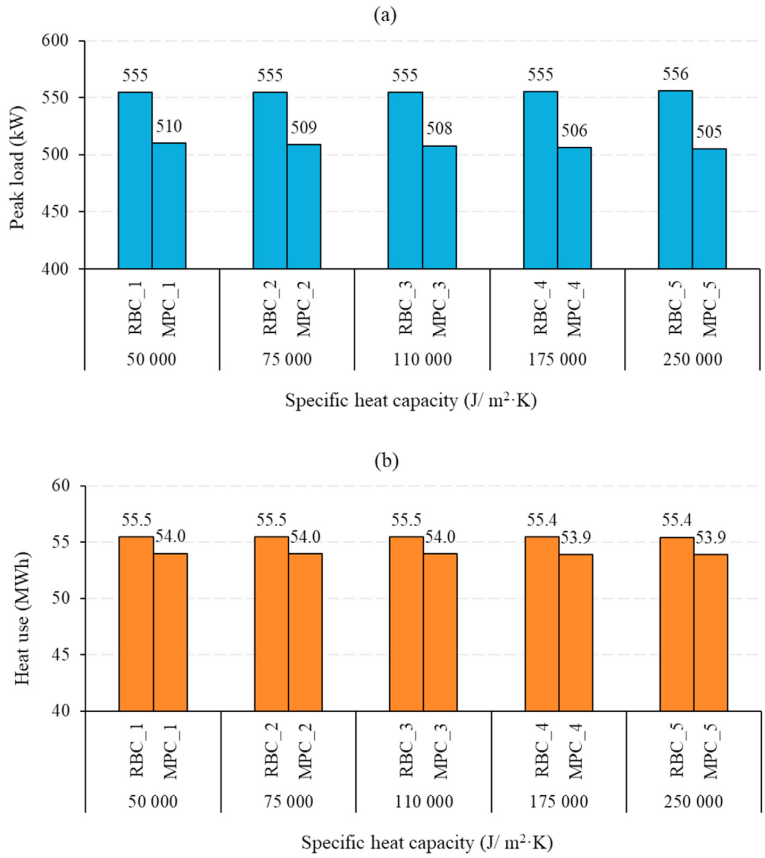

Fig. 11. Comparison between simulated peak loads and simulated heat use of space heating system in different research scenarios dedicated to the sensitivity analysis.

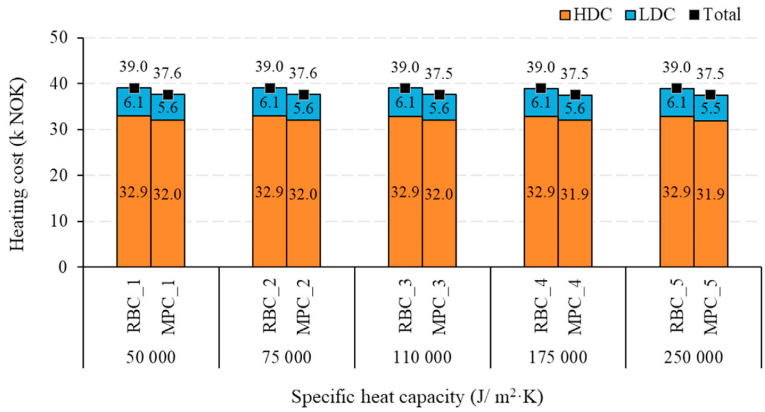

Fig. 12. Comparison between simulated heating costs of space heating system in different research scenarios dedicated to the sensitivity analysis.

the actual information. In the real-world implementation of MPC, the MPC controller is based on the prediction of future disturbances to generate control actions while the building is acted by the actual disturbances. When the prediction information varies largely from the actual disturbances, the MPC controller receives inaccurate prediction information and may generate incorrect control actions, which may impair its performance [42]. Many researchers have confirmed this challenge as well and pointed out that providing accurate prediction and uncertainty information was crucial to achieving reliable MPC performance. For example, Oldewurtel et al. reported that the MPC controllers based on the weather forecast data did not work well, especially when the actual weather differed largely from the forecast [52]. Henze et al. investigated the effect of weather forecast uncertainty on the MPC performance. The result was that MPC seemed to be a promising building control approach, but only in the presence of perfect weather forecasts [53]. Therefore, to improve and achieve the reliable performance of MPC, the uncertainty of future disturbances prediction may be considered and addressed in future work. Meanwhile, a sensitivity analysis may be conducted to assess how sensitive different building construction classes are to future disturbance prediction uncertainty.

6. Conclusions

In this study, an MPC strategy was proposed to realize the optimal control of the SH system, aiming to reduce the energy use, shave the peak load, and cut the heating costs with satisfying indoor temperature. Building thermal mass was incorporated into the MPC design to further improve the energy and economic performance of the SH system. A nonlinear system model was developed to be embedded into the MPC controller to predict the thermal behaviour of the building and the SH system. Considering the future disturbances and the energy price variations, the proposed MPC strategy controlled the output heat flow rate by optimizing the manipulated variables to achieve the maximum peak load shaving and heat use saving, while satisfying acceptable indoor temperatures. The proposed method was tested by the simulation method on a university building located in Norway. The MPC control strategy together with a conventional RBC strategy was evaluated in terms of achieved indoor temperature and heating cost.

Compared to the conventional RBC, the proposed MPC controller shaved the heat peak load by 8.8% and saved the heat use by 2.8% during one week. In addition, the MPC controller demonstrated the weekly heating cost saving of 3.8%, while providing an improved thermal comfort level in terms of indoor temperature, with a reduction of 59% for the indoor temperature violations.

To get more generalized conclusions, a sensitivity analysis was conducted to investigate the impact of building thermal mass on the MPC performance. Simulation results showed that even with 'Very light' building exterior envelopes, the MPC controller still took full advantage of the building thermal mass as TES to shift the heat load away from peak hours, although larger building thermal mass tended to have a larger peak load shaving effect.

Finally, this study considered a perfect future disturbance prediction to explore the theoretical potential of the MPC controller. To achieve these theoretical potentials, further research should be included to tackle the uncertainty of future disturbance prediction.

Declaration of competing interest

The authors declare that they have no known competing financial interests or personal relationships that could have appeared to influence the work reported in this paper.

Acknowledgement

The authors gratefully acknowledge the support from the Research Council of Norway through the research project Understanding behaviour of district heating systems integrating distributed sources under the FRIPRO/FRINATEK program (project number 262707).

Appendix A. Simulation inputs

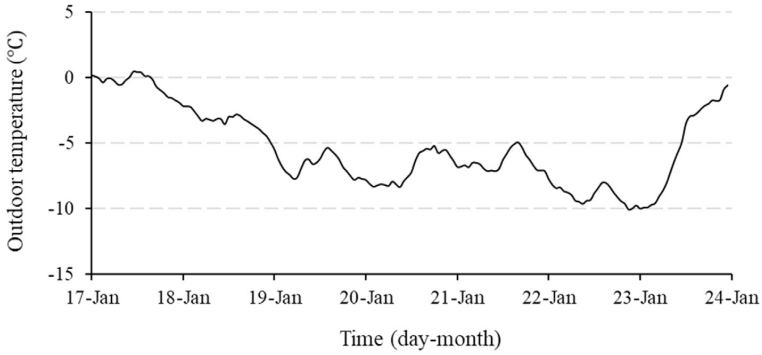

Fig. A 1. Measured outdoor air temperature for the simulation period

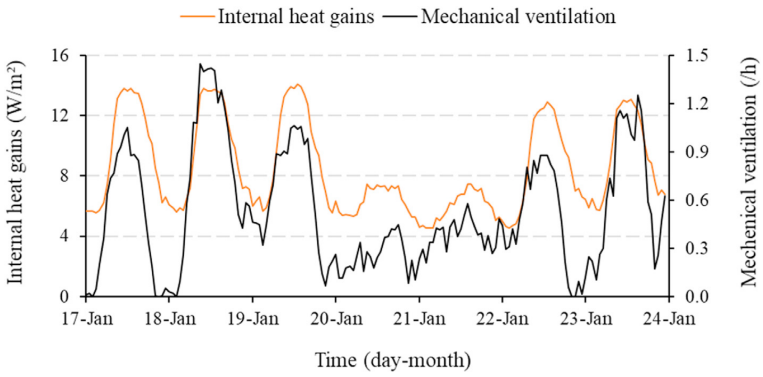

Fig. A 2. Estimated internal heat gains and mechanical ventilation for the simulation period

References

[1] European Commission. Energy performance of buildings directive. 2021. https://ec.europa.eu/energy/topics/energy-efficiency/energy-efficient-buildings/energy-performance-buildings-directive_en. [Accessed 6 April 2021].

[2] European Commission. Heating and cooling. 2022. https://energy.ec.europa.eu/topics/energy-efficiency/heating-and-cooling_en. [Accessed 11 March 2022].

[3] Sorrentino M, Acconcia M, Panagrosso D, Trifirò A. Model-based energy monitoring and diagnosis of telecommunication cooling systems. Energy 2016;116:761–72.

[4] D'Aniello F, Sorrentino M, Rizzo G, Trifirò A, Bedogni F. Introducing innovative energy performance metrics for high-level monitoring and diagnosis of telecommunication sites. Appl Therm Eng 2018;137:277–87.

[5] Sorrentino M, Bruno M, Trifirò A, Rizzo G. An innovative energy efficiency metric for data analytics and diagnostics in telecommunication applications. Appl Energy 2019;242:1539–48.

[6] European Commission. Heating and cooling. 2021. https://ec.europa.eu/energy/topics/energy-efficiency/heating-and-cooling_en?redir=1. [Accessed 6 April 2021].

[7] Li H, Nord N. Transition to the 4th generation district heating-possibilities, bottlenecks, and challenges. Energy Proc 2018;149:483–98.

[8] Killian M, Kozek M. Ten questions concerning model predictive control for energy efficient buildings. Build Environ 2016;105:403–12.

[9] Hilliard T, Kavgic M, Swan L. Model predictive control for commercial buildings: trends and opportunities. Adv Build Energy Res 2016;10(2):172–90.

[10] Aoun N, Bavière R, Vallee M, Aurousseau A, Sandou G. Modelling and flexible predictive control of buildings space-heating demand in district heating systems. Energy 2019;188:116042.

[11] Seal S, Boulet B, Dehkordi VR. Centralized model predictive control strategy for thermal comfort and residential energy management. Energy 2020;212:118456.

[12] Ławryńczuk M, Ocłoń P. Model Predictive Control and energy optimisation in residential building with electric underfloor heating system. Energy 2019;182:1028–44.

[13] Privara S, Široký J, Ferkl L, Cigler J. Model predictive control of a building heating system: the first experience. Energy Build 2011;43(2–3):564–72.

[14] Široký J, Oldewurtel F, Cigler J, Prívara S. Experimental analysis of model predictive control for an energy efficient building heating system. Appl Energy 2011;88(9):3079–87.

[15] Weissmann C, Hong T, Graubner C-A. Analysis of heating load diversity in German residential districts and implications for the application in district heating systems. Energy Build 2017;139:302–13.

[16] Guelpa E, Barbero G, Sciacovelli A, Verda V. Peak-shaving in district heating systems through optimal management of the thermal request of buildings. Energy 2017;137:706–14.

[17] Song J, Wallin F, Li H. District heating cost fluctuation caused by price model shift. Appl Energy 2017;194:715–24.

[18] Rohde D, Knudsen BR, Andresen T, Nord N. Dynamic optimization of control setpoints for an integrated heating and cooling system with thermal energy storages. Energy 2020;193:116771.

[19] Li H, Hou J, Hong T, Ding Y, Nord N. Energy, economic, and environmental analysis of integration of thermal energy storage into district heating systems using waste heat from data centres. Energy 2021;219:119582.

[20] Le Dréau J, Heiselberg P. Energy flexibility of residential buildings using short term heat storage in the thermal mass. Energy 2016;111:991–1002.
[21] Dominković D, Gianniou P, Münster M, Heller A, Rode C. Utilizing thermal building mass for storage in district heating systems: combined building level simulations and system level optimization. Energy 2018;153:949–66.
[22] Pedersen TH, Hedegaard RE, Petersen S. Space heating demand response potential of retrofitted residential apartment blocks. Energy Build 2017;141:158–66.
[23] Hu M, Xiao F, Jørgensen JB, Li R. Price-responsive model predictive control of floor heating systems for demand response using building thermal mass. Appl Therm Eng 2019;153:316–29.
[24] Petersen S, Bundgaard KW. The effect of weather forecast uncertainty on a predictive control concept for building systems operation. Appl Energy 2014;116:311–21.
[25] Frederiksen S, Werner S. District heating and cooling, vol. 579. Studentlitteratur Lund; 2013.
[26] Cígler J, Gyalistras D, Široky J, Tiet V, Ferkl L. Beyond theory: the challenge of implementing model predictive control in buildings. In: Proceedings of 11th Rehva world congress. Clima; 2013.
[27] Bacher P, Madsen H. Identifying suitable models for the heat dynamics of buildings. Energy Build 2011;43(7):1511–22.
[28] The Modelica association. 2020. https://www.modelica.org/. [Accessed 20 December 2020].
[29] Hagos DA, Gebremedhin A, Zethraeus B. Solar water heating as a potential source for inland Norway energy mix. Journal of Renewable Energy 2014;2014.
[30] Ogunsola OT, Song L. Review and evaluation of using RC thermal modeling of cooling load prediction for HVAC system control purpose. ASME International Mechanical Engineering Congress and Exposition 2012;45233:735–43.
[31] European standard. Energy performance of buildings- Energy needs for heating and cooling, internal temperatures and sensible and latent heat loads-Part 1: calculation procedures; ISO 52016-1:2017.
[32] Standard norge. Energy performance of buildings- Calculation of energy needs and energy supply (in Norwegian). SN-NSPEK 2020;3031.
[33] EN 442-2 Radiators and convectors - Part 2: test methods and rating. 2014.
[34] Xu B, Fu L, Di H. Dynamic simulation of space heating systems with radiators controlled by TRVs in buildings. Energy Build 2008;40(9):1755–64.
[35] Li H, Nord N. Operation strategies to achieve low supply and return temperature in district heating system. In: E3S web Conf, vol. 111; 2019, 5022.
[36] IBPSA Project 2019;1.
[37] Purmo. Panel radiators. 2020. https://www.purmo.com/docs/Purmo_tech_catalogue_panel_radiators_full_PR_05_2017_EN_PL.pdf. [Accessed 22 December 2020].
[38] Li H, Hou J, Tian Z, Hong T, Nord N, Rohde D. Optimize heat prosumers' economic performance under current heating price models by using water tank thermal energy storage. Energy 2022;239:122103.
[39] Statkraft varme at Tronheim. Products and services. 2020. https://www.statkraftvarme.no/globalassets/0/statkraft-varme/produkter-og-tjenester/prisark/jan-2021/trondheim-bedrift-uten-volumledd-bt1.pdf. [Accessed 17 December 2020].
[40] Li H, Hou J, Hong T, Nord N. Distinguish between the economic optimal and lowest distribution temperatures for heat-prosumer-based district heating systems with short-term thermal energy storage. Energy 2022:123601.
[41] Raković SV, Levine WS. Handbook of model predictive control. Springer; 2018.
[42] Drgoňa J, Arroyo J, Cupeiro Figueroa I, Blum D, Arendt K, Kim D, et al. All you need to know about model predictive control for buildings. Annu Rev Control 2020;50:190–232.
[43] Åkesson J, Årzén K-E, Gäfvert M, Bergdahl T, Tummescheit H. Modeling and optimization with Optimica and JModelica. org—languages and tools for solving large-scale dynamic optimization problems. Comput Chem Eng 2010;34(11):1737–49.
[44] Amrit R, Rawlings JB, Biegler LT. Optimizing process economics online using model predictive control. Comput Chem Eng 2013;58:334–43.
[45] Hou J, Li H, Nord N, Huang G. Model predictive control under weather forecast uncertainty for HVAC systems in university buildings. Energy Build 2021:111793.
[46] Guan J, Nord N, Chen S. Energy planning of university campus building complex: energy usage and coincidental analysis of individual buildings with a case study. Energy Build 2016;124:99–111.
[47] European standard. Building components and building elements- Thermal resistance and thermal transmittance- Calculation methods; ISO 6946. 2017.
[48] Yang S, Wan MP, Chen W, Ng BF, Zhai D. An adaptive robust model predictive control for indoor climate optimization and uncertainties handling in buildings. Build Environ 2019;163:106326.
[49] ASHRAE. ASHRAE Guideline 14–2014, measurement of energy, demand, and water savings. ASHRAE Atlanta; 2014.
[50] Gholamibozanjani G, Tarragona J, De Gracia A, Fernández C, Cabeza LF, Farid MM. Model predictive control strategy applied to different types of building for space heating. Appl Energy 2018;231:959–71.
[51] Hedegaard RE, Pedersen TH, Knudsen MD, Petersen S. Towards practical model predictive control of residential space heating: eliminating the need for weather measurements. Energy Build 2018;170:206–16.
[52] Oldewurtel F, Parisio A, Jones CN, Gyalistras D, Gwerder M, Stauch V, et al. Use of model predictive control and weather forecasts for energy efficient building climate control. Energy Build 2012;45:15–27.
[53] Henze GP, Kalz DE, Felsmann C, Knabe G. Impact of forecasting accuracy on predictive optimal control of active and passive building thermal storage inventory. HVAC R Res 2004;10(2):153–78.

PAPER 2

Hou J, Li H, Nord N, Huang G. Model predictive control under weather forecast uncertainty for HVAC systems in university buildings. Energy and Buildings. 2022; 257: 111793.

APPENDIX- PUBLICATIONS

Energy & Buildings 257 (2022) 111793

Contents lists available at ScienceDirect

Energy & Buildings

journal homepage: www.elsevier.com/locate/enb

Model predictive control under weather forecast uncertainty for HVAC systems in university buildings

Juan Hou [a,*], Haoran Li [a], Natasa Nord [a], Gongsheng Huang [b]

[a] Department of Energy and Process Technology, Norwegian University of Science and Technology, Kolbjørn Hejes vei 1 B, Trondheim 7491, Norway
[b] Department of Architecture and Civil Engineering, City University of Hong Kong, Y6621 AC1 Tat Chee Ave, Kowloon, Hong Kong

ARTICLE INFO

Article history:
Received 26 March 2021
Revised 22 November 2021
Accepted 15 December 2021
Available online 20 December 2021

Keywords:
Nonlinear model predictive control
Weather forecast uncertainty
Error model
Thermal comfort
Peak load
Heating cost

ABSTRACT

In buildings, there are two yet conflicting optimization goals: 1) minimize energy use and energy cost and 2) maximize thermal comfort. Model predictive control (MPC) is an ideal control strategy to deal with the above conflicting optimization goals. However, one challenge hindering the implementation of the MPC in buildings is the weather forecast uncertainty. This study aimed to improve the performance of the MPC under weather forecast uncertainty by introducing an error model. The error model used a straightforward approach based on easily measurable and accessible data to improve the quality of weather forecast data. The proposed method was tested by simulation on a university building located in Norway, while the detailed information and measured data from this real building were used to develop and validate the building model used in this study. Results showed that the MPC with the error model was able to achieve almost the full theoretical potential of the MPC in terms of the energy cost and thermal comfort, with 3.4% of weekly energy cost saving and 73% of indoor temperature violation numbers reduction compared to a conventional rule-based controller. In contrast, due to the existence of weather forecast error and a lack of error addressing mechanism, the MPC without error model did not perform well and gave the energy cost saving of only 0.7% and the indoor temperature violation numbers even increased by 20%. Meanwhile, the results indicated the introduction of the error model always benefited the MPC performance even under the condition of the low error of weather forecast. This study may facilitate the real application of the MPC in buildings.
© 2021 The Authors. Published by Elsevier B.V. This is an open access article under the CC BY license (http://creativecommons.org/licenses/by/4.0/).

1. Introduction

The energy use in buildings in the European Union (EU) countries accounts for 40% of the final energy use and 36% of the greenhouse gas emissions [1]. In EU countries, 76% of this energy goes towards comfort control in buildings for heating, ventilation and air conditioning (HVAC) [2]. Therefore, it is essential to investigate the methods for reducing energy use and energy cost of these systems. However, the demand for better comfort in buildings is expected to continue as it has been within the last few decades. This leads to two main yet conflicting optimization goals occurring in buildings: 1) maximize the thermal comfort, and 2) minimize both the energy use and the energy cost. Model predictive control (MPC) is an ideal control strategy to deal with the above conflicting optimization goals [3–6]. A building MPC uses a dynamic building model to predict the future thermal behaviour of the building and generates a control vector that minimizes a certain objective function over the prediction horizon in the presence of disturbances and constraints. The objective function used in an MPC can combine several conflicting optimization goals, and an optimal trade-off between these conflicting optimization goals may be secured by running the MPC control strategy [5,7].

Researchers have proven that MPC controllers could result in a theoretical potential for energy saving and improved thermal comfort compared to other conventional rule-based controllers (RBCs). A test case for simulating predictive control in building systems shows the theoretical annual energy saving for heating, lighting, and ventilation of 7% with improved thermal comfort [8]. An on–off controller and an MPC system in a combined solar thermal collector and heat pump system are simulated and the results show that the MPC performs better by providing desired thermal comfort and less energy use, and finally giving the 9% theoretical operating cost saving [9]. A simulation study of MPC applied to the HVAC system in a typical Swiss office building shows a comparison of the MPC with an RBC, and the results indicate theoretical energy saving of about 17% while providing an improved level of comfort [10]. In [11], an MPC strategy for space heating (SH) demand in

* Corresponding author.
E-mail address: juan.hou@ntnu.no (J. Hou).

https://doi.org/10.1016/j.enbuild.2021.111793
0378-7788/© 2021 The Authors. Published by Elsevier B.V.
This is an open access article under the CC BY license (http://creativecommons.org/licenses/by/4.0/).

Nomenclature

AHU	Air-handling unit
CV(RMSE)	Coefficient of variation of the root mean square error
DH	District heating
EDC	Energy demand component
FXC	Fix component
FDC	Flow demand component
HVAC	Heating, ventilation and air conditioning
LDC	Load demand component
MEPS	MetCoOp ensemble prediction system
MPC	Model predictive control
NLP	Nonlinear programming
NMBE	Normalized mean bias error
NMPC	Nonlinear model predictive control
NWPM	Numerical weather prediction model
RBC	Rule-based controller
RC	Resistance-capacitance
RMSE	Root mean square error
SH	Space heating
TES	Thermal energy storage
WCC	Weather-compensation controller

buildings is compared to a conventional weather-compensation controller (WCC). The MPC proves to give operating cost savings theoretically, while maintains decent thermal comfort conditions. Furthermore, in recent years, the effectiveness of MPC in real-world applications has been reported. MPC in real buildings and experiment chambers is described in the article [12]. These examples demonstrate that MPC can save 10–30% of energy use, with the potential for improved thermal comfort for building occupants [13–16]. However, some challenges are hindering the wide-scale implementation of the MPC in buildings. One challenge is the uncertainty of the weather forecast. A building MPC is based on the prediction of future weather, and many studies considered a perfect weather forecast for MPC. However, any prediction has some uncertainties that may influence system performance such as energy use and thermal comfort. Therefore, the MPC controller may receive inaccurate information, leading to incorrect control actions that may cause thermal discomfort or energy waste [12].

Oldewurtel et al. found that the MPC controllers using the weather forecast data did not perform well, especially when the actual weather varied from the forecast [17]. Henze et al. evaluated the impact of weather forecast uncertainty on the MPC performance. The conclusion was that MPC appeared to be a promising building control strategy, but only when perfect weather forecasts were available [18]. Lamoudi et al. assessed the MPC performance considering the uncertainty of the weather forecast. They found the degradation of weather forecast quality generated an increase in the energy cost. A maximum increase of 4% in energy cost was noted due to weather forecast uncertainty [19]. Hedegaard et al. reported that the performance of an MPC controller may be reduced by 4% in terms of heating cost savings due to the weather forecast error [20]. Zavala et al. also pointed out that using accurate forecasts and uncertainty information was critical to achieving reliable MPC performance [21].

One way to address the effect of the weather forecast uncertainty on MPC is to use the stochastic MPC [17,22]. However, for building systems, a stochastic MPC often requires an additive Gaussian disturbance model that does not hold for the weather uncertainty. Furthermore, building systems are usually nonlinear systems. The exact solutions for the stochastic MPC for nonlinear systems subject to non-Gaussian disturbances are, in general, computationally intractable [23,24]. Introducing weather forecast models is another way to tackle the weather forecast uncertainty in MPC. Henze et al. introduced several short-term weather forecast models to improve the performance of MPC. Those weather forecast models predicted the future weather based on historical patterns such as using the same data as the previous day, typical days of a month, etc. It was highlighted that almost the full theoretical potential of MPC may be realized by using simple but accurate short-term weather forecast models [18]. Zavala et al. used a machine learning approach to obtain weather information for MPC [21]. Salque et al. developed a self-learning artificial neural networks model for weather forecast considering the uncertainty of weather [25]. Chakraborty et al. proposed a support vector machine regression model to predict future weather variables [26]. However, the above weather forecast models either need lots of historical data or are too complex. In actual buildings, MPC controllers may require more straightforward approaches based on easily measurable and accessible data.

In summary, applying an MPC controller to HVAC systems has a high potential for improving the performance of buildings in terms of thermal comfort, energy use, and energy cost. However, the effect of weather forecast uncertainty on the MPC performance has to be considered. Furthermore, as Petersen and Bundgaard in [27] pointed out, the effect of weather forecast uncertainty on the MPC performance depended on the climatic regions and test cases. Further research should be conducted to test the concept in other types of climates and buildings. Therefore, this paper presented a simulation-based study to apply an MPC controller for the SH system in a university building located in Trondheim, Norway. The detailed information of building properties and the measured data from the building energy platform were used to develop and validate the building model. An error model was introduced to improve the quality of the weather forecast data, and hence improve the performance of the MPC controller. Two metrics were used to evaluate the MPC performance: the heating cost saving and the achieved indoor air temperature. Shaving the peak load of heat users has great potential for contributing to the heating cost saving. According to a survey in [28], 87% of the existing heating price models in Sweden consider heat users' peak load, and the charging fee based on peak load accounts for 10–50% of the total heating bill. Many researchers have proven both by simulation and real-life experiments that integrating thermal energy storage (TES) is one way to shave the peak load and consequently reduce the heating cost in a heating system. Romanchenko et al. investigated the benefits of applying TESs (a hot water tank or the building thermal mass) in district heating (DH) systems to decrease peak load by developing a detailed techno-economic optimisation model for a DH system of Göteborg, Sweden. The results showed that TESs smoothed the heat load variations of the DH system and the annual heating cost was decreased by 1–2% compared to the scenario without any TES [29]. Pedersen et al. conducted a simulation-based study to investigate how the economic MPC schemes for SH operation can utilize the building thermal mass as the TES in buildings to perform peak load shift and reduce heating cost. The simulation results showed that the proposed method shifted the energy use away from peak load periods and yielded increased heating cost savings (up to approximate 6%) [30]. Dominković et al. explored the potential of utilizing existing building thermal

mass as the TES in a DH system to optimize the operation of the energy system by coupling a detailed building simulation model with a linear optimization model of the energy system. The results showed that the economic savings in operational costs of the studied DH system were in the range of 0.7%–4.6%, not taking the cost of smart controls into account [31]. Kensby et al. conducted a pilot test of utilizing the building thermal mass as the TES in DH systems to decrease the heat load daily variation by periodically overheating and underheating buildings. The results indicated that buildings could tolerate variations in heat deliveries while still maintaining a good indoor climate. In this way, the heat generation could be moved from peak load plants that run on fossil fuels to base load plants with better fuel economy and lower environmental impact [32]. Therefore, the proposed MPC scheme in this study took into account the TES techniques as well.

The novelty of this study is summarized as the following. Firstly, this research introduced an accurate yet simple error model to handle the uncertainty of weather forecast in MPC. This error model only required easily measurable and accessible data, but could explore almost the full theoretical potential of the MPC without increasing any computational complexity. Secondly, a university building located in Norway was used as the case study to test the MPC performance by simulation, which is rarely addressed for this climatic region and building type by existing studies. Thirdly, real historical measured data were used to develop and validate the dynamic building model used in the MPC controller, which provides a good compromise between model accuracy and problem complexity. This study may facilitate the real application of MPC in buildings.

The remainder of this article is organised as follows. Section 2 presents the proposed MPC concept for SH system control in buildings, the modelling approach, the formulation method for MPC, the algorithm for solving nonlinear MPC (NMPC), and the method used for developing the error model. Section 3 introduces the case study, the weather forecast data, and the research scenarios. Section 4 explains the model validation, the evaluation of the error model and the simulation results. Section 5 shows a new set of simulation-based experiments and the corresponding results. Meanwhile, the limitation of this study is discussed. Finally, in Section 6, conclusions are summarized.

2. Method

This section first presents how the MPC concept is applied to the SH system control in buildings, and then the detailed information on building modelling, optimization formulation, optimization algorithm, and the error model for weather forecast are introduced.

2.1. Description of the MPC concept for space heating system control in buildings

Fig. 1 illustrates the fundamental components of an MPC controller for SH system control in buildings. The basic elements of the MPC are 1) a dynamic building model, 2) predictions of future disturbances, 3) an optimization algorithm, and 4) an objective function and constraints. At each time step, the predictions of the future disturbances (e.g., weather) together with the candidate MPC control inputs are used as simulation inputs to the dynamic building model. This simulation is carried out over the prediction horizon. The optimizer evaluates the objective function for each simulation run and adapts the candidate MPC inputs until an optimal solution is obtained. Only the first control inputs are supplied to the building. At the next time step, the MPC changes the initial states of the dynamic building model according to the actual states of the building, and restart the optimization [5]. In this study, occupant behaviour was assumed to be perfectly predicted and the focus was on the consideration of uncertainty in weather predictions.

MPC may realize the optimal management of building energy including energy cost saving and thermal comfort improving, as the future disturbances, energy price, energy demand, and the dynamic building model are incorporated into the controller. In addition, energy storage strategies can be easily integrated into the MPC design. Energy storage strategies together with control strategies play an increasingly important role in shifting peak energy demand and reducing the energy cost in buildings. Some researchers have explored the potential for energy cost saving by integrating water tank or borehole (TES) into building-related systems [33,34]. However, incorporating these (TESs) into buildings requires additional initial investment and maintenance cost. Buildings with large thermal capacity themselves may be utilized as energy storages that present opportunities for peak load shifting and energy cost saving. In this study, the passive thermal mass storage of the buildings was integrated into the MPC control strategy to realize the optimal management of building energy, energy peak load shaving, and energy cost saving.

2.2. Dynamic building model

MPC inherently requires an appropriate dynamic building model, which is then used for the computation of the optimal control inputs. This model must be sufficiently precise to yield valid predictions of building thermal behaviour, but at the same time, the model must be as simple as possible for the optimization task to be computationally tractable and numerically stable [35]. Amidst several models, the simplified resistance–capacitance (RC) model has proven to provide more robust and accurate estimates of the building thermal behaviour [36,37]. Therefore, a simplified RC model was developed by Modelica language in this study to grasp the key characteristics of buildings. The components for this simplified building model and the heat fluxes exchanged among them are presented in Fig. 2.

The individual model parts are the outdoor environment, building envelopes, indoor air, and internal thermal mass. Choosing a suitable order for the building RC model has been discussed in a significant amount of literature, especially in the literature considering the identifiability of parameters when the RC model is a grey-box model [36,38,39]. When the RC model is a grey-box model, the first and second-order RC models are preferred in many studies due to the feasibility of parameter identification. However, these first and second orders of RC models generally lump the entire thermal mass of a building to a single capacity or only make the distinction between the fast dynamics of indoor air and the slow dynamics of the structural mass [39]. The distinction between the exterior thermal mass (envelopes including exterior walls and roof et al. exposed to outdoor environment) and the interior thermal mass (e.g. interior walls, furniture et al. not exposed to outdoor environment) is not made. In this study, the RC model structure with particular attention to the building envelopes' thermal mass and the interior thermal mass was proposed, because their respective thermal inertia is necessary for the short-term heat storage in the intended MPC [11,40]. Therefore, a third-order thermal RC model that had heat capacitances for the building envelopes, interior thermal mass and indoor air was formulated in this study as shown in Fig. 2. The values of the heat resistance and the heat capacitance may be obtained by two common methods: 1) direct calculation based on the detailed information of the building, or 2) system identification technique [41]. Corresponding, the RC models can be classified as white-box models or grey-box models. The white-box RC models applied in many studies have shown satisfactory prediction performance when the detailed

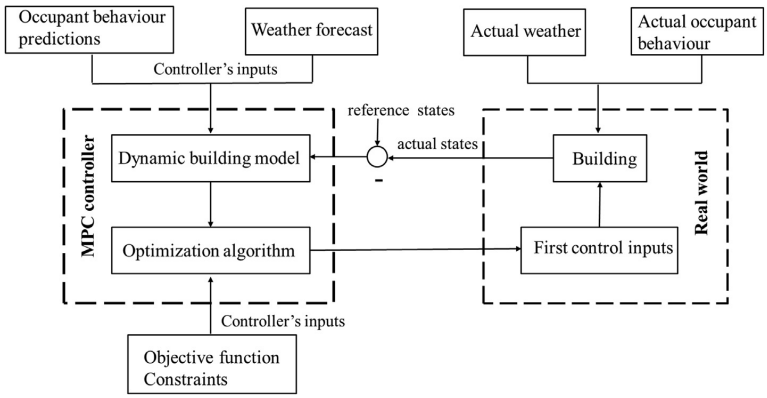

Fig. 1. Model predictive control applied to space heating system control in buildings.

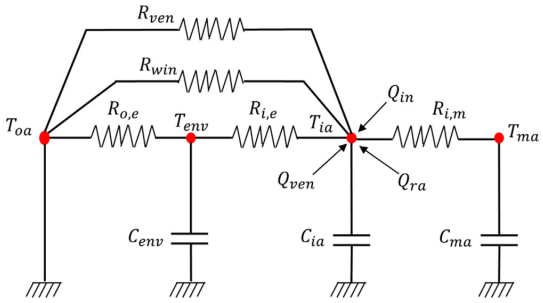

Fig. 2. Schematic of simplified dynamic building model.

information of the building are known [40,42,43]. In this study, the proposed RC model was a white-box model, because the values of the heat resistance and the heat capacitance were determined by direct calculation method based on the known information of the case building and the reference values in the related standard [44]. Furthermore, solar radiation was not considered in this study due to the low solar radiation in the studied area during the studied period [45]. The energy balances for the building envelopes, the indoor air, and the internal thermal mass given in Fig. 2 are illustrated as the following Equations (1-3):

$$C_{env} \cdot \frac{dT_{env}}{dt} = \frac{T_{ia} - T_{env}}{R_{i,e}} + \frac{T_{oa} - T_{env}}{R_{o,e}} \tag{1}$$

$$C_{ia} \cdot \frac{dT_{ia}}{dt} = \frac{T_{ma} - T_{ia}}{R_{i,m}} + \frac{T_{env} - T_{ia}}{R_{i,e}} + \frac{T_{oa} - T_{ia}}{R_{win}} + \frac{T_{oa} - T_{ia}}{R_{ven}} + \dot{Q}_{ra} + \dot{Q}_{ven} + \dot{Q}_{in} \tag{2}$$

$$C_{ma} \cdot \frac{dT_{ma}}{dt} = \frac{T_{ia} - T_{ma}}{R_{i,m}} \tag{3}$$

where C and R represent the heat capacitance and resistance, which were obtained by the direct calculation method in this study. T is the temperature. Subscripts env, ia, oa, ma, win, and ven denote building envelopes, indoor air, outdoor air, internal thermal mass, window, and ventilation (including infiltration and mechanical ventilation), respectively. In addition, $R_{i,e}$ is the heat resistance between the indoor air and the building envelopes, $R_{o,e}$ is the heat resistance between the outdoor air and the building envelopes, and $R_{i,m}$ is the heat resistance between indoor air and interior thermal mass. $\dot{Q}_{in}$ is the internal heat gains, which was obtained based on historical measurement data and related standards in this study [46]. $\dot{Q}_{ven}$ is the heat flow rate from mechanical ventilation system, and it is described as Equation (4) according to Norwegian standard [46]. $\dot{Q}_{ra}$ is the heat flow rate from the radiator system. All the introduced heat capacitances, thermal resistances, temperatures, and heat flow rates in Equations (1-3) are marked in Fig. 2.

A discrete-element radiator model was employed in this study to achieve a more precise dynamical description of the radiator, as shown in Fig. 3. This radiator model is based on the European Standard EN 442–2 [47], which refers to this radiator model as the characteristic equation. Furthermore, previous studies have confirmed this discrete form of the radiator model, in which the radiator is divided into multiple parts while the indoor air is treated as uniform [48–52]. This discrete radiator model is also used by the Modelica IBPSA library [53], which is co-developed by research teams from RWTH Aachen University and the Lawrence Berkeley National Laboratory, etc. Finally, this discrete radiator model is validated using measured data in the study [54], and the results suggest that the discrete radiator model is capable of accurately describing the dynamics of radiators. Therefore, $\dot{Q}_{ra}$ is determined by Equations (5-8). Finally, $\dot{Q}$ is the total heat flow rate supplied from the building heat substation and presented as Equation (9).

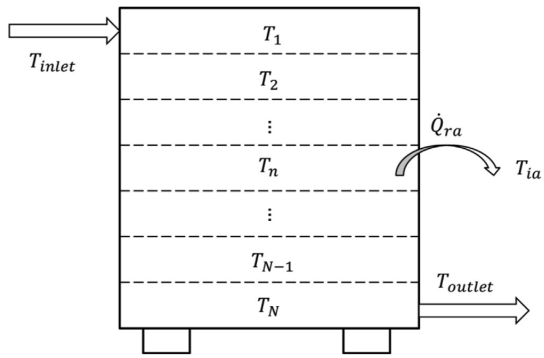

Fig. 3. Discrete-element model of radiator.

$$\dot{Q}_{ven} = 0.33 \cdot \dot{V}_{air} \cdot (1 - \eta_T) \cdot \left(T_{ia}^{ref} - T_{oa}\right) \tag{4}$$

$$\dot{Q}_{ra} = \sum_{n=1}^{N} \dot{q}_n \tag{5}$$

$$\dot{q}_n = K_n \cdot F_n \cdot (T_n - T_{ia}) \tag{6}$$

$$K_n = (T_n - T_{ia})^a \tag{7}$$

$$c_{ra} \cdot \frac{dT_n}{dt} = c_w \cdot \dot{m}_{ra} \cdot (T_{n-1} - T_n) - \dot{q}_n \tag{8}$$

$$\dot{Q} = \dot{Q}_{ven} + \dot{Q}_{ra} \tag{9}$$

where T_{ia}^{ref} is the reference value of indoor temperature. $\dot{V}_{air}$ is the mechanical ventilation volume flow rate, which was obtained from measurement data and related standards in this study [46]. η_T is the temperature efficiency of heat recovery in the mechanical ventilation system. $\dot{q}_n$ is the heat flow rate in each radiator section n. T_n denotes the average water temperature in the radiator section n, as shown in Fig. 3. F_n is the surface area of radiator section n. K_n denotes the equivalent heat transfer coefficient which depends on the temperature difference between the radiator water and the ambient temperature, as described in Equation (7). a is a characteristic coefficient of the radiator, which can be gained from radiator manufacturers and was 0.28 in this study [55]. c_{ra} represents the heat capacity of the radiator material for each section n. c_w and $\dot{m}_{ra}$ denote the specific heat capacity and the flow rate of water, respectively. With the current definition of K_n, it is not constant and makes the energy balance equation of the radiator nonlinear. Therefore, the dynamic building model in this study was nonlinear, and the nonlinearity was mainly derived from the radiator as shown in Equation (7).

2.3. Optimization formulation

This study aimed to reduce energy cost and maintain thermal comfort in buildings by utilizing the MPC. In general, the heating price models include four components, including fixed component (FXC), flow demand component (FDC), energy demand component (EDC), and load demand component (LDC). The FXC represents the cost that a user needs to pay for staying in the DH network. The FDC is a cost charged based on the volume of hot water needed to deliver the heat to a user. The EDC is used to cover the production cost of DH companies and charged based on users' heat use. The LDC is used to cover DH companies' cost to maintain a certain level of capacity for peak heat rate, investment costs of new facilities, depreciation, etc., and it is charged based on the peak load of users. However, the FXC and the FDC usually account for a very small share in existing models. In contrast, the EDC and the LDC together account for up to 96% of the total heating cost [28,56]. Therefore, only the EDC and the LDC were considered for the heating price model in this study, and a multi-objective optimization problem including two conflicting optimization goals is formulated as Equations (10-14).

Minimize:

$$\int_0^H EP(t) \cdot \dot{Q}(t) \cdot dt + LP \cdot \dot{Q}_p + W \cdot \int_0^H \left(T_{ia}(t) - T_{ia}^{ref}(t)\right)^2 \cdot dt \tag{10}$$

subject to:

$$x(0) = A \tag{11}$$

$$\dot{x}(t) - F(x(t), u(t)) = 0 \tag{12}$$

$$\dot{Q}(t) \le \dot{Q}_p \tag{13}$$

$$u_{min} \le u(t) \le u_{max} \tag{14}$$

where H is the predictive horizon, which was 12 h in this study. $EP(t)$ and $\dot{Q}(t)$ are the EDC heating price and the heat rate at time t, respectively. LP is the LDC heating price, and $\dot{Q}_p$ is the peak heat rate which is a free parameter needed to be optimized. In this study, the EDC heating price fluctuated around 0.6 NOK[1]/kWh, and the LDC heating price was 47 NOK/kW/month, which were obtained from the local DH company, Statkraft Varme, in Trondheim [57]. The first and the second terms in Equation (10) are the heating cost including EDC and LDC. In addition, the thermal comfort target was integrated into the objective function as a quadratic form to track the reference values of indoor air temperatures and avoid high indoor temperature violations, as shown with the third term in Equation (10). The quadratic form, also known as the Sum of Squared Errors, is commonly used in the trajectory-tracking target of an objective function [4,58–61]. Similar to the energy price in the heating cost term of the objective function, the thermal comfort term uses W to represent the "price" that occupants are willing to pay for their thermal comfort [4]. The value of W in this study was determined by the following criteria: when the deviation between indoor temperature and its reference value was 0.5 °C, the thermal comfort term and the heating cost term in the objective function contributed equally. However, it can be adjusted to other values based on the system operators' preferences. $T_{ia}(t)$ and $T_{ia}^{ref}(t)$ are the actual indoor temperature and its reference value at time t. Equation (11) is the initial states of the dynamic building system, and the vector A is the values of these initial states. Equation (12) is the nonlinear dynamic building model as described in Section 2.2. The system state vector $x(t)$ was defined as $x(t) = [T_{env}(t) T_{ia}(t) T_{ma}(t) T_n(t)]^T$. The control input $u(t)$ was defined as $u(t) = [T_s(t) \dot{m}_w(t)]^T$. $T_s(t)$ and $\dot{m}_w(t)$ are the supply water temperature and the water flow rate of SH system at time t. u_{min}, and u_{max} are the lower and the upper limits for the control variables.

2.4. Optimization algorithm

As described in Section 2.2 and Section 2.3, the optimization problem in this study was an NMPC optimization problem. However, in practice, the solution to such NMPC dynamic control problems can be challenging due to the nonlinearity of the dynamic model. In this study, we proposed the use of a direct method to formulate a standard nonlinear programming (NLP) problem. The basic idea of the direct method is to transcribe the original infinite-dimensional problem into a finite-dimensional NLP, which can be solved by using an NLP solver. The direct methods can be categorized into sequential and simultaneous approaches. The sequential approach, also known as control parametrization, only discretizes the control variables. The simultaneous approach, however, discretizes the state and control variables simultaneously [62]. Direct collocation is a simultaneous approach and was used in this study.

A time grid $t_0 < t_1 < \cdots < t_N$ was generated over the predictive horizon $[t_0, t_0 + H]$ by dividing the period into N intervals with a constant time step equal to the sample time. The continuous states $x(t)$ were discretized, and the discrete states on the time grid points t_k was denoted as s_k. Meanwhile, the control variables $u(t)$ was parameterized on the same time grid typically as piecewise constant, with control parameters q_k, which yielded on each interval $[t_k, t_{k+1}]$ a constant control $u(t) = q_k$. In addition, on each collocation interval $[t_k, t_{k+1}]$, a set of d collocation times $t_{k,i} \in [t_k, t_{k+1}]$

[1] The currency rate between NOK and EUR can be found from https://www.xe.com/, in this study 1 EUR=10.0 NOK.

was chosen, with $i = 0, 1, \cdots d$. The trajectory of each state on the time interval $[t_k, t_{k+1}]$ was approximated by a polynomial $p_k(t, v_k)$ which had the property $p_k(t_{k,i}, v_k) = v_{k,i}$. Therefore, the states of the dynamic system as described in Equation (12) were discretized, and the collocation-based integration of the state dynamic on a time interval $[t_k, t_{k+1}]$ starting from the initial value s_k hinged on solving the collocation Equation (15). The above discretization processes are illustrated in Fig. 4.

$$c_k(v_k, s_k, q_k) = \begin{bmatrix} v_{k,0} - s_k \\ \dot{p}_k(t_{k,1}, v_k) - F(v_{k,1}, t_{k,1}, q_k) \\ \vdots \\ \dot{p}_k(t_{k,i}, v_k) - F(v_{k,i}, t_{k,i}, q_k) \\ \vdots \\ \dot{p}_k(t_{k,d}, v_k) - F(v_{k,d}, t_{k,d}, q_k) \end{bmatrix} = 0 \tag{15}$$

In addition to solving the collocation Equations (15) for $k = 0, 1, \cdots N-1$, continuity across the interval boundaries was required, i.e. the lengths of red solid lines presented in Fig. 4 should be zero. Therefore, Equation (16) was required and held for $k = 0, 1, \cdots N-1$.

$$p_k(t_{k+1}, v_k) - s_{k+1} = 0 \tag{16}$$

The direct collocation method yielded an NLP, and it can typically be written in the following general form as Equations (17-21).

Minimize:

$$\sum_{k=0}^{N-1} L_k(v_k, s_k, q_k) \cdot (t_{k+1} - t_k) + P \tag{17}$$

subject to:

$$x(0) = s_0 \tag{18}$$

$$c_k(v_k, s_k, q_k) = 0 \tag{19}$$

$$p_k(t_{k+1}, v_k) - s_{k+1} = 0 \tag{20}$$

$$h(s_k, v_k) \leq 0 \tag{21}$$

where $k = 0, 1, \cdots N-1$. Equation (17) is the general form of Equation (10) after discretization by using the direct collocation method. The first rectangular quadrature term is the approximation of integration terms in Equation (10), and the second term is the parameter to be optimized in Equation (10). In addition, Equation (18) is the system initial states. Equations (19) and (20) are the collocation conditions and the continuity conditions as described above. Equation (21) is the path constraints and the general form of Equations (13) and (14) after discretization.

Finally, the above NLP is solved by using the NLP solvers. There are many methods available for solving the NLP. The most common methods are based on either active-set sequential quadratic programming or interior-point methods. The active-set sequential quadratic programming is to iteratively approximate the NLP by a quadratic program, and the interior-point method can be viewed as approximating the NLP by an equality-constrained NLP [63]. In this study, the NLP problem got rid of the inequality constraints by using the interior-point method firstly, and then a local optimum to the NLP was found by solving the first order Karush-Kuhn-Tucker condition, using the iterative techniques based on Newton's method. The above optimization algorithm was illustrated by the flow chart in Fig. 5, and the open-source software JModelica.org was used as the optimization platform to achieve the above process in this study.

2.5. Error model for weather forecast

One challenge with the direct use of the weather forecast data in the MPC is the uncertainty of forecasted data resulted from the uncertainty of the numerical weather prediction model (NWPM). Inherent uncertainty lies in the NWPM due to the stochastic nature of atmospheric processes, the imperfect knowledge of the weather model's initial conditions, as well as modelling errors [17]. Therefore, the exact actual weather data may not be reflected by the forecasted data well. The forecast weather data in this study considered only the outdoor temperature due to the low solar radiation in the studied area during the studied period [45]. The actual outdoor temperature acting on the building can be decomposed as in Equation (22):

$$T_k = \overline{T}_k + e_k \tag{22}$$

where T_k and $\overline{T}_k$ denote the actual and the NWPM forecasted outdoor temperature at the time step k, and e_k is the prediction error of NWPM at the time step k.

To improve the prediction of future disturbance acting on the building, the prediction error of the NWPM, e_k, may be estimated by an error model. The prediction error of the NWPM means the deviation between the actual outdoor temperature and the corresponding NWPM forecasted data. In practice, the current prediction error is known, because of the availability of the measured data. According to [20,64], this study assumed that the unknown future prediction error of the NWPM was correlated to the known current prediction error, however, the correlation decreased along with the increasing time distance. For example, the NWPM predic-

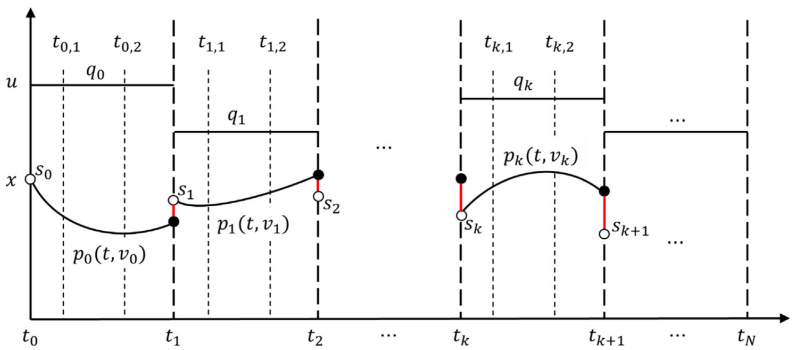

Fig. 4. Illustration of direct collocation for approximating the dynamic system with $d = 2$

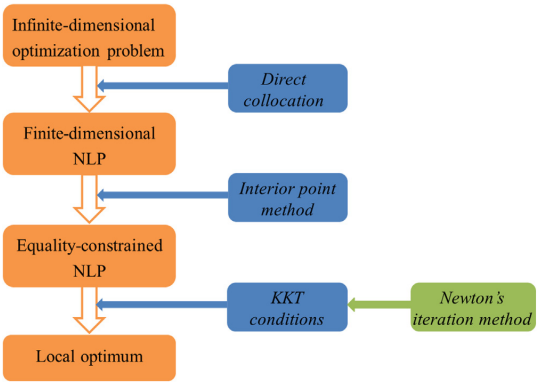

Fig. 5. The flow chart of the optimization algorithm.

tion error in the near future was approximated by the current prediction error, while the NWPM prediction error in the distant future had a limited relationship with the current prediction error and hence the forecasted data from the NWPM was the best estimation for the outdoor temperature. The error model is illustrated as Equation (23).

$$e_{k+t} = r(t) \cdot e_k, t = 1, 2, 3, \cdots, 12 \tag{23}$$

where e_{k+t} is the estimated prediction error of the NWPM in the future, e_k is the known prediction error of the NWPM at the current time step k. Parameter $0 \leq r(t) \leq 1$ which is a weighting function, describes the decreasing predictive effect of the current prediction error to the future NWPM prediction error along with the increasing time distance. In this study, the value of parameter $r(t)$ was given by Equation (24) based on [64]. Therefore, the future outdoor temperature was estimated as Equation (25).

$$r(t) = 1 - \frac{e^{t-6}}{1 + e^{t-6}}, t = 1, 2, 3, \cdots, 12 \tag{24}$$

$$T_{k+t} = \overline{T}_{k+t} + e_{k+t}, t = 1, 2, 3, \cdots, 12 \tag{25}$$

where T_{k+t} is the estimated outdoor temperature in the future, $\overline{T}_{k+t}$ is the forecasted outdoor temperature from NWPM, and e_{k+t} is the estimated prediction error of NWPM given by the error model as illustrated by Equation (23).

Fig. 6 illustrates an example that how the future outdoor temperature is estimated. The outdoor temperature is estimated based on the forecasted data from the NWPM and the estimated prediction error of the NWPM given by the error model. The current prediction error e_k is calculated based on the NWPM forecasted and the corresponding actual outdoor temperature at the current time step k, as shown in Fig. 6. The NWPM prediction error for the near future highly relies on and is approximated by the current prediction error, as shown in Fig. 6 for the time step $k + t$ when t has small values. However, the correlation is decreasing along with the increasing time distance, as shown in Fig. 6 for the time step $k + t$ when the value of t is increasing. Finally, the correlation disappears for the distant future and the estimated future outdoor temperature is only determined by the NWPM forecasted data, as shown in Fig. 6 for the time step $k + t$ when t is 12.

3. Case study and scenarios

The proposed method in Section 2 was tested by a university building. The background of the case study, the weather forecast data from the NWPM, and the research scenarios are introduced in this section.

3.1. Background of the case study

A university building located in Trondheim, Norway, was chosen as the case study as shown in Fig. 7 a). Built in 1962, it has six floors with a floor area of 15 026 m^2. The main functions of this building are education, offices, and laboratory [65]. Fig. 7 b) presents the SH system in this building and how an MPC controller is used as a supervisory control for the SH system. As presented in Fig. 7 b), the SH system in this building is connected to a DH system via a heat exchanger in the building heat substation. The SH system consists of a radiator system and a mechanical ventilation system. The radiator system is responsible for compensating the heat transmission to the environment through building envelopes and heating the incoming cold air caused by air infiltration. The mechanical ventilation system, which consists of several air-handling units (AHUs), is responsible for heating the incoming cold air caused by mechanical ventilation and supplying the heated and fresh air for occupants in the building. The MPC controller used as a supervisory control in this study aimed to optimize the set-points for supply water temperature and water flow rate of the SH system.

The key information about the building is listed in Table 1. The values of the heat resistance and the heat capacitance for the RC

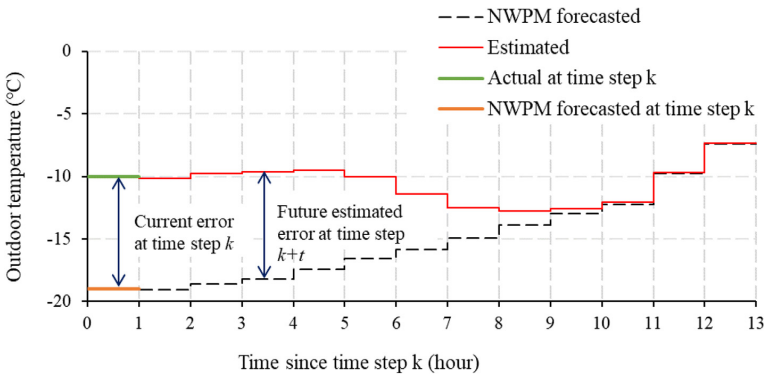

Fig. 6. The relationship between estimated outdoor temperature, NWPM forecasted data and prediction error.

a) The university building

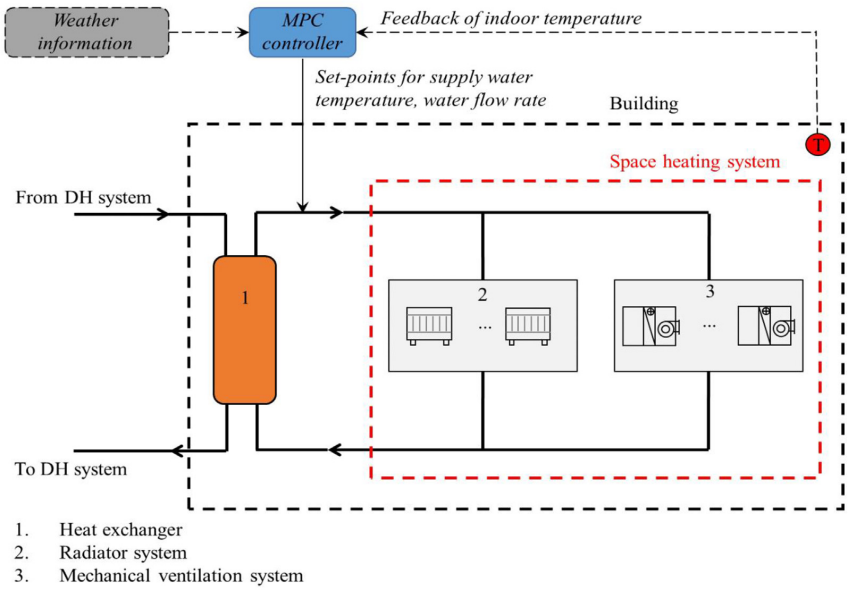

b) Space heating system and MPC controller in the building

Fig. 7. The university building used as the case study.

model proposed in Section 2.2 were obtained by the direct calculation method. Firstly, according to the information on building thermal properties, the heat resistance and capacitance of the individual exterior thermal mass element, including the exterior walls and roof et al. exposed to the outdoor environment, were calculated using the method provided in European standard EN ISO 6946 [66]. Afterwards, the heat resistances and the heat capacitances of all the building exterior thermal mass elements were lumped into one equivalent heat resistance and one equivalent heat capacitance, respectively. These equivalent heat resistance and capacitance represented the overall thermal performance of all the exterior thermal mass elements, and they were obtained by equations (26) and (27), respectively [40]. Specifically, an assumption was made when calculating the heat capacitance of the window- its thermal mass was set as zero because it could be ignorable compared to the other exterior thermal mass elements.

$$R_e = 1/\left(\frac{1}{R_1}+\frac{1}{R_2}+\cdots+\frac{1}{R_i}+\cdots+\frac{1}{R_n}\right) \tag{26}$$

$$C_e = C_1 + C_2 + \cdots + C_i + \cdots + C_n \tag{27}$$

where R_e and C_e are the equivalent heat resistance and capacitance for the overall exterior or interior thermal mass. R_i and C_i are the heat resistance and capacitance of exterior or interior thermal mass element i.

The same method was used to calculate the heat resistance and capacitance of the individual interior thermal mass element. However, in the first step, calculating the heat resistance of the individual element, no thermal conduction through interior thermal mass

Table 1
The key information about the building.

Category	Parameter	Value
Areas of building elements (m^2)	Exterior wall	5 504
	Roof	4 315
	Windows, doors, and glass	2 293
	Interior wall	8 256
U-values of building elements ($W/(m^2 \cdot K)$)	Exterior wall	0.35
	Roof	0.35
	Windows, doors, and glass	2.04
Specific heat capacities of elements ($J/ m^2 \cdot K$) [1]	Exterior opaque	175 000
	Interior wall	75 000
	Air and furniture	10 000
Ventilation	Air infiltration (h^{-1})	2.70[2]
	Mechanical ventilation (h^{-1})	0–1.50[3]
	Temperature efficiency of heat recovery (%)	62
	Heated air volume (m^3)	73 600
Internal heat gains	Equipment, lighting, person (W/ m^2)	5.5–19.0[4]

[1] Based on the building thermal properties and standards [44,46].
[2] Air change rate at 50 Pa, n_{50}.
[3] Operated based on the building occupancy schedule.
[4] Estimated based on the measurement data and standard [46].

element was assumed, therefore, only the surface resistance between the indoor air and the interior thermal mass element was considered. The calculation results for the values of the heat resistance and the heat capacitance are shown in Table A.1.

3.2. Weather forecast data from the numerical weather prediction model

This study was performed using the weather forecast data and corresponding actual weather data for January of 2018 for the university building (coordinates: 63.4°N 10.4°E, elevation 60 m). The weather forecast data were given by the archived forecasts of the NWPM, MetCoOp Ensemble Prediction System (MEPS), which is cooperated by the meteorological services of Norway, Sweden, and Finland. The location of the case building was used as the input for the NWPM to download the corresponding historical weather forecast data. MEPS delivers hourly predictions for the next 66 h with an update cycle of 12 h [67]. In addition, according to the review paper [7], the typical prediction horizon of MPC in HVAC systems that feature slow-moving processes lies in the range from 5 to 48 h. In this study, the prediction horizon of the MPC was chosen as 12 h. Therefore, at each time step, the MPC controller used the latest available 12 h' weather forecast data. In addition, for Fig. 8 and Fig. 9, the actual outdoor temperature was always compared to the available most recent forecast data with an update cycle of 12 h.

Fig. 8 shows the comparison between the MEPS forecasted and the corresponding actual outdoor temperature. The forecasted data predicted the trend of the outdoor temperature well. However, the exact value of the actual outdoor temperature was not reflected by the forecasted data very well. As presented in Fig. 8, the deviation between them could be even up to almost 10 K.

Fig. 9 illustrates the distribution of deviation between the forecasted and the actual outdoor temperature for January of 2018. The temperature deviation had the mean value of −1.2 K and the standard deviation of 2.5 K. On average, the forecasted data were close to the actual outdoor temperature. However, the standard deviation indicated the presence of a considerable amount of overestimated and underestimated values. The distribution graph in Fig. 9 shows that the outdoor temperature was mainly underestimated by the MEPS forecasted data for the studied period.

3.3. Suggested scenarios to include the MPC controller

This research is a simulation-based study to investigate the impact of weather forecast uncertainty on the performance of MPC. Moreover, to improve the performance of the MPC controller, an error model was introduced to address the error of the weather forecast. To test the effectiveness of the MPC controller integrated with the error model, four research scenarios including a reference scenario, two benchmark MPC scenarios, and one improved MPC scenario integrated with the error model were proposed in this research. The reference scenario represented the current RBC strategy for the SH system without using any MPC controller. The other scenarios represented the MPC strategies with different weather information provided for their MPC controllers. The ideal benchmark MPC scenario assumed perfect weather forecasts, i.e. providing the actual weather data for its MPC controller. The standard benchmark MPC scenario did not address the weather forecast error, i.e. directly providing the forecasted weather data for its MPC controller. Finally, the improved MPC scenario handles the weather forecast error by integrating with the error model, i.e. providing the estimated weather data from the error model for its MPC controller. Due to the different weather information provided for different MPC controllers, the SH system of the building in individual MPC scenarios received different optimal control signals. Afterwards, the same building and system model disturbed by actual weather conditions was simulated to obtain the indoor air temperature and the heating cost based on the different control signals, respectively.

The research was conducted through the following four steps. Firstly, the building model was developed based on the method proposed in Section 2.2 and validated as presented in Section 4.1. Secondly, the MPC framework was formulated as described in Sec-

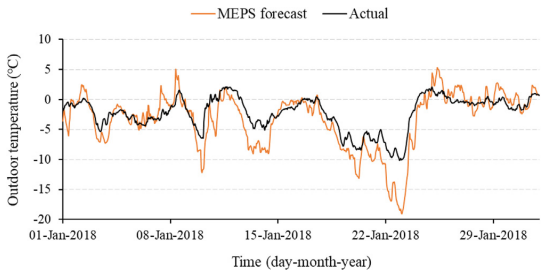

Fig. 8. The comparison between forecasted and corresponding actual outdoor temperature.

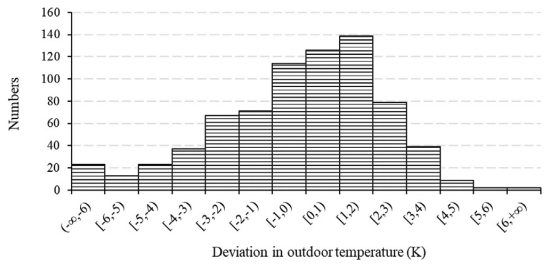

Fig. 9. Distribution of deviation between forecasted and actual outdoor temperature (deviation equals forecasted value minus actual value) for January of 2018.

tion 2.3. Thirdly, four simulation-based experiments were created and simulated as introduced in Section 3.3, respectively, including a reference scenario and three MPC scenarios. Finally, the simulation results of different scenarios were investigated and compared in Section 4 and Section 5.

The proposed four scenarios were presented in Fig. 10. The reference scenario, *RBC* in Fig. 10 a), presented the current RBC strategy for the SH system and was therefore used as a benchmark. In this scenario, a WCC was used to determine the supply water temperature of the SH system according to the actual outdoor temperature. A P controller, which attempted to perform better than the on–off controller, was applied to adjust the water flow rate of the SH system based on the deviation between indoor temperature and its reference value. In this scenario, the optimal management of the building energy is not possible, as the future disturbances, energy price, energy demand, and the dynamic building model cannot be incorporated into controllers.

The ideal MPC scenario, *MPC_actu* in Fig. 10 b) was an ideal MPC control strategy, which was defined as optimal control with the perfect weather prediction, i.e. assuming no deviation between the forecasted weather and the actual weather. As shown in Fig. 10 b), the actual outdoor temperature was used by the MPC controller to present the perfect weather prediction. This is not an implementable controller but a concept, which was used to investigate the theoretical potential of MPC.

The standard MPC scenario, *MPC_fore* in Fig. 10 c), was a standard MPC control strategy in practice. It used the imperfect weather forecast of the NWPM but determined its control actions under the assumption that the predictions were correct. As presented in Fig. 10 c), the forecasted outdoor temperature from the MEPS was used by the MPC controller. This scenario demonstrated the practical potential of MPC.

The improved MPC scenario, *MPC_esti* in Fig. 10 d), was proposed considering the uncertainty of weather predictions in the MPC control strategy. As shown in Fig. 10 d), the error model described in Section 2.5 was integrated to improve the quality of forecasted outdoor temperature from the MEPS, and then the high-quality estimated outdoor temperature was used by the MPC controller. This scenario made the handling of the weather forecast uncertainty straightforward, meanwhile maintained the computationally tractable of MPC.

4. Results

This section firstly presents the model validation and the evaluation of the error model for weather forecast, and then evaluates the three MPC scenarios during a typical week in terms of achieved indoor air temperature and heating cost.

4.1. Model validation

The dynamic building model proposed in Section 2.2 was validated by one month's measured data from the campus energy management platform. For the validation procedure, the simulated control strategy for the SH system was based on the current RBC strategy. As described in Section 3.2, a WCC was used to determine the supply water temperature of the SH system according to the actual outdoor air temperature, and a P controller was used to adjust the water flow rate based on the deviation between indoor air temperature and its reference value. The reference values for the indoor temperature were set as 21℃ from 8:00 am to 10:00 pm, and 19℃ from 10:00 pm to 8:00 am based on the measured data and adjusted by the requirement of the Norwegian standard [46]. The mechanical ventilation and the internal heat gains listed in Table 1 were set as inputs for the dynamic building model. Afterwards, with a reasonable initial guess for the state variables and the control strategy described above, the dynamic building model was simulated in the Dymola environment to track the reference values of the indoor temperature. The simulated hourly heat rate was validated against the measured hourly heat rate.

The validation results are presented in Fig. 11. The simulated and measured hourly heat rate of the building exhibited the same trend. During working hours, the hourly heat rate was higher due to the higher airflow rate in the AHUs of the mechanical ventilation system. During non-working hours or weekends, fewer occupants led to the lower airflow rate in the AHUs of the mechanical ventilation system and hence the lower hourly heat flow rate. In summary, the simulated results were able to capture the key characteristics of building heat flow rate.

To quantify the deviation of the simulated data from the measured data, two indicators, i.e. coefficient of variation of the root mean square error (CV(RMSE)) and normalized mean bias error (NMBE), were used to evaluate the prediction performance of building model according to ASHRAE Guideline 14–2014 [68]. CV (RMSE) characterizes the variability of the errors between the measured and the simulated values. NMBE quantifies the percentage error between the measured and the simulated values. The validation criteria required in ASHRAE Guideline 14–2014 is within ± 30% for CV(RMSE) and within ± 10% for NMBE when using hourly data [68]. In this study, the resulted values of the two indicators were 16.9% for CV(RMSE) and 0.4% for NMBE, respectively, when comparing the hourly simulated and measured heat flow rate. These indicators showed that the dynamic building model developed in this study was able to predict the thermal behaviour of building well and be used for MPC control strategy.

4.2. Evaluation of error model for weather forecast

The three MPC scenarios together with the reference scenario, *RBC*, were tested during a typical week (from 17th to 23th of January of 2018). As shown in Fig. 12, the deviations between the MEPS forecasted and the actual outdoor temperature were large and most of the forecasted values were lower than the actual values. The mean value of these deviations was −2.7 K, and the maximum deviation was −9.2 K.

To improve the quality of MEPS forecasted outdoor temperature as shown in Fig. 12, the error model proposed in Section 2.5 was used to estimate the prediction error of MEPS, and then the estimated MEPS prediction error together with the MEPS forecasted outdoor temperature were combined as described in Equation (25) to generate a sequence of estimated outdoor temperature. According to [18,26], the accuracy of these estimated outdoor temperatures was quantified using a standard metric, root mean square error (RMSE). RMSE represents the sample standard deviation of the differences between predicted values and actual values, as described in Equation (28) [68].

$$RMSE = \sqrt{\frac{\sum_{i=1}^{n} (y_i - \hat{y}_i)^2}{n}} \tag{28}$$

where n is the number of observations of data points, y_i is the actual value, and $\hat{y}_i$ is the predicted value.

Fig. 13 presents the RMSEs of each hour in the predictive horizon, in which the black line represents the RMSE of the MEPS forecasted outdoor temperature, and the orange line represents the RMSE of the estimated outdoor temperature. As mentioned in Section 2, the predictive horizon was 12 h in this study, and hence the X-axis of Fig. 13 ranged from 1 to 12. In addition, the studied typical week had 168 h, and therefore the RMSEs of each hour in the

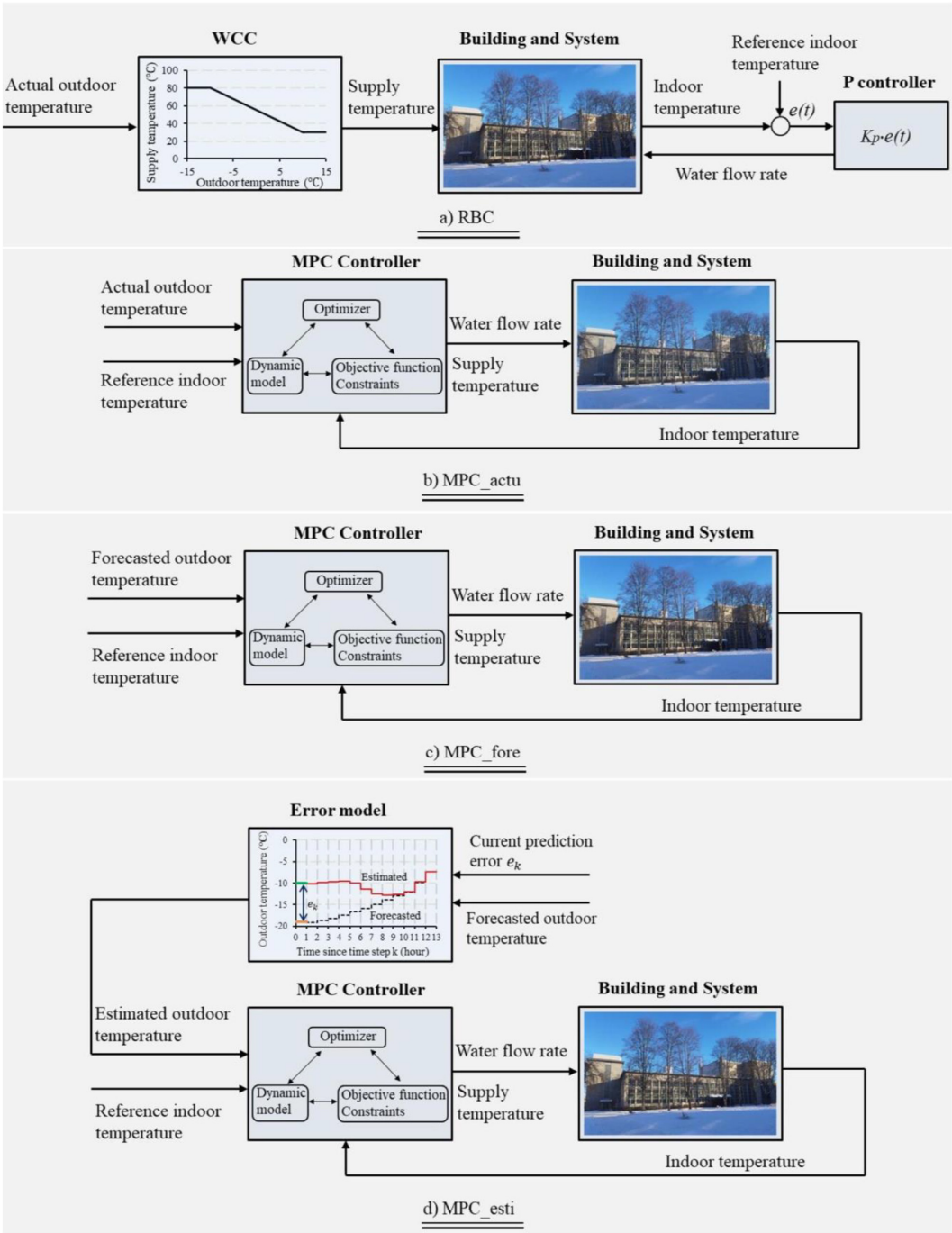

Fig. 10. Schematics of the four scenarios.

predictive horizon was calculated based on 168 pairs of data including actual and predicted values. As described in Section 2.5, one challenge with the direct use of the weather forecast data from NWPM is the inherent prediction error of the NWPM. Therefore, the RMSEs of the forecasted outdoor temperature direct from MEPS were larger and fluctuated around 4.2 K for each hour in the

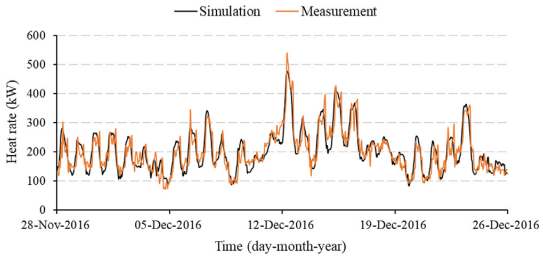

Fig. 11. Comparison between the simulated and measured heat flow rate.

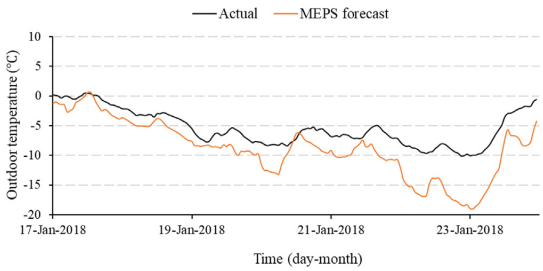

Fig. 12. Outdoor temperature.

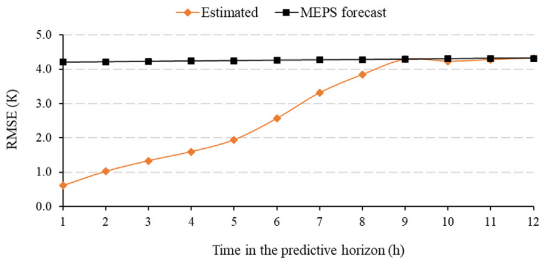

Fig. 13. RMSEs of MEPS forecasted and estimated outdoor temperature.

predictive horizon. In contrast, after introducing the error model for MEPS forecasted outdoor temperature, the accuracy of the outdoor temperature was increased. As shown in Fig. 13, the estimated outdoor temperatures had higher accuracy with the lower RMSEs from 0.5 to 4.2 K, especially for the near future as presented on the left side of Fig. 13.

4.3. Achieved indoor air temperature

Fig. 14 presents the indoor air temperature and its reference values for different scenarios. The reference values for the indoor temperature were set as 21.0℃ from 8:00 am to 10:00 pm, and 19.0℃ from 10:00 pm to 8:00 am for all the scenarios according to Norwegian standard [46], as depicted by the red solid line in Fig. 14. The ideal MPC scenario, *MPC_actu*, demonstrated the theoretical control performance of the MPC for maintaining the indoor temperature as expected. This ideal MPC scenario eliminated the over-heating phenomenon occurring in the reference scenario *RBC*, and reduced the deviations between indoor temperature and its reference values, as shown in Fig. 14. In addition, the violation numbers of the indoor temperature are presented in Fig. 15. The indoor temperature was recorded every ten minutes, and the occurrence of violation was counted when the deviation between the indoor temperature and its reference value was larger than 0.5 K. The ideal MPC scenario, MPC_{actu}, decreased the violation numbers from 430 to 152, with the reduction of almost 65%. Moreover, the ideal MPC scenario considered the peak load shaving target involved in its objective function, and hence slightly lowered the indoor temperature during the peak hours and slightly higher the indoor temperature during the non-peak hours, as shown in Fig. 14.

The standard MPC scenario, *MPC_fore*, which presents the practical indoor temperature control performance of MPC, is depicted in Fig. 14 by the green solid line. The MEPS forecasted outdoor temperature was directly used by the MPC controller in this scenario. Due to receiving inaccurate outdoor temperature, this scenario did not perform well, especially when the MEPS forecasted weather largely varied from the actual one. The over-heating phenomenon in this scenario was even worse than with the reference scenario *RBC*, as shown in Fig. 14 . In addition, compared to the reference scenario, *RBC*, the deviations between the indoor temperature and its reference values were increased and the violation numbers of the indoor temperature were even higher, an increase of 20%, as shown in Fig. 15. Due to receiving the low-quality predictions for the future weather, this standard MPC scenario presented even worse control performance than the conventional RBC in terms of the indoor temperature.

In contrast, the improved MPC scenario, *MPC_esti*, was able to guarantee thermal comfort by introducing the error model. As presented in Fig. 13, the error model together with the MEPS forecasted outdoor temperature generated the high-quality estimated future outdoor temperature, and then the estimated outdoor temperature was used by the MPC controller in this scenario. Due to receiving the high-quality weather data, this scenario achieved almost the same indoor temperature control performance as the ideal MPC scenario, as depicted in Fig. 14 by the orange solid line. The over-heating phenomenon was removed and the deviations between the indoor temperature and its reference values were small in this scenario. The peak load shaving target was also considered as the indoor temperature was controlled to be slightly lower and higher than its reference values during the peak and the non-peak hours, respectively. Moreover, as presented in Fig. 15, the violation numbers of the indoor temperature dropped by almost 80 % compared to the standard MPC scenario (*MPC_fore*) and by 73% compared to the reference scenario *RBC*.

4.4. Heating cost

As described in Section 2.3, the heating cost was charged based on the peak heat rate and the heat use of end-users. Therefore, the peak heat rate and the heat use for the different scenarios will be discussed firstly in this section.

Fig. 16 presents the peak heat rate for different scenarios. As described in Section 2.1, the passive thermal mass storage of the building was integrated into the MPC control strategy to shave the peak load in the building. Therefore, the ideal MPC scenario, *MPC_actu*, presented a remarkable peak load shaving effect and decreased the peak load from 549 kW to 506 kW, a reduction of 7.8% compared to the reference scenario *RBC*. However, due to receiving inaccurate weather data, the peak load shaving performance of the MPC deteriorated. As shown in Fig. 16, the standard MPC scenario, *MPC_fore*, shaved the peak load to 529 kW, with the reduction of only 3.6% compared to the reference scenario *RBC*. In contrast, introducing the error model was able to improve the peak load shaving performance of MPC a bit. As the improved MPC scenario (*MPC_esti*) showed, the peak load was decreased by 4.6%, which was higher than the standard MPC scenario (*MPC_fore*).

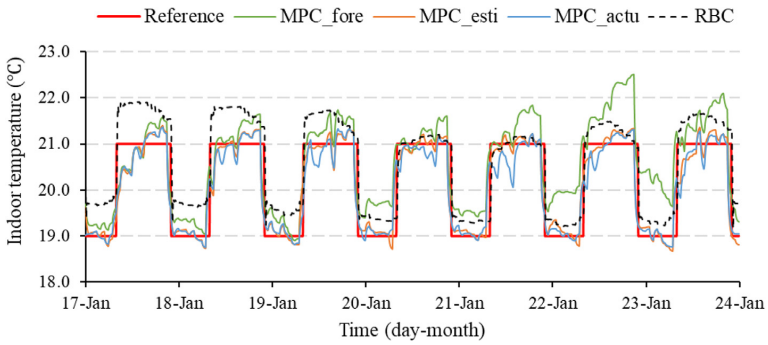

Fig. 14. Indoor temperature.

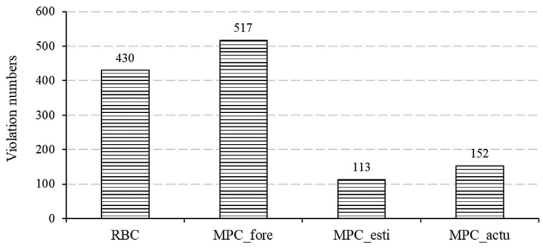

Fig. 15. Violation numbers of indoor temperature.

Fig. 17 presents the heat use for different scenarios. The ideal MPC scenario, *MPC_actu*, demonstrated the theoretical heat use saving potential of the MPC. A theoretical heat use saving of 3.3% was able to be achieved by this ideal MPC scenario. However, the low-quality predictions of weather degraded the heat use saving performance of the MPC. As the standard MPC scenario (*MPC_fore*) showed, its heat use was almost the same as the reference scenario *RBC* and no obvious heat use saving was observed. In this scenario, its MPC controller received lower forecasted outdoor temperature, as presented in Fig. 12, which led to incorrect control actions of MPC. The MPC controller provided more heat than the building demand and hence resulted in the over-heating phenomenon and heat waste. Introducing the error model was able to improve the quality of weather information and significantly improve the MPC performance in terms of heat use saving. As shown in Fig. 17, the improved MPC scenario (*MPC_esti*) reduced the heat use from 54.9 MWh to 53.3 MWh, a reduction of 3.0%, which was very close to the theoretical heat use saving potential of the MPC.

Finally, Fig. 18 presents the heating cost for different scenarios. The theoretical heating cost saving was 4.1%, as the ideal MPC scenario *MPC_actu* showed. This cost saving came from the reduction in both the LDC and the EDC of the heating price model, which was caused by the peak load shaving and the heat use saving effects of the MPC controller. The standard MPC scenario, *MPC_fore*, saved only 0.7% of heating cost compared to the reference scenario *RBC*. The heating cost saving performance of the MPC was degraded a lot due to the low-quality weather forecast information. However, introducing the error model for the weather forecast brought remarkable improvement in terms of heat use saving for the MPC controller, as described above. Therefore, about 3.4% of the heating cost was saved by the improved MPC scenario *MPC_esti*.

5. Discussion

Sections 4.2-4.4 present the simulation results from a week that had a big deviation between the MEPS forecasted and the actual outdoor air temperature. This section, however, investigates the situation with a small deviation between the forecasted and the actual outdoor air temperature. Therefore, the impacts of the low error weather forecast on the performance of MPC controllers were analysed, moreover, the effectiveness of the error model is further discussed. Following that, this section discusses the limitation of this study.

The three MPC scenarios together with the reference scenario were tested during another week (from 24th to 30th of January of 2018). As presented in Fig. 19, the deviations between the MEPS forecasted and the actual outdoor temperature were small. Compared to the tested week presented in Section 4.2 with a mean and a maximum deviation value of −2.7 K and −9.2 K, respectively, this week had a much smaller deviation range with a mean and a maximum deviation value of 0.8 K and 4.7 K. As the steps described in Section 3.3, firstly, the MPC controllers of individual MPC scenarios were provided with different weather information, i.e. the

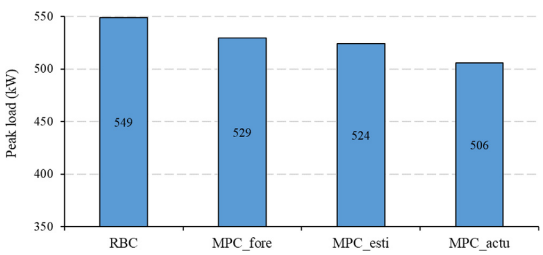

Fig. 16. Peak load for different scenarios.

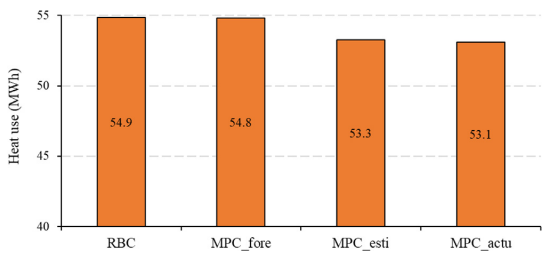

Fig. 17. Heat use for different scenarios.

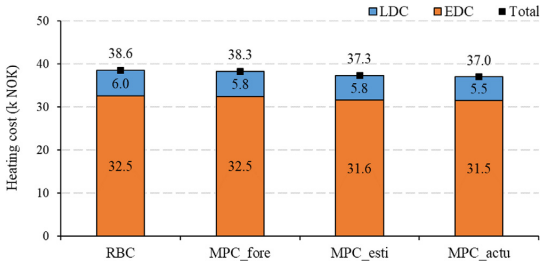

Fig. 18. Heating cost for different scenarios.

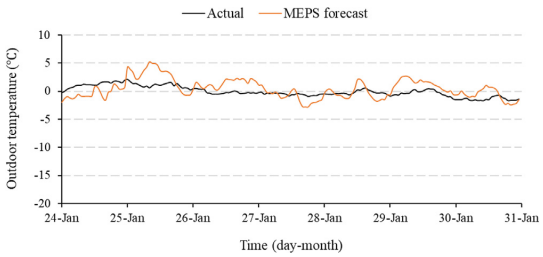

Fig. 19. Outdoor temperature.

actual outdoor temperature for Scenario *MPC_actu*, the forecasted outdoor temperature from MEPS for Scenario *MPC_fore*, and the estimated outdoor temperature from the error model for Scenario *MPC_esti*. Afterwards, these MPC controllers generated control signals based on the provided weather information and the feedback of the building. Finally, the SH system received and executed these control signals, and the processes were simulated under the condition of the actual outdoor temperature. The simulated results for the MPC scenarios and the reference scenario are presented in Fig. 20 and Fig. 21.

Fig. 20 shows the violation numbers of the indoor air temperature for each research scenario during the week from 24th to 30th of January of 2018. In Fig. 20, smaller violation numbers mean better performance in terms of indoor temperature tracking. Different from the results achieved in Section 4.3 that the MPC scenario with the forecasted outdoor temperature, *MPC_fore*, obtained the worest perfromance on indoor temperature tracking, the results in Fig. 20 showed that all the three MPC scenarios presented better performance than the reference scenario, *RBC*. However, similar with the results observed in Section 4.3, Fig. 20 also demonstrates that introducing the error model could improve the performance of MPC controllers regarding the indoor temperature tracking, which

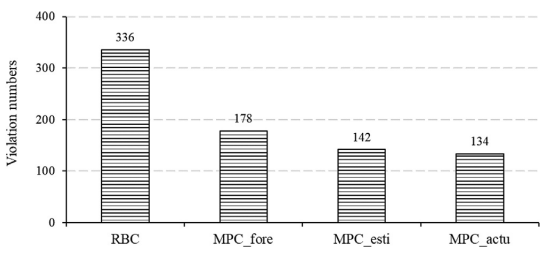

Fig. 20. Violation numbers of indoor temperature (from 24th to 30th of January of 2018).

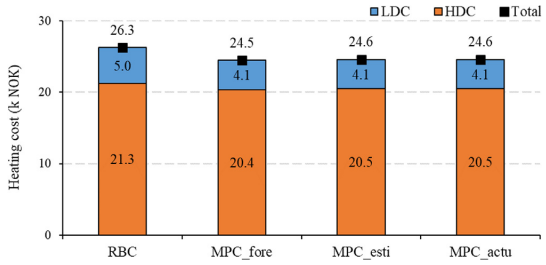

Fig. 21. Heating cost for different scenarios (from 24th to 30th of January of 2018).

can be found when comparing the results of Scenario *MPC_fore* with Scenario *MPC_esti*. The above findings indicated that the better weather forecast guaranteed better indoor temperature tracking performance for MPC controllers than direct use of the forecasted weather data. However, as the prediction error cannot be avoided, introducing the error model always benefited the performance of an MPC controller.

Fig. 21 presents the heating cost for the four research scenarios during the week from 24th to 30th of January of 2018. Different from the results obtained in Section 4.4 that the MPC scenario with the forecasted outdoor temperature, *MPC_fore*, had no obvious heating cost savings, the results in Fig. 21 show that all the three MPC scenarios including the *MPC_fore* scenario, reduced the heating cost of the SH system by around 6.5% compared to the reference scenario. This indicates that the small deviations between the actual and the MEPS forecasted outdoor temperature had no obvious impacts on the MPC performance in terms of heating cost saving. Therefore, some conclusions from this discussion together with the results presented in Section 4.3 and 4.4 may be summarized as follows. Firstly, the quality of weather information provided for the MPC controller had a big impact on the performance of MPC, which was identical with the previous studies, e.g. [17,18]. Secondly, the introduction of an error model to improve the quality of weather information always benefited the MPC performance even when the deviations between the forecasted and measured weather data were small.

Furthermore, there are several limitations of this study. Solar radiation was not considered in this study due to the low solar radiation during the studied period. In this study, there were no available on-site measured solar radiation values for the case building. Therefore, the measured global solar radiation from the nearest weather station, Skjetlein, were collected to infer the situation of solar radiation for the case building [69]. Fig. 22 presents the measured average hourly global solar radiation from the weather station during the studied period. The studied period was January of 2018 and had 31 days, and therefore the average

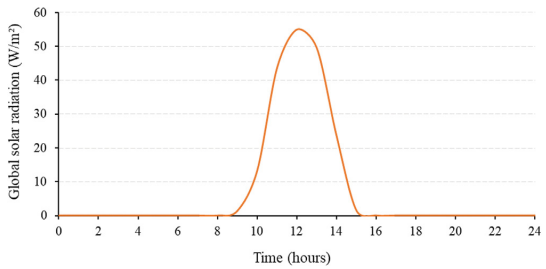

Fig. 22. Measured average hourly global solar radiation during January of 2018.

hourly value was obtained based on the 31 measured global solar radiation for the same hour.

As shown in Fig. 22, the average global solar radiation varied in the range of 10–55 W/m^2 from 10:00 am to 02:00 pm yet only last 4 h in a day and was zero for the rest of day. Furthermore, the nearest weather station is located in the rural area of the city where no shading effect for the weather station. During the studied period, the case building located in the city centre may receive even less solar radiation because of the effect of shading in high-density urban areas [70]. Based on the above explanation, ignoring the solar radiation during the studied period for the case building is reasonable. However, solar gains are significant during the late spring and early autumn, resulting in a shortening of the heating season for almost all locations in Europe [70]. Therefore, solar radiation should be considered when the study is conducted during the late spring and early autumn.

The RC model used in this study was a white-box RC model, and the parameters of this RC model were obtained based on the known detailed information of the case building, the on-site measured data, and related standards. However, for many buildings, detailed building information and complete on-site measured data are often unavailable. In this case, it is challenging to develop a white-box model based on the limited information of the building. Many researchers have investigated using system identification techniques to develop a suitable grey-box model when the building information is limited [38,39,71,72]. Grey-box models have better generalization properties and usually require less building information compared to white-box models. Therefore, to have a more generalized research method, a grey-box RC model may be developed in future work to test the methods proposed in this study.

6. Conclusions

In this study, an error model was proposed to address the effect of weather forecast uncertainty on the MPC performance in buildings. The error model used easily measurable and accessible data to improve the quality of the forecasted weather data from the NWPM, and consequently improved the performance of MPC. The proposed method was tested on a university building located in Norway under the condition of the high error of weather forecast. The three MPC scenarios together with a conventional RBC scenario were evaluated in terms of thermal comfort and heating cost.

Compared to the conventional RBC, the ideal MPC controller with perfect weather data demonstrated the theoretical heating cost saving of 4.1% during one week, while providing an improved level of thermal comfort, with a reduction of 65% for the indoor temperature violations. However, the standard MPC controller with the NWPM forecasted weather data did not perform well, especially when the actual weather varied from the forecast. In that case, the heating cost saving was only 0.7% during this week. Meanwhile, the low-quality weather forecast information resulted in an even worse level of thermal comfort than that of the conventional RBC, an increase of 20% for the violation numbers of the indoor air temperature. In contrast, by introducing the error model, the quality of weather information used in MPC was improved and hence the performance of the MPC controller was significantly improved. The weekly heating cost saving was increased to 3.4%, which was very close to the ideal MPC controller heating cost saving of 4.1%. In addition, the violation numbers of indoor temperature were dropped by 80% and hence the thermal comfort was substantially improved.

To get more generalized conclusions, the proposed method was tested under the condition of the low error of weather forecast as well. Simulation results indicated that the introduction of the error model to improve the quality of weather information always benefited the MPC performance even when the deviations between the forecasted and measured weather data were small.

In summary, integrating a simple but accurate error model into an MPC controller is a practical and feasible approach to tackle the weather forecast uncertainty of MPC in buildings. This study can facilitate the real application of MPC in buildings.

Declaration of Competing Interest

The authors declare that they have no known competing financial interests or personal relationships that could have appeared to influence the work reported in this paper.

Acknowledgement

The authors gratefully acknowledge the support from the Research Council of Norway through the research project Understanding behaviour of district heating systems integrating distributed sources under the FRIPRO/FRINATEK program (project number 262707).

Appendix A. Parameter for the RC model

Table A.1
Parameter for the RC building model.

Parameter	Value
$R_{o,e}$	1.39×10^{-4} K/W
$R_{i,e}$	1.52×10^{-4} K/W
$R_{i,m}$	7.37×10^{-6} K/W
R_{win}	2.13×10^{-4} K/W
C_{env}	1.72×10^{9} J/K
C_{ia}	8.74×10^{7} J/K
C_{ma}	6.88×10^{8} J/K

References

[1] European Commission. Energy Performance of Buildings Directive, https://ec.europa.eu/energy/topics/energy-efficiency/energy-efficient-buildings/energy-performance-buildings-directive_en; 2020 [Accessed 17 December 2020].
[2] J. Laustsen, Energy efficiency requirements in building codes, energy efficiency policies for new buildings., IEA Information Paper. Support of the G8 Plan of Action, 2008.
[3] F. Ascione, N. Bianco, C. De Stasio, G.M. Mauro, G.P. Vanoli, Simulation-based model predictive control by the multi-objective optimization of building energy performance and thermal comfort, Energy Build. 111 (2016) 131–144.
[4] J. Drgoňa, J. Arroyo, I. Cupeiro Figueroa, D. Blum, K. Arendt, D. Kim, E.P. Ollé, J. Oravec, M. Wetter, D.L. Vrabie, L. Helsen, All you need to know about model predictive control for buildings, Ann. Rev. Control. 50 (2020) 190–232.
[5] M. Killian, M. Kozek, Ten questions concerning model predictive control for energy efficient buildings, Build. Environ. 105 (2016) 403–412.
[6] H. Liu, S. Lee, M. Kim, H. Shi, J.T. Kim, K.L. Wasewar, C. Yoo, Multi-objective optimization of indoor air quality control and energy consumption minimization in a subway ventilation system, Energy Build. 66 (2013) 553–561.
[7] A. Afram, F. Janabi-Sharifi, Theory and applications of HVAC control systems–A review of model predictive control (MPC), Build. Environ. 72 (2014) 343–355.
[8] S. Petersen, S. Svendsen, Method for simulating predictive control of building systems operation in the early stages of building design, Appl. Energy 88 (12) (2011) 4597–4606.
[9] M.W. Ahmad, M. Eftekhari, T. Steffen, A.M. Danjuma, Investigating the performance of a combined solar system with heat pump for houses, Energy Build. 63 (2013) 138–146.
[10] D. Sturzenegger, D. Gyalistras, M. Morari, R.S. Smith, Model predictive climate control of a swiss office building: Implementation, results, and cost–benefit analysis, IEEE Trans. Control Syst. Technol. 24 (1) (2016) 1–12.
[11] N. Aoun, R. Bavière, M. Vallée, A. Aurousseau, G. Sandou, Modelling and flexible predictive control of buildings space-heating demand in district heating systems, Energy. 188 (2019) 116042.

[12] H. Thieblemont, F. Haghighat, R. Ooka, A. Moreau, Predictive control strategies based on weather forecast in buildings with energy storage system: A review of the state-of-the art, Energy Build. 153 (2017) 485–500.
[13] S.H. Cho, S.-k. Hong, S.-C. Li, M. Zaheeruddin, An optimal predictive control strategy for radiant floor district heating systems: Simulation and experimental study, Build. Serv. Eng. Res. Technol. 34 (3) (2013) 295–315.
[14] B. Dong, K.P. Lam, A real-time model predictive control for building heating and cooling systems based on the occupancy behavior pattern detection and local weather forecasting, Build. Simul. 7 (1) (2014) 89–106.
[15] S. Prívara, J. Široký, L. Ferkl, J. Cigler, Model predictive control of a building heating system: The first experience, Energy Build. 43 (2-3) (2011) 564–572.
[16] J. Široký, F. Oldewurtel, J. Cigler, S. Prívara, Experimental analysis of model predictive control for an energy efficient building heating system, Appl. Energy 88 (9) (2011) 3079–3087.
[17] F. Oldewurtel, A. Parisio, C.N. Jones, D. Gyalistras, M. Gwerder, V. Stauch, B. Lehmann, M. Morari, Use of model predictive control and weather forecasts for energy efficient building climate control, Energy Build. 45 (2012) 15–27.
[18] G. Henze, D. Kalz, C. Felsmann, G. Knabe, Impact of forecasting accuracy on predictive optimal control of active and passive building thermal storage inventory, HVAC&R Research. 10 (2) (2004) 153–178.
[19] M.Y. Lamoudi, P. Béguery, M. Alamir, Use of simulation for the validation of a model predictive control strategy for energy management in buildings, Proceedings of the Building Simulation, 2011.
[20] R.E. Hedegaard, T.H. Pedersen, M.D. Knudsen, S. Petersen, Towards practical model predictive control of residential space heating: Eliminating the need for weather measurements, Energy Build. 170 (2018) 206–216.
[21] Zavala VM, Constantinescu EM, Krause T, Anitescu M. Weather forecast-based optimization of integrated energy systems. Argonne National Lab.(ANL), Argonne, IL (United States); 2009.
[22] Y. Ma, F. Borrelli, Fast stochastic predictive control for building temperature regulation, in: 2012 American Control Conference (ACC): IEEE, 2012, pp. 3075–3080.
[23] Y. Ma, J. Matusko, F. Borrelli, Stochastic model predictive control for building HVAC systems: Complexity and conservatism, IEEE Trans. Control Syst. Technol. 23 (1) (2015) 101–116.
[24] X. Zhang, G. Schildbach, D. Sturzenegger, M. Morari, Scenario-based MPC for energy-efficient building climate control under weather and occupancy uncertainty, in: 2013 European Control Conference (ECC): IEEE, 2013, pp. 1029–1034.
[25] T. Salque, D. Marchio, P. Riederer, Neural predictive control for single-speed ground source heat pumps connected to a floor heating system for typical French dwelling, Build. Serv. Eng. Res. Technol. 35 (2) (2014) 182–197.
[26] D. Chakraborty, H. Elzarka, R. Bhatnagar, Generation of accurate weather files using a hybrid machine learning methodology for design and analysis of sustainable and resilient buildings, Sustainable Cities and Society. 24 (2016) 33–41.
[27] S. Petersen, K.W. Bundgaard, The effect of weather forecast uncertainty on a predictive control concept for building systems operation, Appl. Energy 116 (2014) 311–321.
[28] J. Song, F. Wallin, H. Li, District heating cost fluctuation caused by price model shift, Appl. Energy 194 (2017) 715–724.
[29] D. Romanchenko, J. Kensby, M. Odenberger, F. Johnsson, Thermal energy storage in district heating: Centralised storage vs. storage in thermal inertia of buildings, Energy Convers. Manage. 162 (2018) 26–38.
[30] T.H. Pedersen, R.E. Hedegaard, S. Petersen, Space heating demand response potential of retrofitted residential apartment blocks, Energy Build. 141 (2017) 158–166.
[31] D.F. Dominković, P. Gianniou, M. Münster, A. Heller, C. Rode, Utilizing thermal building mass for storage in district heating systems: Combined building level simulations and system level optimization, Energy. 153 (2018) 949–966.
[32] J. Kensby, A. Trüschel, J.-O. Dalenbäck, Potential of residential buildings as thermal energy storage in district heating systems–Results from a pilot test, Appl. Energy 137 (2015) 773–781.
[33] H. Li, J. Hou, T. Hong, Y. Ding, N. Nord, Energy, economic, and environmental analysis of integration of thermal energy storage into district heating systems using waste heat from data centres, Energy. 219 (2021) 119582.
[34] D. Rohde, B.R. Knudsen, T. Andresen, N. Nord, Dynamic optimization of control setpoints for an integrated heating and cooling system with thermal energy storages, Energy. 193 (2020) 116771.
[35] Cígler J, Gyalistras D, Široky J, Tiet V, Ferkl L. Beyond theory: the challenge of implementing model predictive control in buildings. Proceedings of 11th Rehva world congress, Clima 2013.
[36] P. Bacher, H. Madsen, Identifying suitable models for the heat dynamics of buildings, Energy Build. 43 (7) (2011) 1511–1522.
[37] Z. O'Neill, S. Narayanan, R. Brahme, Model-based thermal load estimation in buildings, Proceedings of SimBuild. 4 (1) (2010) 474–481.
[38] R.E. Hedegaard, S. Petersen, Evaluation of grey-box model parameter estimates intended for thermal characterization of buildings, Energy Procedia 132 (2017) 982–987.
[39] G. Reynders, J. Diriken, D. Saelens, Quality of grey-box models and identified parameters as function of the accuracy of input and observation signals, Energy Build. 82 (2014) 263–274.
[40] S. Yang, M.P. Wan, W. Chen, B.F. Ng, D. Zhai, An adaptive robust model predictive control for indoor climate optimization and uncertainties handling in buildings, Build. Environ. 163 (2019) 106326.
[41] O.T. Ogunsola, L. Song, Review and evaluation of using RC thermal modeling of cooling load prediction for HVAC system control purpose, ASME Internat. Mech. Eng. Congress Exp. 45233 (2012) 735–743.
[42] T.T. Gorecki, F.A. Qureshi, C.N. Jones, OpenBuild: An integrated simulation environment for building control, IEEE Conf. Control Appl. (CCA). 2015 (2015) 1522–1527.
[43] T.R. Nielsen, Simple tool to evaluate energy demand and indoor environment in the early stages of building design, Sol. Energy 78 (1) (2005) 73–83.
[44] European standard. Energy performance of buildings- Energy needs for heating and cooling, internal temperatures and sensible and latent heat loads- Part 1: Calculation procedures; ISO 52016-1:2017.
[45] D.A. Hagos, A. Gebremedhin, B. Zethraeus, Solar water heating as a potential source for inland Norway energy mix, J. Renew. Energy 2014 (2014) 1–11.
[46] Standard norge. Energy performance of buildings- Calculation of energy needs and energy supply (in Norwegian); SN-NSPEK 3031:2020.
[47] EN 442-2 Radiators and convectors - Part 2: Test methods and rating. 2014.
[48] O. Paulsen, S. Gundtoft, Dynamisk afprøvning af små varmecentraler, Teknologisk Instituts Forlag (1985).
[49] F. Tahersima, J. Stoustrup, H. Rasmussen, An analytical solution for stability-performance dilemma of hydronic radiators, Energy Build. 64 (2013) 439–446.
[50] T.H. Pedersen, R.E. Hedegaard, K.F. Kristensen, B. Gadgaard, S. Petersen, The effect of including hydronic radiator dynamics in model predictive control of space heating, Energy Build. 183 (2019) 772–784.
[51] F. Tahersima, J. Stoustrup, H. Rasmussen, P.G. Nielsen, Thermal analysis of an hvac system with trv controlled hydronic radiator, in: 2010 IEEE International Conference on Automation Science and Engineering: IEEE, 2010, pp. 756–761.
[52] B. Xu, L. Fu, H. Di, Dynamic simulation of space heating systems with radiators controlled by TRVs in buildings, Energy Build. 40 (9) (2008) 1755–1764.
[53] IBPSA Project 1. 2019.
[54] H. Li, N. Nord, Operation strategies to achieve low supply and return temperature in district heating system, E3S Web Conf. 111 (2019) 05022.
[55] Purmo. Panel radiators, https://www.purmo.com/docs/Purmo_tech_catalogue_panel_radiators_full_PR_05_2017_EN_PL.pdf; 2020 [accessed 22 December 2020].
[56] H. Li, J. Hou, Z. Tian, T. Hong, N. Nord, D. Rohde, Optimize heat prosumers' economic performance under current heating price models by using water tank thermal energy storage, Energy. 239 (2022) 122103.
[57] Statkraft varme at Tronheim. Products and services, https://www.statkraftvarme.no/globalassets/0/statkraft-varme/produkter-og-tjenester/prisark/jan-2021/trondheim-bedrift-uten-volumledd-bt1.pdf; 2020 [accessed 17 December 2020].
[58] S.V. Raković, W.S. Levine, Handbook of model predictive control, Springer, 2018.
[59] H.F. Scherer, M. Pasamontes, J.L. Guzmán, J.D. Álvarez, E. Camponogara, J.E. Normey-Rico, Efficient building energy management using distributed model predictive control, J. Process Control 24 (6) (2014) 740–749.
[60] S.S. Walker, W. Lombardi, S. Lesecq, S. Roshany-Yamchi, Application of distributed model predictive approaches to temperature and CO2 concentration control in buildings, IFAC-PapersOnLine. 50 (1) (2017) 2589–2594.
[61] J. Drgoňa, M. Kvasnica, Comparison of MPC strategies for building control, Internat. Conf. Process Control (PC). 2013 (2013) 401–406.
[62] R. Amrit, J.B. Rawlings, L.T. Biegler, Optimizing process economics online using model predictive control, Comput. Chem. Eng. 58 (2013) 334–343.
[63] J. Nocedal, S. Wright, Numerical Optimization, Springer Science & Business Media, 2006.
[64] A. Groß, C. Wittwer, M. Diehl, Stochastic model predictive control of photovoltaic battery systems using a probabilistic forecast model, Eur. J. Control 56 (2020) 254–264.
[65] J. Guan, N. Nord, S. Chen, Energy planning of university campus building complex: Energy usage and coincidental analysis of individual buildings with a case study, Energy Build. 124 (2016) 99–111.
[66] European standard. Building components and building elements- Thermal resistance and thermal transmittance- Calculation methods; ISO 6946:2017.
[67] The Norwegian Meteorological Institute. Free meteorological data, https://www.met.no/en/free-meteorological-data; 2020 [accessed 17 December 2020].
[68] ASHRAE. ASHRAE Guideline 14–2014, Measurement of Energy, Demand, and Water Savings. ASHRAE Atlanta; 2014.
[69] Agricultural Meteorological Service. Get weather data, https://lmt.nibio.no/agrometbase/getweatherdata_new.php?weatherStationId=43; 2021 [accessed 25 August 2021].
[70] Frederiksen S, Werner S. District heating and cooling, Vol. 579, Studentlitteratur Lund, 2013.
[71] Z. Wang, Y. Chen, Y. Li, Development of RC model for thermal dynamic analysis of buildings through model structure simplification, Energy Build. 195 (2019) 51–67.
[72] X. Yu, L. Georges, L. Imsland, Data pre-processing and optimization techniques for stochastic and deterministic low-order grey-box models of residential buildings, Energy Build. 236 (2021) 110775.

PAPER 3

Hou J, Li H, Nord N, Huang G. Model predictive control for a university heat prosumer with data centre waste heat and thermal energy storage. Submitted to Journal of Energy (Status: Under review).

This paper is awaiting publication and is not included in NTNU Open

APPENDIX- PUBLICATIONS

PAPER 4

Li H, Hou J, Tian Z, Hong T, Nord N, Rohde D. Optimize heat prosumers' economic performance under current heating price models by using water tank thermal energy storage. Energy. 2022; 239: 122103.

APPENDIX- PUBLICATIONS

Energy 239 (2022) 122103

Contents lists available at ScienceDirect

Energy

journal homepage: www.elsevier.com/locate/energy

Optimize heat prosumers' economic performance under current heating price models by using water tank thermal energy storage

Haoran Li [a, *], Juan Hou [a], Zhiyong Tian [b], Tianzhen Hong [c], Natasa Nord [a], Daniel Rohde [d]

[a] Department of Energy and Process Technology, Norwegian University of Science and Technology, Kolbjørn Hejes vei 1 B, Trondheim, 7491, Norway
[b] School of Environmental Science and Engineering, Huazhong University of Science and Technology, Wuhan, PR China
[c] Building Technology and Urban Systems Division, Lawrence Berkeley National Laboratory, 1 Cyclotron Road, Berkeley, CA, 94720, USA
[d] SINTEF Energy Research, Sem Sælands vei 11, 7034, Trondheim, Norway

ARTICLE INFO

Article history:
Received 29 March 2021
Received in revised form
19 August 2021
Accepted 19 September 2021
Available online 22 September 2021

Keywords:
4th generation district heating
Thermal energy storage
Distributed heat sources
Heating price model
Peak load
Mismatch problem

ABSTRACT

Due to heat prosumers' dual roles of heat producer and heat consumer, the future district heating (DH) systems will become more flexible and competitive. However, the current heating price models have not yet supported the reverse heat supply from prosumers to the central DH system, which means the prosumers would gain no economic benefit from supplying heat to the central DH system. These unidirectional heating price models will reduce interest in prosumers, and thus hinder the promotion of prosumers in DH systems. This study aimed to optimize prosumers' economic performance under the current heating price models by introducing water tank thermal energy storage (WTTES). A dynamic optimization problem was formulated to explore prosumers' economic potentials. The size parameter of WTTESs was swept in prosumers to obtain the optimal storage size considering the trade-off between the payback period and the heating cost saving. The proposed method was tested on a campus DH system in Norway. The results showed that the prosumer's annual heating cost was saved up to 9%, and the investment of WTTES could be recovered in less than ten years. This study could provide guidelines on improving prosumers' economic performance and promote the development of prosumers during the transformation period of DH systems.
© 2021 The Author(s). Published by Elsevier Ltd. This is an open access article under the CC BY license (http://creativecommons.org/licenses/by/4.0/).

1. Introduction

Buildings account for a large share of total energy use and contribute to global warming considerably. In the European Union (EU), buildings are responsible for approximately 40% of total energy use and 36% of greenhouse gas emissions [1]. Space heating (SH) and domestic hot water (DHW) systems, as essential parts of building energy systems, play an important role in buildings' energy use. For example, in the residential sector of the EU countries, about 80% of the energy use is for SH and DHW [2,3]. District heating (DH) systems can satisfy buildings' heat demand in an energy-efficient and environment-friendly way [4]. Due to these merits, DH systems are competitive compared with alternative heating technologies, especially for urban areas with concentrated heat demand. Currently, more than four thousand DH systems are working successfully in Europe [5], and the national heat market share for DH systems can reach 60% for some areas [6–8]. However, DH systems' competitiveness is weakened by several challenges, such as the considerable distribution heat loss caused by high distribution temperature and the shrinking heat market due to the improving building efficiency [4]. To deal with these challenges and stay competitive, the current second and third generation DH systems are transforming to the fourth and fifth generation DH systems [9–12]. The transformation includes decreasing distribution temperature and upgrading infrastructure, and hence reduces the distribution heat loss and opens the door to more free heat such as renewables and waste heats.

For the future DH systems, renewables and waste heats may be integrated into the user side as distributed heat sources (DHSs) besides the central DH system. These end-users with DHSs are called heat prosumers due to their dual roles of producer and consumer. Fig. 1 illustrates examples of heat prosumers in a DH system. The block *Individual Prosumers* in the upper right of Fig. 1 shows different types of individual prosumers that integrated into the central DH system, these prosumers maybe a building installed with solar panels, a food store with waste heat from the

* Corresponding author.
E-mail address: haoranli@ntnu.no (H. Li).

https://doi.org/10.1016/j.energy.2021.122103
0360-5442/© 2021 The Author(s). Published by Elsevier Ltd. This is an open access article under the CC BY license (http://creativecommons.org/licenses/by/4.0/).

Nomenclature

CHP	Combine heat and power plant
CV(RMSE)	Coefficient of variation of the root mean square error
DC	Data centre
DH	District heating
DHW	Domestic hot water
DHS	Distributed heat source
EDC	Energy demand component
FDC	Flow demand component
FXC	Fixed component
HE	Heat exchanger
LDC	Load demand component
MS	Main substation
NLP	Nonlinear programming
NMBE	Normalized mean bias error
R2R	Extraction from the return line and feed into the return line
R2S	Extraction from the return line and feed into the supply line
S2S	Extraction from the supply line and feed into the supply line
SH	Space heating
TES	Thermal energy storage
WTTES	Water tank thermal energy storage

refrigeration system, or a factory with waste heat from the production process. In addition, the block *Community Prosumer* in the lower right of Fig. 1 presents a community prosumer with end-users and DHSs. These end-users are a cluster of buildings that may contain residential buildings and commercial buildings, and the DHSs may be a data centre (DC) with waste heat from its cooling system and a micro combine heat and power plant (CHP). Different from the individual prosumers connecting to the central DH system directly, the community prosumer is connected to the central DH system via the main substation (MS), and hence the management of the community DH system can be separated from the central DH system. For both the individual prosumers and the community prosumers, it allows bidirectional heat flow between the prosumers and the central DH system. Therefore, the prosumers may be supplied with heat from the central DH system during high heat demand periods, and feed surplus heat from their DHSs to the central DH system during low heat demand periods.

There is a growing interest in prosumers in DH systems. Nord et al. [13] and Lickleder et al. [14] proposed methods to model heat prosumer-based DH systems. Marguerite et al. introduced a tool to optimize the design and operation of prosumers [15]. Pipiciello et al. developed a new type of substation for heat prosumers in DH systems [16]. Nielsen et al. [17], Brand et al. [18], and Gross et al. [19] investigated the impacts of prosumers on DH systems. Huang et al. reviewed the applications of DCs as prosumers in DH systems [20], and Kauko et al. studied the impacts of DCs and supermarkets as prosumers in DH systems [21]. Previous research has proposed the methods to design and operate prosumers and demonstrated the economic benefits of introducing prosumers in

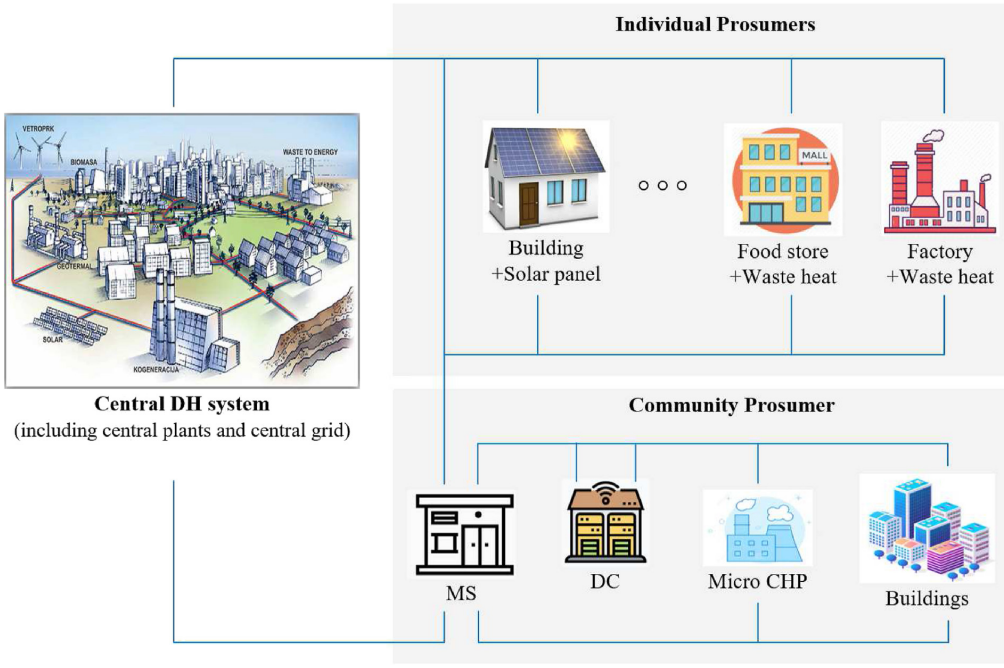

Fig. 1. Schematic illustrates examples of prosumers in a DH system.

DH systems. However, there is limited research focusing on optimizing prosumers' economic performance, especially under the current heating price models. During the transformation period of the DH system, despite some successful projects with bidirectional heating price models, the widely used heating price models have not supported the reverse heat supply from the heat prosumers to the central DH system, which means the prosumers would gain no economic benefit from supplying heat to the central DH system [22]. These unidirectional heating price models are reducing people's interest in heat prosumers, and thus hindering the promotion of prosumers in DH systems. Therefore, further research is needed to optimize prosumers' economic performance under the current widely used heating price models during the transformation period of the DH system.

The current widely used heating price models charge the heating cost of heat prosumers based on both the heat use and the peak load [22]. Therefore, the two possible ways to optimize heat prosumers' economic performance are: 1) increasing the self-utilization rate of heat supply from prosumers' DHSs, and hence reducing the heat supply from the central DH system, and 2) shaving prosumers' peak load by shifting parts of central DH system's heat supply from peak hours to non-peak hours. Thermal energy storages (TESs) have been proven to be good at achieving the above goals. Firstly, TESs may be used to relieve the mismatch between prosumers' heat supply from DHSs and buildings' heat demand [23–27]. Consequently, less heat is fed to the central DH system when surplus heat exists, and the self-utilization rate of the heat supply from prosumers' DHSs is increased. Secondly, TESs may shift the central DH system's heat supply from peak hours to non-peak hours, thereby shaving the peak load of the heat prosumers [28–30]. However, one barrier to the integration of TESs into prosumers is their high investment costs and the economic risk of long payback periods. Therefore, further research is needed to explore the economic feasibility of introducing TESs to prosumers under current heating price models.

This study aimed to break the above economic barrier through the optimal operation of heat prosumers with TESs and the optimal sizing of TESs. Firstly, a water tank thermal energy storage (WTTES) was chosen as short-term TES and integrated into a prosumer. Afterwards, a dynamic optimization problem was formulated aiming to explore the economic potential of the heat prosumer with TES. The economic performance of the prosumer with TES was evaluated in terms of heating cost saving and payback period. Finally, the size parameter of WTTES was swept to obtain the optimal storage size considering the trade-off between the payback period and the heating cost saving. The proposed method was tested on a campus DH system in Norway, which received heat from the central DH system, meanwhile, had its own DHS with waste heat recovery from the university DC. The main contributions of this study are summarized as the following. Firstly, the technical contribution is to support the transformation of current DH systems towards completely renewable-based DH systems with DHSs by optimizing prosumers' economic performance under the current heating price models, which is a practical but rarely addressed problem. Secondly, the scientific contribution is to use the technique of combining dynamic optimization and parameter' sweeping to explore prosumers' economic potentials considering the economic feasibility after introducing TESs. Thirdly, the practical contribution is to provide more comprehensive recommendations for heat prosumers and DH companies to understand the effect of the peak load definition on the economic performance of heat prosumers. This study provides guidelines on improving prosumers' economic performance during the transformation period of the DH system, and thus promote the development of the heat prosumers in DH systems.

The remaining of the article is organized as follows. Section 2 proposes a generalized heating price model based on the current widely used heating price models, afterwards introduces the system design and operation strategy aiming to optimize prosumers' economic performance under the generalized heating price model by using short-term TESs. Section 3 introduces the background of the case study, meanwhile provides information on research scenarios and simulation settings. Section 4 investigates and compares different scenarios' performance in terms of energy and economic indicators. Section 5 discusses the effects of the peak load definition on prosumers' economic performance and investigates the WTTESs' thermoclines during charging and discharging processes. Section 6 concludes this study.

2. Method

This section introduces the method to optimize prosumers' economic performance under current heating price models by using WTTESs. Firstly, a generalized heating price model is proposed based on the current widely used heating price models. Afterwards, considering the generalized heating price model, the system design for prosumers with the WTTESs and the optimization problem aiming to minimize the prosumers' heating cost are given. Meanwhile, the models and constraints used in the optimization problem are presented. Finally, the economic indicators used to evaluate prosumers' performance are introduced.

This study was based on numerical simulation. The DH system model was built using the Modelica language, which is an object-oriented language to conveniently model physical systems [31]. The optimization was performed with JModelica.org, which is an open-source platform for the simulation and optimization of complex dynamic systems [32]. For the optimization process based on the JModelica.org platform, the formulated infinite-dimensional optimization problem was transcribed into a finite-dimensional nonlinear programming (NLP) problem through Direct collocation [33]. Afterwards, the obtained NLP problem was solved by NLP solvers in the following steps. Firstly, the inequality constraints in the NLP problem were eliminated using the interior-point method [34]. Then a local optimum for the NLP was achieved by solving the first order Karush-Kuhn-Tucker condition, using iterative techniques through Newton's method.

2.1. Generalized heating price model

Although heating price models vary with local DH companies, a generalized heating price model was defined and was used in the optimization of prosumers' economic performance. This generalized heating price model was defined as suggested in the review paper of [22], where the current heating price models may include four components: fixed component (FXC), flow demand component (FDC), energy demand component (EDC), and load demand component (LDC). The FXC is paid to connect to the central DH system. The FDC is charged based on the volume of the hot water used to deliver heat and is intended to motivate the low return temperature. The LDC covers the DH companies' cost to maintain a certain level of capacity for the peak load, the initial investment of new facilities, depreciation, etc. It is charged based on the peak load of the end-users. The EDC covers the fuel cost and is charged based on the total heat use of end-users.

Based on the review article of [22], the existence and the average share of each component for the Swedish DH systems are illustrated in Fig. 2. About half of the heating price models include the FXC (60%) and the FDC (50%), however, they only account for 1–2% of the total heating cost. In contrast, the LDC and the EDC are the most commonly used components. About 87% of the current

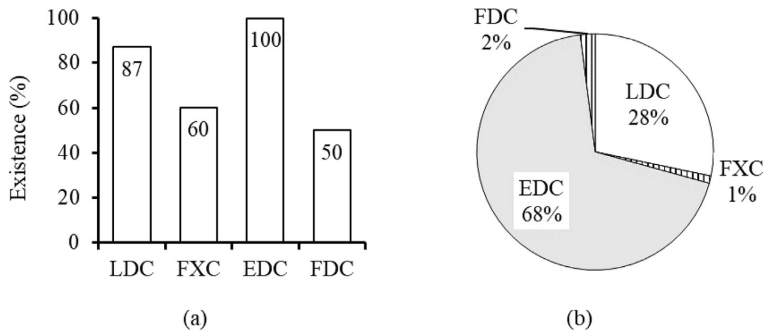

Fig. 2. The existence (a) and average share (b) of each component in investigated heating price models [22].

heating price models have the LDC, and all the current heating price models have the EDC. They together account for 96% of the total heating cost. There are technical-economic reasons for the configuration of a heating price model. All the DH companies want to cover their production cost and therefore the EDC is always included. For newer DH companies that may be oversized than the current heat demand, the most important component to charge the customers is the EDC. In addition, for existing DH companies that may have issues in further capacity increase, more effective utilization of the existing capacities is crucial and therefore the LDC is becoming very important and valuable. According to the above discussion, a generalized heating price model was proposed considering only the LDC and EDC as shown in Equation (1). The introduced generalized heating price model is just a theoretical suggestion and DH companies may organize their models based on their needs.

$$C_{tot} = C_{ldc} + C_{edc} \tag{1}$$

where C_{tot} is the total heating cost, C_{ldc} is the LDC, and C_{edc} is the EDC.

The LDC, C_{ldc}, was calculated as Equation (2):

$$C_{ldc} = LP \cdot \dot{Q}_{pea} \tag{2}$$

where LP is the LDC heating price, and $\dot{Q}_{pea}$ is the yearly peak load according to Refs. [35,36].

The EDC, C_{edc}, was calculated as Equation (3):

$$C_{edc} = \int_{t_0}^{t_f} EP(t) \cdot \dot{Q}(t) dt \tag{3}$$

where $\dot{Q}(t)$ is the heat flow rate supplied to the heat user and $EP(t)$ is the EDC heating price.

2.2. System design for a heat prosumer with WTTES

As introduced in Section 1, WTTES may be integrated into a heat prosumer to improve the economic performance of the heat prosumer under the current heating price models. Fig. 3 illustrates the proposed system design for a prosumer with WTTES, which may increase the self-utilization rate of the heat supply from the prosumer's DHSs and shave the prosumer's peak load. In the system, the DHS may be low-temperature heat sources from renewables or waste heat. There are mainly three configurations to integrate the DHSs into DH grids: 1) extraction from the return line and feed into the supply line (R2S), 2) extraction from the return line and feed into the return line (R2R), and 3) extraction from the supply line and feed into the supply line (S2S). In this study, the R2R mode was chosen, because it is preferable for low-temperature heat sources [4].

In addition, the MS connects the prosumer with the central DH system. The heat exchanger 1 (HE1) in the MS is connected to the TES and used for the heat charging of the WTTES. During the warm period with lower heat demand, the HE1 may supplement the heat supply from the prosumer's DHS. During the cold period with higher heat demand, the HE1 contributes to the peak load shaving, because it may charge the TES at non-peak hours and thus the stored heat can be used at peak hours. Heat exchanger 2 (HE2) is connected to the prosumer's distribution system directly and acts as a high-temperature heat source. It boosts the supply temperature of the prosumer to the required level after the preheating by low-temperature DHSs.

Moreover, the WTTES in the system is a short-term TES. As described in Section 1, it has two key functions. Firstly, it relives the mismatch problem between the DHS's heat supply and the buildings' heat demand during the warm period. When the DHS's heat supply is higher than the buildings' heat demand, the surplus heat supply from the DHS is stored in the WTTES instead of being fed into the central DH system. When the DHS's heat supply is lower than the buildings' heat demand, the stored heat in the WTTES together with the heat from DHS is supplied to the buildings. Secondly, the WTTES shaves the prosumer's peak load during the cold period. The WTTES is charged at non-peak hours and discharged at peak hours, therefore part of the central DH system's heat supply is shifted to non-peak hours and the peak load is shaved.

Finally, the heat-users in the system are buildings. As illustrated in Fig. 1, the heat-user may be one building when the prosumer is an individual prosumer or a cluster of buildings when the prosumer is a community prosumer.

2.3. Optimal operation for a prosumer with WTTES

To optimize prosumers' economic performance, the optimal operation strategy should minimize prosumers' heat use from the central DH system by increasing the self-utilization rate of the heat supply from prosumer's DHSs, minimize the prosumers' peak load. In addition, the operation should track the reference indoor temperature by minimizing the deviation between the simulated indoor temperature and its reference value. To achieve the above

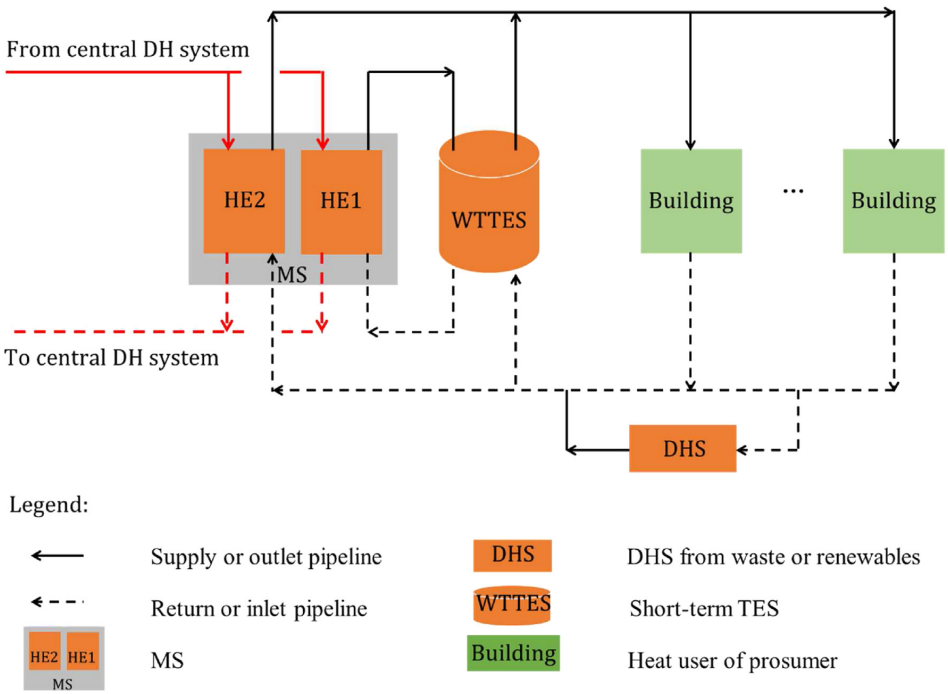

Fig. 3. Schematic illustrates the system design for a prosumer with WTTES.

goals, a multi-objective dynamic optimization problem was formulated as Equations (4), (5), (6), (7), and (8):

Minimize:

$$\int_{t_0}^{t_f} EP(t)\cdot\dot{Q}(t)dt + LP\cdot\dot{Q}_{pea} + W\cdot\int_{t_0}^{t_f}\left(T_{ia}(t) - T_{ia}^{ref}(t)\right)^2\cdot dt \tag{4}$$

subject to:

$$\dot{Q}(t) \le \dot{Q}_{pea} \tag{5}$$

$$F(t, \boldsymbol{z}(t)) = 0 \tag{6}$$

$$F_0(t_0, \boldsymbol{z}(t_0)) = 0 \tag{7}$$

$$z_L \le \boldsymbol{z}(t) \le z_U \tag{8}$$

where $\dot{Q}(t)$ is the heat flow rate supplied from the central DH to the prosumer. $\dot{Q}_{pea}$ and LP are the peak load and the LDC heating price, respectively. $EP(t)$ is the heating price for the EDC. $T_{ia}(t)$ and $T_{ia}^{ref}(t)$ are the simulated indoor temperature and its reference value at time t. $\boldsymbol{z}\in\mathbb{R}^{n_z}$ represents the time-dependent variables, which includes the manipulated variable $\boldsymbol{u}\in\mathbb{R}^{n_u}$ to be optimized, the differential variable $\boldsymbol{x}\in\mathbb{R}^{n_x}$, and the algebraic variable $\boldsymbol{y}\in\ \mathbb{R}^{n_y}$. Equation (6) defines the system dynamics and Equation (7) is the initial conditions of the system. $z_L\in[-\infty,\infty]^{n_z}$ and $z_U\in\ [-\infty,\infty]^{n_z}$ are the lower and upper bounds, respectively.

The system dynamics defined in Equation (6) included the dynamics of the MS, TES, DHS, buildings, and pipelines, as illustrated in Fig. 3. The energy and mass flow exchanged between these components were described by Equations (9), (10), (11), (12), and (13).

$$\dot{Q}(t) = \dot{Q}_{HE1} + \dot{Q}_{HE2} \tag{9}$$

$$\dot{Q}_{HE1} + \dot{Q}_{HE2} + \dot{Q}_{DHS} = \dot{Q}_{Bui} + \dot{Q}_{TES} + \dot{Q}_{loss,\ TES} + \dot{Q}_{loss,\ pip} \tag{10}$$

$$\dot{Q}_{HE1} = c\cdot\dot{m}_{HE1}\cdot(T_{HE1,sup} - T_{HE1,ret}) \tag{11}$$

$$\dot{Q}_{HE2} = c\cdot\dot{m}_{HE2}\cdot(T_{HE2,sup} - T_{HE2,ret}) \tag{12}$$

$$\dot{Q}_{DHS} = c\cdot\dot{m}_{DHS}\cdot(T_{DHS,sup} - T_{DHS,ret}) \tag{13}$$

where $\dot{m}_{HE1}$, $\dot{m}_{HE2}$, and $\dot{m}_{DHS}$ are the mass flow rate of HE1, HE2, and DHS, respectively. $\dot{Q}_{HE1}$, $\dot{Q}_{HE2}$, and $\dot{Q}_{DHS}$ are the heat flow rate of HE1, HE2, and DHS, respectively. $\dot{Q}_{TES}$ is the charging (positive values) and discharging (negative values) heat flow rate of WTTES. $\dot{Q}_{Bui}$ is the heat demand of buildings. $\dot{Q}_{loss,\ TES}$ and $\dot{Q}_{loss,\ pip}$ are the heat loss from WTTES and pipelines, respectively. $T_{HE1,sup}$, $T_{HE2,sup}$, and $T_{DHS,sup}$ are the supply water temperature of HE1, HE2, and DHS, respectively. $T_{HE1,ret}$, $T_{HE2,ret}$, and $T_{DHS,ret}$ are the return water temperature of HE1, HE2, and DHS, respectively. c is the specific heat capacity of water.

In this study, the manipulated variables, $\boldsymbol{u}$ in Equations (6), are the supply water temperature of HEs in the MS ($T_{HE1,sup}$ and $T_{HE2,sup}$), the mass flow rate of HEs and buildings ($\dot{m}_{HE1}$, $\dot{m}_{HE2}$, and $\dot{m}_{Bui}$), and the heat supply flow rate from the radiator to the

building ($\dot{Q}_{rad}$). The heat flow rate of a prosumer, $\dot{Q}(t)$ in Equation (4), means the total heat flow rate of the two HEs in MS ($\dot{Q}_{HE1}$ and $\dot{Q}_{HE2}$) as shown in Equation (9). In addition, the variables $\dot{Q}_{TES}$, $\dot{Q}_{loss,\ TES}$, $\dot{Q}_{Bui}$, and $\dot{Q}_{loss,\ pip}$ are described in the models of WTTES, buildings, and pipelines, which are explained in Sections 2.3.1-2.3.3.

2.3.1. Model for short-term WTTES

WTTES was chosen as the TES in this research because it is easily applied [37,38] and economically reasonable [39] for DH systems. A one-dimensional WTTES model was used to describe the dynamics of the thermocline tank. The model can be represented as a single partial differential equation as Equation (14) [40]:

$$c \cdot \rho \cdot A_{XS} \cdot \frac{\partial T}{\partial t} = c \cdot (\dot{m}_{sou} - \dot{m}_{use}) \cdot \frac{\partial T}{\partial x} - U \cdot P \cdot (T(t,x) - T_{amb}) + \varepsilon \cdot A_{XS} \cdot \frac{\partial^2 T}{\partial x^2} \tag{14}$$

where T is the water temperature in the tank. x is the height of the tank. t is the time. ρ is the density of water. A_{XS} and P are the cross-sectional area and the perimeter of the tank, respectively. $\dot{m}_{sou}$ and $\dot{m}_{use}$ are the water mass flow rate from the heat source side and the user side, respectively. T_{amb} is the ambient temperature. U is the U-value of the tank wall. ε is a parameter representing the combined heat transfer effect of water through diffusion, conduction, and mixing due to turbulent flow.

To solve Equation (14) by using numerical methods, spatial derivatives were approximated by discretizing the tank into n nodes. Using the discretization scheme shown in Fig. 4 and computing energy balances on each node, Equation (14) was converted into a set of ordinary differential equations. The ordinary differential equation for the *ith* node is shown in Equation (15) [40]. Therefore, the heat loss and the heat flow rate of the *ith* node are obtained by Equations (16) and (17), and the total heat loss and heat flow rate of WTTES was calculated as Equations (18) and (19). In addition, the parameter ε has two different types of values representing the situations without and with buoyant mixing effect. When the temperature of a node is lower than the node above it, ε has lower values. Otherwise, the values become several orders of magnitude higher due to the buoyant mixing effect [40].

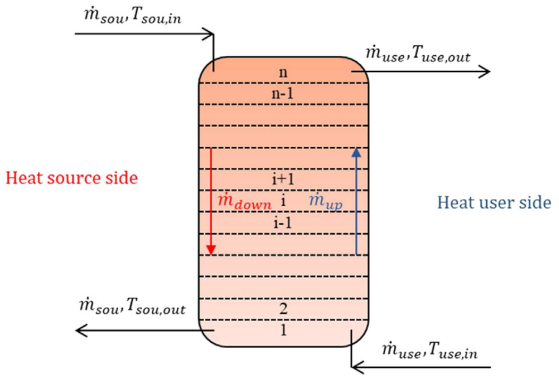

Fig. 4. Diagram illustrates the spatial discretization for a thermocline tank.

$$c \cdot \rho \cdot A_{XS} \cdot \Delta x \cdot \frac{dT_i}{dt} = c \cdot \dot{m}_{use} \cdot (T_{i-1} - T_i) + c \cdot \dot{m}_{sou} \cdot (T_{i+1} - T_i) - U \cdot P \cdot \Delta x \cdot (T_i - T_{amb}) + \frac{\varepsilon \cdot A_{XS}}{\Delta x} \cdot (T_{i+1} - 2 \cdot T_i + T_{i-1}) \tag{15}$$

$$\dot{q}_{loss,\ TES,\ i} = U \cdot P \cdot \Delta x \cdot (T_i - T_{amb}) \tag{16}$$

$$\dot{q}_{TES,i} = c \cdot \dot{m}_{sou} \cdot (T_{i+1} - T_i) \tag{17}$$

$$\dot{Q}_{loss,\ TES} = \sum_{i=1}^{n-1} \dot{q}_{loss,\ TES,\ i} \tag{18}$$

$$\dot{Q}_{TES} = \sum_{i=1}^{n-1} \dot{q}_{TES,i} \tag{19}$$

where Δx is the length of the node, and T_i is the water temperature of the *ith* node. $\dot{q}_{loss,\ TES,\ i}$ and $\dot{q}_{TES,i}$ are the heat loss and heat flow rate of the *ith* node, respectively.

2.3.2. Model for buildings

To improve computational efficiency, a single-equivalent building model was used to represent the overall performance of all the buildings in this study. This simplification has been proved feasibility by previous research [39,41]. After these simplifications, Equation (20) is used to describe the thermal behaviours of all the buildings connected to the prosumer' heating system, and Equations (21)–(23) are the inequality constraints for the variables ΔT_{Bui}, T_{sup}, and $\dot{m}_{Bui}$.

$$\dot{Q}_{Bui} = c \cdot \dot{m}_{Bui} \cdot (T_{sup} - T_{ret}) \tag{20}$$

$$\Delta T_{Bui,\ L} \le \Delta T_{Bui} = T_{sup} - T_{ret} \le \Delta T_{Bui,U} \tag{21}$$

$$T_{sup,L} \le T_{sup} \le T_{sup,U} \tag{22}$$

$$\dot{m}_{Bui,\ L} \le \dot{m}_{Bui} \le \dot{m}_{Bui,\ U} \tag{23}$$

where $\dot{Q}_{Bui}$ is the buildings' heat demand including demand for the SH and the DHW system. $\dot{m}_{Bui}$ and ΔT_{Bui} are the mass flow rate and temperature difference of water at the primary side of the building's substation, respectively. T_{sup} and T_{ret} are the supply and return temperature of water at the primary side of the building's substation, respectively. $\Delta T_{Bui,\ L}$, $T_{sup,L}$, and $\dot{m}_{Bui,\ L}$ are the lower bounds for ΔT_{Bui}, T_{sup}, and $\dot{m}_{Bui}$, respectively. $\Delta T_{Bui,U}$, $T_{sup,U}$, and $\dot{m}_{Bui,\ U}$ are the upper bounds for ΔT_{Bui}, T_{sup}, and $\dot{m}_{Bui}$, respectively.

The lower bound of the supply temperature, $T_{sup,L}$, should be high enough for the SH system and the DHW system to keep a comfortable indoor temperature and avoid hygiene issues, as defined in Equation (24). The lower bound of the supply temperature was defined by Equation (25) for the SH system [42], and the lower bound of the supply temperature for the DHW system was 60 °C as defined in Equation (26), which is required by European standard CEN/TR16355 [43]. In addition, the upper bound for the supply temperature was determined by the supply temperature of

the central DH system, which can be deduced through measured data.

$$T_{sup,L} = max(T_{sup,SH,L}, T_{sup,\ DHW,L}) \tag{24}$$

$$T_{sup,SH,L} = T_{ia} + 0.5 \cdot \left(T_{sup,SH,des} + T_{ret,SH,des} - 2 \cdot T_{ia,des}\right) \cdot \left(\frac{T_{ia,des} - T_{oa}}{T_{ia,des} - T_{oa,des}}\right)^{1/b} + 0.5 \cdot \left(T_{sup,SH,des} - T_{ret,SH,des}\right) \cdot \left(\frac{T_{ia,des} - T_{oa}}{T_{ia,des} - T_{oa,des}}\right) \tag{25}$$

$$T_{sup,\ DHW,L} = 60 \tag{26}$$

where $T_{sup,SH,L}$ and $T_{sup,\ DHW,L}$ are the lower bound of the supply temperature for the SH and the DHW system, respectively. T_{ia} and T_{oa} are the indoor and the outdoor temperature, respectively. $T_{sup,SH}$ and $T_{ret,SH}$ are the supply and the return temperature of the SH system, respectively. b is a parameter depending on the characteristic of the radiator. The subscript *des* refers to the design conditions.

The lower bound of the water mass flow rate $\dot{m}_{Bui,L}$ is zero, and the upper bound of the water mass flow rate $\dot{m}_{Bui,U}$ is constrained by the capacity of the distribution system. In this study, the upper bound of the water mass flow rate $\dot{m}_{Bui,U}$ was obtained by the measurement data. In addition, the characteristics of the system and equipment determine the feasible region of the water temperature difference as described in Equation (21). In this study, the lower bound of the water temperature difference $\Delta T_{Bui,\ L}$ was zero, and the upper bound of the water temperature difference $\Delta T_{Bui,U}$ was obtained by the linear regression using measured data as Equation (27).

$$\Delta T_{Bui,U} = a_0 + a_1 \cdot T_{sup} \tag{27}$$

where a_0 and a_1 are parameters.

The buildings' heat demand, $\dot{Q}_{Bui}$, includes the heat demand for the SH and the DHW system, as in Equation (28).

$$\dot{Q}_{Bui} = \dot{Q}_{SH} + \dot{Q}_{DHW} \tag{28}$$

where $\dot{Q}_{SH}$ and $\dot{Q}_{DHW}$ are the heat demand of the SH and the DHW systems, respectively. $\dot{Q}_{SH}$ can be further divided into the demand for the radiator heating system $\dot{Q}_{rad}$ and the demand for the ventilation system $\dot{Q}_{ven}$, as described in Equation (29).

$$\dot{Q}_{SH} = \dot{Q}_{rad} + \dot{Q}_{ven} \tag{29}$$

Considering the thermal inertia of buildings, a simplified-lumped-capacity model derived from resistance-capacitance networks analogue to electric circuits was used to describe the building dynamics, as defined in Equations (30)–(32).

$$C_{env} \cdot \frac{dT_{env}}{dt} = \frac{T_{ia} - T_{env}}{R_{i,e}} + \frac{T_{oa} - T_{env}}{R_{o,e}} \tag{30}$$

$$C_{ia} \cdot \frac{dT_{ia}}{dt} = \frac{T_{ma} - T_{ia}}{R_{i,m}} + \frac{T_{env} - T_{ia}}{R_{i,e}} + \frac{T_{oa} - T_{ia}}{R_{win}} + \frac{T_{oa} - T_{ia}}{R_{ven}} + \dot{Q}_{rad} + \dot{Q}_{ven} + \dot{Q}_{in} \tag{31}$$

$$C_{ma} \cdot \frac{dT_{ma}}{dt} = \frac{T_{ia} - T_{ma}}{R_{i,m}} \tag{32}$$

where C and R represent the heat capacitance and resistance, T is the temperature. Subscripts *env*, *ia*, *oa*, *ma*, *win*, and *ven* denote building envelopes (including exterior walls and roofs), indoor air, outdoor air, internal thermal mass, window, and ventilation (including infiltration and mechanical ventilation), respectively. In addition, $R_{i,e}$ is the heat resistance between the indoor air and the building envelopes, $R_{o,e}$ is the heat resistance between the outdoor air and the building envelopes, and $R_{i,m}$ is the heat resistance between indoor air and interior thermal mass. $\dot{Q}_{in}$ is the internal heat gains. All the introduced heat capacitances, thermal resistances, temperatures, and heat flow rates in Equations (30)–(32) are marked in Fig. 5.

2.3.3. Model for pipelines

The pipeline model representing the heat loss from the pipelines was described as the following Equations (33)–(35) [44]:

$$\dot{Q}_{loss,\ pip} = \dot{Q}_{loss,\ pip,sup} + \dot{Q}_{loss,\ pip,ret} \tag{33}$$

$$\dot{Q}_{loss,\ pip,sup} = L \cdot \pi \cdot d \cdot \frac{(R_g + R_i) \cdot \Delta T_{pip,sup} - R_c \cdot \Delta T_{pip,ret}}{(R_g + R_i)^2 - R_c^2} \tag{34}$$

$$\dot{Q}_{loss,\ pip,ret} = L \cdot \pi \cdot d \cdot \frac{(R_g + R_i) \cdot \Delta T_{pip,ret} - R_c \cdot \Delta T_{pip,sup}}{(R_g + R_i)^2 - R_c^2} \tag{35}$$

where $\dot{Q}_{loss,\ pip}$, $\dot{Q}_{loss,\ pip,sup}$, and $\dot{Q}_{loss,\ pip,ret}$ are the total heat loss from pipes, the heat loss from supply pipes, and the heat loss from return pipes, respectively. L is the route length for the pair of pipes. d is the outer pipe diameter. R_i, R_g, and R_c are the resistances for insulation, ground, and coinciding, respectively, and they can be obtained by Equations (36)–(38). In addition, $\Delta T_{pip,sup}$ and $\Delta T_{pip,ret}$ are the temperature difference for the supply pipe and the return pipe, and can be obtained by Equations (39) and (40):

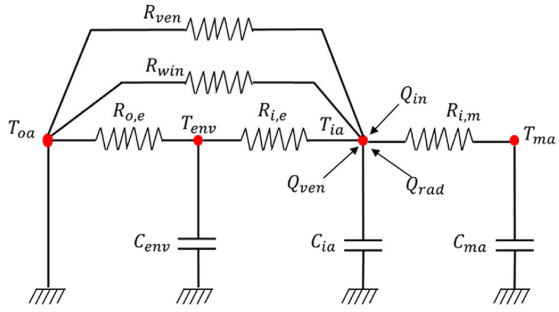

Fig. 5. Schematic of the simplified-lumped-capacity building model.

$$R_i = \frac{d}{2 \cdot \lambda_i} \cdot ln \frac{D}{d} \tag{36}$$

$$R_g = \frac{d}{2 \cdot \lambda} \cdot ln \frac{4 \cdot h}{D} \tag{37}$$

$$R_c = \frac{d}{2 \cdot \lambda} \cdot ln \left(\frac{2 \cdot h}{s} \right) \left(\frac{2 \cdot h}{s} \right) \left(\left(\frac{2 \cdot h}{s} \right)^2 + 1 \right)^{0.5} \tag{38}$$

$$\Delta T_{pip,sup} = T_{pip,sup} - T_{grou} \tag{39}$$

$$\Delta T_{pip,ret} = T_{pip,ret} - T_{grou} \tag{40}$$

where D is the outer insulation diameter, h is the distance between the pipe centres and the ground surface, s is the distance between pipe centres, and λ and λ_i are the heat conductivity for the ground and insulation. In addition, T_{grou} is the ground temperature, which was obtained from Equations (41)–(43). $T_{pip,sup}$ and $T_{pip,ret}$ are the water temperature in the supply pipe and the return pipe, respectively.

2.3.4. Model for the ground

In this study, the WTTES model and pipelines model used the ground temperature to calculate the heat losses. Equations (41)–(43) were applied to estimate the ground temperature as follows [45]:

$$T_{grou}(z,t) = T_{oa,aver} - T_{peak} \cdot e^{-z \cdot \sqrt{\frac{\omega}{2 \cdot \alpha}}} \cdot cos\left(\omega \cdot t - \phi - z \cdot \sqrt{\frac{\omega}{2 \cdot \alpha}} \right) \tag{41}$$

$$\omega = \frac{2 \cdot \pi}{T_{peri}} \tag{42}$$

$$\alpha = \frac{k}{\rho \cdot C} \tag{43}$$

where $T_{grou}(z,t)$ is the ground temperature in the depth z and at time t. $T_{oa,aver}$ is the annual average temperature of the outdoor air. T_{peak} is the peak deviation of the function from zero. ω is the angular frequency, T_{peri} is the period of the temperature cycle, and ϕ is the phase. α, k, ρ, and C are the thermal diffusivity, thermal conductivity, density, and heat capacity of the ground, respectively.

2.4. Indicators to evaluate the economic performance

In this section, the economic indicators including the initial investment cost and the payback period are introduced to evaluate the economic performance of the heat prosumers with TESs. The initial investment cost required for the WTTES depends strongly on the storage size. Fig. 6 illustrates the relationship between the initial investment cost and the size of WTTESs that with storage volumes larger than 200 m^3. The black dots in Fig. 6 present previous projects [52]. Fig. 6 shows that a power function approximates the relationship very well, with a coefficient of determination (R^2) of 0.99 and without obvious overfitting. In this study, the power function in Equation (44) was used to estimate the initial investment cost for large scale WTTESs in DH systems.

$$Invt = 0.0047 \cdot V^{0.6218} \tag{44}$$

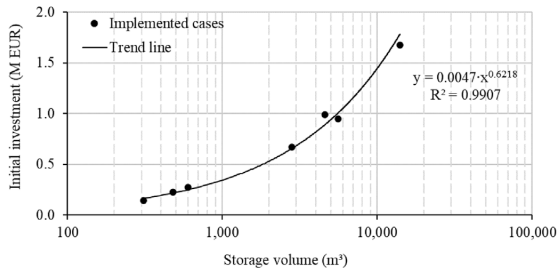

Fig. 6. The initial investment cost for WTTES.

where $Invt$ is the initial investment cost and V is the storage volume of WTTES.

The payback period is the time taken to fully recover the initial investment cost. It is one of the most commonly used methods for evaluating the economic performance of a system [47]. The payback period, PB, was calculated by using Equation (45):

$$B_{sav} \cdot \frac{(1+i)^{PB} - 1}{i \cdot (1+i)^{PB}} - Invt = 0 \tag{45}$$

where B_{sav} is the annual energy bill saving and i is the prevailing interest rate.

3. Case study

The proposed method in Section 2 was tested on a campus DH system in Norway. The background of the case study, research scenarios, and simulation settings are introduced below.

3.1. Background for the case study

A campus DH system in Trondheim, Norway, was chosen as the case study. As illustrated in Fig. 7, the campus DH system is a prosumer with DHS and heat users. The DHS is the university DC, which recovers the condensing waste heat from its cooling system. The heat users are buildings at the campus with a total building area of 300,000 m^2. The campus DH system is connected to the central DH system via the MS. Detailed information on the campus DH system can be found in Refs. [48,49]. According to the measurements from June 2017 to May 2018, the total heat supply for the campus DH system was 32.8 GWh. About 80% of the heat supply comes from the central DH system through the MS. The other 20% comes from the waste heat recovery from the DC.

Fig. 8 plots the heat demand for buildings and waste heat from the DC for the year 2017–2018. As shown with the green line in Fig. 8, the waste heat supply from the DC was around 1.0 MW throughout the year. However, as shown with the black line in Fig. 8, the building heat demand fluctuated from 0.2 MW to 13.8 MW. The mismatch between the waste heat supply and the building heat demand resulted in the surplus waste heat supply, especially for the period between June to October, as shown with the red line of Fig. 8. This surplus waste heat supply was fed into the central DH system via the MS. However, the university got no economic benefit from this surplus waste heat fed in, because as introduced in Section 1, the current heating price models do not support the reverse heat supply from the end-users to the central DH system.

In addition, the building heat demand was not equally distributed and there were high peak loads during the period from

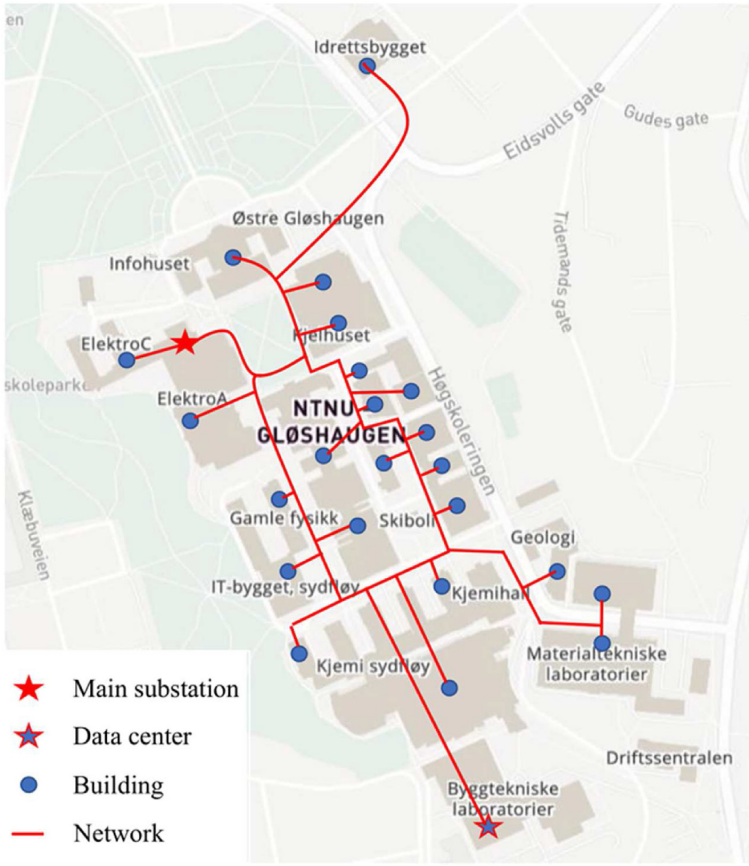

Fig. 7. Campus district heating system.

November to March, as shown with the black line of Fig. 8. The local DH company charged the heating bill also considering the peak load and the university paid about 5.3 million NOK[1] for the peak load each year, which accounted for 26% of the total heating bill.

3.2. Scenarios and simulation settings

To explore the economic feasibility after introducing a WTTES to the prosumer, different research scenarios were proposed based on the storage capacity of WTTES. The storage capacity meant the maximum discharging time for a WTTES under the discharging heat flow rate equals buildings' annual average heat demand. Eight scenarios including the reference scenario were proposed as listed in Table 1. The reference scenario, *Ref*, represented the current campus DH system without any TES. The other scenarios represented the WTTES solutions with storage capacities ranging from three hours to one week. The WTTESs were cylinder-shaped. All the tanks had the same height of 15 m, while the diameters were modified to provide certain storage capacities.

This research was conducted through three steps. Firstly, WTTESs with different storage capacities were integrated into the prosumer's campus DH system, respectively, as introduced in Section 2.2. Secondly, the optimal operation trajectories for the prosumer's campus DH system with the different storage capacities were obtained through the method provided in Section 2.3. Finally, these operation trajectories were evaluated in terms of economic indicators explained in Section 2.4. This study was based on the conditions of the year 2017–2018, and the detailed settings for the simulations are explained as follows. The used buildings' heat demand and the DC's waste heat came from the measured data as shown in Fig. 8. The key parameter settings are presented in Table A 1 in Appendix A. Among them, the parameters for the WTTES model were set according to the research [50], and the parameters of the pipeline model were set based on the book [44]. In addition, the heating prices were obtained from the website of the local DH company [51]. The local DH company used the monthly EDC heating price as shown in Fig. A 1 in Appendix A. Meanwhile, the used LDC heating price was 33 NOK/kW/month. Measured air temperature and estimated ground temperature of the simulation year are presented in Fig. A 2 in Appendix A.

4. Results

This section firstly presents the model validation results and

[1] The currency rate between NOK and EUR can be found from https://www.xe.com/, in this study 1 EUR = 10 NOK.

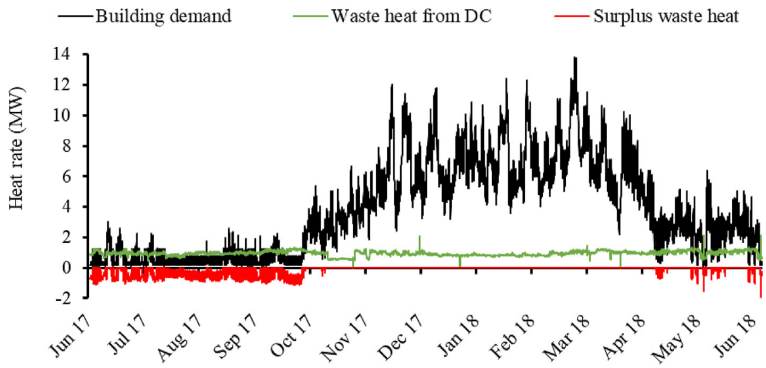

Fig. 8. Heat demand and waste heat supply.

Table 1
Information for the scenarios.

Scenario abbreviation	Storage capacity (hour)	Storage volume (m^3)	Tank diameter (m)
Ref	N/A	N/A	N/A
3 h	3	200	4.1
6 h	6	400	5.8
12 h	12	900	8.7
1 d	24	1700	12.0
3 d	72	5200	21.0
5 d	120	8600	27.0
7 d	168	12,000	31.9

then evaluates the proposed scenarios in terms of energy and economic analyses.

4.1. Model validation

As introduced in Section 2.3, the system model includes the following components: the WTTES, the building, and pipelines. In this study, the current campus DH system does not have any WTTES, and there is no measured data for the heat loss from the pipelines as well. Therefore, the WTTES and the pipeline model were validated according to the reference values from technical reports and textbooks instead of measured data. In a report from the International Energy Agency on large scale TESs [52], the reference storage efficiency for a WTTES is 50–90%. In this study, the corresponding value was about 90%, which was within the reference range. In practice, the low storage efficiency is caused by moistened insulation, because these WTTESs' envelopes are often deficient to protect against moisture penetration. However, it was assumed that the WTTES's envelope had a good quality to protect moisture penetration. Therefore, the WTTES used in this research had high storage efficiency.

According to the textbook *District Heating and Cooling* [44], for the DH systems in high heat density areas, the reference values for pipeline heat loss is 5–8% of the total heat supply. In this study, the corresponding value was close to 5%. This low pipeline heat loss was caused by two reasons. Firstly, compared to the typical DH systems with linear heat densities lower than 20 MWh/(m·a), the studied campus DH system had a higher linear heat density of 22 MWh/(m·a). The higher linear heat density made it more efficient during the distribution process and hence led to less pipeline heat loss. Secondly, the studied campus DH system had an annual average supply temperature of 65 °C that was lower than the typical DH system with 70–80 °C. Therefore, the low-temperature difference between the pipelines and the ground led to low pipeline heat loss.

The building model proposed in Section 2.3.2 was validated against the measured data. To quantify the deviation of the simulated data from the measured data, two indicators, i.e. coefficient of variation of the root mean square error (CV(RMSE)) and normalized mean bias error (NMBE), were used to evaluate the prediction performance of building model according to ASHRAE Guideline 14–2014 [53]. The validation criteria required in ASHRAE Guideline 14–2014 is within ±30% for CV(RMSE) and within ±10% for NMBE when using hourly data [53]. Fig. 9 shows the hourly simulated and measured building heat demand. As shown in Fig. 9, the values of the two indicators satisfied the requirements. In addition, Fig. 9 shows that the simulated building heat demand captured the trend in the measured data very well, with coefficients of determination (R^2) higher than 0.9 and no obvious overfitting.

4.2. Peak load shaving and heat use saving

The heat load duration diagram for the proposed scenarios is illustrated in Fig. 10, and the corresponding peak load is presented in Fig. 11. As shown in Fig. 10, compared to the reference scenario, *Ref*, part of the heat load for the scenarios with WTTES was shifted from the peak hours (the area highlighted with red colour) to the non-peak hours (the area highlighted with green colour). This load shifting contributed to the peak load shaving effect. As shown in Fig. 11, all the scenarios with WTTES had a lower peak load compared to the reference scenario. Furthermore, the load shifting effect was more significant for the scenarios with the larger WTTES. The maximal peak load shaving effect was achieved by scenario *7 d*, which had the largest WTTES. The peak load was shaved from 10.8 MW to 6.6 MW, a reduction of 39%. In contrast, the scenario with the smallest WTTES, *3 h*, had minimal peak load shaving, a reduction of only 4%.

Fig. 12 presents the annual heat use for the proposed scenarios. As introduced in Section 2.3, the prosumer's heat use means the heat supply from the central DH system via the MS. As shown in Fig. 12, the scenarios with the medium size WTTES (*3h*, *6 h*, *12 h*, and *1 d*) had minimal heat use, about 26.1 GWh, a heat use saving of 0.4 GWh compared to the reference scenario, *Ref*. However, the scenarios with the larger WTTES (*3 d*, *5 d* and *7 d*) had more heat use and hence less heat use saving. These results may be explained by Fig. 13. As shown by the columns filled with the orange colour in Fig. 13, the larger WTTES showed better performance on the

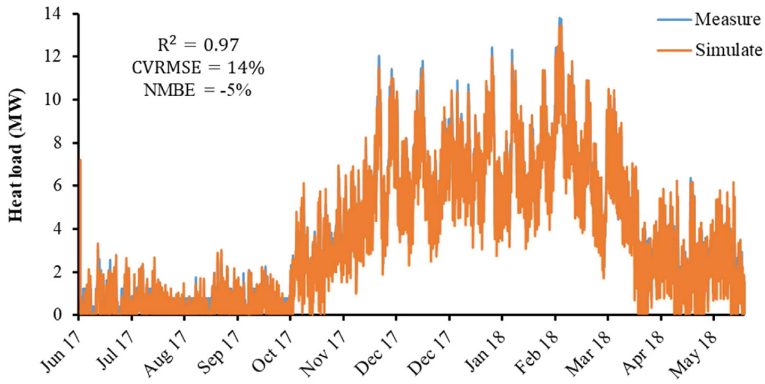

Fig. 9. Comparison between the simulated and measured building heat demand.

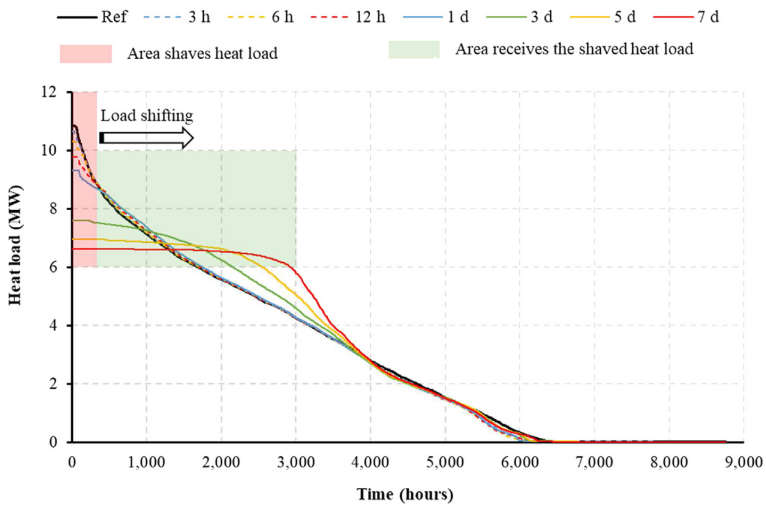

Fig. 10. Heat load duration diagram for the proposed scenarios.

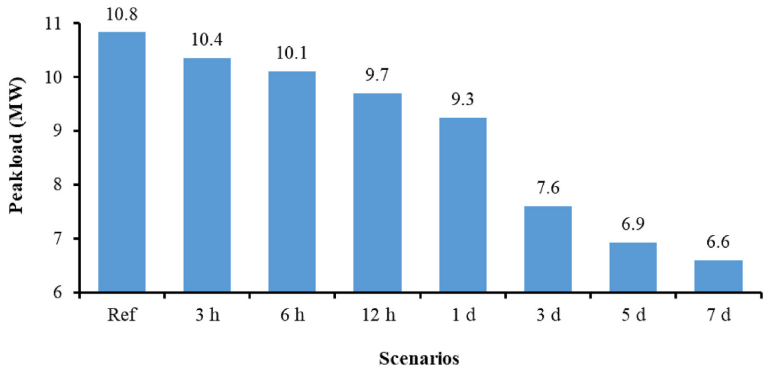

Fig. 11. Peak load for the proposed scenarios.

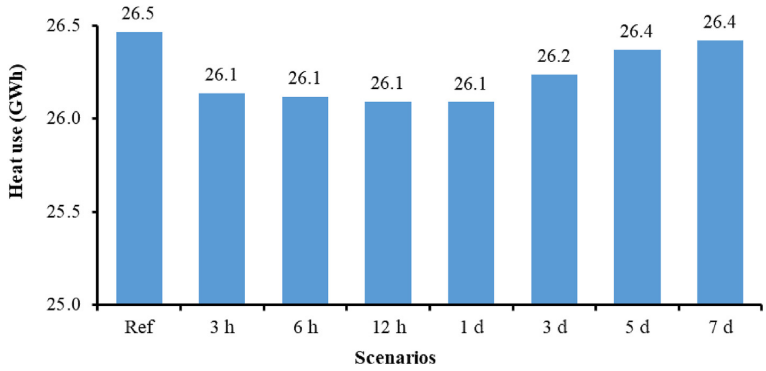

Fig. 12. Annual heat use for the proposed scenarios.

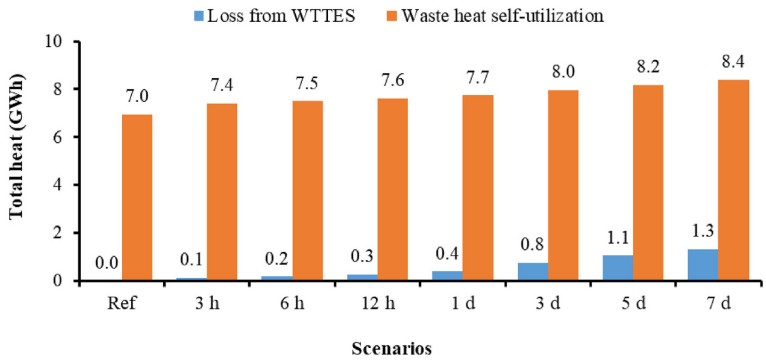

Fig. 13. Annual WTTES's heat loss and DC's waste heat self-utilization for the proposed scenarios.

mismatch relieving, and the waste heat self-utilization rate was increased from 79% to 96% (7.0 GWh to 8.4 GWh). However, the larger WTTES had higher heat loss to the environment as the columns filled with the blue colour in Fig. 13, because of its larger heat transfer area. The overall heat use saving performance of the WTTES depended on the sum of the above two effects. For the smaller WTTES, the mismatch relieving effect dominated the overall heat use performance. In contrast, for the larger WTTES, the heat loss effect dominated the overall heat use performance. Consequently, in this study, the WTTESs with three hours' to one day's storage capacity were the optimized storage size in terms of heat use saving.

4.3. Heating cost saving and payback period

The annual heating cost for the proposed scenarios is presented in Fig. 14 and the corresponding heating cost saving is shown in Fig. 15. Please note that all the currency in this section is presented in NOK. Two phenomena could be observed through Figs. 14 and 15: 1) the heating cost saving mainly came from the LDC, and 2) the larger WTTES brought more significant heating cost saving. As shown in Fig. 14, the annual EDC heating cost for the proposed scenarios was 15.4±0.1 million NOK, and the difference among these scenarios was less than 1%. In contrast, the annual LDC heating cost ranged from 4.7 million NOK to 2.8 million NOK with the increasing storage capacity of the WTTES, meaning a maximum difference of 39%. This significant reduction in the LDC contributed to the total heating cost saving. As shown in Fig. 15, as increasing the storage capacity of the WTTES, the annual heating cost saving increased from 0.4 million NOK to 1.9 million NOK, meaning a saving of 2%–9%. In this study, despite the waste heat self-utilization rate was increased up to 96%, as explained in Section 4.2, the relieving mismatch problem played a limited role in heating cost saving due to the original high waste heat self-utilization rate of 79%. However, for other cases with lower waste heat self-utilization rates, the relieving mismatch problem may contribute more to heating cost savings.

Fig. 16 presents the payback periods for the scenarios with the WTTES. It can be seen that the payback periods ranged from four years to ten years with the increasing WTTES storage size. Although the scenario with the largest WTTES needed the longest payback period, it achieved the highest heating cost saving. In contrast, the scenario with the smallest WTTES saved the lowest heating cost, while its payback period was the shortest. Therefore, the prosumer should make a trade-off between the payback period and the heating cost saving based on its own economic situation.

5. Discussion

This section first discusses the impacts of peak load definition on prosumers' economic performance. Afterwards, the thermoclines of the WTTESs during the charging and discharging processes are investigated.

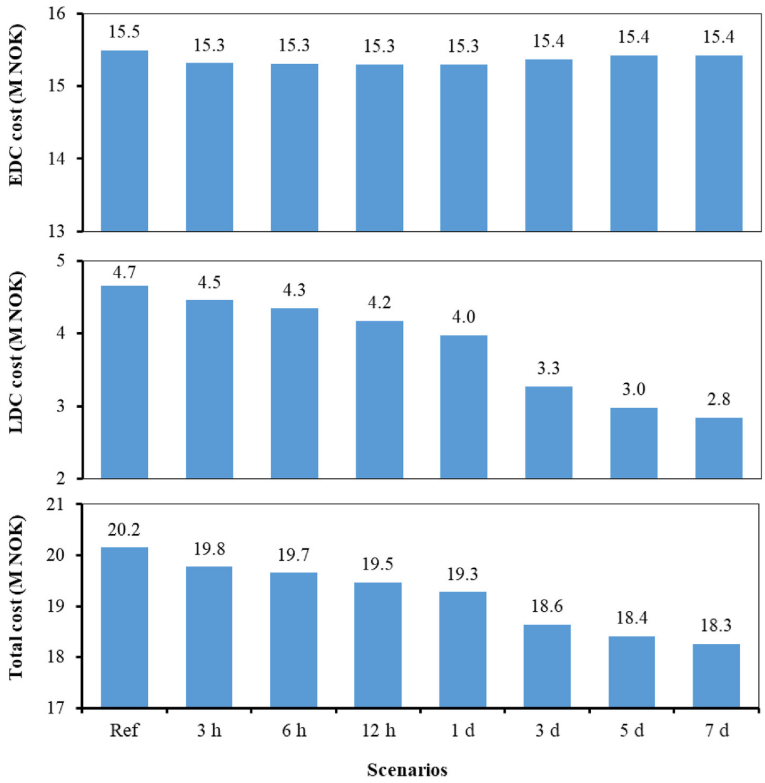

Fig. 14. Annual heating cost for the proposed scenarios.

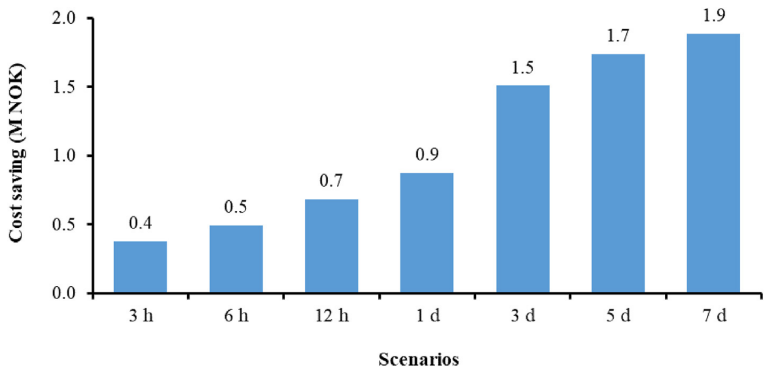

Fig. 15. Annual heating cost saving for the proposed scenarios.

5.1. Impacts of peak load definition

Based on a survey of heating contracts, methods of defining the peak load may be divided into two categories: hourly method and daily method [54]. For the hourly method, the peak load was the maximum hourly heat use, while the daily method was the maximum daily heat use. For this case study, the total heating cost saving was mainly determined by the reduction in LDC as observed in Section 4.3, which was linked to the peak load. Therefore, the way of defining the peak load may have a significant impact on the economic performance of prosumers with WTTESs. The results presented in Section 4 are based on the hourly method and this section presents further results based on the daily method.

The peak load under the daily method for the proposed scenarios is illustrated in Fig. 17, and the corresponding heating cost saving and the payback period are presented in Fig. 18 and Fig. 19,

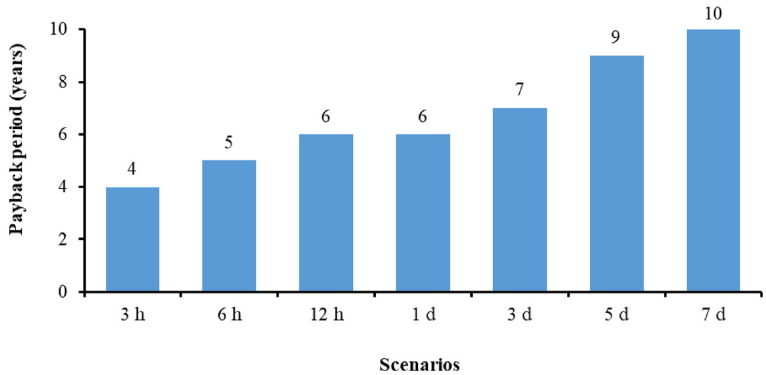

Fig. 16. The payback period for the scenarios with WTTES.

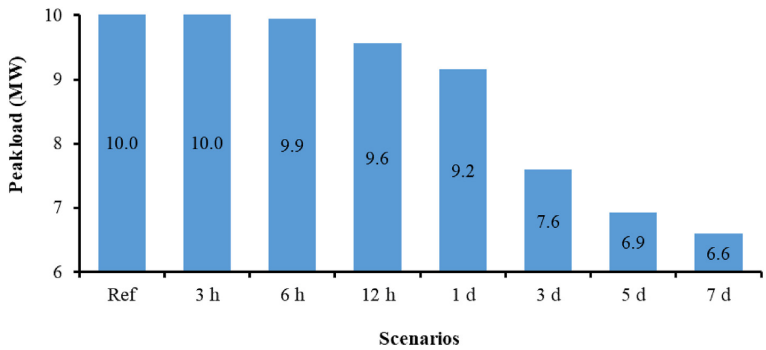

Fig. 17. Peak load for the proposed scenarios under the daily method.

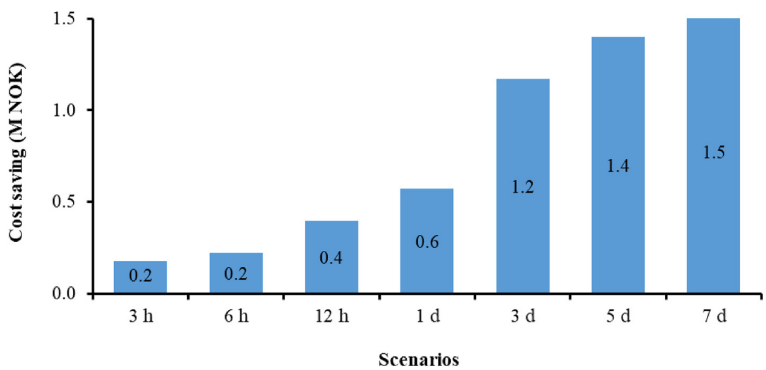

Fig. 18. Heating cost saving for the proposed scenarios under the daily method.

respectively. Similar to the hourly method, the larger WTTES brought a higher peak load shaving effect under the daily method as presented in Fig. 17. The peak load shaving increased from 0.1 MW to 3.4 MW as the increasing storage capacity of the WTTES from six hours to one week. However, compared to the hourly method, the peak load shaving effect under the daily method was different in two aspects: 1) it was less significant, and 2) it was not observed for the scenarios with the small WTTES. As shown in Fig. 17, the maximal peak load shaving effect was 3.4 MW, which was 19% less compared to the hourly method. Moreover, no peak load shaving effect was observed for the scenarios with the storage capacity smaller than six hours, their peak loads equalled that of the reference scenario, *Ref*, with the same value of 10.0 MW. The smaller WTTESs had a limited peak load shifting effect and was only capable to shift the heat load at the hourly level instead of the daily level. Therefore, the daily heat load kept almost the same.

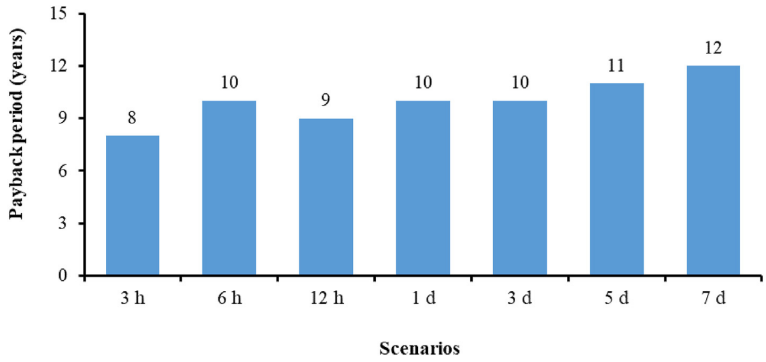

Fig. 19. The payback period for the proposed scenarios under the daily method.

The above impacts on the peak load shaving led to further impacts on the prosumer's economic performance. The prosumer obtained less heating cost saving under the daily method. As shown in Fig. 18, the heating cost saving ranged from 0.2 million NOK to 1.5 million NOK under the daily method, which was 18%–54% less compared to the hourly method. Furthermore, the payback period under the daily method ranged from 8 years to 12 years, and it was longer than the hourly method, especially for the WTTESs with smaller storage volumes.

Some recommendations from the discussion on the peak load definition are given as follows. Firstly, for the heat prosumers, special attention should be paid to the effect of the peak load definition. It may bring economic risk due to the changing of the heating contract. For example, DH companies may change their methods of defining the peak load from the hourly method to the daily method, and hence the economic benefit on heating cost saving may be drastically reduced and the payback period for TESs may be significantly prolonged. Secondly, for DH companies, it is better to use the hourly method to define the peak load, because the heat prosumers would be more motivated to introduce TESs and participate in user-side heat load management. One vital advantage brought by the user-side heat load management is peak load shaving, which may bring significant economic and technical benefits for DH companies.

5.2. Thermocline of the WTTES

In a WTTES, a thermocline is a layer where the water temperature changes more dramatically with depth than in the layers above and below it. It separates the lower density hot water at the top of the tank from the higher density cold water at the bottom of the tank. Generally, the thermocline should be as thin as possible to obtain a better thermal stratification and a less mixing effect between the hot and cold water [55]. Moreover, the position of the thermocline should be adjusted as the result of the optimized charging and discharging processes. Research showed that an optimal thermocline condition guaranteed high performance of the WTTES. For example, according to a study, the storage efficiency may be improved by 6% by optimizing the charging and discharging processes that led to an optimal thermocline condition [56]. Similar results were obtained in this study, which highlighted the importance of the thermocline of the WTTES. To assist the analysis of thermocline, the variable dimensionless temperature was used. As calculated by Equation (46), the water temperature of an individual layer in the WTTES was scaled into a real number ranging from 0 to 1. The two extreme values, 0 and 1, indicated the lowest and highest water temperature among all the layers in the WTTES. In a figure that illustrates the distribution of dimensionless temperature of layers in a WTTES, the thermocline can be identified as the layer that has significantly higher dimensionless temperature gaps between the layers above and below it.

$$T_{i,nonD} = \frac{T_i - T_{i,min}}{T_{i,max} - T_{i,min}} \tag{46}$$

where $T_{i,nonD}$ is the dimensionless water temperature of the Layer i. T_i is the water temperature of the Layer i. $T_{i,max}$ and $T_{i,min}$ are the highest and lowest water temperatures among all the layers in the WTTES.

Fig. 20 gives an example that illustrates an optimal thermocline condition of the WTTES, in which the plotted data were collected from Scenario *5 d* from February 06 to March 02 of 2018. As shown in Fig. 20 (c), the original heat load ranged from 4 MW to 14 MW during the presented period. However, after the load shifting by the WTTES, the heat load was almost constant at around 7 MW. To achieve this flattened heat load, the WTTES adjusted its operation strategies based on the heat load conditions and the whole period was divided into four subperiods. From February 06 to February 18, the WTTES might work for peak load shaving or valley filling depending on the heat load condition. However, as shown in Fig. 20 (a), the charging process dominated the period, which featured a rising water temperature in the tank. In addition, as illustrated in Fig. 20 (b), a thermocline was gradually formulated and enhanced around Layer 2, which was indicated by increasing dimensionless temperature gaps between the layers above and below it. Moreover, the position of the thermocline was at the lower side of the tank, therefore, more space was available to store the hot water above it. From February 18 to February 21, the WTTES serviced for peak load shaving, as shown in Fig. 20 (c). This period demanded a continually discharging process, and thus the water temperature in the tank was decreased as observed in Fig. 20 (a). Moreover, opposite to the charging dominated process in the previous period, the thermocline attenuated with reducing dimensionless temperature gaps, as observed in Fig. 20 (b). The following two periods, from February 21 to February 25 and from February 25 to March 02, repeated the above two periods with a charging dominated process and a discharging dominated process, which was characterised by an enhanced and attenuated thermocline, respectively.

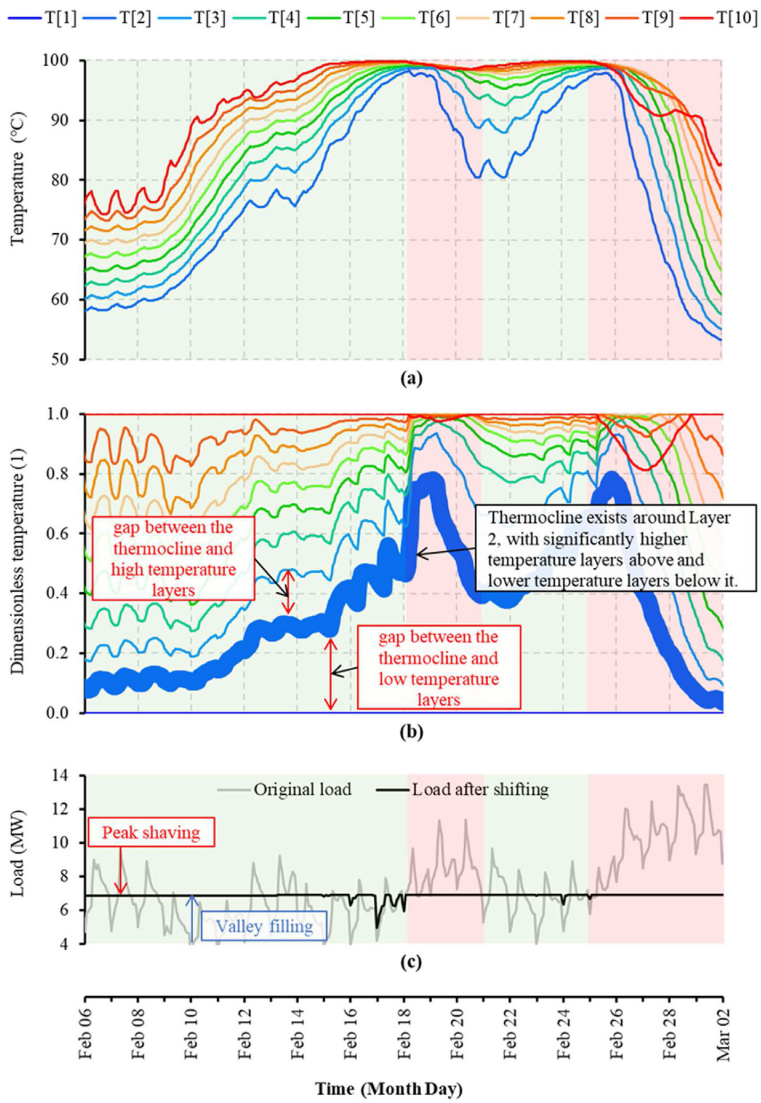

Fig. 20. An example of the charging and discharging processes of the WTTES, T [10] to T [1] refers to the water temperature from the top layer to the bottom layer, (a) temperature, (b) dimensionless temperature, and (c) heat load.

Some recommendations from the investigation of the thermocline of the WTTES are summarized as follows. Firstly, thermocline can be used as an effective indicator to understand the conditions and forecast the performance of WTTESs. Secondly, both the thickness and position are important to evaluate the conditions of the thermocline.

6. Conclusions

This study aimed to optimize prosumers' economic performance under the current unidirectional heating price models by using short-term TESs. A WTTES was chosen as the short-term TES and integrated into the prosumer. A dynamic optimization problem was formulated to explore the economic potential of the prosumer with TES. The size parameters of the TESs were swept to obtain the optimal storage size considering the trade-off between the payback period and the heating cost saving. The proposed method was tested on a campus DH system in Trondheim, Norway.

Results showed that by introducing the WTTES into the heat prosumer, the peak load was shaved by up to 39%, and the waste heat self-utilization rate was increased from 79% to 96%. These significantly improved the economic performance of the heat prosumer during the transformation period of the DH system. The annual heating cost was saved up to 1.9 million NOK, a saving of 9%, meanwhile, the initial investment of the WTTES was able to be fully recovered in less than ten years.

In addition, the effects of the peak load definition on the economic performance of the heat prosumers were discussed. It was found that the prosumers' economic performance was much better when using the hourly method to define the peak load instead of the daily method. Therefore, it was recommended that prosumers should consider the potential economic risk of introducing WTTES when the daily method is used in the heating contract. Moreover, research results highlighted the importance of the thermocline and showed that an optimal thermocline condition can lead to the high performance of the WTTES.

This study may provide guidelines on improving the heat prosumers' economic performance during the transformation period of the DH system, and hence promote the development of prosumers in DH systems.

Declaration of competing interest

The authors declare that they have no known competing financial interests or personal relationships that could have appeared to influence the work reported in this paper.

Acknowledgement

The authors gratefully acknowledge the support from the Research Council of Norway through the research project understanding behaviour of district heating systems integrating distributed sources under the FRIPRO/FRINATEK program (project number 262707) and the innovation project low-temperature thermal grids with surplus heat utilization under the EnergiX program (project number 280994).

Appendix A. Setting for the case study

Table A 1
Parameter setting for the simulation.

Category	Parameter	Value
WTTES and ground	U	1.2 W/(m^2·K)
	$T_{oa,aver}$	5.0 °C
	T_{peak}	4.5 °C
	T_{peri}	31,536,000 s
	k	2.7 W/(m·K)
	ρ	2800 kg/(m^3)
	C	840 J/(K·kg)
	ϕ	4.25 rad
Pipeline	L	1500 m
	d	0.273 m
	D	0.4 m
	h	1.2 m
	s	1.2 m
	λ	1.5 W/(m·K)
	λ_i	0.03 W/(m·K)
Buildings	C_{env}	45,000,000,000 J/K
	C_{ia}	1,300,000,000 J/K
	C_{ma}	2,900,000,000 J/K
	$R_{i,e}$	1.18 (m^2·K)/W
	$R_{o,e}$	1.03 (m^2·K)/W
	$R_{i,m}$	0.35 (m^2·K)/W
	R_{win}	0.48 (m^2·K)/W
	$\dot{Q}_{sen}$	0-8,000,000 W
	$\dot{Q}_{in}$	0-4,500,000 W
	$\dot{Q}_{DHW}$	0-1,200,000 W

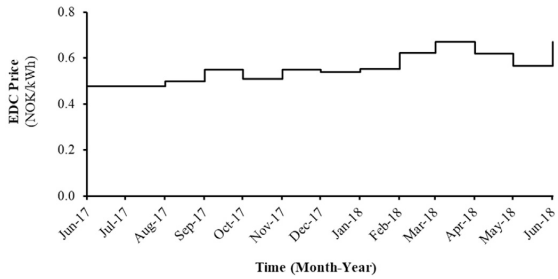

Fig. A 1. The EDC heating price [51]

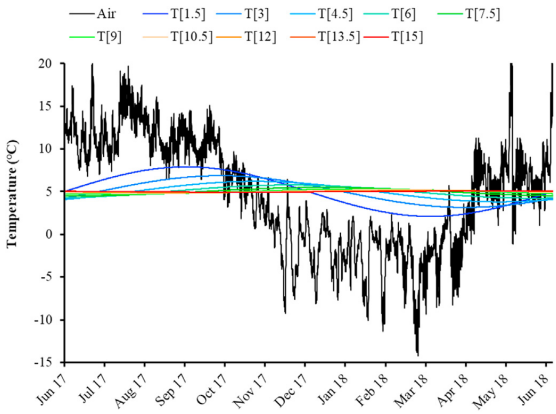

Fig. A 2. Measured air temperature and estimated ground temperature of the simulation year, T [15] to T[1.5] refers to the ground temperature from the 15 m depth to 1.5 m depth

Author statement

Haoran Li: Conceptualization, Methodology, Software, Validation, Writing – original draft Juan Hou: Conceptualization, Methodology, Writing – original draft Zhiyong Tian: Writing – review & editing Tianzhen Hong: Conceptualization, Writing – review & editing Natasa Nord: Conceptualization, Writing – review & editing, Supervision Daniel Rohde: Software, Writing – review & editing

References

[1] In focus: Energy efficiency in buildings, https://ec.europa.eu/info/news/focus-energy-efficiency-buildings-2020-feb-17en#:∼:text=Collectively%2C%20buildings%20in%20the%20EU,%2C%20usage%2C%20renovation%20and%20demolition, accessed September 2020.
[2] Heating and cooling, https://ec.europa.eu/energy/topics/energy-efficiency/heating-and-cooling_en?redir=1, accessed September 2020.
[3] Mapping and analyses of the current and future (2020-2030) heating/cooling fuel deployment (fossil/renewables), https://ec.europa.eu/energy/studies/mapping-and-analyses-current-and-future-2020-2030-heatingcooling-fuel-deployment_en, accessed September 2020.
[4] Li H, Nord N. Transition to the 4th generation district heating - possibilities,

bottlenecks, and challenges. Energy Procedia 2018;149:483–98.
[5] Sayegh MA, Danielewicz J, Nannou T, Miniewicz M, Jadwiszczak P, Piekarska K, et al. Trends of European research and development in district heating technologies. Renew Sustain Energy Rev 2017;68:1183–92.
[6] Åberg M, Fälting L, Lingfors D, Nilsson AM, Forssell A. Do ground source heat pumps challenge the dominant position of district heating in the Swedish heating market? J Clean Prod 2020;254:120070.
[7] Connolly D, Lund H, Mathiesen BV, Werner S, Möller B, Persson U, et al. Heat Roadmap Europe: combining district heating with heat savings to decarbonise the EU energy system. Energy Pol 2014;65:475–89.
[8] Werner S. International review of district heating and cooling. Energy 2017;137:617–31.
[9] Buffa S, Cozzini M, D'Antoni M, Baratieri M, Fedrizzi R. 5th generation district heating and cooling systems: a review of existing cases in Europe. Renew Sustain Energy Rev 2019;104:504–22.
[10] Christian Holmstedt Hansen OG, Hanne Kortegaard Støchkel, Detlefsen Nina. The competitiveness of district heating compared to individual heating. 2018.
[11] Dalla Rosa A, Li H, Svendsen S, Werner S, Persson U, Ruehling K, et al. IEA DHC Annex X report:Toward 4th generation district heating. Experience and Potential of Low-Temperature District Heating; 2014.
[12] Persson U, Werner S. Heat distribution and the future competitiveness of district heating. Appl Energy 2011;88(3):568–76.
[13] Nord N, Shakerin M, Tereshchenko T, Verda V, Borchiellini R. Data informed physical models for district heating grids with distributed heat sources to understand thermal and hydraulic aspects. Energy 2021;222:119965.
[14] Lickleder T, Hamacher T, Kramer M, Perić VS. Thermohydraulic model of Smart Thermal Grids with bidirectional power flow between prosumers. Energy 2021;230:120825.
[15] Marguerite C, Schmidt R-R, Pardo Garcia N. Concept development of an industrial waste heat based micro DH network. Conference Concept development of an industrial waste heat based micro DH network. LESO-PB, EPFL, p. 597-602.
[16] Pipiciello M, Caldera M, Cozzini M, Ancona MA, Melino F, Di Pietra B. Experimental characterization of a prototype of bidirectional substation for district heating with thermal prosumers. Energy 2021;223:120036.
[17] Nielsen S, Möller B. Excess heat production of future net zero energy buildings within district heating areas in Denmark. Energy 2012;48(1):23–31.
[18] Brand L, Calvén A, Englund J, Landersjö H, Lauenburg P. Smart district heating networks – a simulation study of prosumers' impact on technical parameters in distribution networks. Appl Energy 2014;129:39–48.
[19] Gross M, Karbasi B, Reiners T, Altieri L, Wagner H-J, Bertsch V. Implementing prosumers into heating networks. Energy 2021;230:120844.
[20] Huang P, Copertaro B, Zhang X, Shen J, Löfgren I, Rönnelid M, et al. A review of data centers as prosumers in district energy systems: renewable energy integration and waste heat reuse for district heating. Appl Energy 2020;258:114109.
[21] Kauko H, Kvalsvik KH, Rohde D, Nord N, Utne Å. Dynamic modeling of local district heating grids with prosumers: a case study for Norway. Energy 2018;151:261–71.
[22] Song J, Wallin F, Li H. District heating cost fluctuation caused by price model shift. Appl Energy 2017;194:715–24.
[23] Tian Z, Perers B, Furbo S, Fan J. Thermo-economic optimization of a hybrid solar district heating plant with flat plate collectors and parabolic trough collectors in series. Energy Convers Manag 2018;165:92–101.
[24] Shah SK, Aye L, Rismanchi B. Seasonal thermal energy storage system for cold climate zones: a review of recent developments. Renew Sustain Energy Rev 2018;97:38–49.
[25] Köfinger M, Schmidt RR, Basciotti D, Terreros O, Baldvinsson I, Mayrhofer J, et al. Simulation based evaluation of large scale waste heat utilization in urban district heating networks: optimized integration and operation of a seasonal storage. Energy 2018;159:1161–74.
[26] Rohde D, Andresen T, Nord N. Analysis of an integrated heating and cooling system for a building complex with focus on long–term thermal storage. Appl Therm Eng 2018;145:791–803.
[27] Rohde D, Knudsen BR, Andresen T, Nord N. Dynamic optimization of control setpoints for an integrated heating and cooling system with thermal energy storages. Energy 2020;193:116771.
[28] Verrilli F, Srinivasan S, Gambino G, Canelli M, Himanka M, Del Vecchio C, et al. Model predictive control-based optimal operations of district heating system with thermal energy storage and flexible loads. IEEE Trans Autom Sci Eng 2017;14(2):547–57.
[29] Verda V, Colella F. Primary energy savings through thermal storage in district heating networks. Energy 2011;36(7):4278–86.
[30] Harris M. Thermal energy storage in Sweden and Denmark: potentials for technology transfer. IIIEE Master thesis; 2011.
[31] The Modelica Association, https://www.modelica.org/, accessed Jan 2021.
[32] Åkesson J, Gäfvert M, Tummescheit H. Jmodelica—an open source platform for optimization of modelica models. Conference Jmodelica—an open source platform for optimization of modelica models.
[33] Amrit R, Rawlings JB, Biegler LT. Optimizing process economics online using model predictive control. Comput Chem Eng 2013;58:334–43.
[34] Nocedal J, Wright S. Numerical optimization. Springer Science & Business Media; 2006.
[35] Sernhed K, Gåverud H, Sandgren A. Customer perspectives on district heating price models. International Journal of Sustainable Energy Planning and Management 2017;13:47–60.
[36] Song J, Wallin F, Li H, Karlsson B. Price models of district heating in Sweden. Energy Procedia 2016;88:100–5.
[37] Bott C, Dressel I, Bayer P. State-of-technology review of water-based closed seasonal thermal energy storage systems. Renew Sustain Energy Rev 2019;113:109241.
[38] Pinel P, Cruickshank CA, Beausoleil-Morrison I, Wills A. A review of available methods for seasonal storage of solar thermal energy in residential applications. Renew Sustain Energy Rev 2011;15(7):3341–59.
[39] Li H, Hou J, Hong T, Ding Y, Nord N. Energy, economic, and environmental analysis of integration of thermal energy storage into district heating systems using waste heat from data centres. Energy 2021;219:119582.
[40] Powell KM, Edgar TF. An adaptive-grid model for dynamic simulation of thermocline thermal energy storage systems. Energy Convers Manag 2013;76:865–73.
[41] Li H, Hou J, Nord N. Using thermal storages to solve the mismatch between waste heat feed-in and heat demand: a case study of a district heating system of a university campus. 2019.
[42] He P, Sun G, Wang F, Wu H, Wu X. Heating engineering (in Chinese). China Architecture & Building Press; 2009.
[43] CEN. CEN/TR16355 Recommendations for prevention of Legionella growth in installations inside buildings conveying water for human consumption. 2012.
[44] Frederiksen S, Werner S. District heating and cooling. Studentlitteratur Lund; 2013.
[45] Andújar Márquez JM, Martínez Bohórquez MÁ, Gómez Melgar S. Ground thermal diffusivity calculation by direct soil temperature measurement. Application to very low enthalpy geothermal energy systems. Sensors 2016;16(3):306.
[47] Jaluria Y. Design and optimization of thermal systems. CRC press; 2007.
[48] Nord N, Sandberg NH, Ngo H, Nesgård E, Woszczek A, Tereshchenko T, et al. Future energy pathways for a university campus considering possibilities for energy efficiency improvements. Conference Future energy pathways for a university campus considering possibilities for energy efficiency improvements, vol. vol. 352. IOP Publishing, p. 012037.
[49] Guan J, Nord N, Chen S. Energy planning of university campus building complex: energy usage and coincidental analysis of individual buildings with a case study. Energy Build 2016;124:99–111.
[50] Cruickshank CA. Evaluation of a stratified multi-tank thermal storage for solar heating applications. Doctoral thesis; 2009.
[51] Charging method for heating bill in Trondheim, https://www.statkraftvarme.no/globalassets/2-statkraft-varme/statkraft-varme-norge/om-statkraft-varme/prisark/20190901/fjernvarmetariff-trondheim-bt1.pdf, accessed September 2020.
[52] Mangold D, Deschaintre L. Task 45 Large Systems Seasonal thermal energy storage Report on state of the art and necessary further R+ D. International Energy Agency Solar Heating and Cooling Programme; 2015.
[53] ASHRAE. ASHRAE guideline 14–2014, measurement of energy, demand, and water savings. ASHRAE Atlanta; 2014.
[54] Larsson O. Pricing models in district heating. Master thesis; 2011.
[55] Li G. Sensible heat thermal storage energy and exergy performance evaluations. Renew Sustain Energy Rev 2016;53:897–923.
[56] Ghaddar NK. Stratified storage tank influence on performance of solar water heating system tested in Beirut. Renew Energy 1994;4(8):911–25.

PAPER 5

Hou J, Li H, Nord N. Model predictive control for a data centre waste heat-based heat prosumer in Norway. Submitted to BuildSim Nordic 2022 conference. (Status: Accepted for full paper, and oral presentation).

This is an open access article under the CC BY license

APPENDIX- PUBLICATIONS

Model predictive control for a data centre waste heat-based heat prosumer in Norway

Juan Hou*, Haoran Li, Natasa Nord
Department of Energy and Process Technology, Norwegian University of Science and Technology (NTNU), Trondheim, Norway
* *corresponding author: juan.hou@ntnu.no*

Abstract

Waste heat from a data centre (DC) is a promising heat source because of the evenly distributed load profile and intensive waste heat generation. Many studies have proven the substantial financial benefits for the district heating (DH) operators by integrating DC waste heat with DH systems. However, there is a scarcity of research focusing on the optimal control of the DH system after integrating DC waste heat to further improve the system's economic performance. Therefore, this study aimed to further improve the economic performance of a DH system with DC waste heat by utilizing a model predictive control (MPC) scheme. This MPC scheme employed an economic-related objective function and formulated technical operational constraints. The proposed MPC scheme was tested on a campus DH system in Norway by simulation. Compared to a traditional rule-based control approach, the MPC scheme reduced the monthly energy cost by 1.8% while providing more stable chilled water for the DC cooling system.

Introduction

A data centre (DC) is a location where information technology (IT) equipment is housed. Moreover, a DC usually incorporates environmental control devices to guarantee that the IT equipment operates in a safe environment. These two major energy end-user equipment, i.e. the IT equipment and environmental control devices, results in a DC an energy-intensive facility. A DC can use more than 40 times the energy of a typical office building, and the majority of electricity used in DCs is converted into waste heat [1]. As a result, given the concern on the energy and climate crises, it is critical to investigate techniques for improving the energy efficiency of DCs [2]. The integration of DC waste heat into district heating (DH) systems is an effective way for the sustainability of DC as well as the improvement of the DH system's economic performance, and many researchers have proven it [3-5]. However, there is a scarcity of research focusing on the optimal control of the DH system after integrating DC waste heat to further improve the system economic performance, particularly for a DC waste heat-based heat prosumer with thermal energy storage (TES).

An optimal control technique may fully unlock the system's flexibility and hence further improve the DH system's economic performance. Model predictive control (MPC), which can use an economic-related objective function, is an ideal optimal control technique for achieving the system's maximum feasible economic performance while meeting various technical operational restrictions [6, 7]. In the presence of disturbances and technical operational restrictions, an MPC technique employs a system dynamic model to predict the system's future behaviour and provides an optimal control vector that minimizes an objective function over the prediction horizon.

This study, therefore, aimed to contribute to the optimal control of the DH system after integrating DC waste heat to further improve the system's economic performance by utilizing an MPC scheme. In the MPC scheme, an economic-related objective function based on an economic boundary was defined, a system dynamic model was developed and optimization constraints were formulated based on a real system's measured data. A campus DH system located in central Norway, which is a DC waste heat-based heat prosumer, was chosen as the case system to test the proposed MPC scheme by simulation. Moreover, the campus DH system was monitored by its energy management platform, which provided extensive operational data to aid this study. The DC performance, the total energy use and the energy bill of the system were used to evaluate the proposed MPC scheme. The main contributions of this study are listed as follows. Firstly, this study aimed to explore the optimal control of a DH system after integrating DC waste heat, which is a realistic yet rarely addressed issue. Secondly, the economic boundary was formulated by considering the dynamic pricing schemes of heating and electricity in Nordic countries at the same time, which may contribute to the study of the energy system involving both thermal and electrical networks. Lastly, real measured data from the case system was used to formulate the optimization constraints, which may supplement the recommended values from the standards and support the simulation and optimization to reveal the operation of a real system.

The remainder of this article is organised as follows. Section 2 describes the campus DH system, presents the developed system dynamic model, the developed economic boundary and the formulated MPC scheme. The information on simulation settings and research scenarios is introduced as well in Section 2. The model validation and simulation results are presented in Section 3. Lastly, conclusions are given in Section 4.

Methods

This section describes the campus DH system, as well as the system modelling method and economic boundary

condition. Finally, the MPC formulation, simulation settings and research scenarios are demonstrated.

Campus district heating system

Figure 1 presents the studied campus DH system, which is located in Trondheim, Norway. The campus DH system is connected to the city DH system via heat exchangers (HEs) in the main substation (MS), allowing the campus DH system to be managed independently. The waste heat from the university DC is captured by heat pump (HP) units and reused for the heating demand of the campus so that the DC waste heat is a distribution heat source (DHS). The connection method between the DC and campus DH system is that the water is extracted from the return pipe of the campus DH system and heated by the high-temperature refrigerant vapour at the HP condenser, and then fed back into the return pipe [8, 9]. Based on the measured data from June 2017 to May 2018, as shown in Figure 2, the total building heating demand was 32.8 GWh. The DC waste heat recovery accounted for about 20% of the total heating supply, and the rest 80% was supplied from the city DH system via the MS. As a result, the DH system on campus is a DC waste heat-based heat prosumer. In addition, buildings with a total building area of around 300 000 m^2 are the heat users in this campus DH system [10].

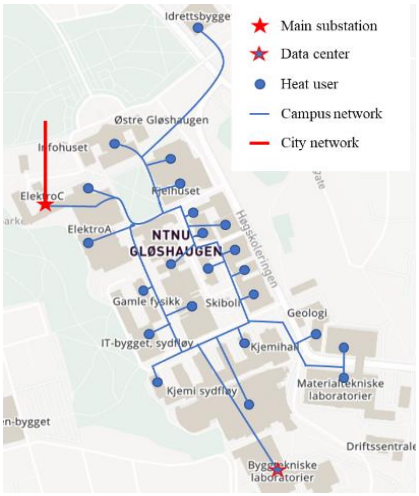

Figure 1. Campus district heating system

Another feature noticed in Figure 2 is that the building heating demand was not equally distributed and hence the peak heat loads were needed from the MS because the DC waste heat supply was almost constant throughout the year. However, the local DH company considers heat users' peak loads and the charging fee based on the peak loads accounted for around 26% of the total heating bill each year. The previous study has shown that using a short-term TES, water tank TES (WTTES), for the case system could solve the high peak load problem while also improving the system's economic performance [11]. Furthermore, research has been conducted to determine the optimal storage size for the introduced WTTES [12]. Therefore, this study was further research based on this previous research and introduced a WTTES with optimal storage size. The introduced WTTES had a storage volume of 900 m^3 and was able to supply heat to the campus DH system for up to 12 hours. In addition, the introduced WTTES was charged by a HE in the MS.

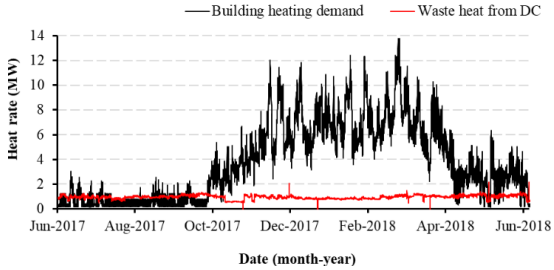

Figure 2. Building heating demand and data centre waste heat recovery

System modelling method

MPC uses a system dynamic model to predict the system's future behaviour and provides an optimal control vector. The Modelica language was used in this study to build the system dynamic model, which was based on the energy and mass flow exchanging connection between the individual component models. The individual components consisted of the MS, DC, buildings, WTTES, circulator pump (CP) and pipeline. The energy and mass flow exchanges between various components, as well as the modelling method for each component of the MS, buildings, WTTES and pipelines, are elaborated in previous research [12]. The modelling methods of the DC's HP and CP are discussed in this section.

Based on research [13], the operational conditions are the key factors that determine an HP's electricity use, aside from the HP's inherent performance characteristics. The operational conditions include the inlet and outlet water temperature as well as the water mass flow rate both at the evaporator and condenser sides of an HP. Moreover, extensive measured data on these operational conditions were available in this study. Therefore, an HP model including these operational conditions was developed, as shown in Equation (1).

$$\hat{E}_{HP} = a \cdot T_{in\_eva} + b \cdot T_{out\_eva} + c \cdot T_{in\_con} + d \cdot T_{out\_con} + e \cdot \dot{m}_{eva} + f \cdot \dot{m}_{con} \quad (1)$$

where $\hat{E}_{HP}$ is the simulated HP compressor power. T_{in_eva} and T_{out_eva} are the inlet and outlet water temperatures at the evaporator side. T_{in_con} and T_{out_con} are the inlet and outlet temperatures at the condenser side. $\dot{m}_{eva}$ and $\dot{m}_{con}$ are the water mass flow rate at the evaporator and condenser sides, respectively. a, b, c, d, e, and f are the parameters needed to be identified. In this study, the Evolutionary engine provided by the Excel Solver was used to identify these parameter values.

To overcome pipeline hydraulic resistance and local pipeline accessory resistance, a CP was employed to circulate warm water for the campus DH network. This study used a variable-speed CP because it can dramatically minimize pumping electricity use [14]. The total pumping power needed to circulate the water in a distribution system can be calculated by Equations (2) and (3).

$$E_{CP} = \frac{\Delta P \cdot \dot{V}}{\eta_{CP}} \tag{2}$$

$$\Delta P = S \cdot \dot{m}^2 \tag{3}$$

where E_{CP} is the CP electricity use. $\dot{V}$ is the water volume flow rate. η_{CP} is the total conversion efficiency of the CP and was 0.7 in this study [15]. ΔP is the total pressure drop of the DH distribution network. $\dot{m}$ is the mass flow rate of water. S is the resistance friction coefficient of the DH distribution network that is related to the characteristics of the pipeline. One assumption was adopted in this study: the water flow rate was regulated by the variable-speed CP, and the pipeline valves had no actions. As a result, the resistance friction coefficient S was a constant value that could be inferred from the DH system's design condition.

Economic boundary condition

The energy bill of the campus DH system includes two parts: 1) heating bill paid for the DH use and 2) electricity bill paid for the electricity use. Heat is provided by the DH company for the HEs in the MS, while electricity is provided by the electricity company for the HP of DC and the CP. As a result, this section defines the economic boundary condition by considering the pricing mechanisms of heating and electricity in Norway at the same time.

A generalized heating price model has been proposed in research [12], and this study used it as well. A generalized electricity price model was proposed in this study based on the investigation of electricity contracts in Norway. When using electricity in Norway, end-users must pay for two components: 1) power price for the electricity purchased from a power supplier, and 2) grid rent to the local grid distribution company for the power's transportation [16, 17].

In terms of the power price paid for a power supplier, a spot-price contract was used in this study. Because it is the most commonly used contract type in Norway based on Statistics Norway [18]. The price of the spot-price contract is calculated by Equations (4), (5) and (6).

$$C_{ele\_pow} = C_{spo} + C_{sur} + C_{mfi} \tag{4}$$

$$C_{spo} = \int_{t_0}^{t_f} PP_{spo}(t) \cdot \dot{E}(t) \cdot dt \tag{5}$$

$$C_{sur} = \int_{t_0}^{t_f} PP_{sur} \cdot \dot{E}(t) \cdot dt \tag{6}$$

where C_{ele_pow} denotes the power price paid by consumers. C_{spo} is the spot price-related fee and C_{sur} is a mark-up fee that must be paid by the customer [19]. C_{mfi} is the monthly fixed fee. Moreover, $PP_{spo}(t)$ represents the spot price at time t and gained from Nord Pool [20]. PP_{sur} is the mark-up fee per energy unit. Finally, $\dot{E}(t)$ is the electricity use at time t.

In terms of the grid rent paid for the grid distribution company, it is determined by the local grid distribution company. The grid rent for a big electricity user includes an energy link fee, a power link fee and an annual fixed fee, as shown by Equations (7), (8) and (9) [21].

$$C_{ele\_gri} = C_{ene} + C_{pow} + C_{afi} \tag{7}$$

$$C_{ene} = \int_{t_0}^{t_f} GP_{ene} \cdot \dot{E}(t) \cdot dt \tag{8}$$

$$C_{pow} = GP_{pow} \cdot \dot{E}_p \tag{9}$$

where C_{ele_gri} denotes the grid rent paid by consumers. C_{ene} and C_{pow} are the energy link fee and the power link fee, respectively. C_{afi} is the annual fixed fee. GP_{ene} is the energy link fee per energy unit and $\dot{E}(t)$ is the electricity use at time t. GP_{pow} is the power extraction price per power unit and $\dot{E}_p$ is the highest hourly power output.

As a result, a generalized electricity price model was suggested in this study, which is determined by Equation (10).

$$C_{ele} = C_{ele\_pow} + C_{ele\_gri} \tag{10}$$

where C_{ele} is the total electricity cost.

Model predictive control formulation

The MPC scheme developed in this study employed an economic-related objective function to further improve the economic performance of the campus DH system. The generalized heating price model and electricity model were used in this objective function. However, the monthly fixed fee in the power price and the annual fixed fee in grid rent were not involved, because they are not determined by the real-time electricity use. Furthermore, the power link fee included in the grid rent of the electricity price model was not taken into account. This is because the optimization problem in MPC only considered the electricity use of the HP and CP, the electricity use by other equipment, lighting, etc. was not considered, while the power link fee is calculated based on the highest hourly total electricity use of the entire energy system. As a result, the MPC controller solves the following optimization problem at each time step:

Minimize:

$$\begin{aligned} \int_0^H EP(t) \cdot \dot{Q}_{MS}(t) \cdot dt + LP \cdot \dot{Q}_{MS\_p} \\ + \int_0^H (PP_{spo}(t) \\ + PP_{sur} + GP_{ene}) \\ \cdot (\dot{E}_{HP}(t) + \dot{E}_{CP}(t)) \\ \cdot dt \end{aligned} \tag{11}$$

subject to:

$$\dot{Q}_{MS}(t) \le \dot{Q}_{MS\_p} \quad (12)$$

$$F(t, \boldsymbol{z}(t)) = 0 \quad (13)$$

$$F_0(t_0, \boldsymbol{z}(t_0)) = 0 \quad (14)$$

$$z_L \le \boldsymbol{z}(t) \le z_U \quad (15)$$

where H is the predictive horizon and was 12 hours in this study. $\dot{Q}_{MS}(t)$ is the heat flow rate from the MS at time t. $\dot{Q}_{MS\_p}$ is the peak heat rate from the MS, and it was a parameter to be optimized in this study. The peak heat rate was determined by the maximum hourly heat use in one month in this study [22]. $EP(t)$ is the energy demand component (EDC) heating price at time t, and LP is the load demand component (LDC) heating price [12]. $\dot{E}_{HP}(t)$ and $\dot{E}_{CP}(t)$ denote the HP electricity use and the CP electricity use at time t, respectively. The system dynamic model and its initial condition are the equality constraints as shown by Equations (13) and (14). Equation (15) defines the inequality constraint, which includes the technical operational constraints. $\boldsymbol{z} \in \mathbb{R}^{n_z}$ is the set of time-dependent variables and includes the manipulated variables $\boldsymbol{u} \in \mathbb{R}^{n_u}$ to be optimized, the differential variables $\boldsymbol{x} \in \mathbb{R}^{n_x}$, and the algebraic variables $\boldsymbol{y} \in \mathbb{R}^{n_y}$. $z_L \in [-\infty, \infty]^{n_z}$ and $z_U \in [-\infty, \infty]^{n_z}$ are the lower and upper limits, respectively.

Finally, the above-formulated optimization problem was solved on the optimization platform JModelica.org [23]. The detailed information on the optimization algorithm used in JModelica .org was elaborated on in the research [24].

Simulation settings and research scenarios

The building heating demand presented in Figure 2 was used as simulation inputs in the study. The energy prices, which included both heating and electricity, were collected from the local DH company [25] and a power supplier [26]. The used LDC in heating price was 39 NOK/kW (The currency rate between NOK and EUR used in this study was 1 EUR=10.0 NOK). The used EDC in heating price ranged from 0.484 to 0.868 NOK/kWh, while the electricity use-related price ranged from 0.485 to 0.870 NOK/kWh. The measured inlet water temperature and water mass flow rate of the evaporator in DC were almost constant values, with the average values of 11°C and 36.5 kg/s, and were directly used as simulation inputs in this study.

An MPC scenario together with an RBC scenario was proposed in the study. The RBC scenario was a reference scenario based on an RBC strategy, as shown in Figure 3 (a). A weather compensation controller (WCC) and a proportional-integral (PI) controller were used to control the supply water temperature and water flow rate of HE2. Another PI controller was utilized to control the compressor power of HP according to the feedback from the outlet water temperature of the evaporator, whose reference value was set as 6.5 °C. Moreover, a pre-defined schedule based on the heating demand characteristics was used to control the charging and discharging processes of WTTES.

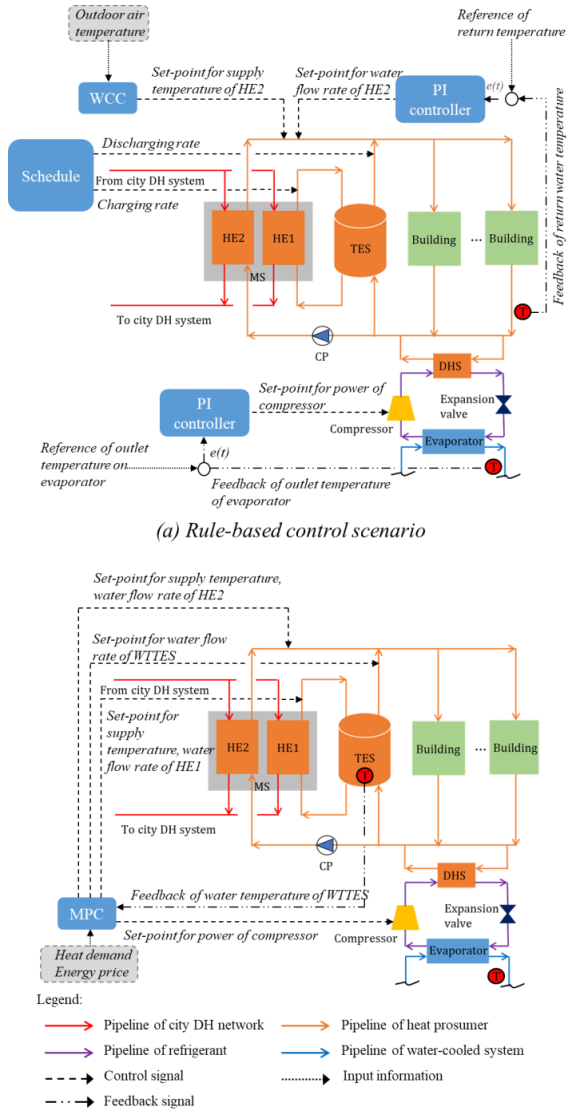

Figure 3. Research scenarios

The MPC scenario was based on the proposed MPC scheme, as shown in Figure 3 (b). Its manipulated variables included the supply water temperature and mass flow rate of the HEs, the water mass flow rate of the WTTES and the power of the HP compressor. In the real system, these manipulated variables were constrained to their feasible regions, formulating the MPC's technique operational constraints. The bounds of the HP compressor power were obtained by the measured data. The range of the outlet water temperature at the evaporator was set as

6.0- 7.0°C based on measured data. The bound settings of other manipulated variables can be found in [12].

Results

This section firstly introduces the model validation and then evaluates the MPC scheme in terms of the DC performance as well as the total energy use and energy bill of the system. In addition, January of 2018 was chosen as a typical month in the heating season of the year 2017-2018 to conduct this simulation-based study.

Model validation

Table 1 shows the values for the identified parameters in the HP model. The HP model was validated by the measured data from the campus energy management platform, as shown in Figure 4. Mean absolute error (MAE), mean absolute percentage error (MAPE) and root mean square error (RMSE) were utilized to evaluate the developed model, as presented in Figure 4 [27, 28]. Moreover, as shown in Figure 4, the simulated compressor hourly power matched the measured data well with the coefficient of determination (R^2) of 0.93.

Table 1. Values of the identified parameters

Parameter	*a*	*b*	*c*	*d*	*e*	*f*
Value	-1.5	10.6	-17.0	24.4	-5.7	-9.3

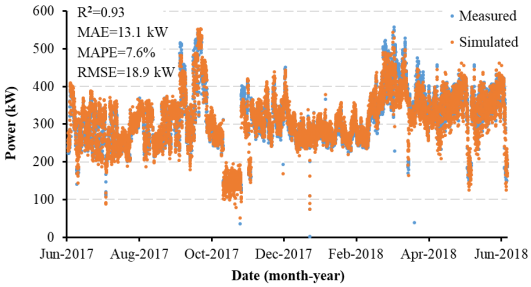

Figure 4. Simulated and measured hourly compressor power of heat pump

Data centre performance

Figure 5 presents the outlet temperature of the evaporator in HP. Compared to the RBC scenario, the MPC scenario had a smaller outlet temperature fluctuating range and preferred lower outlet temperatures with an average value of 6.0. Moreover, one result was obtained as well: the cooling requirement of DC was satisfied in both MPC and RBC scenarios because the evaporator's outlet water temperatures were mostly between 6.0 and 7.0°C, which was the feasible range based on the measured data. Figure 6 presents the coefficient of performance (COP) of HP. Similar to the outlet temperature of the evaporator, the MPC scenario had a lower COP fluctuating range yet higher COP values with an average value of 3.1. These results showed that the MPC scenario was more robust than the RBC scenario, expressed as the lower fluctuation ranges of both the evaporator's outlet temperature and the HP's COP, both of which are critical for the DC cooling system's safe operation.

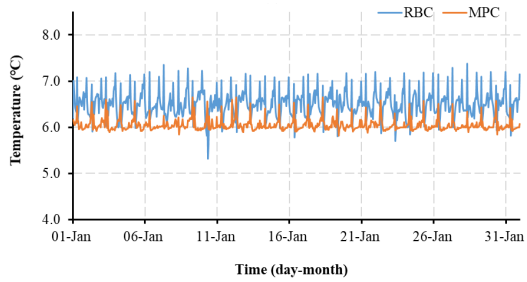

Figure 5. Simulated outlet temperatures of the evaporator

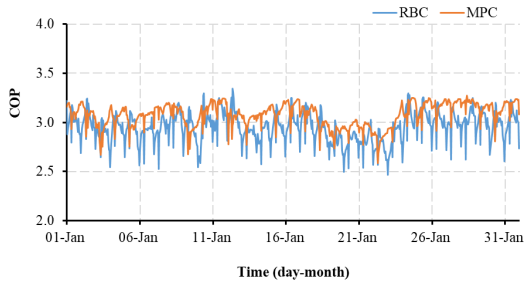

Figure 6. Simulated coefficient of performance of heat pump

Total energy use and energy bill

The total energy use consisted of the heat use from the MS and the electricity use to power the HP of DC and the CP. Figure 7 presents the simulated total energy use in January of 2018 for the two research scenarios. Compared to the RBC scenario, more electricity but less heat were used in the MPC scenario. As shown in Figure 7, the total heat use in the MPC scenario was 5.02 GWh, with a reduction of 2.0% compared to the RBC scenario. In contrast, electricity use was increased by 8.1% in the MPC scenario. The reason can be explained as follows: the MPC scenario preferred to produce more waste heat from the DC by utilizing more electricity because the HP's COPs were usually higher than 1 and fluctuated at 3.1. In addition, during the study period, the electricity prices were only slightly higher than the heating prices. As a result, the MPC scheme depended on obtaining as much heat as possible from the HP to achieve the best possible economic performance.

Figure 8 presents the monthly total energy bill for the two research scenarios. The energy bill included heating and electricity costs. Thereof, the heating cost consisted of the LDC based on the heat user's peak load and the EDC based on the total heat users' heat use. As shown in Figure 8, the MPC scenario saved the total energy bill by 1.8% compared to the RBC scenario. Specifically, the reduced heating costs in the MPC scenario, which were brought

by both the reductions of the LDC and the EDC, with a total cost reduction of 2.3%. On the other hand, the MPC scenario increased the electricity cost by 8.2% due to the increased electricity use. However, the electricity cost contributed to less than 10% of the total energy bill and hence the overall economic performance of the MPC scenario was not impaired by the increased electricity cost. In summary, the MPC scheme optimized the trade-off between heat and electricity use so that the possible maximum economic performance of the heat prosumer was achieved in the MPC scenario.

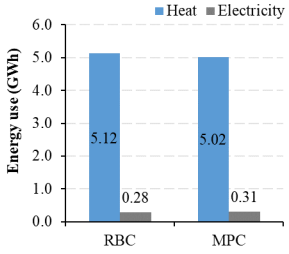

Figure 7. Energy use for the two research scenarios

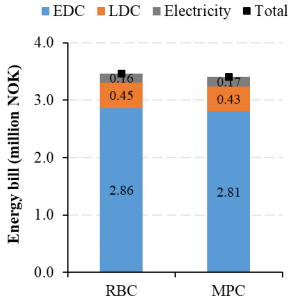

Figure 8. Energy bill for the two research scenarios

Conclusion

This study aimed to further improve the economic performance of a DH system after integrating DC waste heat by utilizing an MPC scheme. The MPC scheme employed an economic-related objective function, formulated the economic boundary condition and the technical operational constraints. The proposed MPC scheme was tested on a campus DH system in Norway by simulation.

Results showed that the MPC scheme was found to be more stable and robust, as seen by smaller fluctuating ranges of both the evaporator outlet temperatures and the COPs of the HP in DC, which are critical for the safe operation of the DC cooling system. To achieve the best possible economic performance, the MPC scheme tended to extract waste heat from the DC as much as possible by utilizing more electricity for the HP but extracting less heat from the MS, resulting in a 1.8% monthly energy cost saving. In summary, the MPC scheme optimized the trade-off between heat and electricity use so that the possible maximum economic performance of the heat prosumer was achieved in the MPC scenario.

Acknowledgement

The authors gratefully acknowledge the support from the Research Council of Norway through the research project Understanding behaviour of district heating systems integrating distributed sources under the FRIPRO/FRINATEK program (project number 262707).

Nomenclature

COP	Coefficient of performance
CP	Circulator pump
DC	Data centre
DH	District heating
DHS	Distributed heat source
EDC	Energy demand component
HE	Heat exchanger
HP	Heat pump
IT	Information technology
LDC	Load demand component
MAE	Mean absolute error
MAPE	Mean absolute percentage error
MPC	Model predictive control
MS	Main substation
PI	Proportional-integral
RBC	Rule-based control
RMSE	Root mean square error
TES	Thermal energy storage
WCC	Weather compensation controller
WTTES	Water tank thermal energy storage

References

[1] Greenberg S, Mills E, Tschudi B, Rumsey P, Myatt B. Best practices for data centers: Lessons learned from benchmarking 22 data centers. Proceedings of the ACEEE Summer Study on Energy Efficiency in Buildings in Asilomar, CA ACEEE, August. 2006;3:76-87.

[2] Huang P, Copertaro B, Zhang X, Shen J, Löfgren I, Rönnelid M, et al. A review of data centers as prosumers in district energy systems: Renewable energy integration and waste heat reuse for district heating. Applied Energy. 2020;258:114109.

[3] Wahlroos M, Pärssinen M, Manner J, Syri S. Utilizing data center waste heat in district heating–Impacts on energy efficiency and prospects for low-temperature district heating networks. Energy. 2017;140:1228-38.

[4] Davies G, Maidment G, Tozer R. Using data centres for combined heating and cooling: An investigation for London. Applied Thermal Engineering. 2016;94:296-304.

[5] He Z, Ding T, Liu Y, Li Z. Analysis of a district heating system using waste heat in a distributed cooling data center. Applied Thermal Engineering. 2018;141:1131-40.

[6] Drgoňa J, Arroyo J, Cupeiro Figueroa I, Blum D, Arendt K, Kim D, et al. All you need to know about model predictive control for buildings. Annual Reviews in Control. 2020;50:190-232.

[7] Killian M, Kozek M. Ten questions concerning model predictive control for energy efficient buildings. Building and Environment. 2016;105:403-12.

[8] Li H, Nord N. Transition to the 4th generation district heating-possibilities, bottlenecks, and challenges. Energy Procedia. 2018;149:483-98.

[9] Nord N, Shakerin M, Tereshchenko T, Verda V, Borchiellini R. Data informed physical models for district heating grids with distributed heat sources to understand thermal and hydraulic aspects. Energy. 2021;222:119965.

[10] Guan J, Nord N, Chen S. Energy planning of university campus building complex: Energy usage and coincidental analysis of individual buildings with a case study. Energy and Buildings. 2016;124:99-111.

[11] Li H, Hou J, Hong T, Ding Y, Nord N. Energy, economic, and environmental analysis of integration of thermal energy storage into district heating systems using waste heat from data centres. Energy. 2021;219:119582.

[12] Li H, Hou J, Tian Z, Hong T, Nord N, Rohde D. Optimize heat prosumers' economic performance under current heating price models by using water tank thermal energy storage. Energy. 2022;239:122103.

[13] Shu H-W, Duanmu L, Zhu Y-X, Li X-L. Critical COP value of heat pump unit for energy-saving in the seawater-source heat pump district heating system and the analysis of its impact factors. Harbin Gongye Daxue Xuebao(Journal of Harbin Institute of Technology). 2010;42(12):1995-8.

[14] Liu X, Zheng ON, Niu F. A simulation-based study on different control strategies for variable speed pump in distributed ground source heat pump systems. ASHRAE Transactions. 2016;122.

[15] Grundfos. Circulator pump, https://product-selection.grundfos.com/no/products/nbg-nbge/nbg/nbg-100-80-160177-97839346?pumpsystemid=1406357823&tab=variant-sizing-results; 2021 [accessed 15 December 2021].

[16] Norwegian Water Resources and Energy Directorate. Energy Regulatory Authority, https://www.nve.no/reguleringsmyndigheten/kunde/nett/nettleie/?ref=mainmenu; 2021 [Accessed 3 November 2021].

[17] Karlsen SS. Investigation of Grid Rent Business Models as Incentive for Demand-Side Management in Buildings-A case study on fully electric operated houses in Norway. Master thesis: Norwegian University of Science and Technology. 2018.

[18] Statistics Norway. Energy and Manufacturing, https://www.ssb.no/en/energi-og-industri/artikler-og-publikasjoner/twofold-increase-in-electricity-price-for-households; 2021 [Accessed 3 November 2021].

[19] Energy Facts Norway. Norway's Energy Supply System, https://energifaktanorge.no/en/utskrift/#toc-2; 2021 [Accessed 3 November 2021].

[20] Nord Pool. https://www.nordpoolgroup.com/; 2021 [Accessed 3 November 2021].

[21] Tensio. Grid Rental, https://ts.tensio.no/kunde/nettleie-priser-og-avtaler; 2021 [Accessed 3 November 2021].

[22] Li H, Hou J, Hong T, Nord N. Distinguish between the economic optimal and lowest distribution temperatures for heat-prosumer-based district heating systems with short-term thermal energy storage. Energy. 2022:123601.

[23] Åkesson J, Årzén K-E, Gäfvert M, Bergdahl T, Tummescheit H. Modeling and optimization with Optimica and JModelica. org—Languages and tools for solving large-scale dynamic optimization problems. Computers & Chemical Engineering. 2010;34(11):1737-49.

[24] Hou J, Li H, Nord N, Huang G. Model predictive control under weather forecast uncertainty for HVAC systems in university buildings. Energy and Buildings. 2021:111793.

[25] Statkraft varme at Tronheim. Products and services, https://www.statkraftvarme.no/globalassets/0/statkraft-varme/produkter-og-tjenester/prisark/jan-2021/trondheim-bedrift-uten-volumledd-bt1.pdf; 2021 [accessed 16 December 2021].

[26] NordlysEnergi. Company, https://www.nordlysenergi.com/bedrift; 2021 [accessed 16 December 2021].

[27] Ahmad T, Chen H, Shair J. Water source heat pump energy demand prognosticate using disparate data-mining based approaches. Energy. 2018;152:788-803.

[28] Wang J, Li G, Chen H, Liu J, Guo Y, Sun S, et al. Energy consumption prediction for water-source heat pump system using pattern recognition-based algorithms. Applied Thermal Engineering. 2018;136:755-66.

ISBN 978-82-326-6697-3 (printed ver.)
ISBN 978-82-326-5523-6 (electronic ver.)
ISSN 1503-8181 (printed ver.)
ISSN 2703-8084 (online ver.)

NTNU

Norwegian University of
Science and Technology